

REPORT DOCUMENTATION PAGE			Form Approved OMB NO. 0704-0188		
<p>The public reporting burden for this collection of information is estimated to average 1 hour per response, including the time for reviewing instructions, searching existing data sources, gathering and maintaining the data needed, and completing and reviewing the collection of information. Send comments regarding this burden estimate or any other aspect of this collection of information, including suggestions for reducing this burden, to Washington Headquarters Services, Directorate for Information Operations and Reports, 1215 Jefferson Davis Highway, Suite 1204, Arlington VA, 22202-4302. Respondents should be aware that notwithstanding any other provision of law, no person shall be subject to any penalty for failing to comply with a collection of information if it does not display a currently valid OMB control number.</p> <p>PLEASE DO NOT RETURN YOUR FORM TO THE ABOVE ADDRESS.</p>					
1. REPORT DATE (DD-MM-YYYY) 29-04-2015		2. REPORT TYPE Ph.D. Dissertation		3. DATES COVERED (From - To) -	
4. TITLE AND SUBTITLE Exploring Alkaline Stable Organic Cations for Polymer Hydroxide Exchange Membranes			5a. CONTRACT NUMBER W911NF-10-1-0520		
			5b. GRANT NUMBER		
			5c. PROGRAM ELEMENT NUMBER 611103		
6. AUTHORS Bingzi Zhang			5d. PROJECT NUMBER		
			5e. TASK NUMBER		
			5f. WORK UNIT NUMBER		
7. PERFORMING ORGANIZATION NAMES AND ADDRESSES Colorado School of Mines 1500 Illinois Street, Guggenheim Hall, Room 130  Golden, CO 80401 -1887			8. PERFORMING ORGANIZATION REPORT NUMBER		
9. SPONSORING/MONITORING AGENCY NAME(S) AND ADDRESS (ES) U.S. Army Research Office P.O. Box 12211 Research Triangle Park, NC 27709-2211			10. SPONSOR/MONITOR'S ACRONYM(S) ARO		
			11. SPONSOR/MONITOR'S REPORT NUMBER(S) 58161-CH-MUR.68		
12. DISTRIBUTION AVAILABILITY STATEMENT Approved for public release; distribution is unlimited.					
13. SUPPLEMENTARY NOTES The views, opinions and/or findings contained in this report are those of the author(s) and should not be construed as an official Department of the Army position, policy or decision, unless so designated by other documentation.					
14. ABSTRACT Hydroxide exchange membranes (HEMs) are important polymer electrolytes for electrochemical energy conversion devices. One major concern with the practical application of HEMs is their poor alkaline stabilities which stems from the hydroxide attack on the cationic group. Accordingly, the nature of the cationic group is the top priority in terms of alkaline stability. The most used cation system, which is quaternary ammonium (QA) based, has insufficient alkaline stability for practical applications. In this study, the tertiary sulfoniums (TS) and the quaternary phosphonium (QP) were selected as two candidates to overcome the intrinsic limitation of the QA.					
15. SUBJECT TERMS Anion Exchange Membranes, Stable Organic Cations					
16. SECURITY CLASSIFICATION OF:			17. LIMITATION OF ABSTRACT UU	15. NUMBER OF PAGES	19a. NAME OF RESPONSIBLE PERSON Andrew Herring
a. REPORT UU	b. ABSTRACT UU	c. THIS PAGE UU			19b. TELEPHONE NUMBER 303-384-2082

## Report Title

Exploring Alkaline Stable Organic Cations for Polymer Hydroxide Exchange Membranes

### ABSTRACT

Hydroxide exchange membranes (HEMs) are important polymer electrolytes for electrochemical energy conversion devices. One major concern with the practical application of HEMs is their poor alkaline stabilities which stems from the hydroxide attack on the cationic group. Accordingly, the nature of the cationic group is the top priority in terms of alkaline stability. The most used cation system, which is quaternary ammonium (QA) based, has insufficient alkaline stability for practical applications. In this study, the tertiary sulfoniums (TS) and the quaternary phosphonium (QP) were selected as two candidates to overcome the intrinsic limitation of the QA.

The triaryl-substituted TS (TAS), for the first time, was introduced as the cationic group for HEMs. The methoxy-substituted TAS based HEM exhibits reasonable alkaline stability and hydroxide conductivity. The alkaline stabilities of a series of TAS model compounds showed that more electron density on the central sulfur atom results in enhanced TAS alkaline stability. However, due to the susceptibility of the central sulfur atom to hydroxide attack, the most stable TAS cation in this study is still inferior to the benchmark cation, benzyltrimethylammonium (BTMA). Through degradation kinetics study, Benzyl (tris(2,4,6- trimethoxyphenyl)phosphonium (BTPP-(2,4,6-MeO)) was determined to have higher alkaline stability than the benchmark, BTMA. A new multi-step degradation mechanism related to the degradation of the methoxy groups for BTPP-(2,4,6-MeO) was proposed and verified. It suggested that the elimination of the substituent degradation can further enhance the QP's alkaline stability.

By replacing methoxy substituents with methyl groups, a superior QP cation, methyl tris(2,4,6-trimethoxyphenyl) phosphonium (MTPP-(2,4,6-Me)) was developed. MTPP-(2,4,6-Me) demonstrated a level of stability that has not been achieved by any other known HEM cations. The alkaline degradation kinetics and mechanisms of a wide range of QPs determined that the electronic effect and steric effect combined determine the alkaline stabilities of QP cations.

To take advantage of the outstanding alkaline stability of MTPP-(2,4,6-Me), a feasible synthesis route was developed to synthesize MTPP-(2,4,6-Me) functionalized polymers for constructing HEMs.

**EXPLORING ALKALINE STABLE ORGANIC CATIONS FOR POLYMER  
HYDROXIDE EXCHANGE MEMBRANES**

by

Bingzi Zhang

A dissertation submitted to the Faculty of the University of Delaware in partial fulfillment of the requirements for the degree of Doctor of Philosophy in Chemical Engineering

Spring 2015

© 2015 Bingzi Zhang  
All Rights Reserved

**EXPLORING ALKALINE STABLE ORGANIC CATIONS FOR POLYMER  
HYDROXIDE EXCHANGE MEMBRANES**

by

Bingzi Zhang

Approved: \_\_\_\_\_  
Abraham Lenhoff, Ph.D.  
Chair of the Department of Chemical and Biomolecular Engineering

Approved: \_\_\_\_\_  
Babatunde Ogunnaike, Ph.D.  
Dean of the College of Engineering

Approved: \_\_\_\_\_  
James G. Richards, Ph.D.  
Vice Provost for Graduate and Professional Education

I certify that I have read this dissertation and that in my opinion it meets the academic and professional standard required by the University as a dissertation for the degree of Doctor of Philosophy.

Signed:

---

Yushan Yan, Ph.D.  
Professor in charge of dissertation

I certify that I have read this dissertation and that in my opinion it meets the academic and professional standard required by the University as a dissertation for the degree of Doctor of Philosophy.

Signed:

---

Thomas H. Epps, III, Ph.D.  
Member of dissertation committee

I certify that I have read this dissertation and that in my opinion it meets the academic and professional standard required by the University as a dissertation for the degree of Doctor of Philosophy.

Signed:

---

Arthi Jayaraman, Ph.D.  
Member of dissertation committee

I certify that I have read this dissertation and that in my opinion it meets the academic and professional standard required by the University as a dissertation for the degree of Doctor of Philosophy.

Signed:

---

Timothy E. Mueller, Ph.D.  
Member of dissertation committee

## ACKNOWLEDGMENTS

First and above all, I would like to express the deepest appreciation to my Ph.D. advisor, Prof. Yushan Yan, for his excellent guidance, caring, patience, and providing me with an excellent atmosphere for doing research. Without his guidance and persistent help, this dissertation would not have been possible.

I would also like to thank Prof. Thomas H. Epps, III, Prof. Arthi Jayaraman and Dr. Timothy E. Mueller for being on my dissertation committee and providing useful feedback regarding my research. The comments and suggestions gained from the process were very helpful.

I would like to thank PIs in the MURI team: Prof. Bryan Coughlin from University of Massachusetts, Prof. Andrew M. Herring, Prof. Daniel M. Knauss and Prof. Matthew W. Liberatore from Colorado School of Mines, and Prof. Thomas A. Witten and Prof. Gregory A. Voth from University of Chicago for bringing out insightful questions and offering constructive suggestions in the teleconferences and annual meetings.

My fellow students' support has been continuous fuel during my long journey in finishing this doctoral program. Particularly, I would like to thank my research group members: Qianrong Fang, Junhua Wang, Jie Zheng, Shuang Gu, Yun Zhao, Ke Gong, Laj Xiong, Mingchuan Luo, Wenchao Sheng, Robert Kaspar, Mariah Woodroof, Jarrod Wittkopf, Xiaoya Ma, Andrew Tibbits, Marco Dunwell, Stephen Giles, Hongxia Guo, Hao Wang, Shuyuan Zhou, Kurt Jensen, Jianyu Cao, Minrui Gao, Yu Zhang, Jun Jiang, Shaun Alia, Yanqi Zhang, Ting Luo, Qian Xu, Melissa

Gettel and Rui Cai; I would like to thank my fellow MURI team members: Yating Yang, Wenxu Zhang, Haomiao Yuan, Yifan Li, Ye Liu, Benjamin Carie, Ashley Maes, Piril Ertem, Derek Strasser, Tara Prasad Pandey, Chinomso Nwosu, Himanshu Nitin Sarode, Steve Tse, Debbie Haywood and Melissa Vandiver; I would also like to thank fellow graduate students in University of California, Riverside: Wenting Hou, Yuanqi Tao, Yang Li and Bo Zhao.

I would like to thank Long Hai and Prof. Bryan Pivovar of the National Renewable Energy Laboratory for doing the calculation and theoretic work for my phosphonium project.

I would also like to thank my family members, who have always supported, encouraged and believed in me.

I would like to give my special thanks to Zhongbin Zhuang. He was always there cheering me up and stood by me through the good times and bad.

Finally, I would like to thank the MURI program of the Department of Defense and the ARPA-E program of Department of Energy for funding my Ph.D. work and the Royal Society of Chemistry for permitting me to reprint the following paper:

B. Z. Zhang, S. Gu, J. H. Wang, Y. Liu, A. M. Herring, Y. S. Yan, Tertiary Sulfonium as A Cationic Functional Group for Hydroxide Exchange Membranes. *RSC Advances*, **2012**, 2, 12683-12685.

## TABLE OF CONTENTS

LIST OF TABLES .....	x
LIST OF FIGURES .....	xi
ABSTRACT .....	xix
 1 INTRODUCTION .....	 1
1.1 Fuel cells.....	1
1.1.1 Background.....	1
1.1.2 Proton exchange membrane fuel cells (PEMFCs).....	3
1.1.3 Alkaline fuel cells (AFCs).....	5
1.1.4 Hydroxide exchange membrane fuel cells (HEMFCs) .....	6
1.2 Hydroxide exchange membranes (HEMs) .....	8
1.2.1 Background.....	8
1.2.2 Hydroxide conductivity issue .....	9
1.2.3 Alkaline stability issue .....	11
1.3 Cations for HEMs.....	12
1.3.1 Background.....	12
1.3.2 Nitrogen-based cation systems .....	14
1.3.3 Degradation pathways for quaternary ammonium (QA) cations.	16
1.3.4 Intrinsic limitation of QA cations.....	17
1.3.5 Phosphorus-based cation systems (phosphoniums).....	19
1.3.6 Sulfur-based cation systems (sulfoniums).....	21
1.4 Research aim and objectives .....	21
1.5 Outline of the dissertation .....	22
 2 TERTIARY SULFONIUM AS A CATIONIC FUNCTIONAL GROUP FOR HEMS .....	 24
2.1 Introduction .....	24
2.2 Materials and methods.....	27
2.2.1 Materials and characterization.....	27



2.2.2	Experimental methods .....	28
2.3	Results and Discussion .....	40
2.3.1	Thermal stability of the MeOTAS based HEM.....	40
2.3.2	Hydroxide conductivity of the MeOTAS based HEM .....	42
2.3.3	Alkaline stability of the MeOTAS based HEM .....	43
2.3.4	Comparison of PSf-MeOTASOH HEM and PSf-MeTASOH HEM .....	44
2.3.5	Influence of the phenyl-substituent over the alkaline stability ....	45
2.4	Conclusion .....	53
3	DEGRADATION KINETICS AND DEGRADATION MECHANISMS OF PHOSPHONIUM CATIONS IN ALKALINE ENVIRONMENT .....	55
3.1	Introduction .....	55
3.2	Materials and methods.....	58
3.2.1	Materials and characterization.....	58
3.2.2	Experimental methods .....	58
3.3	Results and discussion .....	61
3.3.1	Degradation kinetics of BTPP-(2,4,6-MeO) and QP analogs .....	61
3.3.2	Degradation mechanisms of of BTPP-(2,4,6-MeO) and QP analog .....	69
3.3.3	Verification of the proposed degradation mechanism of BTPP- (2,4,6-MeO) .....	74
3.4	Conclusion .....	79
4	DESIGN OF AN ALKALINE STABLE PHOSPHONIUM CATION .....	81
4.1	Introduction .....	81
4.2	Materials and methods.....	82
4.2.1	Materials and characterization.....	82
4.2.2	Experimental methods .....	83
4.3	Results and discussion .....	86
4.3.1	Synthesis of the MTPP-(2,4,6-Me) .....	86
4.3.2	Alkaline durability test of MTPP-(2,4,6-Me).....	89

4.3.3	Reasons for the ultra-high alkaline stability of MTPP-(2,4,6-Me) .....	96
4.3.4	Exploration of the structure-property relationship .....	98
4.4	Conclusion .....	105
5	SYNTHESIS OF MTPP-(2,4,6-ME)-FUNCTIONALIZED POLYMER FOR HEMS .....	107
5.1	Introduction .....	107
5.2	Materials and methods .....	110
5.2.1	Materials and characterization .....	110
5.2.2	Experimental methods .....	111
5.2.2.1	Route 1 .....	111
5.2.2.2	Route 2 .....	112
5.2.2.3	Route 3 .....	114
5.2.2.4	Synthesis of 2-bromo-5-vinyl- <i>m</i> -xylene .....	118
5.2.2.5	Alkaline stability study of MTPP-(2,4,6-Me) analog .....	119
5.3	Results and discussion .....	120
5.3.1	Route 1- link the side group of MTPP-(2,4,6-Me)-I to the polymer backbone .....	120
5.3.2	Route 2- link the P center to the polymer backbone .....	121
5.3.3	Route 3- link the side group of the phosphine precursor to the polymer backbone .....	123
5.3.4	Alkaline durability test of MTPP-(2,4,6-Me) analog .....	125
5.4	Conclusion .....	127
6	CONCLUSIONS AND FUTURE WORK .....	128
6.1	Conclusions .....	128
6.2	Future work .....	131
6.2.1	Preparation and characterization of MTPP-(2,4,6-Me) based HEMs .....	131
6.2.2	Further improvement of alkaline stabilities of MTPP-(2,4,6-Me) based HEMs .....	132
6.2.3	Further improvement of hydroxide conductivities of MTPP-(2,4,6-Me) based HEMs .....	134
6.2.4	Further exploration of alkaline stable QP cations .....	135

REFERENCES .....	137
A ABBREVIATIONS AND IMPORTANT VARIABLES .....	155
B TAFT EQUATION AND STERIC SUBSTITUENT CONSTANT ( $E_s$ ) .....	159
C DEGRADATION MECHANISM STUDY OF QP ANALOGS IN CHAPTER 3 AND DEGRADATION KINETICS STUDY OF QP CATIONS IN CHAPTER 4 .....	161

## LIST OF TABLES

Table 1.1:	Selected ion mobilities at infinite dilution in H <sub>2</sub> O at 25 °C. <sup>[42]</sup> .....	9
Table 1.2:	Chemical structures of reported HEM cations. ....	13
Table 2.1:	Thermal decomposition temperature of the pristine PSf and PSf-MeOTASOH. ....	41
Table 2.2:	IEC, HC and HC <sub>IEC</sub> of PSf-MeOTASOH and PSf-MeTASOH HEMs. .	42
Table 3.1:	Summary of $k_{80}$ of cations studied in this chapter.....	68
Table 4.1:	Unsuccessful reaction conditions for quaternization with benzyl halides (BnX) to produce BTPP-(2,4,6-Me). ....	87
Table 4.2:	Structure of QP cations studied in this chapter. ....	99
Table 4.3:	<sup>31</sup> P NMR chemical shift ( $\delta$ ) and degradation rate ( $k$ , $k_{OF}$ and $k_{EH}$ ) of QP cations at 80 °C. ....	100
Table 4.4:	Degradation mechanisms of QP cations studied in this chapter. ....	101
Table 5.1:	Reaction conditions and degree of acylation of acylated PPO.....	114
Table 5.2:	Conditions for and results of polymer quaternization reaction (Route 2).....	123
Table B.1:	Some $E_s$ used in the Taft equation. <sup>[256-258]</sup> .....	160

## LIST OF FIGURES

Figure 1.1:	Schematic diagram of a PEMFC. ....	4
Figure 1.2:	Chemical structure of Nafion. ....	5
Figure 1.3:	Schematic diagram of a HEMFC. ....	7
Figure 1.4:	The change in cell voltage and specific-area resistance during constant current hold test ( $150 \text{ mA cm}^{-2}$ ) at $70^\circ\text{C}$ over 12 h for a membrane-electrode-assembly (MEA) prepared from PPO with benzyl trimethyl ammonium (PPO-TMA <sup>+</sup> ). <sup>[219]</sup> Reproduced by permission of the authors. ....	15
Figure 1.5:	Degradation pathways for QA cation (exemplified by BTMA) in the presence of OH <sup>-</sup> nucleophiles. The inset (dashed box) shows the additional Hofmann Elimination degradation mechanism that can occur with alkyl-bound QA groups (that possess $\beta$ -H atoms). <sup>[2]</sup> Reproduced by permission of The Royal Society of Chemistry. ....	17
Figure 1.6:	Proposed strategies to eliminate the two major degradation pathways of BTMA. ....	19
Figure 1.7:	Chemical structure of tris(2,4,6-trimethoxyphenyl)phosphonium functionalized polysulfone (PSf-TPQP). ....	20
Figure 2.1:	Chemical structures of (a) TS cation and (b) the TAS cation. R <sub>1</sub> , R <sub>2</sub> and R <sub>3</sub> are the substituents. ....	25
Figure 2.2:	Alkaline degradation pathways of ordinary TS cations (trialkyl or arylalkyl substituted TS cations). ....	26
Figure 2.3:	Synthesis route of MeOTASOH-functionalized polysulfone (PSf-MeOTASOH). ....	28
Figure 2.4:	<sup>1</sup> H NMR spectrum (CDCl <sub>3</sub> ) of diphenyl(3-bromomethyl-4-methoxyphenyl) sulfonium triflate. ....	31
Figure 2.5:	<sup>1</sup> H NMR spectrum (CDCl <sub>3</sub> ) of chloromethylated polysulfone (CMPSf). ....	32

Figure 2.6	$^1\text{H}$ NMR spectrum ( $\text{CDCl}_3$ ) of butylaminated polysulfone (PSf-BA). ...	33
Figure 2.7:	$^1\text{H}$ NMR spectrum ( $\text{DMSO-d}_6$ ) of MeOTASCl functionalized polysulfone (PSf-MeOTASCl). .....	34
Figure 2.8:	Optical images of PSf-MeOTASOH HEM. ....	36
Figure 2.9:	Thermal gravimetric analysis (TGA) curves of the pristine PSf (dash line), and PSf-MeOTASOH (solid line). Test conditions: nitrogen atmosphere with $20 \text{ mL min}^{-1}$ of flow rate, and $10 \text{ }^\circ\text{C min}^{-1}$ of heating rate. ....	41
Figure 2.10:	Percent conductivity remaining of PSf-MeOTASOH HEM under alkaline degradation test over 14 days. Test conditions: 1 M KOD/D <sub>2</sub> O for test solution and $60 \text{ }^\circ\text{C}$ for test temperature. ....	43
Figure 2.11:	Chemical structures of two TAS based HEMs: (a) PSf-MeOTASOH and (b) PSf-MeTASOH. ....	44
Figure 2.12:	Percent conductivity remaining of PSf-MeTASOH HEM under alkaline degradation test. Test conditions: 1 M KOD/D <sub>2</sub> O for test solution and $60 \text{ }^\circ\text{C}$ for test temperature. ....	45
Figure 2.13:	Chemical structures of (a) MeOTASCl and (b) MeTASCl. ....	46
Figure 2.14:	$^1\text{H}$ NMR spectra of MeOTASCl: (a) before alkaline durability test and (b) after 14 days durability test. The inset shows the enlarged spectra in the region of 6.8~7.4 ppm. Test conditions: 1 M KOD/D <sub>2</sub> O for test solution and $60 \text{ }^\circ\text{C}$ for test temperature. ....	47
Figure 2.15:	$^1\text{H}$ NMR spectra of MeTASCl: (a) before alkaline durability test, and (b) after 1 day alkaline durability test over 1 day. The inset shows the enlarged spectra in the region of 6.8~7.8 ppm. Test conditions: 1 M KOD/D <sub>2</sub> O for test solution and $60 \text{ }^\circ\text{C}$ for test temperature. ....	47
Figure 2.16:	Chemical structure of 9MeOTASCl. ....	48
Figure 2.17:	Time series of $^1\text{H}$ NMR spectra during durability test of 9MeOTASCl at $80 \text{ }^\circ\text{C}$ . TMS( $\text{CH}_2$ ) <sub>3</sub> SO <sub>3</sub> Na as the internal standard; 1 M KOD in CD <sub>3</sub> OD/D <sub>2</sub> O (5/1 vol) as the solvent. ....	49
Figure 2.18:	Time series of $^1\text{H}$ NMR spectra during durability test of MeOTASCl at $80 \text{ }^\circ\text{C}$ . TMS( $\text{CH}_2$ ) <sub>3</sub> SO <sub>3</sub> Na as the internal standard; 1 M KOD in CD <sub>3</sub> OD/D <sub>2</sub> O (5/1 vol) as the solvent. ....	50

Figure 2.19: (a) Degradation profiles and (b) plots of $\ln(C_0/C)$ versus time of 9MeOTAS and MeOTAS at 80 °C. 1 M KOD in CD <sub>3</sub> OD/D <sub>2</sub> O (5/1 vol) as the solvent. ....	51
Figure 2.20: Time series of <sup>1</sup> H NMR spectra during durability test of the benchmark cation BTMA at 80 °C. TMS(CH <sub>2</sub> ) <sub>3</sub> SO <sub>3</sub> Na as the internal standard; 1 M KOD in CD <sub>3</sub> OD/D <sub>2</sub> O (5/1 vol) as the solvent. ....	52
Figure 2.21: (a) Degradation profile and (b) plot of $\ln(C_0/C)$ versus time of BTMA at 80 °C. 1 M KOD in CD <sub>3</sub> OD/D <sub>2</sub> O (5/1 vol) as the solvent. ....	53
Figure 3.1: 3D chemical structures of (a) triphenylsulfonium and (b) benzyltriphenylphosphonium. ....	56
Figure 3.2: Chemical structures of 9MeOTAS and TPQP. ....	56
Figure 3.3: Chemical structures of (a) BTPP-(2,4,6-MeO) and (b) BTMA. ....	57
Figure 3.4: Chemical structures of three QP analogs: (a) BTPP, (b) BTPP-( <i>p</i> -Me) and (c) BTPP-( <i>p</i> -MeO). ....	57
Figure 3.5: Time series of <sup>1</sup> H NMR spectra during durability test of the BTPP-(2,4,6-MeO) at 80 °C. TMS(CH <sub>2</sub> ) <sub>3</sub> SO <sub>3</sub> Na as the internal standard; 1 M KOD in CD <sub>3</sub> OD/D <sub>2</sub> O (5/1 vol) as the solvent. ....	63
Figure 3.6: Time series of <sup>31</sup> P NMR spectra during durability test of the BTPP-(2,4,6-MeO) at 80 °C. Phosphoric acid as the external standard; 1 M KOD in CD <sub>3</sub> OD/D <sub>2</sub> O (5/1 vol) as the solvent. ....	64
Figure 3.7: (a) Degradation profiles and (b) plots of $\ln(C_0/C)$ versus time of BTPP-(2,4,6-MeO) and BTMA at 80 °C. 1 M KOD in CD <sub>3</sub> OD/D <sub>2</sub> O (5/1 vol) as the solvent. ....	64
Figure 3.8: Time series of <sup>31</sup> P NMR spectra during durability test of (a) BTPP, (b) BTPP-( <i>p</i> -Me) and BTPP-( <i>p</i> -MeO) at 20 °C. Phosphoric acid as the external standard; 1 M KOD in CD <sub>3</sub> OD/D <sub>2</sub> O (5/1 vol) as the solvent. ....	66
Figure 3.9: Degradation profiles of QP analogs at 20 °C. 1 M KOD in CD <sub>3</sub> OD/D <sub>2</sub> O (5/1 vol) as the solvent. ....	67
Figure 3.10: (a) Plots of $\ln(C_0/C)$ of BTPP-( <i>p</i> -Me) versus time at three different temperatures (20 °C, 30 °C and 40 °C); (b) Arrhenius plot ( $-\ln(k)$ vs $1/T$ ) of BTPP-( <i>p</i> -Me). ....	67

Figure 3.11: (a) Plots of $\ln(C_0/C)$ of BTPP-( <i>p</i> -MeO) versus time at three different temperatures (20 °C, 40 °C and 50 °C); (b) Arrhenius plot ( $-\ln(k)$ vs $1/T$ ) of BTPP-( <i>p</i> -MeO).....	68
Figure 3.12: Degradation products of QP analogs if $S_N2$ benzylic substitution takes place.....	69
Figure 3.13: $^{31}\text{P}$ NMR spectra of BTPP before and after degradation at 20 °C. Phosphoric acid as the external standard; 1 M KOD in $\text{CD}_3\text{OD}/\text{D}_2\text{O}$ (5/1 vol) as the solvent. ....	70
Figure 3.14: Degradation mechanism of QP analogs in alkaline media.....	71
Figure 3.15: Evidence that the BTPP-(2,4,6-MeO) degrades by a different mechanism than QP analogs. (a) $^{31}\text{P}$ NMR Spectra of BTPP-(2,4,6-MeO) after 32 days' test, with phosphine oxide (TTMPPO) added; (b) $^{31}\text{P}$ NMR of BTPP-(2,4,6-MeO) after 32 days' test, showing no trace of TTMPPO at 16.8 ppm; (c) $^1\text{H}$ NMR spectrum showing no trace of toluene from 7.09 to 7.23 ppm. The box indicate where the toluene would be found, if present. ....	72
Figure 3.16: Proposed degradation mechanism of BTPP-(2,4,6-MeO) in alkaline media. ....	73
Figure 3.17: Evidence of ether hydrolysis during degradation. Another degradation test was performed in ethanol instead of methanol, resulting in the $^1\text{H}$ NMR spectra shown above. The methanol production peak is boxed. Solvent: 1 M KOD in $\text{CD}_3\text{CD}_2\text{OD}/\text{D}_2\text{O}$ (5/1 vol).....	75
Figure 3.18: Evidence of inner salt formation during degradation. (a) $^{31}\text{P}$ NMR spectrum of degradation products, showing BTPP-(2,4,6-MeO) (peak A) and the inner salt degradation product (peak B); (b) Same spectrum after addition of HCl. The acid protonates the inner salt, eliminating peak B and generating peak C. ....	76
Figure 3.19: Evidence of ketone formation during degradation. This ATR-FTIR spectrum shows a characteristic ketone peak only after degradation.....	77
Figure 3.20: $^{31}\text{P}$ NMR assignment of BTPP-(2,4,6-MeO) after degradation at 80 °C. Phosphoric acid as the external standard. 1 M KOD in $\text{CD}_3\text{OD}/\text{D}_2\text{O}$ (5/1 vol) as the solvent. ....	78
Figure 4.1: Chemical structures of (a) MTPP-(2,4,6-Me), (b) BTPP-(2,4,6-Me) and (c) MTPP-(2,4,6-MeO).....	86



Figure 4.2:	Chemical equation for quaternization of DMF with benzyl chloride. ....	88
Figure 4.3:	$^1\text{H}$ NMR spectrum ( $\text{DMSO-d}_6$ ) of DMF after quaternization with benzyl chloride. ....	88
Figure 4.4:	Time series of $^1\text{H}$ NMR spectra during durability test of the MTPP-(2,4,6-Me) at 80 °C. $\text{TMS}(\text{CH}_2)_3\text{SO}_3\text{Na}$ as the internal standard; 1 M KOD in $\text{CD}_3\text{OD}/\text{D}_2\text{O}$ (5/1 vol) as the solvent.....	90
Figure 4.5:	Time series of $^{31}\text{P}$ NMR spectra during durability test of the MTPP-(2,4,6-Me) at 80 °C. Phosphoric acid as the external standard; 1 M KOD in $\text{CD}_3\text{OD}/\text{D}_2\text{O}$ (5/1 vol) as the solvent.....	91
Figure 4.6:	Time series of $^1\text{H}$ NMR spectra during durability test of the MTPP-(2,4,6-MeO) at 80 °C. $\text{TMS}(\text{CH}_2)_3\text{SO}_3\text{Na}$ as the internal standard; 1 M KOD in $\text{CD}_3\text{OD}/\text{D}_2\text{O}$ (5/1 vol) as the solvent.....	92
Figure 4.7:	Time series of $^{31}\text{P}$ NMR spectra during durability test of the MTPP-(2,4,6-MeO) at 80 °C. Phosphoric acid as the external standard; 1 M KOD in $\text{CD}_3\text{OD}/\text{D}_2\text{O}$ (5/1 vol) as the solvent.....	93
Figure 4.8:	(a) Degradation profiles and (b) plots of $\ln(C_0/C)$ versus time of MTPP-(2,4,6-Me), MTPP-(2,4,6-MeO), BTPP-(2,4,6-MeO) and BTMA at 80 °C. 1 M KOD in $\text{CD}_3\text{OD}/\text{D}_2\text{O}$ (5/1 vol) as the solvent. ....	95
Figure 4.9:	Comparison of alkaline stability of MTPP-(2,4,6-Me) and other reported cations. Test conditions: 1 M KOD or NaOD in $\text{D}_2\text{O}$ , 20% degradation threshold on $^1\text{H}$ NMR basis (unless otherwise noted). Ammonium: trimethyl-benzylammonium [80 °C in 1 M NaOD/( $\text{D}_2\text{O}+\text{CD}_3\text{OD}$ ) <sup>[212]</sup> and 100 °C in 1 M NaOD/ $\text{D}_2\text{O}$ ]. Imidazolium: 1-methyl-benzylimidazolium <sup>[177]</sup> , 2-phenyl benzimidazolium (0.3 M KOH) <sup>[72]</sup> , 1,3-dimethyl-2-(2,4,6-trimethylphenyl)-benzimidazolium (1.3 M KOH) <sup>[72]</sup> . Guanidinium: pentamethyl-benzylguanidium. Pyridinium: benzylpyridinium. Phosphonium: tetrakis(dialkylamino)phosphonium [1 M NaOD/( $\text{D}_2\text{O}+\text{CD}_3\text{OD}$ )] <sup>[212]</sup> . Sulfonium: methoxy-triphenylsulfonium <sup>[261]</sup> . Ruthenium: bis(terpyridine)ruthenium (UV-vis spectroscopy) <sup>[216]</sup> . ....	96
Figure 4.10:	Plot of $-\ln(k_{OF})$ versus $\delta$ for QP cations shown in Table 4.3. (a) MTPP-(2,4,6-Me), (b) MTPP-(2,4,6-MeO), (d) MTPP-(2,6-MeO), (e) BTPP-(2,6-MeO), (f) MTPP-( <i>o</i> -MeO), (g) BTPP-( <i>o</i> -MeO), (h) MTPP-( <i>o</i> -Me), (i) MTPP-( <i>p</i> -MeO), (j) BTPP-( <i>p</i> -MeO) and (k) BTPP-( <i>p</i> -Me).....	103

Figure 4.11: Comparison of cation pairs with different phosphine precursors (cation (i)/cation (j), cation (f)/cation (g) and cation (d)/cation (e)). (a) MTPP-(2,4,6-Me), (b) MTPP-(2,4,6-MeO), (d) MTPP-(2,6-MeO), (e) BTPP-(2,6-MeO), (f) MTPP-( <i>o</i> -MeO), (g) BTPP-( <i>o</i> -MeO), (h) MTPP-( <i>o</i> -Me), (i) MTPP-( <i>p</i> -MeO), (j) BTPP-( <i>p</i> -MeO) and (k) BTPP-( <i>p</i> -Me).....	105
Figure 5.1: Synthesis of MTPP-(2,4,6-Me) functionalized polymer (Route 1).....	108
Figure 5.2: Synthesis of MTPP-(2,4,6-Me) functionalized polymer (Route 2).....	109
Figure 5.3: Synthesis of MTPP-(2,4,6-Me) functionalized polymer (Route 3).....	110
Figure 5.4: <sup>1</sup> H NMR spectrum (CDCl <sub>3</sub> ) of MTPP-(2,4,6-Me) after the bromination. ....	111
Figure 5.5: <sup>31</sup> P NMR spectrum (CDCl <sub>3</sub> ) of MTPP-(2,4,6-Me) after the bromination. ....	112
Figure 5.6: <sup>1</sup> H NMR spectrum (CDCl <sub>3</sub> ) of acylated PPO, L = 2. L is the number of carbons of the acylating agent.....	113
Figure 5.7: <sup>1</sup> H NMR spectrum (CDCl <sub>3</sub> ) of acylated PPO, L = 4. L is the number of carbons of the acylating agent.....	113
Figure 5.8: <sup>1</sup> H NMR spectra (CDCl <sub>3</sub> ) of poly(4-bromostyrene) and 4-vinylphenyl-bis(2,4,6-trimethyphenyl) phosphine functionalized polystyrene.....	116
Figure 5.9: <sup>31</sup> P NMR spectra (CDCl <sub>3</sub> ) of 4-vinylphenyl-bis(2,4,6-trimethyphenyl) phosphine functionalized polystyrene and methyl 4-vinylphenyl-bis(2,4,6-trimethyphenyl)phosphonium functionalized polystyrene.....	117
Figure 5.10: Synthesis route of 4-bromo-3,5-dimethylstyrene.....	124
Figure 5.11: Synthesis route of MTPP-(2,4,6-Me) analog functionalized polymer (verification of Route 3). ....	124
Figure 5.12: Chemical structures of MTPP-(2,4,6-Me) and MTPP-(2,4,6-Me) analog. ....	125
Figure 5.13: Time series of <sup>31</sup> P NMR spectra during durability test of MTPP-(2,4,6-Me) analog at 60 °C. Phosphoric acid as the external standard; 1M KOD in CD <sub>3</sub> OD/D <sub>2</sub> O (5/1 vol) as the solvent. ....	126

Figure 6.1:	A strategy to mitigate the cation-triggered polymer backbone degradation. ....	133
Figure 6.2:	Synthesis route of MTPP-(2,4,6-Me) functionalized polymer with elongated linkage.....	133
Figure 6.3:	A strategy to improve the hydroxide conductivities of MTPP-(2,4,6-Me)-based HEMs. ....	134
Figure 6.4:	A strategy to further improve the alkaline stability of the QP cation. (a) MTPP-(2,4,6-Me) and (b) MTPP-(2,4,6- <i>t</i> -Bu). ....	136
Figure 6.5:	Chemical structure of a possibly superior QP cation, methyl (2,4,6-trimethylphenyl)-bis(2,4,6-tri- <i>t</i> -butylphenyl)phosphonium. ....	136
Figure 6.6:	Proposed synthesis route of the new phosphine precursor.....	136
Figure C.1:	<sup>1</sup> H NMR evidence for the toluene production in the alkaline degradation of BTPP. ....	161
Figure C.2:	<sup>1</sup> H NMR evidence for the toluene production in the alkaline degradation of BTPP-( <i>p</i> -Me).....	162
Figure C.3:	<sup>1</sup> H NMR evidence for the toluene production in the alkaline degradation of BTPP-( <i>p</i> -MeO).....	162
Figure C.4:	Time series of <sup>31</sup> P NMR spectra during durability test of MTPP-(2,6-MeO) at 80 °C. Phosphoric acid as the external standard; 1 M KOD in CD <sub>3</sub> OD/D <sub>2</sub> O (5/1 vol) as the solvent. The degradation percentage is calculated by A <sub>2</sub> /(A <sub>1</sub> + A <sub>2</sub> + A <sub>3</sub> ). A <sub>1</sub> is the peak area of the phosphine oxide; A <sub>2</sub> is the peak area of MTPP-(2,6-MeO); A <sub>3</sub> is the peak area of ether hydrolysis products. ....	163
Figure C.5:	The plot of ln(C <sub>0</sub> /C) versus time of MTPP-(2,6-MeO) at 80 °C. 1 M KOD in CD <sub>3</sub> OD/D <sub>2</sub> O (5/1 vol) as the solvent.....	163
Figure C.6:	Time series of <sup>31</sup> P NMR spectra during durability test of BTPP-(2,6-MeO) at 80 °C. Phosphoric acid as the external standard; 1 M KOD in CD <sub>3</sub> OD/D <sub>2</sub> O (5/1 vol) as the solvent. The degradation percentage is calculated by A <sub>2</sub> /(A <sub>1</sub> + A <sub>2</sub> + A <sub>3</sub> ). A <sub>1</sub> is the peak area of the phosphine oxide; A <sub>2</sub> is the peak area of BTPP-(2,6-MeO); A <sub>3</sub> is the peak area of ether hydrolysis products. ....	164

Figure C.7: The plot of $\ln(C_0/C)$ versus time of BTPP-(2,6-MeO) at 80 °C. 1 M KOD in CD <sub>3</sub> OD/D <sub>2</sub> O (5/1 vol) as the solvent.....	164
Figure C.8: Time series of <sup>31</sup> P NMR spectra during durability test of MTPP-( <i>o</i> -MeO) at 80 °C. Phosphoric acid as the external standard; 1 M KOD in CD <sub>3</sub> OD/D <sub>2</sub> O (5/1 vol) as the solvent. The degradation percentage is calculated by $A_2/(A_1 + A_2)$ . A <sub>1</sub> is the peak area of the phosphine oxide; A <sub>2</sub> is the peak area of MTPP-( <i>o</i> -MeO).....	165
Figure C.9: The plot of $\ln(C_0/C)$ versus time of MTPP-( <i>o</i> -MeO) at 80 °C. 1 M KOD in CD <sub>3</sub> OD/D <sub>2</sub> O (5/1 vol) as the solvent.....	165
Figure C.10: Time series of <sup>31</sup> P NMR spectra during durability test of BTPP-( <i>o</i> -MeO) at 80 °C. Phosphoric acid as the external standard; 1 M KOD in CD <sub>3</sub> OD/D <sub>2</sub> O (5/1 vol) as the solvent. The degradation percentage is calculated by $A_2/(A_1 + A_2)$ . A <sub>1</sub> is the peak area of the phosphine oxide; A <sub>2</sub> is the peak area of BTPP-( <i>o</i> -MeO).....	166
Figure C.11: The plots of $\ln(C_0/C)$ versus time of BTPP-( <i>o</i> -MeO) at 80 °C. 1 M KOD in CD <sub>3</sub> OD/D <sub>2</sub> O (5/1 vol) as the solvent.....	166
Figure C.12: Time series of <sup>31</sup> P NMR spectra during durability test of MTPP-( <i>o</i> -Me) at 80 °C. Phosphoric acid as the external standard; 1 M KOD in CD <sub>3</sub> OD/D <sub>2</sub> O (5/1 vol) as the solvent. The degradation percentage is calculated by $A_2/(A_1 + A_2)$ . A <sub>1</sub> is the peak area of the phosphine oxide; A <sub>2</sub> is the peak area of MTPP-( <i>o</i> -Me).....	167
Figure C.13: The plot of $\ln(C_0/C)$ versus time of MTPP-( <i>o</i> -Me) at 80 °C. 1 M KOD in CD <sub>3</sub> OD/D <sub>2</sub> O (5/1 vol) as the solvent. ....	167
Figure C.14: Time series of <sup>31</sup> P NMR spectra during durability test of MTPP-( <i>p</i> -MeO) at 80 °C. Phosphoric acid as the external standard; 1 M KOD in CD <sub>3</sub> OD/D <sub>2</sub> O (5/1 vol) as the solvent. The degradation percentage is calculated by $A_2/(A_1 + A_2)$ . A <sub>1</sub> is the peak area of MTPP-( <i>p</i> -MeO) oxide; A <sub>2</sub> is the peak area of MTPP-( <i>p</i> -MeO).....	168
Figure C.15: Plots of $\ln(C_0/C)$ versus time of MTPP-( <i>p</i> -MeO) at 80 °C. 1 M KOD in CD <sub>3</sub> OD/D <sub>2</sub> O (5/1 vol) as the solvent. ....	168

## ABSTRACT

Hydroxide exchange membranes (HEMs) are important polymer electrolytes for electrochemical energy conversion devices. One major concern with the practical application of HEMs is their poor alkaline stabilities which stems from the hydroxide attack on the cationic group. Accordingly, the nature of the cationic group is the top priority in terms of alkaline stability. The most used cation system, which is quaternary ammonium (QA) based, has insufficient alkaline stability for practical applications. In this study, the tertiary sulfoniums (TS) and the quaternary phosphonium (QP) were selected as two candidates to overcome the intrinsic limitation of the QA.

The triaryl-substituted TS (TAS), for the first time, was introduced as the cationic group for HEMs. The methoxy-substituted TAS based HEM exhibits reasonable alkaline stability and hydroxide conductivity. The alkaline stabilities of a series of TAS model compounds showed that more electron density on the central sulfur atom results in enhanced TAS alkaline stability. However, due to the susceptibility of the central sulfur atom to hydroxide attack, the most stable TAS cation in this study is still inferior to the benchmark cation, benzyltrimethylammonium (BTMA).

Through degradation kinetics study, Benzyl (tris(2,4,6-trimethoxyphenyl)phosphonium (BTPP-(2,4,6-MeO)) was determined to have higher alkaline stability than the benchmark, BTMA. A new multi-step degradation mechanism related to the degradation of the methoxy groups for BTPP-(2,4,6-MeO)

was proposed and verified. It suggested that the elimination of the substituent degradation can further enhance the QP's alkaline stability.

By replacing methoxy substituents with methyl groups, a superior QP cation, methyl tris(2,4,6-trimethylphenyl)phosphonium (MTPP-(2,4,6-Me)) was developed. MTPP-(2,4,6-Me) demonstrated a level of stability that has not been achieved by any other known HEM cations. The alkaline degradation kinetics and mechanisms of a wide range of QPs determined that the electronic effect and steric effect combined determine the alkaline stabilities of QP cations.

To take advantage of the outstanding alkaline stability of MTPP-(2,4,6-Me), a feasible synthesis route was developed to synthesize MTPP-(2,4,6-Me) functionalized polymers for constructing HEMs.

## **Chapter 1**

### **INTRODUCTION**

The increasing global energy demand and the environmental impact of energy use from conventional sources (e.g. fossil fuels) impose serious challenges to human health, energy security, environmental protection and the sustainability of natural resources.<sup>[1]</sup> To solve these problems, people for a long time have been looking for clean, efficient and sustainable power sources. For the past five decades, fuel cells have been recognized as one of the most promising candidates for the next generation power sources.<sup>[2]</sup>

#### **1.1 Fuel cells**

##### **1.1.1 Background**

A fuel cell is an energy conversion device that converts the chemical energy from a fuel directly to electrical energy through a chemical reaction with oxygen. A fuel cell consists of two catalyst-coated electrodes (anode and cathode) and an electrolyte. The anode is where fuel oxidation reaction takes place while the cathode is where oxygen reduction reaction takes place. Catalysts are needed on the two electrodes to accelerate these two reactions. The electrolyte, which could be either a liquid or a solid, permits only the appropriate ions (not electrons) to pass from one electrode to the other. The electrons generated at the anode go through an external circuit to the cathode to produce direct current electricity.

The concept of a fuel cell was firstly brought up by a number of scientists including Cristian Friedrich Schönbein, Humphry Davy and William Grove in the early nineteenth century. The first commercial fuel cells were used in NASA space programs to generate power for space missions in the late 1950s and early 1960s.<sup>[3]</sup> Since the 1960s, fuel cells have been used to power a large number of electronic and mechanical systems, from portable power and vehicle propulsion to stationary power generation.

Compared to conventional power sources, such as internal combustion engines or batteries, fuel cells have various advantages including: (1) the fuel in fuel cells is not combusted, and the energy instead being generated electrocatalytically, which allows fuel cells to be highly energy efficient; (2) fuel cells, in which hydrogen is used as the fuel, can eliminate pollution caused by burning fossil fuels; (3) most fuel cells operate more silently than internal combustion engines; (4) the maintenance of fuel cells is simple because there are few moving parts in the system; and (5) fuel cell operating time is much longer than that of batteries, because they could work continuously as long as the fuel and oxygen are fed.

Fuel cells are generally classified according to the type of electrolyte they use. Nowadays, there are six major types of fuel cells: proton-exchange membrane fuel cells (PEMFCs), hydroxide exchange membrane fuel cells (HEMFCs), alkaline fuel cells (AFCs), phosphoric acid fuel cells (PAFCs), solid oxide fuel cells (SOFCs) and molten carbonate fuel cells (MCFCs). Each fuel cell type has its own features, offering advantages in particular applications. PAFCs, SOFCs and MCFCs usually operate at high temperatures (PAFCs: 150~200 °C; SOFCs and MCFCs: >500 °C). Whereas,



PEMFCs, AFCs and HEMFCs operate at relatively lower temperature (<100 °C), and they will be discussed in detail as follows.

### 1.1.2 Proton exchange membrane fuel cells (PEMFCs)

For the past two decades, PEMFCs are the leading technology due to their relatively quick start-up, rapid response to varying loads, and low operating temperatures. A PEMFC uses an acidic proton-conducting polymer membrane, i.e. the proton exchange membrane (PEM), as its electrolyte, with platinum-based electrodes.

In a PEMFC (Fig. 1.1), hydrogen (or another fuel) is fed to the anode side, whereas oxygen (pure oxygen or air) is supplied to the cathode side. At the anode, electrons are stripped from hydrogen to produce protons on the surface of a platinum-based catalyst (hydrogen oxidation reaction, HOR, Eq. 1.1). The protons pass through a PEM to the cathode side whereas the electrons travel through an external circuit, generating electrical output of the cell and leading to the cathode. At the cathode, another precious metal electrode combines the protons and electrons with oxygen to form water, which is the only waste product produced (oxygen reduction reaction, ORR, Eq. 1.2). The overall reaction is combining hydrogen and oxygen to produce water and electricity (Eq. 1.3).



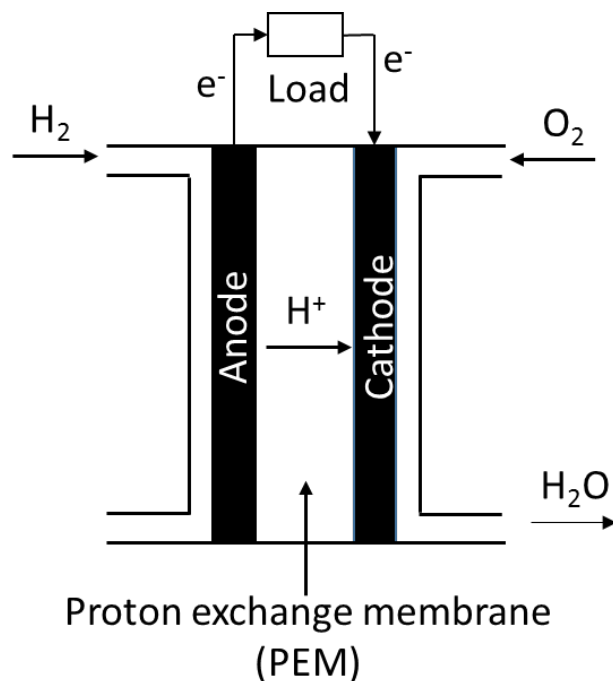


Figure 1.1: Schematic diagram of a PEMFC.

The heart of the PEMFC is a PEM that separates the reactant gases and conducts protons. The primary requirements for a high performance PEM include: (1) excellent proton conductivity; (2) poor electron conductivity; (3) low fuel and oxidant permeability; (4) high chemical and thermal stability; (5) good mechanical strength and dimensional stability; (6) sufficient water transport properties; (7) adequately a long lifetime ( $\sim 5000$  h for transportation applications<sup>[4]</sup>) under real fuel cell operation conditions; and (8) low cost.

The most widely used PEM is Nafion, developed in the late 1960s by Walther Grot of DuPont Inc.<sup>[5]</sup> Nafion is a sulfonated tetrafluoroethylene-based polymer, composed with a hydrophobic perfluorinated polyethylene backbone and a highly hydrophilic sulfonic acid-terminated perfluorovinyl ether pendant (Fig. 1.2). Nafion is

considered as the prototypical membrane for PEMFCs due to its high proton conductivity, excellent chemical stability and longevity in a fuel cell environment.<sup>[6]</sup>

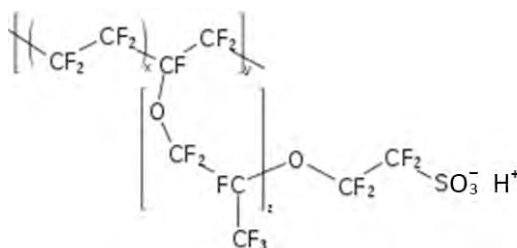


Figure 1.2: Chemical structure of Nafion.

The major drawback of PEMFCs is the high cost and low durability of their precious metal based electrocatalysts, especially platinum (~\$1500/oz., 2014) or platinum group metals (PGMs).<sup>[7]</sup> Although great progress has been made in reducing the catalyst loading and achieving high power density and reasonable energy density, the cost of PEMFCs is still above the reasonable level for commercialization.

### 1.1.3 Alkaline fuel cells (AFCs)

Alkaline catalysis in fuel cells has been demonstrated with non-precious metal catalysts<sup>[8]</sup>, because the kinetics for both fuel oxidation<sup>[9-10]</sup> and oxygen reduction<sup>[11]</sup> are enhanced in alkaline media<sup>[12]</sup> compared to the acidic media. However, AFCs have serious drawbacks associated with their system complexity, electrolyte leakage and carbonate formation, all of which are not existing in PEMFCs. The typical electrolyte used in AFC is concentrated alkaline aqueous solutions (e.g. 6 M KOH solution)<sup>[13-15]</sup>, which could strongly absorb CO<sub>2</sub> from the air,<sup>[13, 16]</sup> so that the charge carrier OH<sup>-</sup> would quickly be converted to HCO<sub>3</sub><sup>-</sup> or CO<sub>3</sub><sup>2-</sup>. Such a carbonate formation process

would (1) reduce the ionic conductivity of the electrolyte because the mobility of  $\text{HCO}_3^-$  or  $\text{CO}_3^{2-}$  is lower than that of  $\text{OH}^-$ ; and (2) block the micro pores of the electrode and break its waterproof property due to the carbonate precipitation, leading to an electrolyte leakage.<sup>[17]</sup>

An effective way to solve the carbonation issue is to replace the liquid alkaline electrolyte with a membrane based alkaline electrolyte<sup>[18-19]</sup> whose basic structure is a positively charged polymer backbone with dissociated hydroxide acting as the charge carrier to conduct ions. With a membrane electrolyte, the negative effects of  $\text{CO}_2$  could be eliminated. The conducting species is now attached to a fixed solid polymer so that there are no mobile cations (i.e.  $\text{K}^+$  in KOH electrolyte). Although there will be some carbonates, the precipitates of metal carbonate will not form to block the porous electrodes. Furthermore, no liquid alkaline solution is present; hence electrolyte leakage and electrode corrosion will be eliminated.

#### **1.1.4 Hydroxide exchange membrane fuel cells (HEMFCs)**

By combining the advantages of both PEMFCs and AFCs, HEMFCs (Fig. 1.3) based on the solid hydroxide exchange membrane (HEM) electrolyte, have recently received considerable attention. Similar to a PEMFC, in a HEMFC, HOR (Eq. 1.4) takes place on the anode side and ORR (Eq. 1.5) on the cathode side, but in a basic condition. The overall reaction (Eq. 1.6) is the same as that of a PEMFC, which is hydrogen combined with oxygen to generate water.



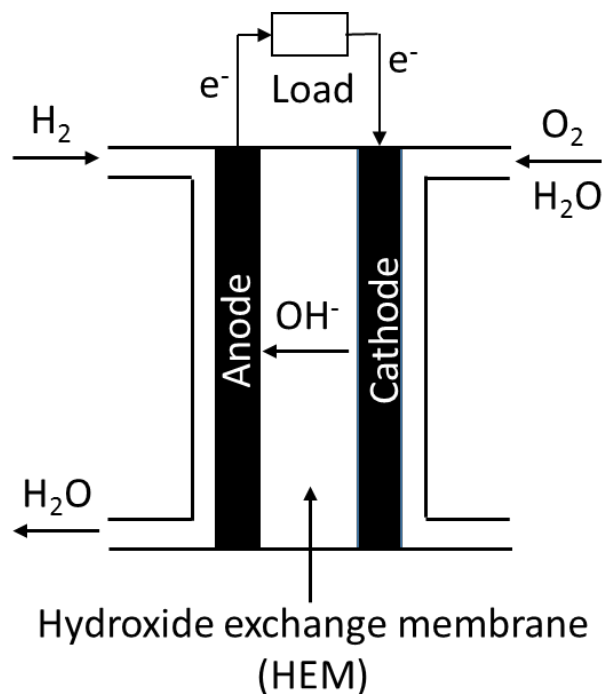


Figure 1.3: Schematic diagram of a HEMFC.

By switching the working ion from proton ( $H^+$ ) to hydroxide ( $OH^-$ ), HEMFCs enable non-precious metals such as silver<sup>[20-21]</sup> and nickel<sup>[21-22]</sup> as electrocatalysts, thus HEMFCs have the potential to solve the catalyst cost and durability problems. For instance, Zhuang<sup>[23]</sup> and Yan<sup>[21]</sup> recently showed HEMFCs that are completely free from PGMs, respectively. Equally important, HEMFCs are not substantially limited by  $CO_2$  contamination that is the major barrier for AFCs. Additionally, HEMFCs can offer fuel flexibility (e.g. methanol, ethanol, ethylene glycol, etc.) because of their low over-potential for hydrocarbon fuel oxidation and reduced fuel crossover.<sup>[24]</sup> Recently, hydrogen, methanol and ethanol have been used as the anode fuels in HEMFCs and promising results have been achieved.<sup>[18, 25-33]</sup> All these advantages make HEMFCs very promising in solving fuel cell commercialization problems.

## 1.2 Hydroxide exchange membranes (HEMs)

### 1.2.1 Background

The most critical technology barrier for HEMFCs is the lack of a high-performance HEM. HEMs are polymer electrolytes that conduct  $\text{OH}^-$  as they possess positively charged cationic groups attached covalently to a polymer backbone. These cationic groups can be linked to the backbone *via* extended side chains, directly onto the backbone, or they can be an integral part of the backbone.

The primary requirements for HEMs are the following: (1) excellent alkaline stability and thermal stability; (2) high hydroxide conductivity and low electronic conductivity; (3) good mechanical and dimensional stability during manufacturing and operation; and (4) low cost.<sup>[3]</sup>

Among all of these requirements, the two major challenges for HEMs are their low alkaline stabilities<sup>[34-38]</sup> and low hydroxide conductivities (compared to the  $\text{H}^+$  conductivities of PEMs)<sup>[39-41]</sup>. The lower conductivities of HEMs vs PEMs stem from two aspects: (1) the lower mobility of  $\text{OH}^-$  vs  $\text{H}^+$  (Table 1.1)<sup>[42]</sup>; and (2) the lower levels of dissociation of the cationic groups compared to the highly acidic sulfonic groups in PEMs. The reason for HEM's low alkaline stability is that the hydroxide is a very strong nucleophile while the positively charged cationic groups are susceptible to nucleophilic attacks. Thus, the hydroxide has a strong tendency to attack the cationic group to form neutral species and thus cause the loss of charge carriers. These two major issues will be discussed in detail as follows.

Table 1.1: Selected ion mobilities at infinite dilution in H<sub>2</sub>O at 25 °C.<sup>[42]</sup>

Ion	Mobility (10 <sup>-8</sup> m <sup>2</sup> s <sup>-1</sup> V <sup>-1</sup> )	Relative mobility (relative to K <sup>+</sup> )
H <sup>+</sup>	36.23	4.75
OH <sup>-</sup>	20.64	2.71
CO <sub>3</sub> <sup>2-</sup>	7.46	0.98
HCO <sub>3</sub> <sup>-</sup>	4.61	0.60
Na <sup>+</sup>	5.19	0.68
Cl <sup>-</sup>	7.91	1.04
K <sup>+</sup>	7.62	1.00

### 1.2.2 Hydroxide conductivity issue

In terms of the low conductivities, based on the mathematical relationship that ionic conductivity  $\propto$  ion mobility  $\times$  ion concentration, with fixed ion mobility, the increase of ion concentration would improve ionic conductivity. Accordingly, one strategy to address this issue is to offset the intrinsically lower mobility by using HEMs with higher ion-exchange capacities (IECs, i.e. the number of cationic groups per unit mass of polymer) compared to PEMs to increase the hydroxide concentration. However, overly high IECs could cause excessive water uptake and dimensional swelling, resulting in HEMs with lower mechanical strengths. Therefore, covalent crosslinking of polymer chains is usually applied to suppress excessive water uptake and membrane swelling. However, it may also lead to less desirable properties such as reduced flexibility and embrittlement, and even a loss of conductivity.<sup>[43-50]</sup>

Another strategy to improve the conductivities of HEMs without introducing excessively high IECs is to enhance the effective mobility of OH<sup>-</sup>. In HEMs, the real motion of OH<sup>-</sup> could be retarded by the resistances from hydrophobic polymer chains, so that the effective mobility of OH<sup>-</sup> is much lower than that in dilute solutions. This is a common drawback of polymer electrolytes including Nafion (where the effective mobility of H<sup>+</sup> is only about 20% of that in dilute solution).<sup>[2]</sup> Therefore, the

development of phase-segregated HEMs containing hydrophobic phases interconnected with hydrophilic ionic clusters and channels is an efficient way to enhance the effective mobility of  $\text{OH}^-$ . There are two major approaches to achieve better phase-segregated HEMs: (1) introduce a longer linkage between the cationic groups and the polymer backbone;<sup>[23]</sup> and (2) more importantly, fabricate the HEMs based on the strong phase-segregated block or grafted copolymers.<sup>[51-54]</sup> Based on these efforts, the conductivities of HEMs have been greatly improved but there still exist some problems, such as complex synthesis and insufficient mechanical strength.

However, in real fuel cell operations, the performance is determined by the overall conductance of the HEM, not the intrinsic conductivity of the cationic group. The overall conductance of the HEM is determined by both intrinsic conductivity and membrane thickness. Therefore, besides improving the intrinsic conductivity, reducing membrane thickness could also effectively raise the overall conductance. In contrast to PEMs, the ion transport within HEMs is from the cathode to anode and the resulting electroosmotic drag suppresses fuel crossover from anode to cathode. Meanwhile, water in HEMs is produced at the anode and partially consumed at the cathode, thus water management is potentially simplified and problems related to the cathode flooding could also be solved.<sup>[24]</sup> Therefore, thick HEMs are not needed to block such mass transport. HEMs could be manufactured much thinner than PEMs to gain better overall conductance. In other words, with the improved material and cell design, the conductivity issue is not insurmountable.<sup>[2]</sup>



### 1.2.3 Alkaline stability issue

A primary concern with the use of HEMs in electrochemical devices is their stabilities in strongly alkaline environments. The alkaline stability of a HEM is dependent on two aspects: the polymer backbone stability and the cation stability.

The polymer backbone stability is a lower concern as wide ranges of chemistries are available to develop robust and alkaline stable polymeric frameworks (e.g. polysulfone backbone was shown to be stable even after exposure to 40% NaOH at 70-80 °C for 300 h<sup>[55]</sup>).

The backbones that have been commonly used for HEMs are polyethylene<sup>[56-58]</sup>, polyphenylenes<sup>[59-61]</sup>, perfluorinated types<sup>[62-65]</sup>, poly(epichlorohydrins)<sup>[18, 39, 66-69]</sup>, polybenzimidazole (PBI) types<sup>[70-77]</sup>, unsaturated polypropylene<sup>[78]</sup>, poly(vinylbenzyl chloride)<sup>[79-81]</sup>, polyphosphazenes<sup>[82]</sup>, poly(vinyl alcohol) [PVA]<sup>[32, 66, 83-90]</sup>, and those based on poly(arylene ethers) of various chemistries<sup>[91-95]</sup>, such as polysulfones<sup>[25, 96-102]</sup>, poly(phenylene oxides) [PPO]<sup>[45-46, 103-109]</sup>, poly(ether ketones)<sup>[43, 110-119]</sup>, poly(ether oxadiazoles)<sup>[44, 120-121]</sup>, and poly(ether imides)<sup>[122-123]</sup>. Some polymer backbones have been constructed by novel techniques, including pore-filled types<sup>[124-130]</sup>, radiation-grafted types<sup>[47, 131-139]</sup>, PTFE-reinforced types<sup>[140-145]</sup>, electrospun fiber types<sup>[146-147]</sup>, and those synthesized using plasma techniques<sup>[140, 148-155]</sup>.

However, in terms of cationic groups, because they are positively charged so that the strong nucleophile ( $\text{OH}^-$ ) could easily attack them, leading to the formation of neutral species. As a result, HEMs would lose their conductivities and functionalities in HEMFCs. Under caustic conditions there are a number of pathways that may lead to destruction of the cationic charge, such as the microscopic reverse of the Menshutkin reaction with  $\text{OH}^-$  acting as a nucleophile,  $\beta$ -hydrogen (Hofmann) elimination, or

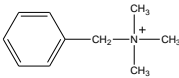
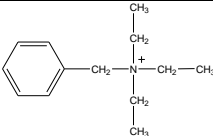
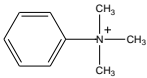
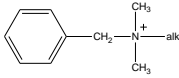
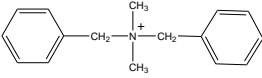
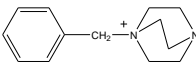
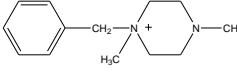
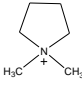
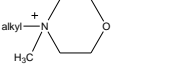
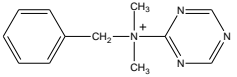
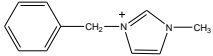
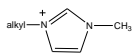
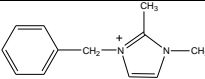
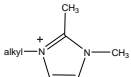
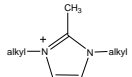
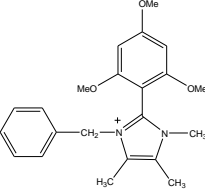
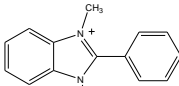
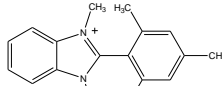
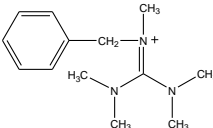
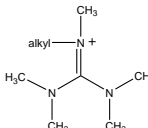
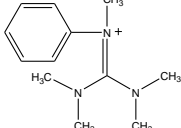
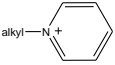
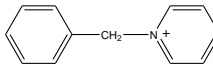
ylide formation as a consequence of  $\alpha$ -hydrogen elimination. Therefore, the nature of the cation is the top priority in terms of stability.

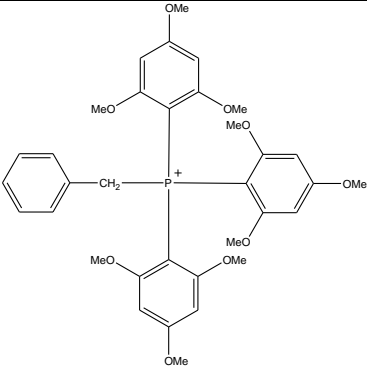
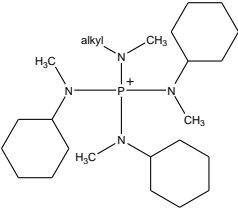
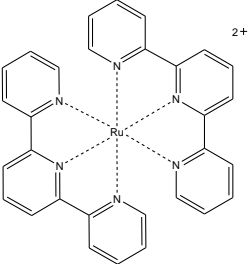
### 1.3 Cations for HEMs

#### 1.3.1 Background

Cations that could be linked to the polymer backbones have the potential to become the cationic groups in HEMs. Table 1.2 summarizes the cations that have been studied for HEMs, include: (a) quaternary ammoniums (QAs) such as benzyltrialkylammoniums<sup>[3, 24, 156-169]</sup>, 1,4-diazabicyclo[2.2.2]octane-based QAs (DABCO-based QAs) and 1-azabicyclo[2.2.2]octane-based QAs (ABCO-based QAs),<sup>[45, 130, 134, 136, 170-174]</sup> and all-alkyl-bound (benzene ring-free) QAs<sup>[56-57]</sup>; (b) heterocyclic systems including imidazoliums<sup>[44, 79, 110, 120-121, 135, 175-189]</sup>, benzimidazoliums<sup>[190]</sup>, pyridiniums<sup>[90, 153-154, 191-196]</sup> and PBI systems where the positive charges are on the backbone<sup>[72, 75, 197]</sup>; (c) guanidiniums<sup>[63, 198-204]</sup>; (d) phosphorus-based (P-based) systems including stabilized phosphoniums [e.g. benzyl tris(2,4,6-trimethoxyphenyl)phosphoniums]<sup>[46, 119, 170, 205-211]</sup> and P–N systems such as tetrakis(dialkylamino)phosphoniums<sup>[212]</sup> and phosphatraniums<sup>[64]</sup>; (e) metal-based systems such as ruthenium-based<sup>[213-216]</sup> and cobalt-based,<sup>[217]</sup> where an attraction is the ability to have multiple positive charges per cationic group. The majority of the HEM based cations are nitrogen-based, with a few of exceptions, such as phosphorus-based and metal-based.

Table 1.2: Chemical structures of reported HEM cations.

Cation	Chemical structure
Ammonium	<div>  <p><b>Trimethyl-benzylammonium (tmbAm)</b></p> </div> <div>  <p><b>Triethyl-benzylammonium (tebAm)</b></p> </div> <div>  <p><b>Trimethyl-phenylammonium (tmpAm)</b></p> </div> <div>  <p><b>Dimethyl-alkyl-benzylammonium (dmabAm)</b></p> </div> <div>  <p><b>Dimethyl-dibenzylammonium (dmdbAm)</b></p> </div> <div>  <p><b>1,4-Diazabicyclo[2.2.2]-octane-benzylammonium (dabcobAm)</b></p> </div> <div>  <p><b>1,4-dimethylpiperazine-benzylammonium (dmpbAm)</b></p> </div> <div>  <p><b>Dimethyl-pyrrolidine-alkyl-ammonium (dmpaAm)</b></p> </div> <div>  <p><b>Methyl-morpholine-alkylammonium (mmaAm)</b></p> </div> <div>  <p><b>Dimethyl-1,3,5-triazine-benzylammonium (dmtbAm)</b></p> </div>
Imidazolium	<div>  <p><b>1-Methyl-benzylimidazolium (mbIm)</b></p> </div> <div>  <p><b>1-Methyl-alkylimidazolium (malIm)</b></p> </div> <div>  <p><b>1,2-Dimethyl-benzylimidazolium (dmbIm)</b></p> </div> <div>  <p><b>1,2-Dimethyl-alkylimidazolium (dmalIm)</b></p> </div> <div>  <p><b>1-Alkyl-2-methyl-alkylimidazolium (amalIm)</b></p> </div> <div>  <p><b>1,4,5-trimethyl-2-(2,4,6-trimethoxyphenyl)-benzylimidazolium (tmmpbIm)</b></p> </div> <div>  <p><b>1,3-Dimethyl-2-phenyl-benzimidazolium (dmpbIm)</b></p> </div> <div>  <p><b>1,3-Dimethyl-2-(2,4,6-trimethylphenyl)-benzimidazolium (dmtpbIm)</b></p> </div>
Guanidinium	<div>  <p><b>Pentamethyl-benzylguanidinium (pmbGu)</b></p> </div> <div>  <p><b>Pentamethyl-alkylguanidinium (pmaGu)</b></p> </div> <div>  <p><b>Pentamethyl-phenylguanidinium (pmpGu)</b></p> </div>
Pyridinium	<div>  <p><b>Alkylpyridinium (aPy)</b></p> </div> <div>  <p><b>Benzylpyridinium (bPy)</b></p> </div>

Phosphonium	  Tris(2,4,6-trimethoxyphenyl)-benzylphosphonium ( <i>tmopbPh</i> ) Tetrakis(dialkylamino)phosphonium ( <i>tkdaaPh</i> )
Ruthenium	 Bis(terpyridine)ruthenium ( <i>btpRu</i> )

### 1.3.2 Nitrogen-based cation systems

At present, the most commonly used HEMs are based on QA functionalized polymers due to their simple structure, easy synthesis and good hydroxide conductivities. Some of these HEMs have already been commercialized, such as FAA and Tokuyama series.<sup>[218]</sup> However, the overall performance of QA based HEMFCs has often been limited by their insufficient alkaline and thermal stabilities. The long-term stability of the QA cations under fuel cell operating conditions remains a concern. For example, Fig. 1.4 shows the durability of a QA-based HEM in a HEMFC. The specific-area resistance increases over the test and the cell voltage drops by 50% after only 12 h.<sup>[219]</sup>

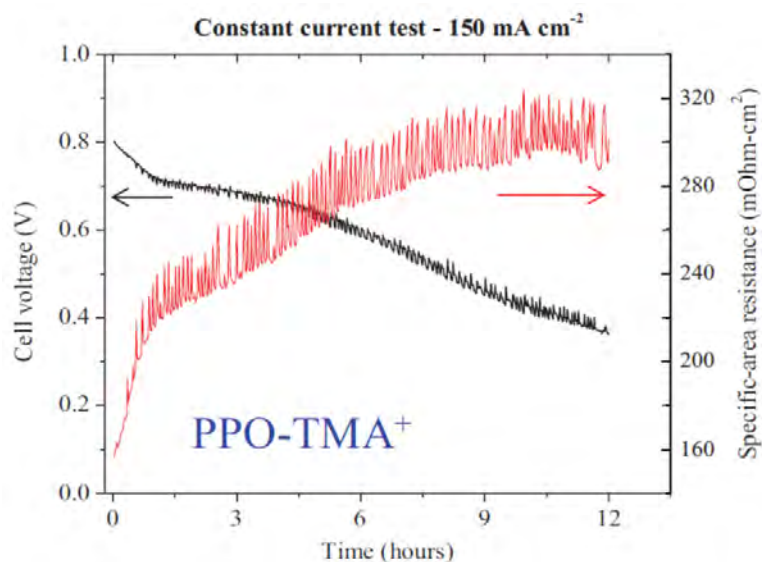


Figure 1.4: The change in cell voltage and specific-area resistance during constant current hold test ( $150 \text{ mA cm}^{-2}$ ) at  $70^\circ\text{C}$  over 12 h for a membrane-electrode-assembly (MEA) prepared from PPO with benzyl trimethyl ammonium ( $\text{PPO-TMA}^+$ ).<sup>[219]</sup> Reproduced by permission of the authors. This article is licensed under [Creativecommons.org/licenses/by/4.0/](https://creativecommons.org/licenses/by/4.0/)

In improving the stabilities of QA systems, researchers have made numerous efforts to develop novel stabilized N-based cations. Some stabilized QA cations have been reported, such as DABCO-base and quinuclidinium-based QA systems<sup>[45, 130, 134, 136, 170-174]</sup>, whose rigid cage structures could to some extent block the  $\text{OH}^-$  attack. N-based systems involving multiple N atoms and ‘resonance stabilization’ have been evaluated, including the non-heterocyclic systems (e.g. pentamethylguanidinium and benzyltetramethylguanidinium)<sup>[198-204]</sup> and the heterocyclic imidazoliums with replacement of protons at different ring positions<sup>[34, 44, 79, 110, 120-121, 135, 175-189]</sup>. Although some of these cations gained improved conductivities and other properties, their alkaline stabilities are still limited for HEMFC operations.

### 1.3.3 Degradation pathways for quaternary ammonium (QA) cations

The QAs' poor alkaline stabilities stem from their facile degradation pathways in the presence of  $\text{OH}^-$ . Fig. 1.5, exemplified by benzyltrimethylammonium (BTMA), shows the multiple degradation pathways.<sup>[2]</sup> The main degradation mechanisms for QAs are *via* direct nucleophilic displacement and Hofmann elimination. In terms of direct nucleophilic displacement at  $\alpha$ -C, there are two different types: methyl substitution ( $\text{S}_{\text{N}}2$  #1) and benzylic substitution ( $\text{S}_{\text{N}}2$  #2). In the first mechanism,  $\text{OH}^-$  performs an  $\text{S}_{\text{N}}2$  attack on the methyl groups to form methanol whereas in the second mechanism,  $\text{OH}^-$  performs an  $\text{S}_{\text{N}}2$  attack on the benzyl groups to form trimethylamine. With respects to Hofmann elimination,  $\text{OH}^-$  attacks a beta-hydrogen ( $\beta$ -H) of the QA, leading to the formation of an alkene, an amine and a water molecule. The  $\beta$ -Hs and the N atoms are required to form the anti-periplanar confirmation for facile Hofmann elimination to occur.<sup>[69, 220-221]</sup> Hofmann elimination reaction cannot occur with BTMA as there are no  $\beta$ -Hs present. However, this is not the case with benzyltriethylammonium groups,<sup>[35, 222]</sup> which contain  $\beta$ -Hs. Besides the above two main degradation pathways, the formation of intermediate ylide has been detected *via* deuterium scrambling experiments, which could potentially lead to Stevens and Sommelet–Hauser rearrangements<sup>[36]</sup>; however, such ylide-derived mechanisms rarely end in a degradation event.<sup>[34]</sup>

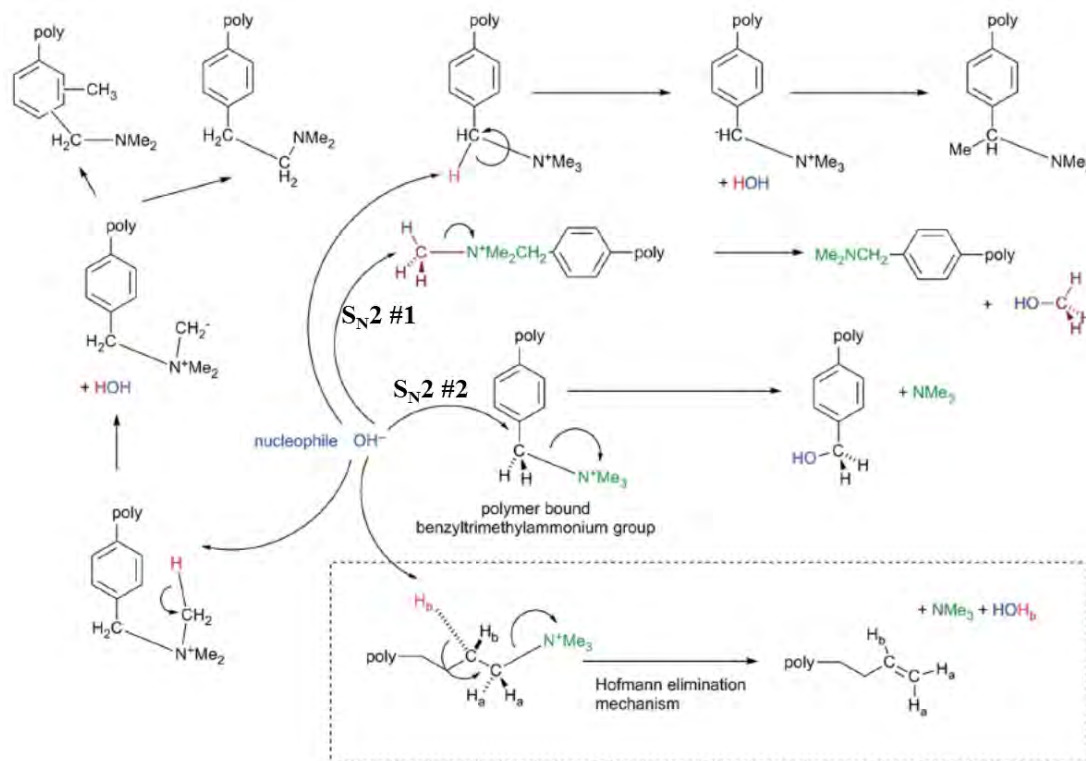


Figure 1.5: Degradation pathways for QA cation (exemplified by BTMA) in the presence of  $\text{OH}^-$  nucleophiles. The inset (dashed box) shows the additional Hofmann Elimination degradation mechanism that can occur with alkyl-bound QA groups (that possess  $\beta$ -H atoms).<sup>[2]</sup> Published by The Royal Society of Chemistry. This article is licensed under a Creative Commons Attribution 3.0 Unported License. The link: [Creativecommons.org/licenses/by/3.0/](https://creativecommons.org/licenses/by/3.0/)

#### 1.3.4 Intrinsic limitation of QA cations

In order to eliminate Hofmann elimination pathway, people designed BTMA cation, a QA cation bears three methyl groups and one benzyl group. The introduction of a benzyl group not only eliminates the presence of  $\beta$ -Hs but also favors the link of the cation to the polymer backbone (most of the cations are linked to the polymer backbone by using polymer-mobilized benzyl halide as the quaternizing agent). Accordingly, BTMA gained decent alkaline stability (e.g. BTMA exhibits negligible

degradation over 30 days in 2 M KOH aqueous solution at 80 °C<sup>[223]</sup>) and became the benchmark cation for HEMs.

Besides the Hofmann elimination, there are still two pathways readily available for BTMA degradations. In an accelerated durability test ( $T = 80\text{ }^{\circ}\text{C}$ ; 1 M KOD;  $\text{CD}_3\text{OD}/\text{D}_2\text{O}$  (5/1 vol)), BMTA degraded 20% in 4 days.<sup>[212]</sup> If we could further eliminate the two  $\alpha\text{-C}$   $\text{S}_{\text{N}}2$  pathways by rational design of cations, the alkaline stabilities of QAs would be further improved. Inspired by BTMA, we propose that by replacing the three methyl groups with three phenyl rings,  $\text{S}_{\text{N}}2$  attack #2 could be eliminated. Furthermore, if we could further replace the benzyl group with another phenyl ring,  $\text{S}_{\text{N}}2$  attack #1 could be eliminated (Fig. 1.6). It may be argued that such tetra-phenyl substituted ammonium structure also has  $\beta\text{-Hs}$  that would cause Hofmann elimination. In fact, without the formation of anti-periplanar conformation for the  $\beta\text{-H}$  and the N atom, Hofmann elimination is unlikely to take place. Unfortunately, the tetra-phenyl substituted ammonium is challenging to prepare and does not exist as a stable species. The cation structure that could block all the degradation pathways in alkaline environment itself is not stable, which is the intrinsic limitation for N-based systems.



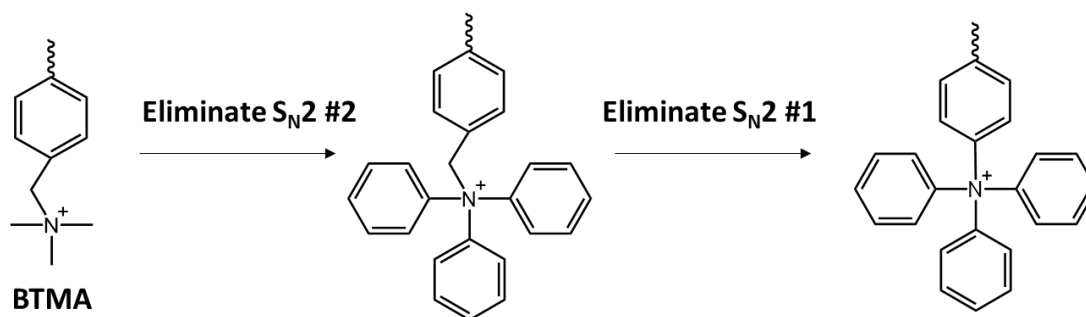


Figure 1.6: Proposed strategies to eliminate the two major degradation pathways of BTMA.

In overcoming the intrinsic limitation of N-based systems, people are looking for other center atoms to replace N. By searching through the periodic table, we expect that phosphorus and sulfur could also form a stable cationic structure similar to nitrogen. More importantly, the triaryl substituted phosphonium and sulfonium are known and much more stable than ammonium analog due to the  $p-\pi$  and  $d-\pi$  bonding between the center atom and the aromatic rings.<sup>[224-227]</sup> By adopting all-phenyl substituted phosphonium or sulfonium, all the three major degradation pathways for QAs in alkaline environment can be eliminated and these two are promising candidates for the cations in HEMs.

### 1.3.5 Phosphorus-based cation systems (phosphoniums)

Regarding phosphorus-based systems, simple alkyl-triaryl-substituted QP analogues (e.g. benzyl triphenylphosphonium) will degrade in aqueous alkaline solutions at ambient temperature in only a few hours. This is due to the formation of phosphine oxide *via* the Cahours-Hofmann reaction.<sup>[228-229]</sup> However, it was expected that strong electron-donation to the center atom and large steric hindrance adjacent to the center atom would enhance QP's alkaline stability. Recently, our group reported a

novel polymer-bound QP system, tris(2,4,6-trimethoxyphenyl) quaternary phosphonium (TPQP), where the additional nine methoxy groups are designed to provide electron donation and additional steric hindrance.<sup>[21, 46, 206, 209-210]</sup> The HEMs based on TPQP hydroxide (TPQPOH) functionalized polysulfone (PSf-TPQPOH, Fig. 1.7) showed not only good solubility in lower alcohol solvents (e.g. methanol, ethanol and n-propanol) and decent hydroxide conductivities ( $45 \text{ mS cm}^{-1}$  at  $20^\circ\text{C}$ ) but also improved alkaline stabilities compared with some QA based HEMs. It can maintain conductivity and flexibility after an immersion treatment in 2 M KOH at  $60^\circ\text{C}$  or 10 M KOH at room temperature for two days; or in 1 M KOH at  $60^\circ\text{C}$  or 5 M KOH at room temperature for one month, while under similar conditions typical commercial QAOH-functionalized FAA membranes become very brittle owing to severe degradation.<sup>[209]</sup> The recent two-dimensional NMR spectroscopic studies showed that PSf-TPQPOH gradually decomposed in 1 M KOH solution at  $60^\circ\text{C}$ ,<sup>[230]</sup> revealing that there is still room for improvement.

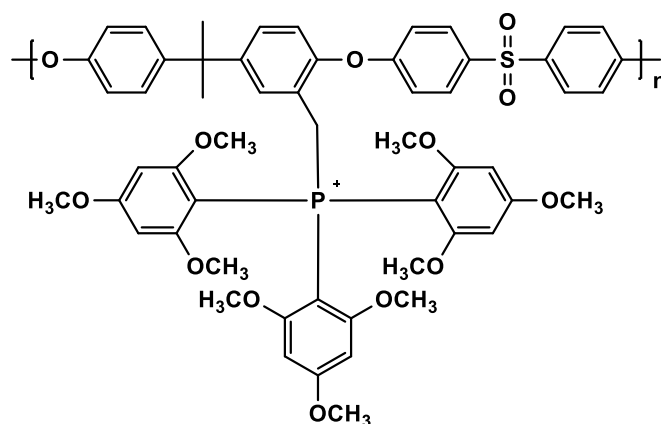


Figure 1.7: Chemical structure of tris(2,4,6-trimethoxyphenyl)phosphonium functionalized polysulfone (PSf-TPQP).

### 1.3.6 Sulfur-based cation systems (sulfoniums)

Similar to quaternary nitrogen or phosphorus, tertiary sulfur (i.e. sulfonium) possesses one unit of positive charge, thus it can be considered as a candidate for the cationic functional group in HEMs. Trialkylsulfonium-based molten salts have already been used as electrolytes in batteries, electrolyzer and other electrochemical devices.<sup>[231-235]</sup> However, trialkylsulfonium and arylalkylsulfonium are reported to have lower chemical and thermal stability than quaternary ammonium,<sup>[3, 163]</sup> limiting their applications in HEMs. Different from P-based systems, the all-aryl substituted sulfoniums (i.e. triarylsulfonium, TAS) are much easier to synthesize. More importantly, TASs have much improved alkaline stabilities<sup>[224]</sup> than trialkylsulfonium, as well as enhanced thermal stability (over 300 °C)<sup>[225-226]</sup>, because of the  $p\pi-d\pi$  bonding between the  $p$  and  $d$  orbitals of the sulfur and the  $\pi$  electrons of the aromatic rings (electronic effect) and the large steric hindrance of the bulky aryl groups (steric effect).<sup>[227]</sup> With such structures, both the Hofmann elimination and  $\alpha$ -C S<sub>N</sub>2 degradation pathways (both #1 and #2) in alkaline environment can be eliminated. Therefore, making TAS might be promising for HEMs.

## 1.4 Research aim and objectives

The research aim of this Ph.D. work is to develop new cation based alkaline stable HEMs for HEMFC applications.

To achieve the above goal, the following objectives were developed: (a) design and synthesize a series of TAS cations and evaluate their alkaline stabilities; (b) construct a feasible synthesis route to obtain TAS functionalized polymers; (c) quantitatively measure the degradation rates of QP cations and find out their degradation mechanisms; (d) design alkaline stable QP cations based on the

mechanism studies and find out the factors that influence the cation stability and (e) design a feasible synthesis route to obtain QP functionalized polymers.

## **1.5 Outline of the dissertation**

In Chapter 2, TAS cations were successfully linked to the polymer backbone *via* a unique synthesis route. For the first time, TAS based HEMs were developed and characterized, confirming that sulfonium cations could work as the cationic groups in HEMs. To understand the factors that influence the alkaline stability, three TAS model compounds with different phenyl substituents were synthesized and their alkaline stabilities were investigated by nuclear magnetic resonance (NMR) spectroscopy. The relationship between the alkaline stability and the substituents was explored.

In Chapter 3, the alkaline stabilities of a typical QP cation, i.e. benzyl tris(2,4,6-trimethoxyphenyl)phosphonium (BTPP-(2,4,6-MeO) and its three QP analogs were quantitatively studied and their degradation rate constants were calculated. The superior alkaline stability of BTPP-(2,4,6-MeO) to that of BTMA was discovered. A multi-step degradation mechanism for BTPP-(2,4,6-MeO) was proposed and verified, which is different from other common QP cations. The chapter ends with explanations for BTPP-(2,4,6-MeO)'s superior stability and a strategy that could further improve the cation stability.

In Chapter 4, inspired by the new degradation mechanism presented in Chapter 3, a new QP cation, methyl tris(2,4,6-trimethylphenyl)phosphonium (MTPP-(2,4,6-Me)) was designed and synthesized and its ultra-high alkaline stability was confirmed. The alkaline stability and degradation mechanism of a wide range of QP cations were studied. The structure-property relationship was explored. This chapter ends with the

conclusion of the determinant factors of cation stabilities under different circumstances.

In Chapter 5, efforts were made to synthesize MTPP-(2,4,6-Me) based polymers. Three synthesis routes were constructed and explored. Based on the unique properties of MTPP-(2,4,6-Me), a unique way of linking the cation to polymer backbones was discovered and verified to be feasible.

## Chapter 2

### TERTIARY SULFONIUM AS A CATIONIC FUNCTIONAL GROUP FOR HEMS

Tertiary sulfonium (TS) was introduced as the cationic functional group for HEMs. The methoxy-substituted triarylsulfonium functionalized HEM (i.e. PSf-MeOTASOH) (Fig. 2.3) exhibited excellent thermal stability (onset decomposition temperature,  $T_{OD} = 242\text{ }^{\circ}\text{C}$ ), decent hydroxide conductivity ( $15.4\text{ mS cm}^{-1}$  at  $20\text{ }^{\circ}\text{C}$ ), and good alkaline stability. This work showed that, similar to nitrogen and phosphorus, sulfonium cations with designed substituents could also be used to construct HEM.

The influence of the phenyl-substituent on TAS cation's alkaline stability was explored. By introducing more or even stronger electron donating groups to the aromatic rings, the alkaline stability of the TAS cation was significantly enhanced.

This Chapter is reprinted with permission from The Royal Society of Chemistry. B. Z. Zhang, S. Gu, J. H. Wang, Y. Liu, A. M. Herring, Y. S. Yan, Tertiary Sulfonium as A Cationic Functional Group for Hydroxide Exchange Membranes. *RSC Advances*, **2012**, 2, 12683-12685.

#### 2.1 Introduction

Similar to nitrogen or phosphorus, sulfur also can bear one unit of positive charge to form TS (Fig. 2.1(a)), and thus has the potential to serve as the cationic functional group in HEMs. In this species, the five electrons of the valence shell of  $\text{S}^+$

are distributed in three bonds and one lone pair of electrons. If all of the three groups on sulfur are aryl groups, it is referred to as the TAS (Fig. 2.1(b)).

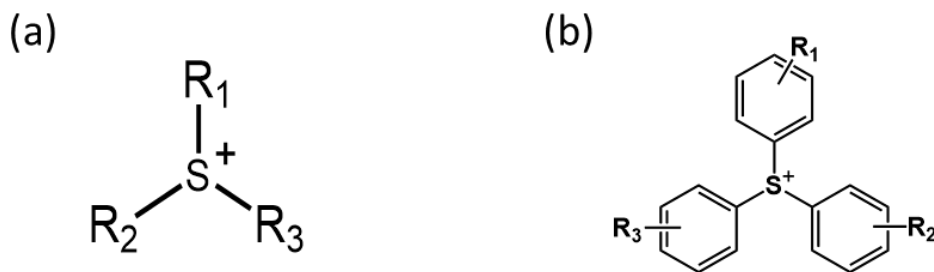
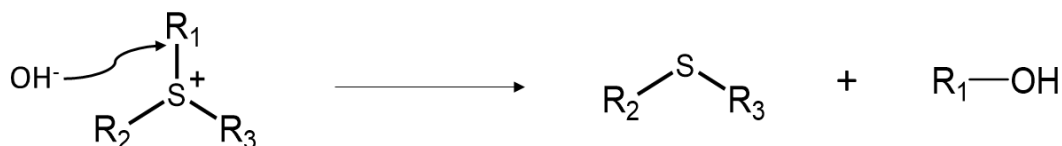


Figure 2.1: Chemical structures of (a) TS cation and (b) the TAS cation. R<sub>1</sub>, R<sub>2</sub> and R<sub>3</sub> are the substituents.

For ordinary TS cations (trialkyl or arylalkyl substituted TS cations), besides the S<sub>N</sub>2 attack at the α-C, which is similar to the QA cations, OH<sup>−</sup> could also attack the S center to form sulfoxide (Fig. 2.2).<sup>[236-238]</sup> Therefore, these TS cations were reported to have lower chemical and thermal stability than QA cations<sup>[3, 163]</sup>, limiting their applications in HEMs. However, if the sulfonium is triaryl-substituted (i.e. TAS), the α-C S<sub>N</sub>2 attack can be eliminated and thus its alkaline stability will be greatly improved.<sup>[224]</sup> TAS cations are also expected to be more resistant to the nucleophilic attack at the central atom. The *d* orbitals of S in the TAS overlap with *π* electrons of the aryl group, thus forming *pπ-dπ* bonding which causes considerable positive charge dispersal throughout the molecule.<sup>[227]</sup> Additionally, the bulky aryl groups on S provides more steric hindrance to the nucleophilic attack. Accordingly, TAS is not readily susceptible to nucleophilic displacement reactions at the central S atom. Introducing electron-donating groups to the aromatic rings further improves the

stability and reduces Lewis acidity of this compound. For example, a methoxy-substituted TAS was observed to have enhanced ion-exchange ability equivalent to ammonium hydroxides.<sup>[239]</sup> TAS also exhibits high thermal stability. For TAS, due to the formation of  $p\pi-d\pi$  bonding, the bond between the central atom and the aryl group becomes stronger and the aryl group can only split off at high temperatures ( $>300\text{ }^{\circ}\text{C}$ )<sup>[227]</sup>, indicating exceptional thermal stability. For example, a phenylthio-substituted TAS has been found to have much higher thermal stability (up to  $408\text{ }^{\circ}\text{C}$ ).<sup>[226]</sup> Therefore, TAS-based polymers are considered attractive candidates for HEMs.

$S_N2$  attack at the  $\alpha$ -carbon



Attack at the S center

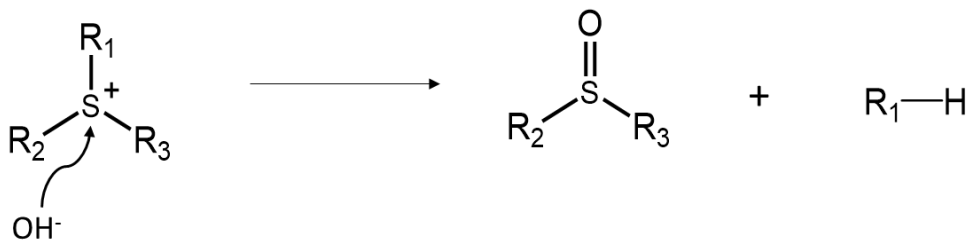


Figure 2.2: Alkaline degradation pathways of ordinary TS cations (trialkyl or arylalkyl substituted TS cations).



In this chapter, the successful synthesis of TAS based polymers and the investigation of their performances as HEMs are presented. The alkaline stabilities of three TAS cations were also investigated to determine the factors that influence the cation stability.

## **2.2 Materials and methods**

### **2.2.1 Materials and characterization**

All the chemicals mentioned in the synthesis were purchased from Sigma-Aldrich and used as received.  $^1\text{H}$  NMR spectra were measured at 400 MHz on a Bruker AV400 spectrometer. The  $^1\text{H}$  NMR chemical shifts are expressed as  $\delta$  downfield from tetramethylsilane (TMS) and calibrated to the residual proton of the deuterated solvent ( $\delta = 7.26$  for chloroform-d and  $\delta = 2.50$  for DMSO-d<sub>6</sub>). Thermogravimetric analysis (TGA) was performed in nitrogen (flow rate: 20 mL min<sup>-1</sup>) with a Mettler Toledo TGA/DSC1 thermogravimetric analyzer at a heating rate of 10 °C min<sup>-1</sup>. The conductivity measurements were carried out by four-point probe alternating current (AC) impedance spectroscopy using a four-point probe system connected with an impedance/gain-phase analyzer (Solartron 1260) and an electrochemical interface (Solartron 1287).

## 2.2.2 Experimental methods

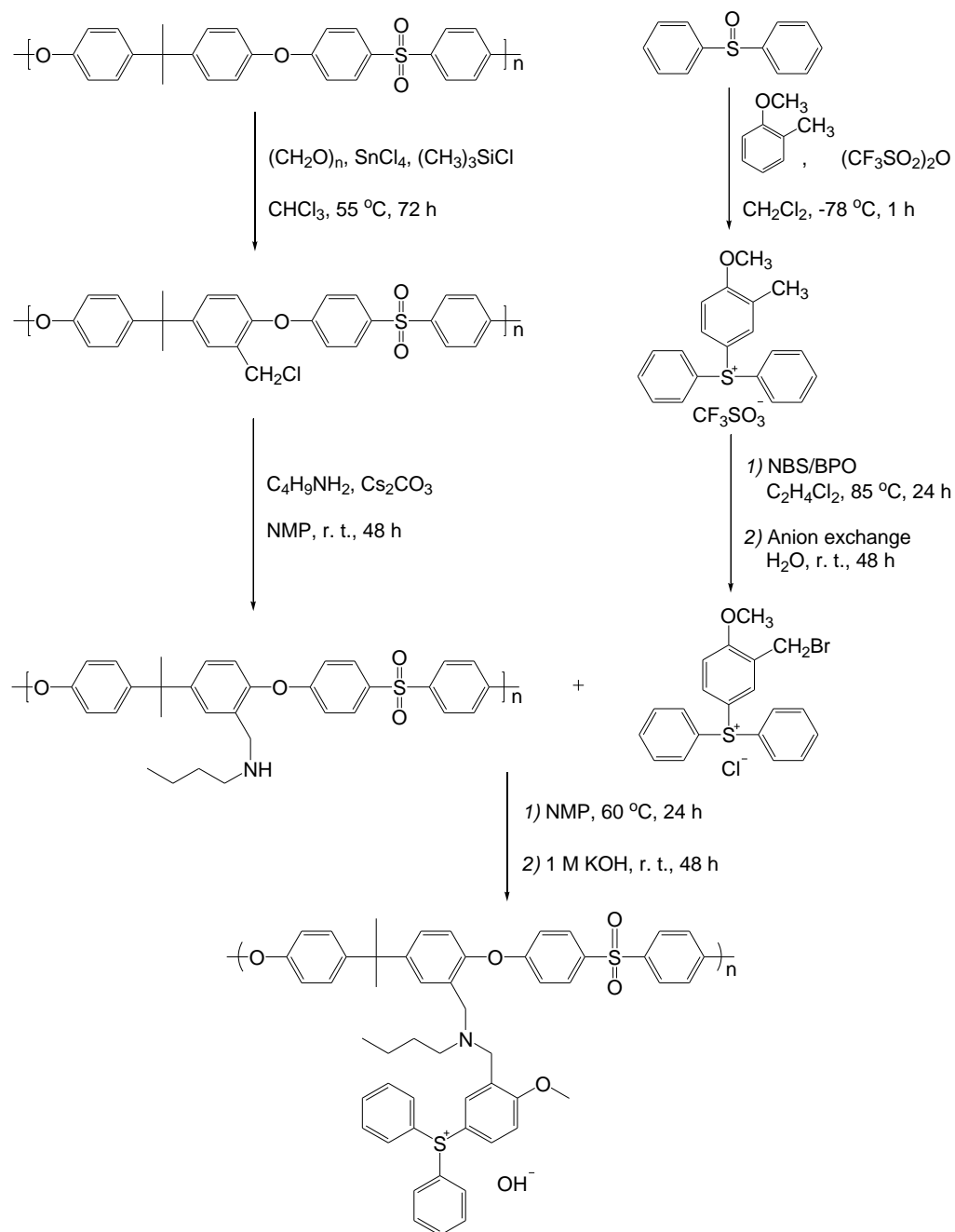


Figure 2.3: Synthesis route of MeOTASOH-functionalized polysulfone (PSf-MeOTASOH).

Because diarylsulfides are significantly less nucleophilic than tertiary amines or tertiary phosphines, the general ‘chloromethylation–quaternization–alkalization’ protocol could not be applied to synthesize TAS functionalized polymer. Therefore, a novel nitrogen-bridge strategy was adopted to synthesize PSf-MeOTAS and PSf-MeTAS, including three major steps (Fig. 2.3): (1) synthesis of diphenyl(3-methyl-4-methoxyphenyl) sulfonium chloride by the condensation reaction between diphenyl sulfoxide and 2-methylanisole, followed by a bromination reaction and anion exchange; (2) synthesis of PSf-BA through a chloromethylation and amination reaction to introduce a nitrogen atom bridge; and (3) incorporation of the MeOTAS cation to the polysulfone backbone *via* the reaction between the bromomethyl group of diphenyl(3-bromomethyl-4-methoxyphenyl) sulfonium chloride and the butylamine group of PSf-BA. The detailed procedure for each step is as follows:

**Synthesis of diphenyl(3-methyl-4-methoxyphenyl)sulfonium triflate (MeOTASTf):** 16.2 g (80 mmol) diphenyl sulfoxide and 9.77 g (80 mmol) methylanisole were dissolved in 800 mL dichloromethane. The solution was cooled to  $-78\text{ }^{\circ}\text{C}$  in a dry ice-acetone bath and 22.6 g (80 mmol) trifluoromethanesulfonic anhydride was added dropwise. The mixture was stirred at room temperature for 1 h. After the reaction, the mixture was washed three times with saturated sodium bicarbonate ( $\text{NaHCO}_3$ ) solution and then with deionized water (DI) water and dried under anhydrous magnesium sulfate ( $\text{MgSO}_4$ ) for 24 h. The treated solution was concentrated to 100 mL by a rotary evaporator and added dropwise into 500 mL diethyl ether to precipitate the product. The white precipitate was separated by filtration and dried under vacuum at room temperature for 24 h.

Diphenyl(3-methyl-4-methoxyphenyl)sulfonium triflate (MeOTASTf):  $^1\text{H}$  NMR (400 MHz,  $\text{CDCl}_3$ )  $\delta$  7.74-7.60 (11H, m), 7.42 (1H, d,  $J = 2.4$  Hz), 7.12 (1H, d,  $J = 8.8$  Hz), 3.87 (3H, s), 2.17 (3H, s). Yield: 90 wt%.

**Synthesis of diphenyl(4-methylphenyl)sulfonium triflate (MeTASTf):** MeTASTf was synthesized by following the same procedure of MeOTASTf, except replacing methylanisole with anisole (8.65 g, 80 mmol).

Diphenyl(4-methoxyphenyl)sulfonium triflate (MeTASTf):  $^1\text{H}$  NMR (400 MHz,  $\text{CDCl}_3$ )  $\delta$  8.12-7.45 (14H, m), 2.06 (3H, s). Yield: 86 wt%.

**Synthesis of diphenyl(3-bromomethyl-4-methoxyphenyl)sulfonium chloride:** 4.56 g (10 mmol) MeOTASTf and 1.78 g (10 mmol) *N*-bromosuccinimide (NBS) was dissolved in 100 mL dichloroethane. The solution was heated to 85 °C, followed by addition of 0.12 g (0.5 mmol) benzoyl peroxide (BPO). The mixture was stirred at room temperature for 24 h. After the reaction, the mixture was added dropwise into 300 mL diethyl ether to precipitate the product. The precipitate was washed three times with diethyl ether and dried under vacuum at room temperature for 24 h to give diphenyl(3-bromomethyl-4-methoxyphenyl)sulfonium triflate. The  $^1\text{H}$  NMR evidence is shown in Fig. 2.4. Then, 3 g diphenyl(3-bromomethyl-4-methoxyphenyl)sulfonium triflate was dissolved in 1000 mL DI water, followed by addition of 120 g IRA-900 anion exchange resin to convert triflate ions to chloride ions. After 48 h, the resin was filtered and the water was evaporated to give diphenyl(3-bromomethyl-4-methoxyphenyl)sulfonium chloride.

The degree of bromination (DB) was calculated from the following equation:  $\text{DB} = 3A_1/2A_2 \times 100\%$ , where  $A_1$  and  $A_2$  are integral area of Peak 1 ( $-\text{CH}_2\text{Br}$ ) and Peak 2 ( $-\text{OCH}_3$ ) in the  $^1\text{H}$  NMR spectrum (Fig. 2.4). The calculated DB is 70 at%.

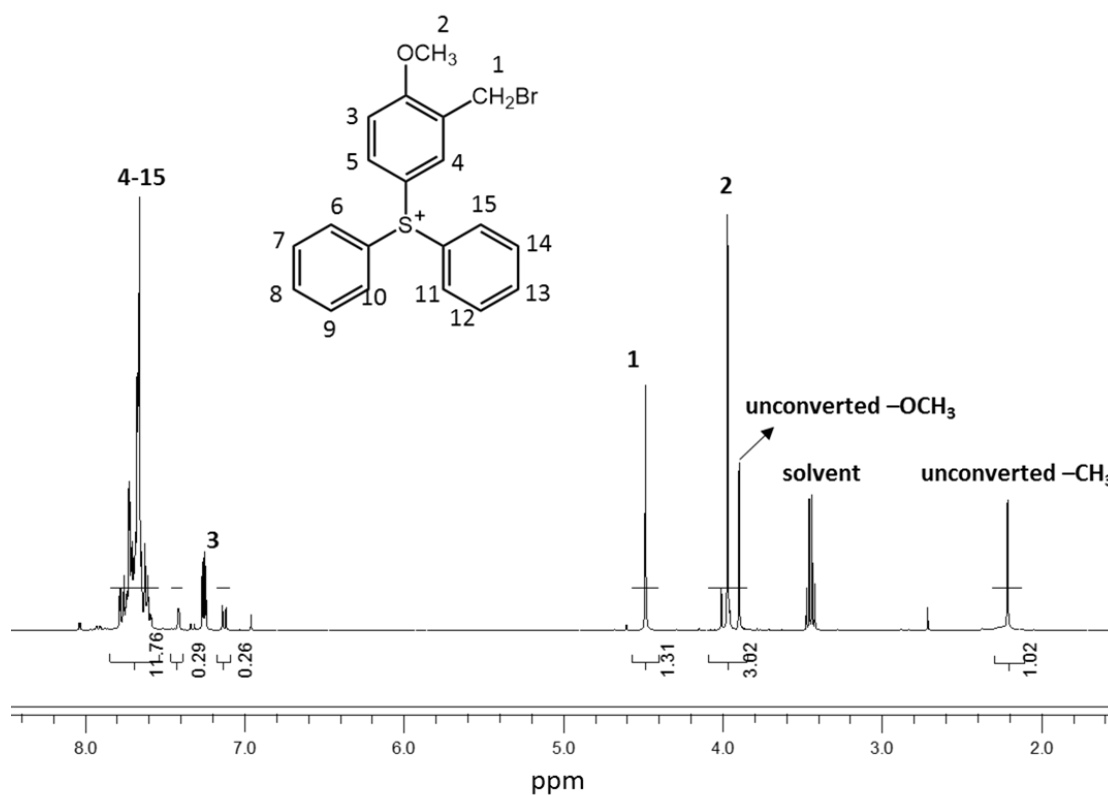


Figure 2.4:  $^1\text{H}$  NMR spectrum ( $\text{CDCl}_3$ ) of diphenyl(3-bromomethyl-4-methoxyphenyl) sulfonium triflate.

**Synthesis of diphenyl(4-bromomethylphenyl)sulfonium chloride:** Follow the same procedure of diphenyl(3-bromomethyl-4-methoxyphenyl)sulfonium chloride, except replacing MeOTASTf with MeTASTf (4.26 g, 10 mmol). The calculated DB is 72 at%.

**Synthesis of chloromethylated polysulfone (CMPSf):** 15 g (33.9 mmol) polysulfone (PSf) was dissolved in 750 mL chloroform. 10.18 g (339 mmol) paraformaldehyde and 36.9 g (339 mmol) trimethylchlorosilane were added into PSf solution, followed by dropwise addition of 1.767 g (6.78 mmol) stannic chloride. The

mixture was stirred at 55 °C for 72 h. After the reaction, the mixture was poured into ethanol to precipitate the product. The precipitate was separated by filtration, washed three times with ethanol and dried under vacuum at room temperature for 24 h. The  $^1\text{H}$  NMR evidence is shown in Fig. 2.5.

The degree of chloromethylation (DC) of CMPSf was calculated from the following equation:  $\text{DC} = \frac{A_9/2}{A_7/4} \times 100\%$ , where  $A_9$  and  $A_7$  are integral area of Peak 9 ( $-\text{CH}_2\text{Cl}$ ) and Peak 7 (proton adjacent to  $-\text{SO}_2-$  group in the aromatic ring) in the  $^1\text{H}$  NMR spectrum (Fig. 2.5). The calculated DC is 128 at%. The DC is larger than 100 at% because there are two sites available in one repeat unit for chloromethylation.

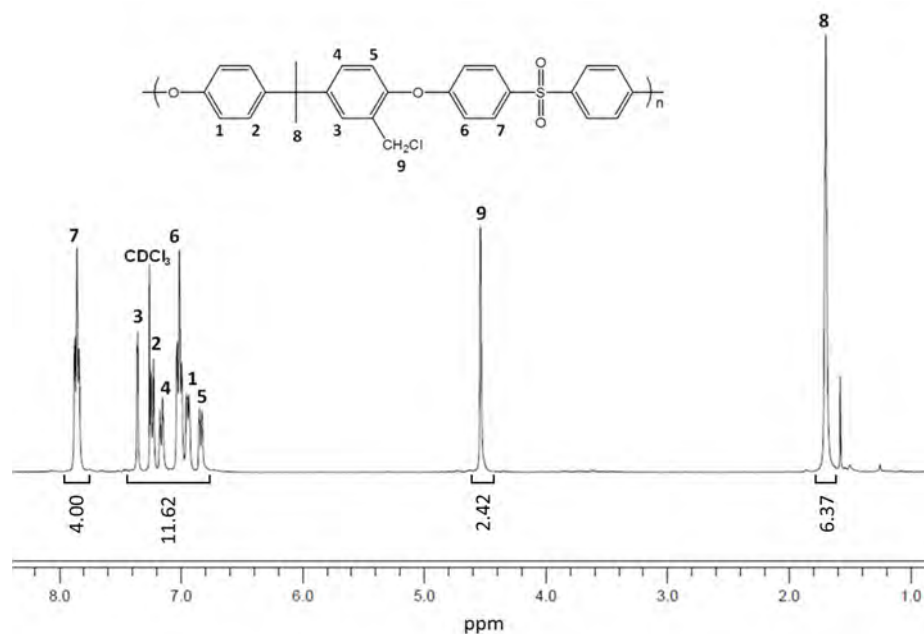


Figure 2.5:  $^1\text{H}$  NMR spectrum ( $\text{CDCl}_3$ ) of chloromethylated polysulfone (CMPSf).

**Synthesis of butylaminated polysulfone (PSf-BA):** 2.02 g (4 mmol) was dissolved in 40 mL 1-methyl-2-pyrrolidinone (NMP), followed by addition of 4.69 mL (40 mmol) butylamine and 3.16 g (8 mmol) cesium carbonate ( $\text{Cs}_2\text{CO}_3$ ). The mixture was stirred at room temperature for 48 h. After the reaction, the mixture was added dropwise into 400 mL DI water to precipitate the polymer. The precipitate was washed three times with DI water, filtered and dried in vacuum at 60 °C for 48 h. The  $^1\text{H}$  NMR evidence is shown in Fig. 2.6.

The disappearance of the chemical shift 4.44 ppm indicates that the conversion of chloromethyl group to butyl amine is close to 100%.

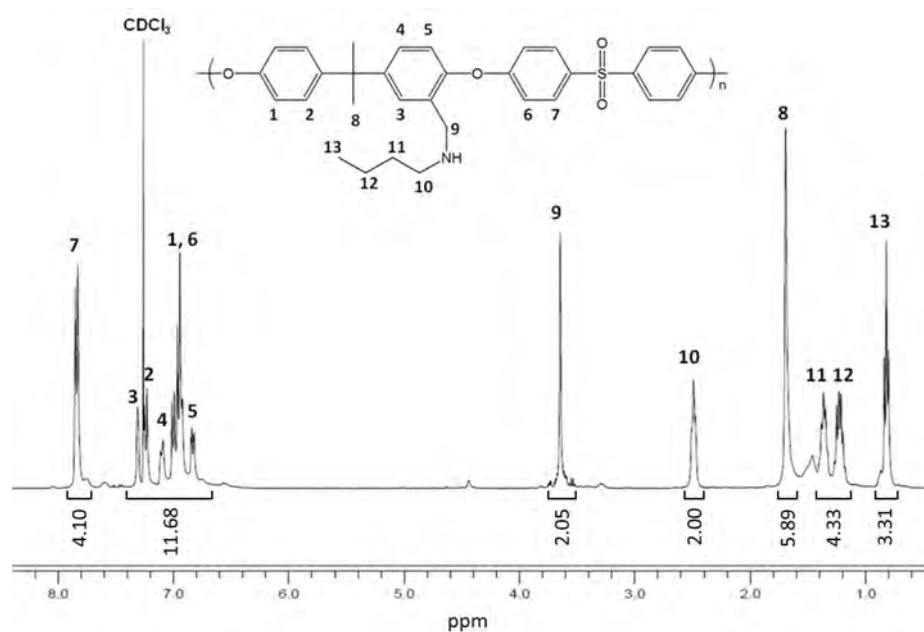


Figure 2.6  $^1\text{H}$  NMR spectrum ( $\text{CDCl}_3$ ) of butylaminated polysulfone (PSf-BA).

**Synthesis of diphenyl(3-methyl-4-methoxyphenyl)sulfonium chloride (MeOTASCl) functionalized polysulfone (PSf-MeOTASCl):** 0.110 g (0.2 mmol) PSf-BA and 0.227 g (0.4 mmol) MeOTASCl were dissolved in 1 mL NMP. The solution was stirred at 60 °C for 24 h. After the reaction, the solution was added dropwise into ethanol to precipitate the polymer. The precipitate was washed with ethanol three times, filtered and dried in vacuum at room temperature for 24 h. The  $^1\text{H}$  NMR evidence is shown in Fig. 2.7.

$\text{H}_{9'-13'}$  are assigned to the unconverted butylamine group. The degree of functionalization of MeOTAS cation (DS) was calculated from the following equation:  $\text{DS} = \frac{A_{10}}{A_{10} + A_{10'}}$ , where  $A_{10}$  and  $A_{10'}$  are integral area of Peak 10 (from functionalized butylamine) and Peak 10' (from unconverted butylamine) in the  $^1\text{H}$  NMR spectrum (Fig. 2.7). The calculated DS of MeOTAS cation is 46 at%.

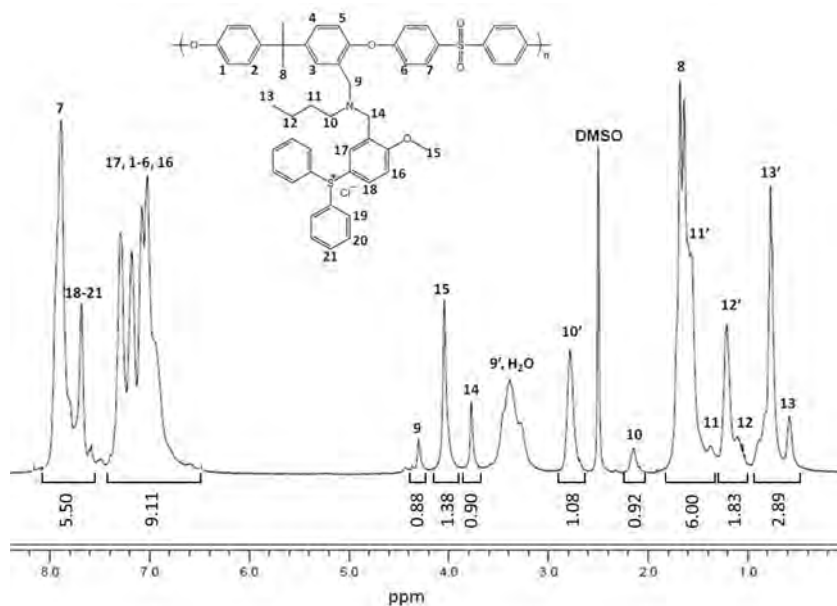


Figure 2.7:  $^1\text{H}$  NMR spectrum ( $\text{DMSO-d}_6$ ) of MeOTASCl functionalized polysulfone (PSf-MeOTASCl).



**Synthesis of triphenylsulfonium chloride (MeTASCl) functionalized polysulfone (PSf-MeTASCl):** Follow the same procedure of PSf-MeOTASCl, except replacing MeOTASCl with MeTASCl (0.215 g, 0.4 mmol). The calculated DS of TAS cation is 44 at%.

**Synthesis of bis(1,3,5-trimethoxyphenyl)sulfoxide:** To a suspension of 13.4 g (80 mmol) 1,3,5-trimethoxybenzene, 25 mL chloroform and 11.5 g (4 mmol) tungstophosphoric acid ( $\text{H}_3\text{PW}_{12}\text{O}_{40}$ ), 3.50 mL (48 mmol) thionyl chloride was added dropwise at the room temperature under argon atmosphere for 4 h. After the reaction, the mixture was extracted with diethyl ether three times, the combined extract was then washed with saturated  $\text{NaHCO}_3$  solution and dried over anhydrous  $\text{MgSO}_4$ , concentrated in vacuum and the resulting product was purified by recrystallization in ethyl acetate/hexane mixed solvent to afford pure bis(1,3,5-trimethoxyphenyl)-sulfoxide.<sup>[240]</sup>

Bis(1,3,5-trimethoxyphenyl)sulfoxide:  $^1\text{H}$  NMR (400 MHz,  $\text{CDCl}_3$ )  $\delta$  6.07 (4H, s), 3.78 (6H, s), 3.73 (12H, s). Yield: 70 wt%.

**Synthesis of tris(1,3,5-trimethoxyphenyl)sulfonium triflate (9MeOTASTf):** 3.83 g (10 mmol) bis(1,3,5-trimethoxyphenyl)sulfoxide and 1.68 g (10 mmol) 1,3,5-trimethoxybenzene were dissolved in 100 mL dichloromethane. The solution was cooled to  $-78\text{ }^\circ\text{C}$  in a dry ice-acetone bath and 2.83 g (10 mmol) trifluoromethanesulfonic anhydride was added dropwise. The mixture was stirred at room temperature for 1 h. After the reaction, the mixture was washed three times with saturated  $\text{NaHCO}_3$  solution and then with DI water and dried under anhydrous  $\text{MgSO}_4$  for 24 h. The treated solution was concentrated to 10 mL by a rotary evaporator and added dropwise into 100 mL diethyl ether to precipitate the product. The brown

precipitate was separated by filtration and dried under vacuum at room temperature for 24 h.

Bis(1,3,5-trimethoxyphenyl)sulfoxide:  $^1\text{H}$  NMR (400 MHz,  $\text{CDCl}_3$ )  $\delta$  6.18 (6H, s), 3.89 (9H, s), 3.70 (18H, s). Yield: 84 wt%.

**Preparation of diphenyl(3-methyl-4-methoxyphenyl)sulfonium hydroxide (MeOTASOH) functionalized polysulfone (PSf-MeOTASOH) based HEM:** The PSf-MeOTASCl/NMP solution (10 wt%) was poured onto a flat glass sheet, followed by evaporating the solvent at 30 °C for 24 h to obtain a PSf-MeOTASCl membrane. The PSf-MeOTASOH HEM was obtained by immersing PSf-MeOTASCl membrane in 1 M KOH aqueous solution at room temperature for 48 h to exchange chloride ions for hydroxide ions. Then, the membrane was washed thoroughly with DI water, followed by immersing in DI water for another 48 h to remove residual KOH. The DI water was refreshed periodically.

Fig. 2.8 shows the optical images of PSf-MeOTASOH HEM. This HEM is colorless, transparent, and flexible.

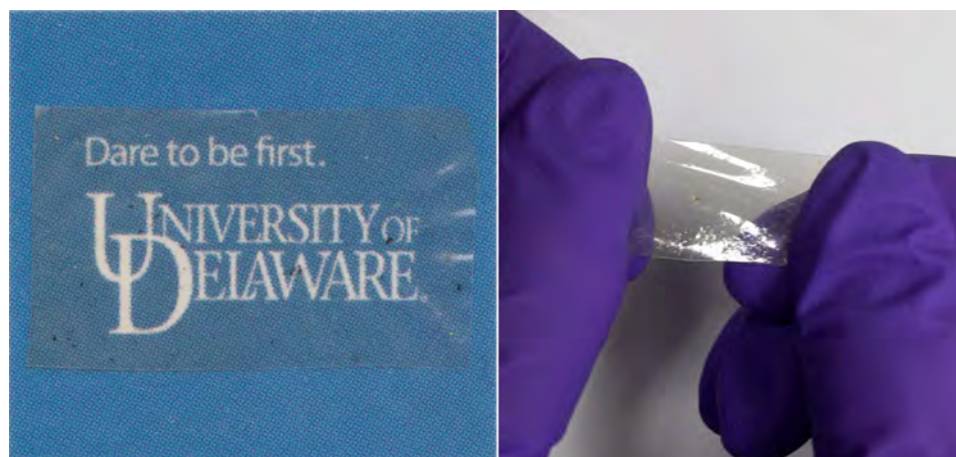


Figure 2.8: Optical images of PSf-MeOTASOH HEM.

**Preparation of triphenylsulfonium hydroxide (MeTASOH) functionalized polysulfone (PSf-MeTASOH) based HEM:** Follow the same procedure of PSf-MeOTASOH HEM.

**Measurement of ion exchange capacity (IEC) of HEMs:** PSf-MeOTASOH or PSf-MeTASOH was immersed in 100 mL of 0.1 M HCl solution for 48 h. The resultant solution was then titrated with a standardized NaOH solution (0.1 M) using phenolphthalein as an indicator.

**Measurement of the water uptake of HEMs:** The HEMs were vacuum-dried at 60 °C for 10 h until constant weights were obtained. They were then immersed in DI water at room temperature for 4 h. After that, the HEMs were taken out, wiped with tissue paper, and quickly weighed. The water uptakes of HEMs were calculated according to Eq. 2.1. Here  $W_{\text{wet}}$  is the weight of the wet membrane, and  $W_{\text{dry}}$  is the weight of the dry membrane.

$$\text{Water uptake (wt\%)} = \left[ \frac{W_{\text{wet}} - W_{\text{dry}}}{W_{\text{dry}}} \right] \times 100\% \quad \text{Eq. 2.1}$$

**Measurement of the swelling ratio of HEMs:** The round-shaped HEMs were vacuum-dried at 60 °C for 10 h until constant diameters were obtained. They were immersed in water at room temperature for 4 h, and the diameters of the wet membrane were measured. The swelling ratio was calculated by Eq. 2.2.  $l_{\text{wet}}$  is the diameter of the wet membrane, and  $l_{\text{dry}}$  is the diameter of the dry membrane.

$$\text{Swelling ratio (wt\%)} = \left[ \frac{l_{\text{wet}} - l_{\text{dry}}}{l_{\text{dry}}} \right] \times 100\% \quad \text{Eq. 2.2}$$

**Measurement of hydroxide conductivity of HEMs:** The hydroxide conductivity ( $\sigma$ , in  $\text{S cm}^{-1}$ ) of each membrane (size: 1 cm  $\times$  4 cm) was obtained according to Eq. 2.3. Here  $d$  is the distance between reference electrodes;  $L_s$  and  $W_s$

are the thickness and width of the membrane, respectively; R is the measured resistance of the membrane.

$$\sigma = d/L_s W_s R \quad \text{Eq. 2.3}$$

R was measured over the frequency range from 1 mHz to 100 kHz by four-point probe AC impedance spectroscopy using an electrode system connected with an impedance/gain-phase analyzer and an electrochemical interface. The membranes and the electrodes were set in a Teflon cell, and the distance between the reference electrodes was 1 cm. The cell was placed in a thermo-controlled chamber in DI water for measurement.

All samples were equilibrated in water for at least 24 h prior to the conductivity measurement. Repeated measurements were then taken with 10 min interval until no change in impedance was observed.

**Alkaline durability test of PSf-MeOTASOH and PSf-MeTASOH HEMs:**

Each of these two HEMs was cut into several small pieces. The membranes were immersed in a 1 M KOH aqueous solution at 60 °C or room temperature. The membrane was taken out at one time and washed thoroughly with DI water, followed by immersing in DI water for another 48 h to remove residual KOH. The DI water was refreshed periodically. Hydroxide conductivity measurements were carried out periodically to monitor the degradation of the HEM.

**Alkaline durability tests of TAS model compounds (MeOTASCl and MeTASCl):** Each of the TAS model compounds (1 mmol) was dissolved in 1 M KOD/D<sub>2</sub>O solution (30 mL), and the solution was kept at 60 °C for a certain duration (14 days for MeOTASCl and 1 day for MeTASCl), followed by periodic sampling and <sup>1</sup>H NMR analysis.

**Accelerated alkaline durability tests of TAS model compounds (MeOTASCl and 9MeOTASCl)<sup>[212]</sup>:** 1 M deuterated potassium hydroxide (KOD) in CD<sub>3</sub>OD/D<sub>2</sub>O (5/1 vol) solution was prepared by dissolving KOD (40 wt% in D<sub>2</sub>O, 4.28 g, 30.0 mmol) in a mixture of deuterated methanol and heavy water (CD<sub>3</sub>OD/D<sub>2</sub>O) (25 mL/2.67 mL). Each of the TAS model compounds (1 mmol) was dissolved in the alkaline solution to obtain a molar ratio of 30 KOD : 1 TAS (i.e. 0.033 M). 3-(trimethylsilyl)-1-propanesulfonic acid sodium salt (TMS(CH<sub>2</sub>)<sub>3</sub>SO<sub>3</sub>Na) (0.107 g, 0.490 mmol) was added to serve as an internal standard for <sup>1</sup>H NMR measurements. The mixture was placed in a fluoropolymer lined autoclave. Before the test (t = 0), an aliquot of the testing solution was removed and analyzed by <sup>1</sup>H NMR spectroscopy to determine the initial quantity of TAS. Then, the testing solution was held at 80 °C. Aliquots of the reaction were removed daily and analyzed by <sup>1</sup>H NMR spectroscopy to determine the quantity of TAS remaining.

**Accelerated alkaline durability tests of benchmark cation BTMA:** 1 M deuterated potassium hydroxide (KOD) in CD<sub>3</sub>OD/D<sub>2</sub>O (5/1 vol) solution was prepared by dissolving KOD (40 wt% in D<sub>2</sub>O, 4.28 g, 30.0 mmol) in a mixture of deuterated methanol and heavy water (CD<sub>3</sub>OD/D<sub>2</sub>O) (25 mL/2.67 mL). BTMA-Br (0.230 g, 1.00 mmol) was added to the alkaline solution to obtain a molar ratio of 30 KOD : 1 model compound (i.e. 0.033 M). TMS(CH<sub>2</sub>)<sub>3</sub>SO<sub>3</sub>Na (0.107 g, 0.490 mmol) was added to serve as an internal standard for <sup>1</sup>H NMR measurements. The mixture was placed in a fluoropolymer lined autoclave. Before the test (t = 0), an aliquot of the testing solution was removed and analyzed by <sup>1</sup>H NMR spectroscopy to determine the initial quantity of BTMA. Then, the testing solution was held at 80 °C. Aliquots of the reaction were removed every 4 days and analyzed by <sup>1</sup>H NMR spectroscopy to

determine the quantity of BTMA remaining. A control sample with the same recipe but without adding KOD was prepared, and submitted to  $^1\text{H}$  NMR measurement.

**Calculation of the degradation rate constant ( $k$ ) of TAS model compounds and BTMA:** The degradation rate is defined by Eq. 2.4.

$$-r_d = -\frac{d[\text{cation}]}{dt} = k[\text{cation}]^m[\text{OH}^-]^n \quad \text{Eq. 2.4}$$

Because  $\frac{[\text{OH}^-]_0}{[\text{cation}]_0} = 30$ , we can consider  $[\text{OH}^-] \approx \text{constant}$ . Thus, the rate

equation becomes Eq. 2.5.

$$-r_d = -\frac{d[\text{cation}]}{dt} = k'[\text{cation}]^m, k' = k[\text{OH}^-]^n, [\text{OH}^-] = 1 \text{ M} \quad \text{Eq. 2.5}$$

Here,  $r_d$  is the degradation rate,  $k$  is the degradation rate constant,  $k'$  is the adjusted degradation rate constant.  $k_{80}$  (the adjusted degradation rate constant at 80 °C) of 9MeOTAS, MeOTAS and BTMA were calculated by correlating  $\ln(C_0/C)$  at 80 °C and time. Here,  $C_0$  is the initial cation concentration, and  $C$  is the concentration at the sampling time.

## 2.3 Results and Discussion

### 2.3.1 Thermal stability of the MeOTAS based HEM

TGA analysis was carried out to determine the thermal stability of PSf-MeOTASOH HEM. Fig. 2.9 showed that the PSf-MeOTASOH HEM has an onset decomposition temperature ( $T_{\text{OD}}$ , defined as the temperature at 1 wt% loss) of 242 °C (Table 2.1). Under the same test conditions ( $\text{N}_2$  atmosphere and  $10 \text{ }^\circ\text{C min}^{-1}$  heating rate), PSf-MeOTASOH HEM has much higher  $T_{\text{OD}}$  than the QA-based HEM (same polysulfone backbone, 140~170 °C)<sup>[95, 241-244]</sup> and QP-based HEM (same polysulfone backbone, 178 °C).<sup>[245]</sup> This  $T_{\text{OD}}$  is also higher than those of quaternary guanidinium

based poly(arylene ether sulfone) (185 °C with 5 wt% loss)<sup>[246]</sup> and imidazolium based polyfluorene (200 °C with 4 wt% loss).<sup>[247]</sup>

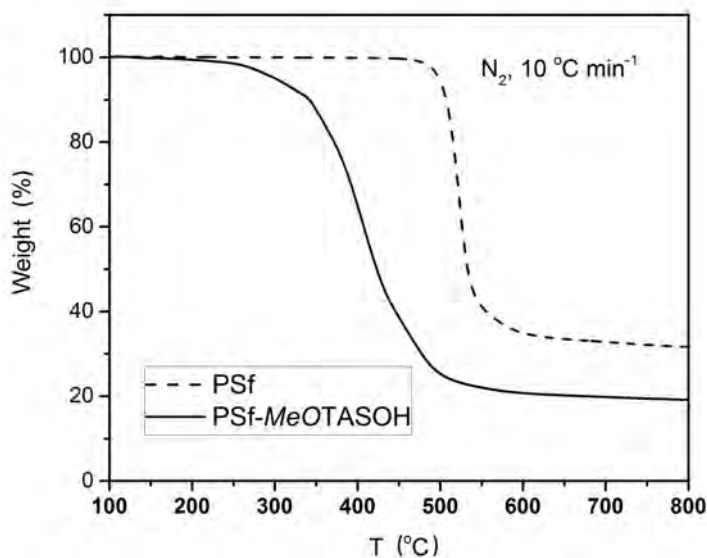


Figure 2.9: Thermal gravimetric analysis (TGA) curves of the pristine PSf (dash line), and PSf-MeOTASOH (solid line). Test conditions: nitrogen atmosphere with 20 mL min<sup>-1</sup> of flow rate, and 10 °C min<sup>-1</sup> of heating rate.

Table 2.1: Thermal decomposition temperature of the pristine PSf and PSf-MeOTASOH.

Polymer	T <sub>OD</sub> <sup>a</sup> (°C)	T <sub>FD</sub> <sup>b</sup> (°C)
PSf	476	523
PSf-MeOTASOH	242	406

<sup>a</sup> T<sub>OD</sub>, onset decomposition temperature. <sup>b</sup> T<sub>FD</sub>, fastest-weight-loss decomposition temperature.

### 2.3.2 Hydroxide conductivity of the MeOTAS based HEM

With an ion exchange capacity (IEC) of  $0.69 \text{ mmol g}^{-1}$ , the PSf-MeOTASOH has a water uptake of 26.9 wt% and a swelling ratio less than 5% at  $20^\circ\text{C}$ . The hydroxide conductivity of PSf-MeOTASOH is  $15.4 \pm 1.4 \text{ mS cm}^{-1}$  at  $20^\circ\text{C}$  (Table 2.2), which meets the basic requirement of HEMFCs ( $>10^{-2} \text{ S cm}^{-1}$ ).<sup>[160]</sup> Generally, the conductivity increases almost linearly with the density of the ionic group (i.e. IEC), and thus an IEC-normalized hydroxide conductivity (hydroxide conductivity over IEC, Table 2.2) is a more objective measure of the intrinsic hydroxide conductivity for HEMs.<sup>[206]</sup> PSf-MeOTASOH shows a high IEC-normalized hydroxide conductivity ( $22.3 \text{ mS g cm}^{-1} \text{ mmol}^{-1}$ ) that is slightly higher than that of quaternary ammonium-based polysulfone HEMs ( $19 \text{ mS g cm}^{-1} \text{ mmol}^{-1}$ )<sup>[23]</sup>, indicating a similar efficiency of hydroxide conduction. This value is also higher than those of imidazolium-based polysulfone HEMs ( $8.4 \text{ mS g cm}^{-1} \text{ mmol}^{-1}$ )<sup>[145]</sup>, but lower than those of the QP-based polysulfone HEMs ( $39 \text{ mS g cm}^{-1} \text{ mmol}^{-1}$ )<sup>[209]</sup>. **Note:** there is significant room to increase the hydroxide conductivity of PSf-MeOTASOH HEM by adjusting the synthesis conditions to introduce more TAS cations to the polymer backbone.

Table 2.2: IEC, HC and  $\text{HC}_{\text{IEC}}$  of PSf-MeOTASOH and PSf-MeTASOH HEMs.

HEM	IEC <sup>a</sup> ( $\text{mmol g}^{-1}$ )	HC <sup>b</sup> ( $\text{mS cm}^{-1}$ )	$\text{HC}_{\text{IEC}}$ <sup>c</sup> ( $\text{mS g cm}^{-1} \text{ mmol}^{-1}$ )
PSf-MeOTASOH <sup>d</sup>	0.69	$15.4 \pm 1.4$	22.3
PSf-MeTASOH <sup>e</sup>	0.68	$7.7 \pm 1.3$	11.3

<sup>a</sup> IEC, theoretical ion exchange capacity based on the degree of functionalization. <sup>b</sup> HC, hydroxide conductivity measured in water at  $20^\circ\text{C}$ . <sup>c</sup>  $\text{HC}_{\text{IEC}}$ , IEC-normalized hydroxide conductivity. <sup>d</sup> 46 at% of the degree of functionalization. <sup>e</sup> 44 at% of the degree of functionalization.



### 2.3.3 Alkaline stability of the MeOTAS based HEM

The alkaline stability test of PSf-MeOTASOH HEM was carried out in 1 M KOH at 60 °C. The conductivity loss was used to determine the cation degradation percentage. Over the test, a slow decline of the hydroxide conductivity was observed (Fig. 2.10). After 12 days, the HEM still maintained 80% of its conductivity, indicative an enhanced alkaline stability. Under similar conditions the commercial QA-based FAA membranes became very brittle due to severe degradation.<sup>[209]</sup> Additionally, there was no obvious loss of conductivity observed for PSf-MeOTASOH HEM after immersion in 1 M KOH for 30 days at 20 °C, indicating long-term stability.

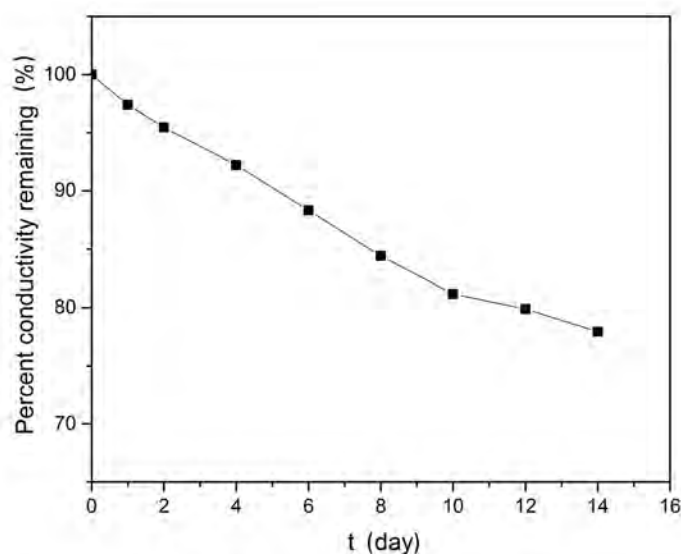


Figure 2.10: Percent conductivity remaining of PSf-MeOTASOH HEM under alkaline degradation test over 14 days. Test conditions: 1 M KOD/D<sub>2</sub>O for test solution and 60 °C for test temperature.

### 2.3.4 Comparison of PSf-MeOTASOH HEM and PSf-MeTASOH HEM

To determine the influences of phenyl-substituents on HEM performances, MeO-free TAS cation-based polysulfone HEM (PSf-MeTASOH) (chemical structure in Fig. 2.11(b)) was synthesized through the analogous synthesis route (Fig. 2.3) and compared with PSf-MeOTASOH HEM (chemical structure in Fig. 2.11(a)).

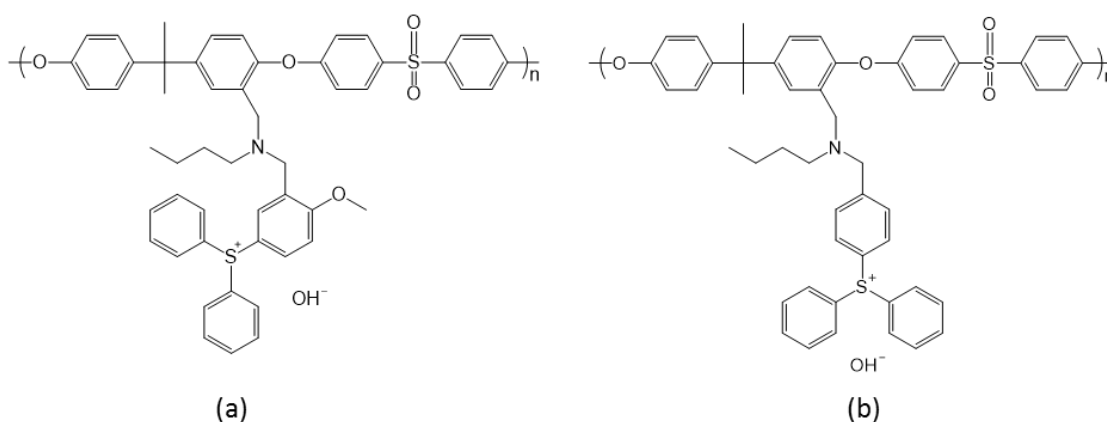


Figure 2.11: Chemical structures of two TAS based HEMs: (a) PSf-MeOTASOH and (b) PSf-MeTASOH.

With almost the same IEC, PSf-MeTASOH HEM has a conductivity of only half of that of PSf-MeOTASOH (7.7 vs 15.4 mS cm<sup>-1</sup>, Table 2.2). Also, the alkaline stability of PSf-MeTASOH HEM is significantly inferior to that of PSf-MeOTASOH HEM. The immersion of PSf-MeTASOH HEM in 1M KOH at 60 °C causes a serious decline of the hydroxide conductivity (Fig. 2.12). This HEM completely degraded within only 2 days, indicating significantly decreased alkaline stability.

The comparison between PSf-MeOTASOH and PSf-MeTASOH HEMs indicates that the methoxy substituent is likely to be critical for the TAS cations in terms of alkaline stabilities and hydroxide conductivities, as it helps delocalize the positive charge on sulfur and increase the basicity, simultaneously through the strong electron donation.

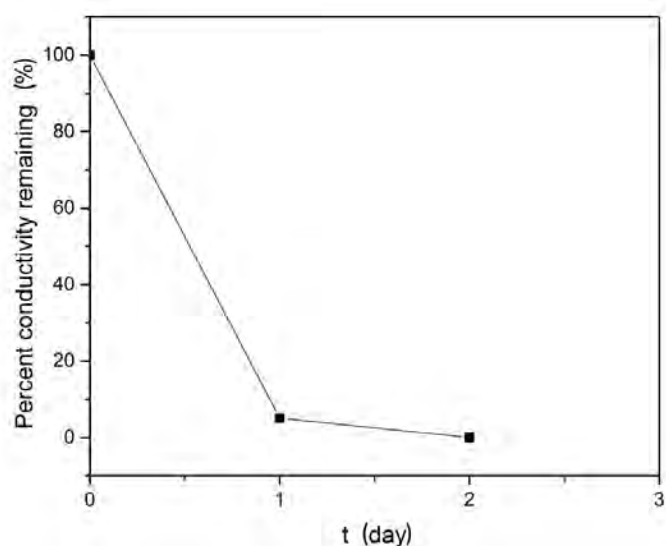


Figure 2.12: Percent conductivity remaining of PSf-MeTASOH HEM under alkaline degradation test. Test conditions: 1 M KOD/D<sub>2</sub>O for test solution and 60 °C for test temperature.

### 2.3.5 Influence of the phenyl-substituent over the alkaline stability

To further determine the influence of the phenyl-substituents over the alkaline stability, two TAS model compounds (Fig. 2.13) were submitted to alkaline durability tests to investigate the intrinsic cation stabilities. MeOTAS cation remained almost intact after the degradation test in 1 M KOD/D<sub>2</sub>O solution at 60 °C for 14 days (Fig. 2.14). In contrast, the MeTAS completely degraded within 1 day, evidenced by the <sup>1</sup>H

NMR spectra (Fig. 2.15). It underwent central atom degradation procedure to form diphenylsulfoxide and toluene. Apparently, MeOTAS is indeed much more stable than MeTAS, which confirms that the electron-donating phenyl-substituent improves cation stability and thus HEM stability. This result also suggests that the alkaline stability of TAS cation could be further improved by introducing more or even stronger electron-donating groups.



Figure 2.13: Chemical structures of (a) MeOTASCl and (b) MeTASCl.

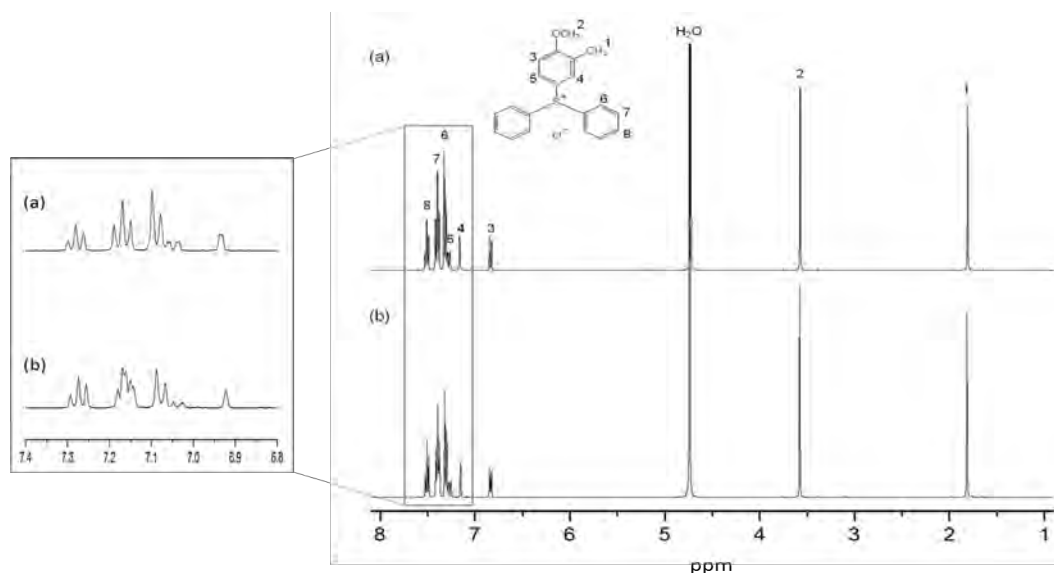


Figure 2.14:  $^1\text{H}$  NMR spectra of MeOTASCl: (a) before alkaline durability test and (b) after 14 days durability test. The inset shows the enlarged spectra in the region of 6.8~7.4 ppm. Test conditions: 1 M KOD/D<sub>2</sub>O for test solution and 60 °C for test temperature.

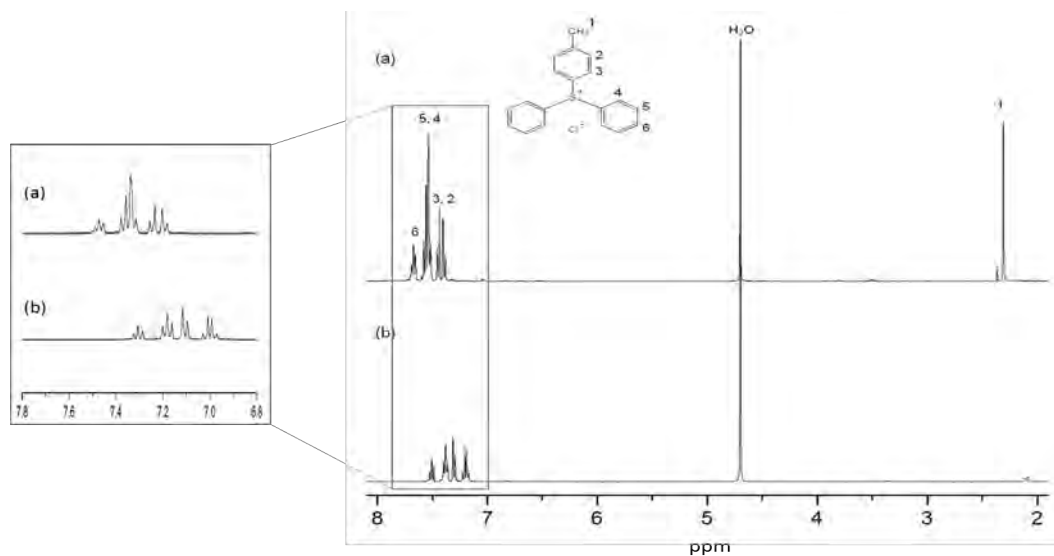


Figure 2.15:  $^1\text{H}$  NMR spectra of MeTASCl: (a) before alkaline durability test, and (b) after 1 day alkaline durability test over 1 day. The inset shows the enlarged spectra in the region of 6.8~7.8 ppm. Test conditions: 1 M KOD/D<sub>2</sub>O for test solution and 60 °C for test temperature.

Based on the analysis above, a new TAS cation with nine methoxy substituents on phenyl rings (9MeOTAS, chemical structure in Fig. 2.16) was designed and synthesized to provide strong electron donation to the central sulfur atom. For the alkaline durability test, because of the low solubility of this cation in pure water, a new strategy was adopted to do the test. The test temperature was increased to 80 °C, and methanol was introduced as the solvent to better dissolve this cation. Meanwhile, the methanol could accelerate the cation degradation to shorten the duration of the test. For comparison, the alkaline stability of MeOTAS was also tested *via* the same procedure.

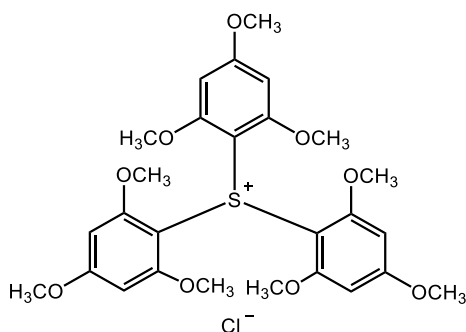


Figure 2.16: Chemical structure of 9MeOTASCl.

For each test, a 1 M alkaline solution was prepared by dissolving deuterated potassium hydroxide (KOD) in a 5/1 (vol) mixture of deuterated methanol and heavy water ( $\text{CD}_3\text{OD}/\text{D}_2\text{O}$ ).<sup>[212]</sup> 9MeOTASCl or MeOTASCl was added to the alkaline solution to obtain a molar ratio of 30 KOD : 1 TAS model compound (i.e. 0.033 M) so that the alkali concentration could be considered constant over the test.  $\text{TMS}(\text{CH}_2)_3\text{SO}_3\text{Na}$  was added to serve as an internal standard for  $^1\text{H}$  NMR

measurements. The mixture was held at 80 °C, with  $^1\text{H}$  NMR spectra taken periodically (Fig. 2.17 and 2.18).

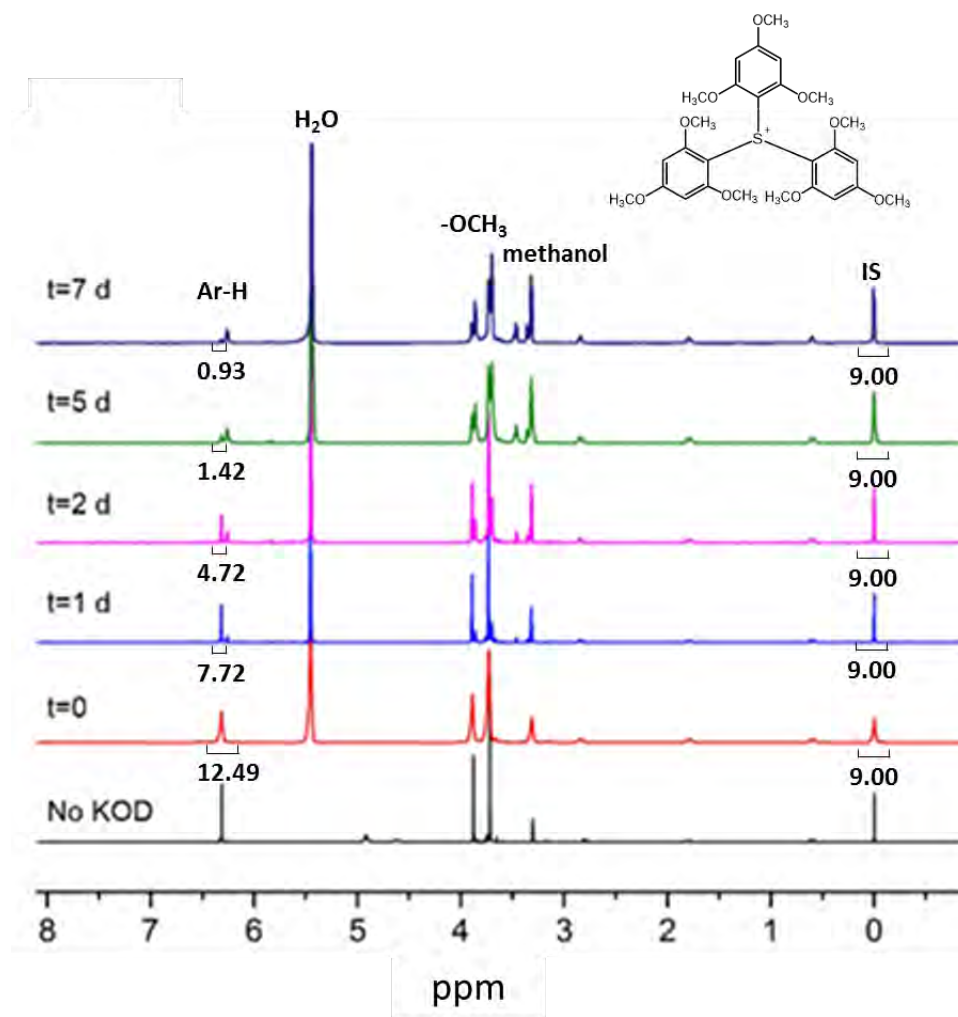


Figure 2.17: Time series of  $^1\text{H}$  NMR spectra during durability test of 9MeOTASCl at 80 °C. TMS(CH<sub>2</sub>)<sub>3</sub>SO<sub>3</sub>Na as the internal standard; 1 M KOD in CD<sub>3</sub>OD/D<sub>2</sub>O (5/1 vol) as the solvent.

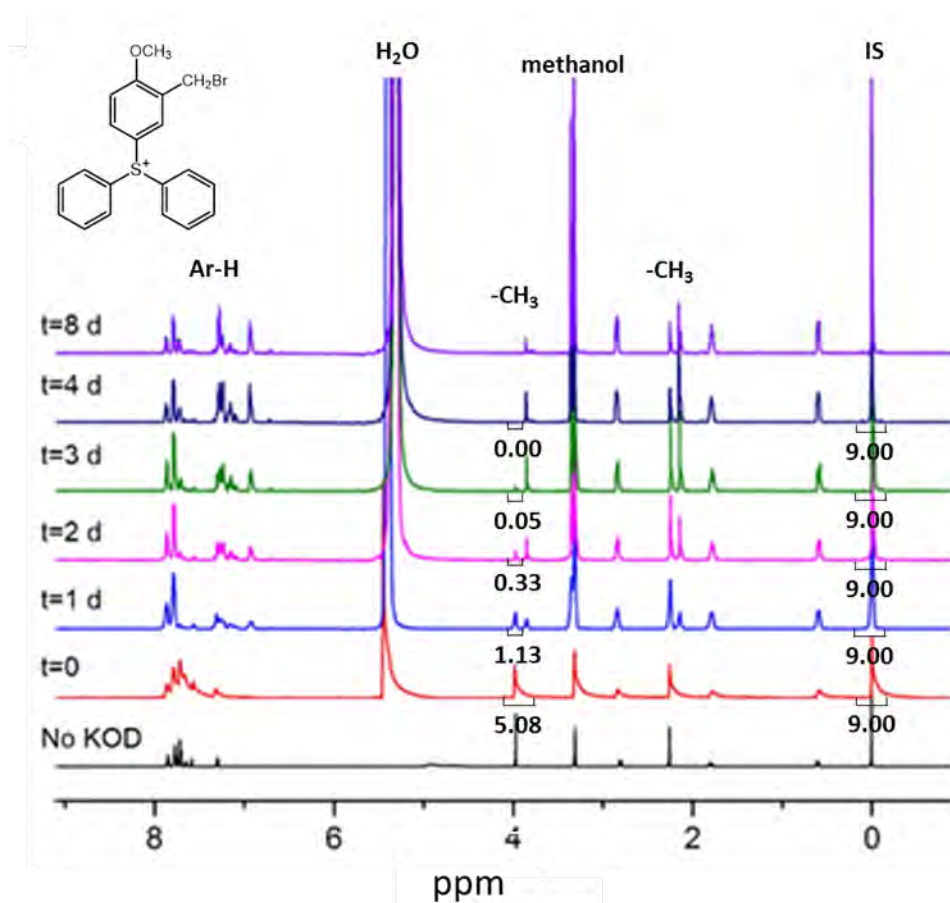


Figure 2.18: Time series of  $^1\text{H}$  NMR spectra during durability test of MeOTASCl at 80 °C. TMS(CH<sub>2</sub>)<sub>3</sub>SO<sub>3</sub>Na as the internal standard; 1 M KOD in CD<sub>3</sub>OD/D<sub>2</sub>O (5/1 vol) as the solvent.

The degradation percentages of 9MeOTAS were judged by the gradual decrease in area of the aromatic protons ( $\delta = 6.32$  ppm) as compared to the constant area of the largest internal standard peak (methyl proton,  $\delta = 0$  ppm) (Fig. 2.17). The degradation percentage of MeOTAS was judged by the gradual decrease in area of the methoxy protons ( $\delta = 3.98$  ppm) as compared to the constant area of the largest internal standard peak (methyl proton,  $\delta = 0$  ppm) (Fig. 2.18).



The degradation profiles of these two TAS model compounds (Fig. 2.19(a)) suggested that 9MeOTAS has better alkaline stability than MeOTAS. Fig. 2.19(b) showed that the degradation reactions of these two TAS cations are first-order. The adjusted degradation rate constant at 80 °C ( $k_{80}$ ) of each model compounds is calculated from the slope of the fitted line. 9MeOTAS ( $k_{80} = 4.7\text{E-}6 \text{ s}^{-1}$ ) is 3.6 times as stable as MeOTAS ( $k_{80} = 1.7\text{E-}5 \text{ s}^{-1}$ ), confirming that by introducing more electron-donating substituents to the phenyl rings, the alkaline stability of TAS cation can be enhanced.

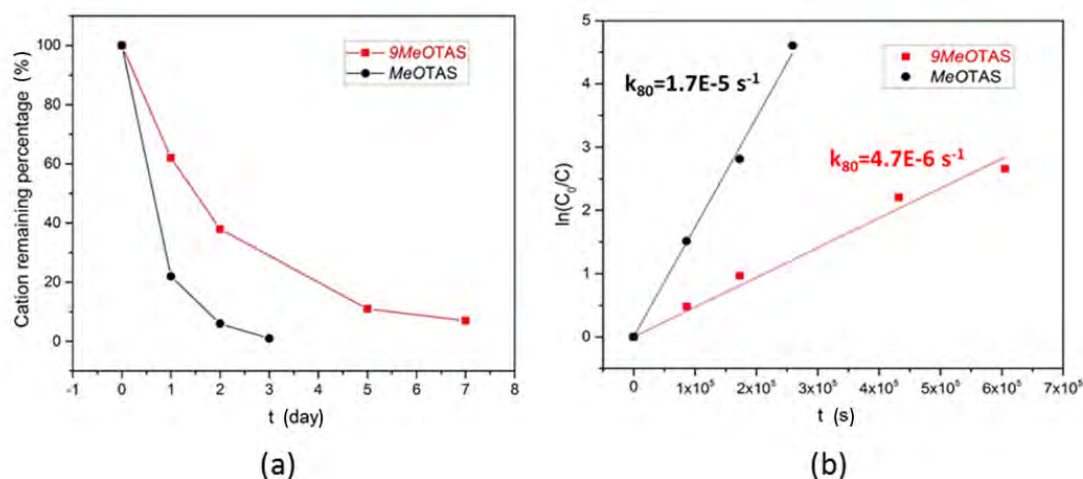


Figure 2.19: (a) Degradation profiles and (b) plots of  $\ln(C_0/C)$  versus time of 9MeOTAS and MeOTAS at 80 °C. 1 M KOD in  $\text{CD}_3\text{OD}/\text{D}_2\text{O}$  (5/1 vol) as the solvent.

For further comparison, we also tested the alkaline stability of the benchmark cation BTMA under the same conditions as that of 9MeOTAS ( $^1\text{H}$  NMR in Fig. 2.20, summary of the degradation rates in Fig. 2.21(a)). The degradation percentage of

BTMA was judged by the gradual decrease in area of the aromatic region ( $\delta = 7.50\sim 7.62$  ppm) as compared to the constant area of the largest internal standard peak (methyl proton,  $\delta = 0$  ppm).

Fig. 2.21(b) showed that BTMA has a  $k_{80}$  of  $8.3\text{E}-7\text{ s}^{-1}$  which is 5.7 time as stable as 9MeOTAS ( $k_{80} = 4.7\text{E}-6\text{ s}^{-1}$ ). It suggested that although by increasing the electron density on the central sulfur, 9MeOTAS gained more alkaline stability than MeOTAS, it is still inferior to the benchmark BTMA.

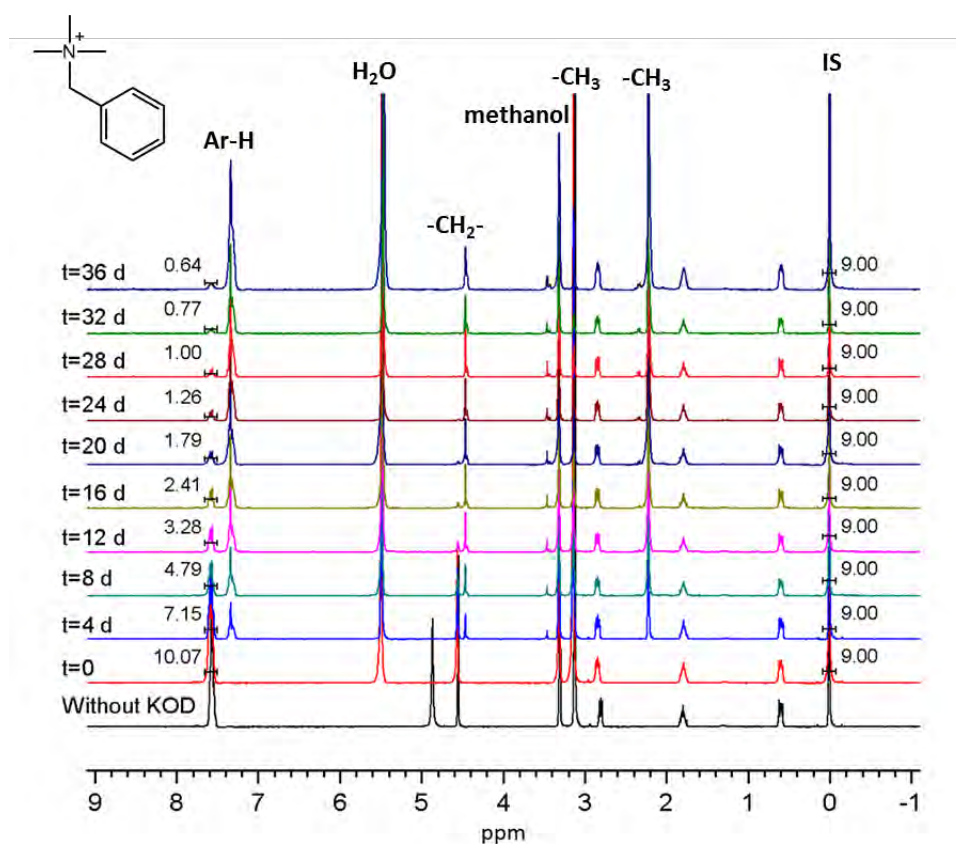


Figure 2.20: Time series of  $^1\text{H}$  NMR spectra during durability test of the benchmark cation BTMA at  $80\text{ }^\circ\text{C}$ .  $\text{TMS}(\text{CH}_2)_3\text{SO}_3\text{Na}$  as the internal standard; 1 M KOD in  $\text{CD}_3\text{OD}/\text{D}_2\text{O}$  (5/1 vol) as the solvent.

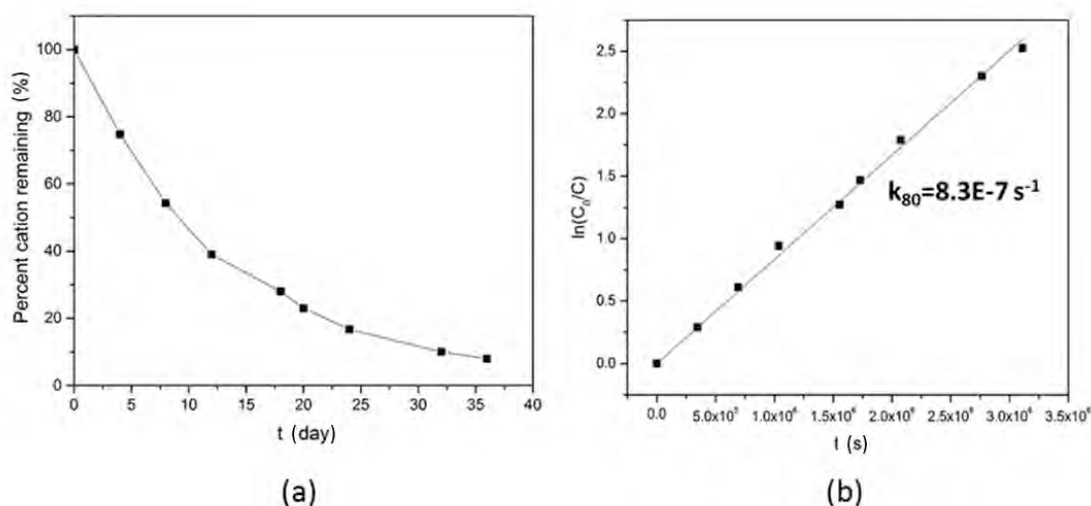


Figure 2.21: (a) Degradation profile and (b) plot of  $\ln(C_0/C)$  versus time of BTMA at 80 °C. 1 M KOD in  $\text{CD}_3\text{OD}/\text{D}_2\text{O}$  (5/1 vol) as the solvent.

The possible explanation for TAS's lower alkaline stability is that in TAS, the central S atom has available  $d$  orbitals for nucleophilic attack. Although the  $\text{S}_{\text{N}}2$  attack at the  $\alpha$ -C has been blocked, the degradation of the S center takes place, which is faster than  $\alpha$ -C  $\text{S}_{\text{N}}2$  attack in BTMA.

## 2.4 Conclusion

In summary, a methoxy-substituted triarylsulfonium functionalized polysulfone (PSf-MeOTASOH) has been successfully synthesized. The PSf-MeOTASOH HEMs are colorless, transparent, and flexible. PSf-MeOTASOH HEM shows excellent thermal stability ( $T_{\text{OD}} = 242 \text{ }^\circ\text{C}$ ), higher than QA-based and QP-based HEMs. With an IEC of  $0.69 \text{ mmol g}^{-1}$ , it exhibits a decent hydroxide conductivity of  $15.4 \text{ mS cm}^{-1}$  at  $20 \text{ }^\circ\text{C}$ , and a high IEC-normalized hydroxide conductivity ( $22.3 \text{ mS g cm}^{-1} \text{ mmol}^{-1}$ ).

The alkaline stabilities of TAS model compounds have been investigated. By increasing the quantity of the electron-donating substituents on the aromatic rings, the alkaline stability of the TAS cation is improved (9MeOTAS>MeOTAS>MeTAS). However, the alkaline stability of the most stable TAS cation (9MeOTAS) was determined to be inferior to the benchmark BTMA, which is the intrinsic limitation for TAS cations. Consequently, in order to mitigate the nucleophilic attack on the central atom, a less reactive central atom is preferred for an alkaline stable cation, which we will discuss in Chapter 3.

## Chapter 3

### DEGRADATION KINETICS AND DEGRADATION MECHANISMS OF PHOSPHONIUM CATIONS IN ALKALINE ENVIRONMENT

The alkaline stabilities of benzyl (tris(2,4,6-trimethoxyphenyl)phosphonium (BTTPP-(2,4,6-MeO)) cation and three QP analogs were quantitatively studied. Their degradation rate constants were obtained and compared with that of the benchmark BTMA. A multi-step degradation mechanism for BTTPP-(2,4,6-MeO) was proposed and verified, which was different from that of the three QP analogs. Through the design of BTTPP-(2,4,6-MeO), two degradation pathways for QP cations ( $\alpha$ -carbon degradation and central atom degradation) have been eliminated. The remaining degradation pathway (ether hydrolysis of the methoxy group) provides us important opportunities for further improvement of the cation stability.

#### 3.1 Introduction

Similar to the TS cation, the QP cation undergo central atom degradation *via* the similar mechanism.<sup>[228-229, 248]</sup> However, different from the trivalent TS cation, the QP cation is tetravalent. The 3D chemical structures of triphenylsulfonium and benzyltriphenylphosphonium show that the central atom of the QP is more sterically protected than that of the TS, resulting in mitigated OH<sup>-</sup> attack at the P center. (Fig. 3.1). Although there is still a possibility for  $\alpha$ -C S<sub>N</sub>2 attack at the benzylic position or the methyl position, the large steric hindrance from the other three aromatic rings could help protect this position from S<sub>N</sub>2 attack (Fig. 3.2). Therefore, the QP cations are considered to be more stable than the TS cations in the alkaline environment.

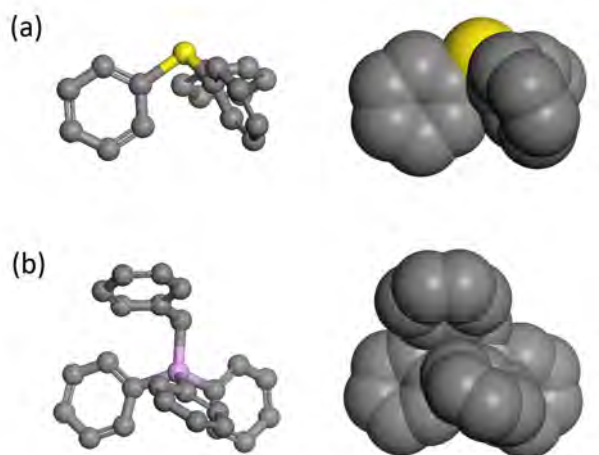


Figure 3.1: 3D chemical structures of (a) triphenylsulfonium and (b) benzyltriphenylphosphonium.

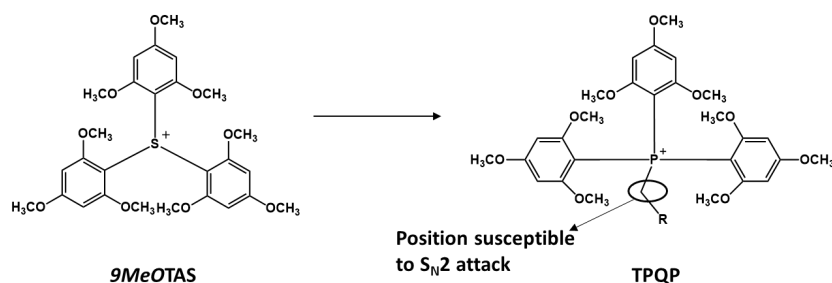


Figure 3.2: Chemical structures of 9MeOTAS and TPQP.

The simple QP cations are unstable and will degrade in aqueous alkaline solution at room temperature in only a few hours.<sup>[248, 250]</sup> To address this problem, our group designed a stabilized QP system (TPQP) by substituting the all of the (2,4,6)-phenyl hydrogens with methoxy groups.<sup>[209]</sup> Benefiting from the strong electron-donating ability and additional steric hindrance of the methoxy groups<sup>[211]</sup>, the alkaline stability of TPQP was significantly improved, and it was found that TPQP based HEMs was more stable than their BTMA analogs. Recently, Ramani et al. observed

the degradation of TPQP functionalized polysulfone in alkali by two-dimensional NMR spectroscopy<sup>[230]</sup>, revealing that there is still room for improvement. However, the intrinsic alkaline stability of TPQP cationic group has not been quantitatively measured and the degradation mechanism is still not clear. Without knowing the exact degradation rate and mechanism, it is not appropriate to compare TPQP with the benchmark cation (in this paper, BTMA) and other further developed cations.

In this chapter, we synthesized a model compound for PSf-TPQP, BTPP-(2,4,6-MeO) (Fig. 3.3), and quantitatively studied its alkaline stability. Three more QP analogs were also synthesized and studied for comparison. Their degradation rate constants were obtained and compared with that of BTMA. A multi-step substituents-related degradation mechanism for BTPP-(2,4,6-MeO) was proposed and verified, which provides us important guidance to further improve the cation stability.

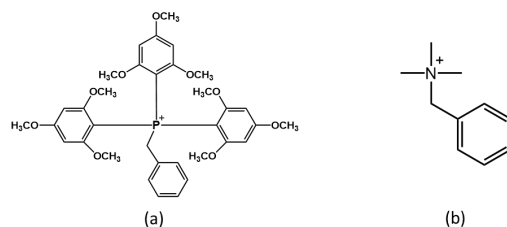


Figure 3.3: Chemical structures of (a) BTPP-(2,4,6-MeO) and (b) BTMA.

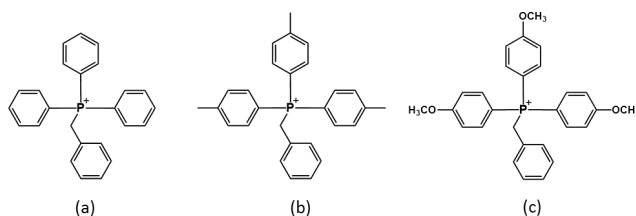


Figure 3.4: Chemical structures of three QP analogs: (a) BTPP, (b) BTPP-(*p*-Me) and (c) BTPP-(*p*-MeO).

## 3.2 Materials and methods

### 3.2.1 Materials and characterization

All the chemicals mentioned in the synthesis were purchased from Sigma-Aldrich and used as received. The  $^1\text{H}$  NMR spectra were measured in deuterated solvents on a Bruker AV400 spectrometer ( $^1\text{H}$ , 400 MHz). The  $^1\text{H}$  NMR chemical shifts are expressed as  $\delta$  downfield from tetramethylsilane (TMS) and calibrated to the residual proton of the deuterated solvent ( $\delta = 7.26$  for chloroform-d). The  $^{31}\text{P}$  NMR spectra were measured in deuterated solvents on a Bruker AV400 spectrometer ( $^{31}\text{P}$ , 161 MHz). The  $^{31}\text{P}$  NMR chemical shifts are expressed as downfield from external 85%  $\text{H}_3\text{PO}_4$ .

### 3.2.2 Experimental methods

**Synthesis of benzyl trimethylammonium bromide (BTMA-Br):** 1.71 g benzyl bromide (10 mmol) and 1.97 g 45 wt% aqueous trimethylamine (15 mmol) were dissolved in 20 mL ethanol. After stirring at room temperature for 24 h, the solvent and trimethylamine were evaporated under vacuum. The residual solid was washed with tetrahydrofuran (THF) three times and dried under vacuum.

BTMA-Br (Fig. 3.3(b)):  $^1\text{H}$  NMR (400 MHz,  $\text{CDCl}_3$ )  $\delta$  7.62-7.51 (5H, m), 4.69 (2H, s), 3.11 (9H, s). Yield: 95 wt%.

**General procedure for synthesizing benzyl based quaternary phosphonium (QP) chloride:** A mixture of the corresponding phosphine (10 mmol) and 2.54 g benzyl chloride (20 mmol) in 10 mL THF was stirred 60 °C for 24 h. The precipitated product was collected by filtration, rinsed three times with THF, and dried under vacuum.<sup>[251]</sup>



Benzyl tris(2,4,6-trimethoxyphenyl)phosphonium chloride (BTPP-(2,4,6-MeO)-Cl) (Fig. 3.3(a)):  $^1\text{H}$  NMR (400 MHz,  $\text{CDCl}_3$ )  $\delta$  7.05-7.03 (3H, m), 6.98-6.95 (2H, m), 6.04 (6H, d,  $J = 4.8$  Hz), 4.59 (2H, d,  $J = 17.2$  Hz), 3.85 (9H, s), 3.61 (18H, s).  $^{31}\text{P}$  NMR (161 MHz,  $\text{CDCl}_3$ )  $\delta$  5.71 (s). Yield: 94 wt%.

Benzyl triphenylphosphonium chloride (BTPP-Cl) (Fig. 3.4(a)):  $^1\text{H}$  NMR (400 MHz,  $\text{CDCl}_3$ )  $\delta$  7.77-7.71 (9H, m), 7.63-7.59 (6H, m), 7.22-7.17 (1H, m), 7.13-7.07 (4H, m), 5.50 (2H, d,  $J = 14.8$  Hz).  $^{31}\text{P}$  NMR (161 MHz,  $\text{CDCl}_3$ )  $\delta$  23.3 (s). Yield: 85 wt%.

Benzyl tris(*p*-methylphenyl)phosphonium chloride (BTPP-(*p*-Me)-Cl) (Fig. 3.4(b)):  $^1\text{H}$  NMR (400 MHz,  $\text{CDCl}_3$ )  $\delta$  7.57-7.51 (6H, m), 7.42-7.38 (6H, m), 7.24-7.19 (1H, m), 7.15-7.11 (2H, m), 7.08-7.05 (2H, m), 5.24 (2H, d,  $J = 14.4$  Hz), 2.46 (9H, s).  $^{31}\text{P}$  NMR (161 MHz,  $\text{CDCl}_3$ )  $\delta$  22.2 (s). Yield: 88 wt%.

Benzyl tris(*p*-methoxyphenyl)phosphonium chloride (BTPP-(*p*-MeO)-Cl) (Fig. 3.4(c)):  $^1\text{H}$  NMR (400 MHz,  $\text{CDCl}_3$ )  $\delta$  7.52-7.46 (6H, m), 7.22-7.17 (1H, m), 7.13-6.99 (10H, m), 4.96 (2H, d,  $J = 14.0$  Hz), 3.86 (9H, s).  $^{31}\text{P}$  NMR (161 MHz,  $\text{CDCl}_3$ )  $\delta$  21.1 (s). Yield: 92 wt%.

#### **Synthesis of tris(2,4,6-trimethoxyphenyl)phosphine oxide (TTMPPO):**

Excess hydrogen peroxide ( $\text{H}_2\text{O}_2$ , 1 mL, 30 wt%) was added to a solution of tris(2,4,6-trimethoxyphenyl)phosphine (TTMPP) (1.00 g, 1.98 mmol) in 10 mL of acetone. The solution was refluxed for 8 h. The resultant solution was cooled, and the volume was reduced to 5 mL under reduced pressure. Diethyl ether (50 mL) was slowly added to give the precipitation of a white crystalline solid. The product was collected by filtration, washed three times with diethyl ether and dried under vacuum.<sup>[252]</sup>

TTMPPO:  $^1\text{H}$  NMR (400 MHz,  $\text{CDCl}_3$ )  $\delta$  6.03 (6H, d,  $J = 4.0$  Hz), 3.79 (9H, s), 3.51 (18H, s).  $^{31}\text{P}$  NMR (161 MHz,  $\text{CDCl}_3$ )  $\delta$  12.6 (s). Yield: 85 wt%.

**Alkaline durability test of BTPP-(2,4,6-MeO):** 1 M deuterated potassium hydroxide (KOD) in  $\text{CD}_3\text{OD}/\text{D}_2\text{O}$  (5/1 vol) solution was prepared by dissolving KOD (40 wt% in  $\text{D}_2\text{O}$ , 4.28 g, 30.0 mmol) in a mixture of deuterated methanol and heavy water ( $\text{CD}_3\text{OD}/\text{D}_2\text{O}$ ) (25 mL/2.67 mL). BTPP-(2,4,6-MeO)-Cl (0.659 g, 1.00 mmol) was added to the alkaline solution to obtain a molar ratio of 30 KOD : 1 model compound (i.e. 0.033 M).  $\text{TMS}(\text{CH}_2)_3\text{SO}_3\text{Na}$  (0.107 g, 0.490 mmol) was added to serve as an internal standard for  $^1\text{H}$  NMR measurements. The mixture was placed in a fluoropolymer lined autoclave. Before the test ( $t = 0$ ), an aliquot of the testing solution was removed and analyzed by  $^1\text{H}$  NMR and  $^{31}\text{P}$  NMR spectroscopy to determine the initial quantity of BTPP-(2,4,6-MeO). Then, the testing solution was held at 80 °C. Aliquots of the reaction were removed periodically (daily for the first 4 days and every 4 days hereafter) and analyzed by  $^1\text{H}$  NMR and  $^{31}\text{P}$  NMR spectroscopy to determine the quantity of BTPP-(2,4,6-MeO) remaining. A control sample with the same recipe but without adding KOD was prepared, and its  $^1\text{H}$  NMR and  $^{31}\text{P}$  NMR were also measured.

**Alkaline durability test of QP analogs:** The three QP analogs were tested under similar condition to the test of BTPP-(2,4,6-MeO), but at lower temperatures (20 °C to 50 °C).

**Calculation of the degradation rate constant ( $k$ ) of BTPP-(2,4,6-MeO) and QP analogs:**  $k_{80}$  (the adjusted degradation rate constant at 80 °C) of BTPP-(2,4,6-MeO) was calculated by plotting  $\ln(C_0/C)$  versus time, and the slope is  $k_{80}$ . Here,  $C_0$  is the initial QP cation concentration, and  $C$  is the QP cation concentration at the

sampling time.  $k_{80}$  of BTPP-(*p*-Me) and BTPP-(*p*-MeO) cannot be acquired directly because of their rapid decomposition at 80 °C. Accordingly, alkaline durability tests under three lower temperatures for each cation were carried out and  $k$  for each temperature was calculated. Arrhenius plot was applied to obtain the activation energy  $E_a$  and then  $k_{80}$ .  $k_{80}$  of BTPP cannot be obtained because it degrades immediately when it mixed with the alkaline solution at room temperature.

### 3.3 Results and discussion

#### 3.3.1 Degradation kinetics of BTPP-(2,4,6-MeO) and QP analogs

This quantitative study focuses on the intrinsic alkaline stabilities of QP model compounds, excluding the influences from the polymer structure, such as phase segregation and the degradation from polymer backbones. Meanwhile, it is essential to ensure that the chemical structure of each QP has sufficient similarity to its polymer-bound form. Polysulfone has been commonly used as the polymer backbone for constructing HEMs.<sup>[25, 96-102]</sup> Accordingly, to mimic the aromatic backbone structure and activated halide functionality of chloromethylated polysulfone, we selected benzyl halide as the quaternizing agent to be attached to the phosphine or amine precursor to acquire BTPP-(2,4,6-MeO) (Fig. 3.3(a)) and BTMA. BTMA was chosen as the benchmark because of its common application in HEMs. Following the same synthesis procedure, three other QP molecules (BTPP, BTPP-(*p*-Me) and BTPP-(*p*-MeO)) (Fig. 3.4) analogous to BTPP-(2,4,6-MeO) were also synthesized, in order to study the influence of the phenyl-substituent on the alkaline stability.

Alkaline durability tests were conducted to BTPP-(2,4,6-MeO) and three QP analogs. Methanol was introduced to acquire better solubility of the model compounds

and to accelerate the cation degradation.<sup>[212]</sup> Each of the model compounds was added to the alkaline solution to obtain a molar ratio of 30 KOD : 1 model compound (i.e. 0.033 M) so that the alkali concentration could be considered constant over the test. TMS(CH<sub>2</sub>)<sub>3</sub>SO<sub>3</sub>Na was added to serve as an internal standard for <sup>1</sup>H NMR measurements. The mixture was held at 80 °C for BTPP-(2,4,6-MeO) or 20 °C for three QP analogs, with <sup>1</sup>H NMR and <sup>31</sup>P NMR spectra taken periodically (Fig. 3.5 and 3.6). The degradation percentage of BTPP-(2,4,6-MeO) was judged by the gradual decrease in area of the largest peak (ortho-methoxy proton,  $\delta = 3.63$  ppm) as compared to the constant area of the largest internal standard peak (methyl proton,  $\delta = 0$  ppm) (Fig. 3.5).

Fig. 3.7(a) showed that over 36 days, BTPP-(2,4,6-MeO) degraded slower than BTMA (e.g., 50% vs 77% degraded after 20 days). As shown in Fig. 3.7(b),  $k_{80}$  for BTPP-(2,4,6-MeO) and BTMA were calculated to be  $4.0\text{E}-7 \text{ s}^{-1}$  and  $8.3\text{E}-7 \text{ s}^{-1}$ , respectively. In other words, BTPP-(2,4,6-MeO) is twice as stable to OH<sup>-</sup> attack as the benchmark BTMA.

Similarly, three QP analogs were subjected to the same durability tests as BTPP-(2,4,6-MeO). All of them completely degraded rapidly (within 5 min) at 80 °C, which is much faster than BTPP-(2,4,6-MeO) and the benchmark BTMA. It indicates that the nine methoxy substituents are the decisive factor for the enhanced stability of the BTPP-(2,4,6-MeO). Because it is hard to achieve  $k_{80}$  of QP analogs directly, the durability tests for QP analogs at three reduced temperatures (20 °C, 30 °C and 40 °C for BTPP-(*p*-Me); and 20 °C, 30 °C and 50 °C for BTPP-(*p*-MeO)) were carried out to slow down the degradations and calculate  $k_{80}$ . The degradation percentage of each QP analogs was judged by  $A_2/(A_1+A_2)$  in <sup>31</sup>P NMR spectra (Fig. 3.8, tested at 20 °C),  $A_1$

is the peak area of generated phosphine oxide peak and  $A_2$  is the peak area of the remaining QP analog.

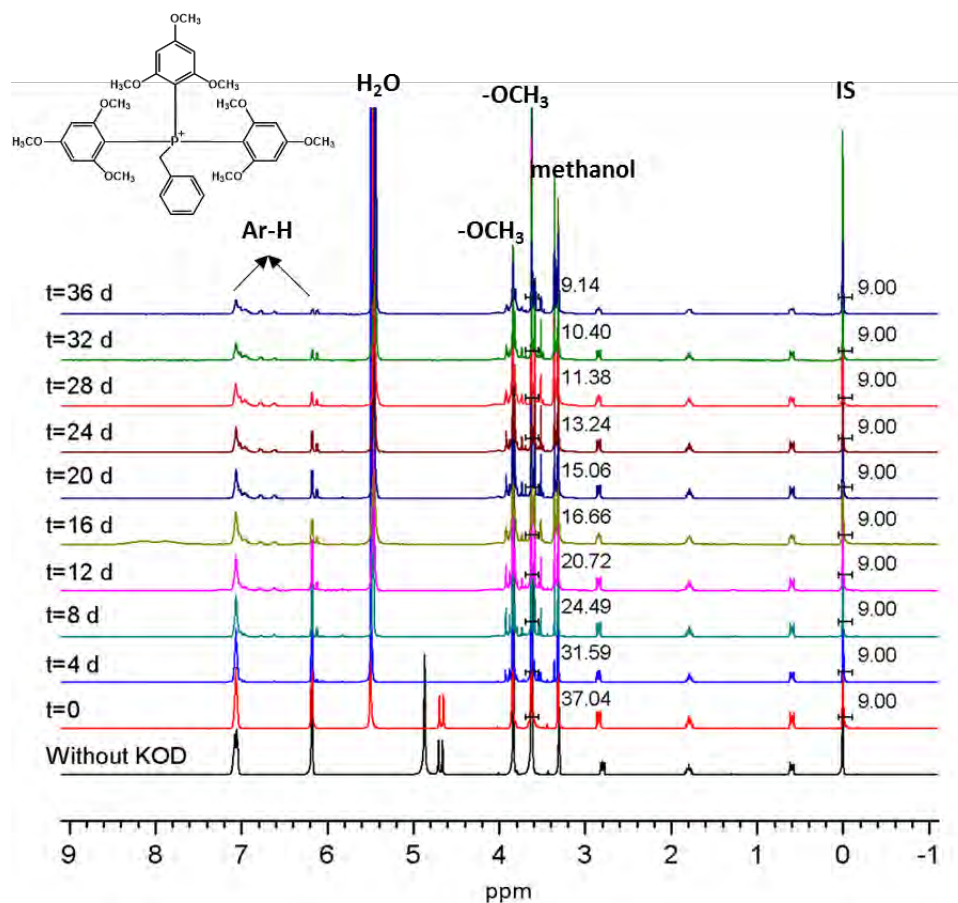


Figure 3.5: Time series of  $^1\text{H}$  NMR spectra during durability test of the BTTP-(2,4,6-MeO) at 80 °C. TMS(CH<sub>2</sub>)<sub>3</sub>SO<sub>3</sub>Na as the internal standard; 1 M KOD in CD<sub>3</sub>OD/D<sub>2</sub>O (5/1 vol) as the solvent.

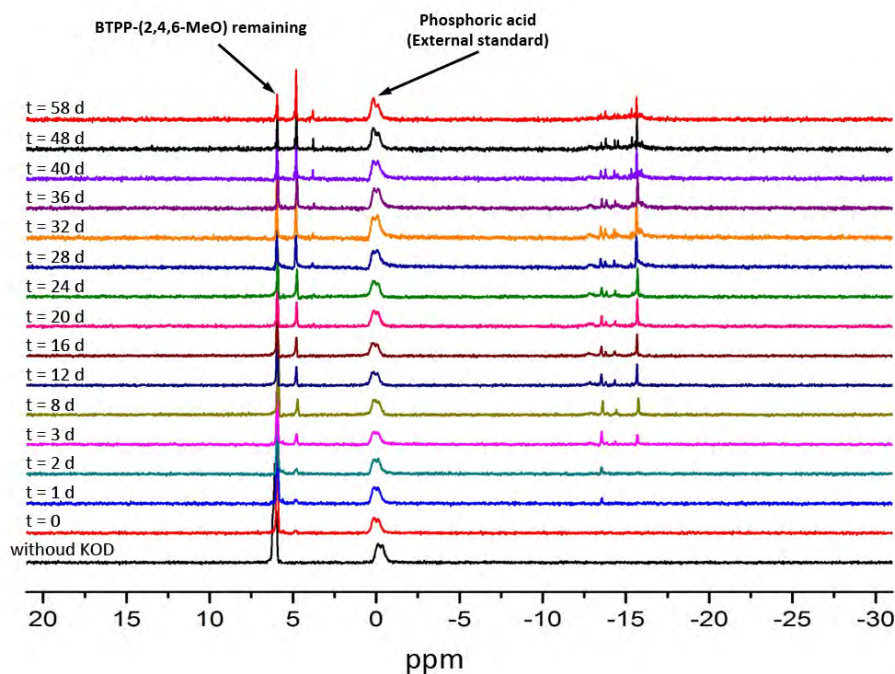


Figure 3.6: Time series of  $^{31}\text{P}$  NMR spectra during durability test of the BTPP-(2,4,6-MeO) at 80 °C. Phosphoric acid as the external standard; 1 M KOD in  $\text{CD}_3\text{OD}/\text{D}_2\text{O}$  (5/1 vol) as the solvent.

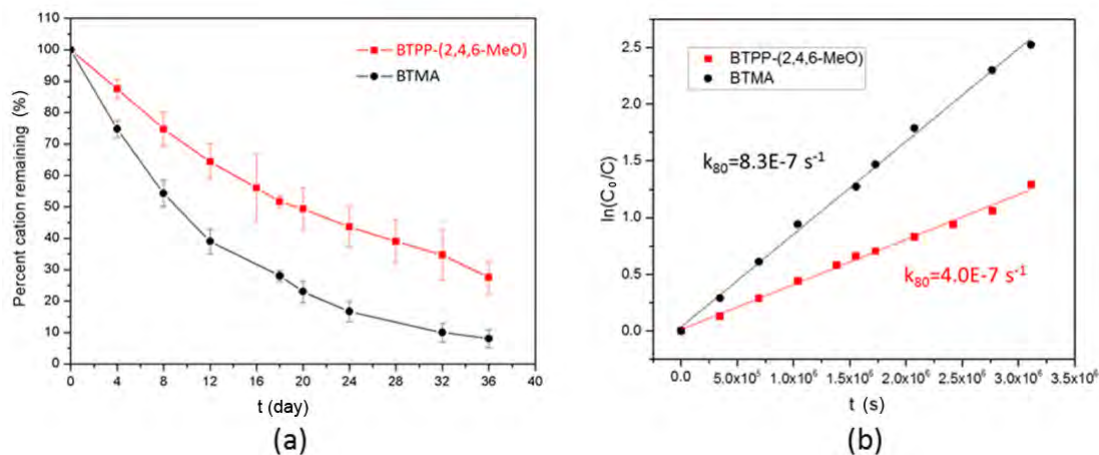
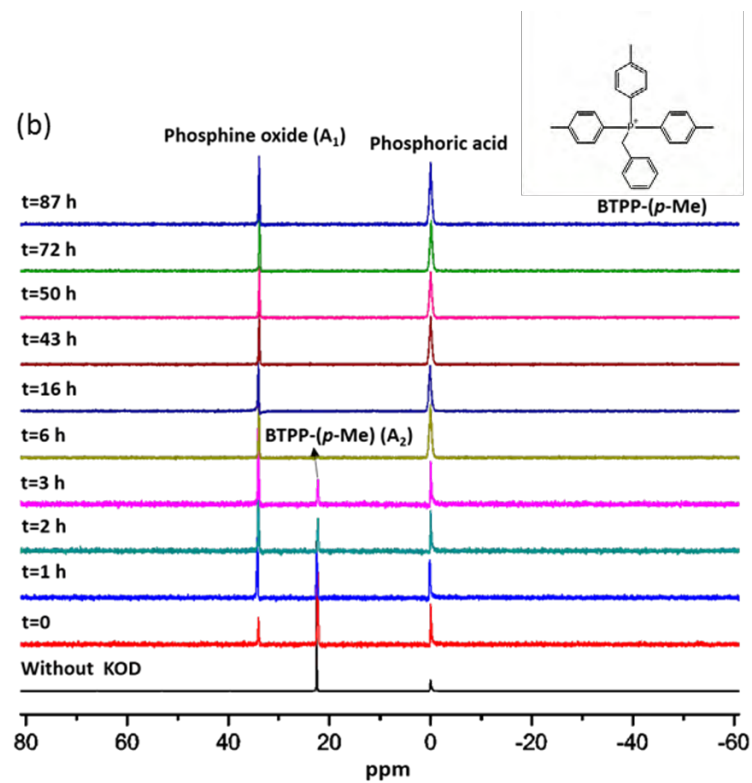
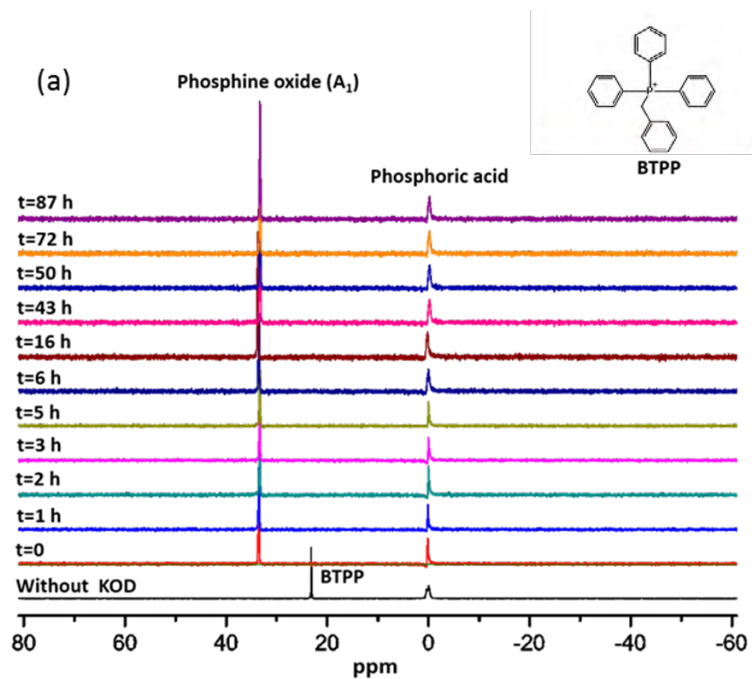


Figure 3.7: (a) Degradation profiles and (b) plots of  $\ln(C_0/C)$  versus time of BTPP-(2,4,6-MeO) and BTMA at 80 °C. 1 M KOD in  $\text{CD}_3\text{OD}/\text{D}_2\text{O}$  (5/1 vol) as the solvent.



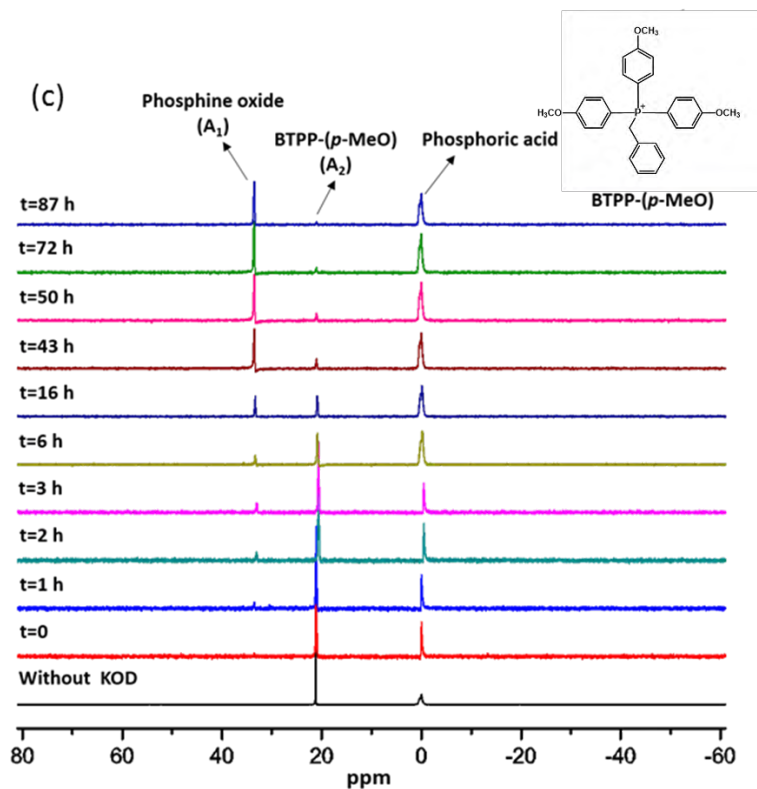


Figure 3.8: Time series of  $^{31}\text{P}$  NMR spectra during durability test of (a) BTTP, (b) BTTP-(*p*-Me) and BTTP-(*p*-MeO) at 20 °C. Phosphoric acid as the external standard; 1 M KOD in  $\text{CD}_3\text{OD}/\text{D}_2\text{O}$  (5/1 vol) as the solvent.

Fig. 3.9 showed that at 20 °C, all of the three QP analogs completely degraded within a week. The alkaline stabilities of three QP analogs rank as BTTP-(*p*-MeO) > BTTP-(*p*-Me) >> BTTP. As the phenyl-substituent changing from -H (weakly electron donating) to -Me to -OMe (strongly electron donating), the alkaline stability increased. By conducting Arrhenius plots (Fig. 3.10 and 3.11),  $k_{80}$  for BTTP-(*p*-Me) and BTTP-(*p*-MeO) were calculated to be  $9.7\text{E}-2 \text{ s}^{-1}$  and  $1.3\text{E}-3 \text{ s}^{-1}$  respectively.



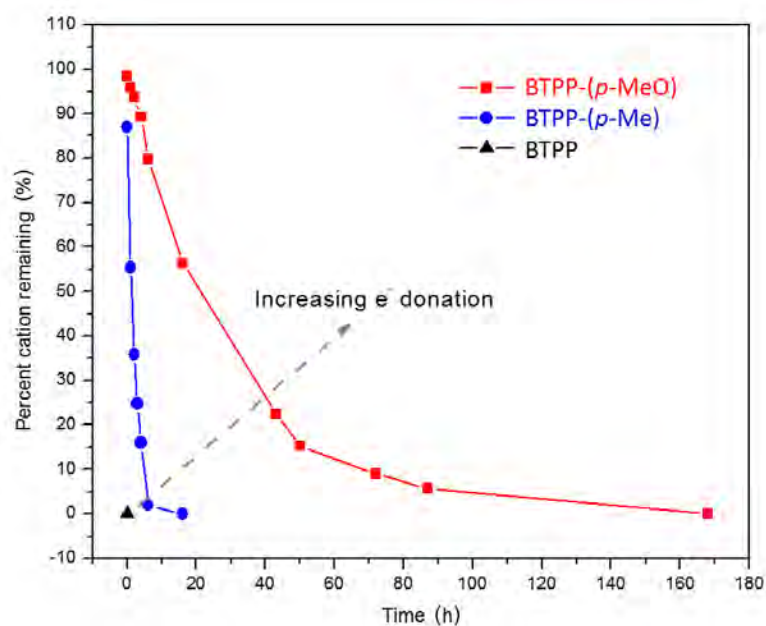


Figure 3.9: Degradation profiles of QP analogs at 20 °C. 1 M KOD in CD<sub>3</sub>OD/D<sub>2</sub>O (5/1 vol) as the solvent.

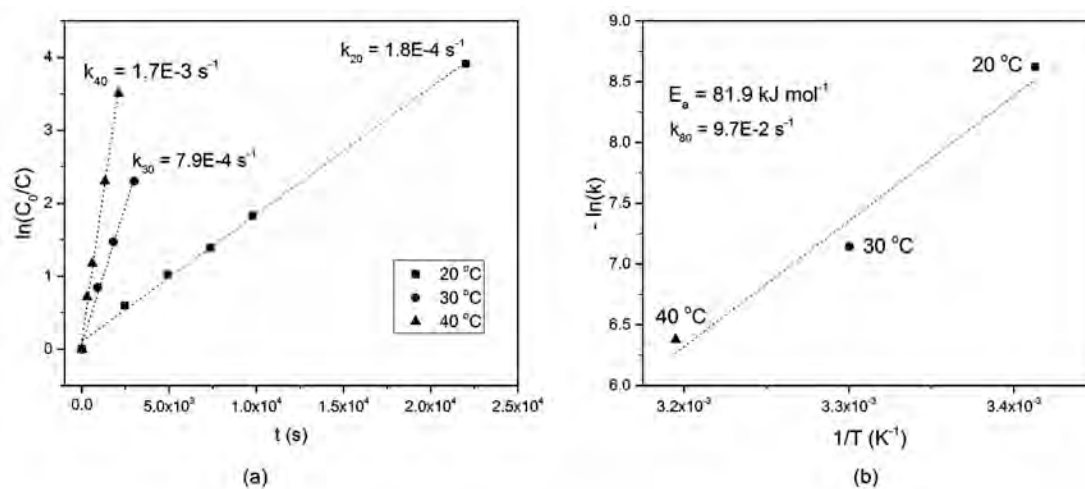


Figure 3.10: (a) Plots of  $\ln(C_0/C)$  of BTPP-(*p*-Me) versus time at three different temperatures (20 °C, 30 °C and 40 °C); (b) Arrhenius plot ( $-\ln(k)$  vs  $1/T$ ) of BTPP-(*p*-Me).

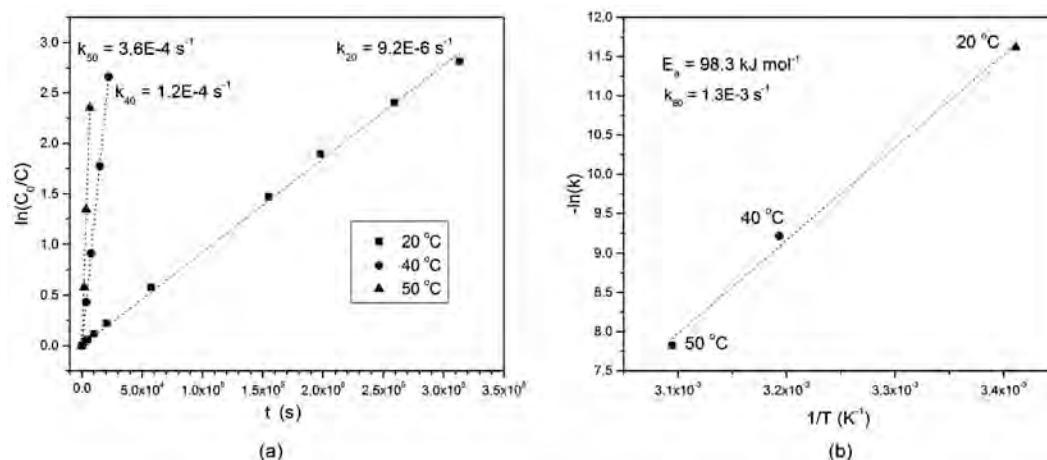


Figure 3.11: (a) Plots of  $\ln(C_0/C)$  of BTTP-(*p*-MeO) versus time at three different temperatures (20 °C, 40 °C and 50 °C); (b) Arrhenius plot ( $-\ln(k)$  vs  $1/T$ ) of BTTP-(*p*-MeO).

Table 3.1 summarizes  $k_{80}$  for all the cations studied in this chapter, except BTTP ( $k_{80}$  for BTTP cannot be measured due to its rapid degradation at room temperature). BTTP-(2,4,6-MeO) is several orders of magnitude more stable to OH<sup>-</sup> attack than the QP analogs (5 orders for BTTP-(*p*-Me) and 3 orders for BTTP-(*p*-MeO)) and twice as stable as the benchmark BTMA.

Table 3.1: Summary of  $k_{80}$  of cations studied in this chapter.

Cation	(a) BTTP	(b) BTTP-( <i>p</i> -Me)	(c) BTTP-( <i>p</i> -MeO)	(d) BTMA	(e) BTTP-(2,4,6-MeO)
$k_{80} \text{ (s}^{-1}\text{)}$	N/A	9.7E-2	1.3E-3	8.3E-7	4.0E-7

### 3.3.2 Degradation mechanisms of BTTP-(2,4,6-MeO) and QP analogs

To understand the factors that influence the alkaline stability, the degradation mechanism for each QP cation was studied in detail by identifying its degradation products. Under our testing conditions, BTMA has been found to undergo two  $\alpha$ -C  $S_N2$  degradation pathways (benzylic substitution and methyl substitution). The degradation products of each QP analog were investigated to see whether such  $S_N2$  degradation pathways take place for QP analogs. If the  $S_N2$  attack at the benzylic position takes place, the corresponding phosphine would be produced (Fig. 3.12). Taking BTTP as an example, after complete decomposition, no phosphine ( $\delta = -6.75$  ppm) but phosphine oxide ( $\delta = 33.3$  ppm) was detected in its degradation products by  $^{31}\text{P}$  NMR measurements (Fig. 3.13). The same degradation behavior was also observed for the other two QP analogs. It reveals that no  $\alpha$ -C  $S_N2$  attack takes place in QP analogs, confirming that the benzylic position in QP cations is resistant to  $\text{OH}^-$  attack.

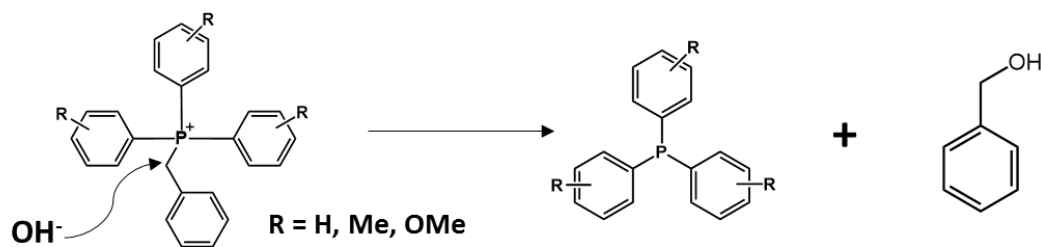


Figure 3.12: Degradation products of QP analogs if  $S_N2$  benzylic substitution takes place.

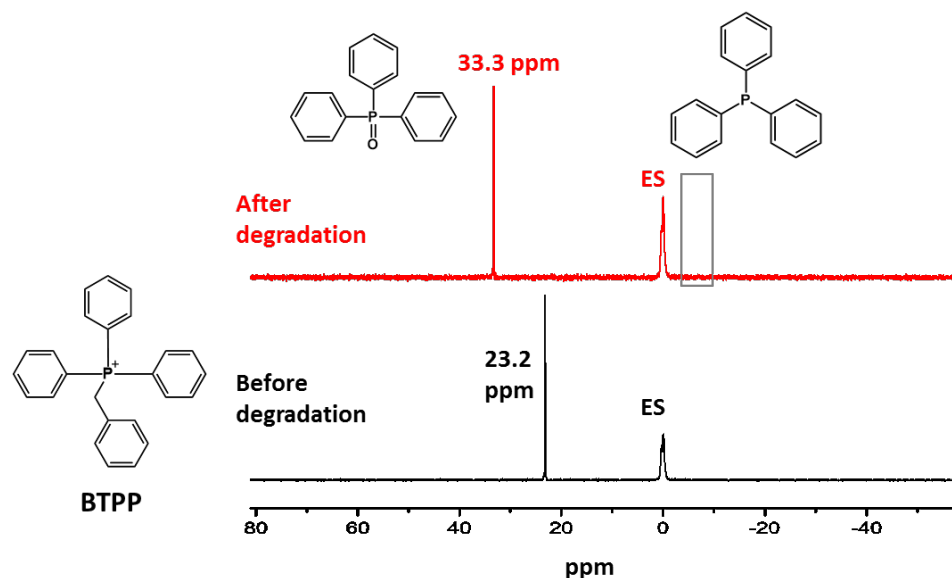


Figure 3.13:  $^{31}\text{P}$  NMR spectra of BTTP before and after degradation at 20 °C. Phosphoric acid as the external standard; 1 M KOD in  $\text{CD}_3\text{OD}/\text{D}_2\text{O}$  (5/1 vol) as the solvent.

The formation of phosphine oxide indicated that the  $\text{OH}^-$  attack takes place at the central atom, similar to the TAS case. For each of the three QP analogs, toluene and the corresponding phosphine oxide were detected in its degradation products, confirming that they all underwent Cahours–Hofmann reaction to degrade.<sup>[250]</sup> This reaction involves the attack of hydroxide ion on a transient pentacovalent adduct arising from a phosphonium cation and a second hydroxide (Fig. 3.14). Based on this degradation mechanism, higher electron density on the central P atom (electronic effect) and larger steric hindrance around the central P atom (steric effect) would reduce the possibility of  $\text{OH}^-$  attack, and thus mitigate the central atom degradation. The contribution from the electronic effect has been clearly demonstrated by the kinetic studies of three QP analogs. The steric effect will be discussed in Chapter 4.

Therefore, protecting the central P atom both electronically and sterically is critical to stabilize QP cations.

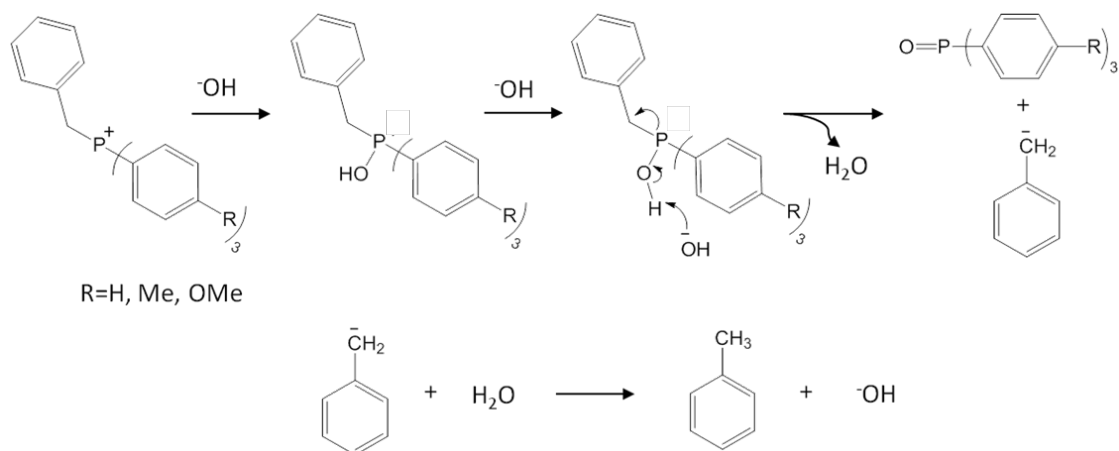


Figure 3.14: Degradation mechanism of QP analogs in alkaline media.

Based on the above trend, it can be expected that the formation of phosphine oxide for BTPP-(2,4,6-MeO) would be even more difficult, because the strong electron donation and additional steric hindrance provided by the nine methoxy groups would better protect the P center. As expected, neither phosphine oxide (synthesized separately,  $^{31}\text{P}$  NMR: 16.8 ppm in  $\text{CDCl}_3$ ) nor toluene ( $^1\text{H}$  NMR:  $\delta = 7.09\sim 7.23$  ppm in  $\text{CDCl}_3$ ) was produced in the degradation products of BTPP-(2,4,6-MeO) (Fig. 3.15), indicating that Cahours–Hofmann reaction did not take place during the durability test. Also, the  $\alpha\text{-C}$   $\text{S}_{\text{N}}2$  attack didn't take place for BTPP-(2,4,6-MeO). Multiple new  $^{31}\text{P}$  peaks generated after degradation (Fig. 3.6) indicates that BTPP-(2,4,6-MeO) was undergoing a completely different degradation process.

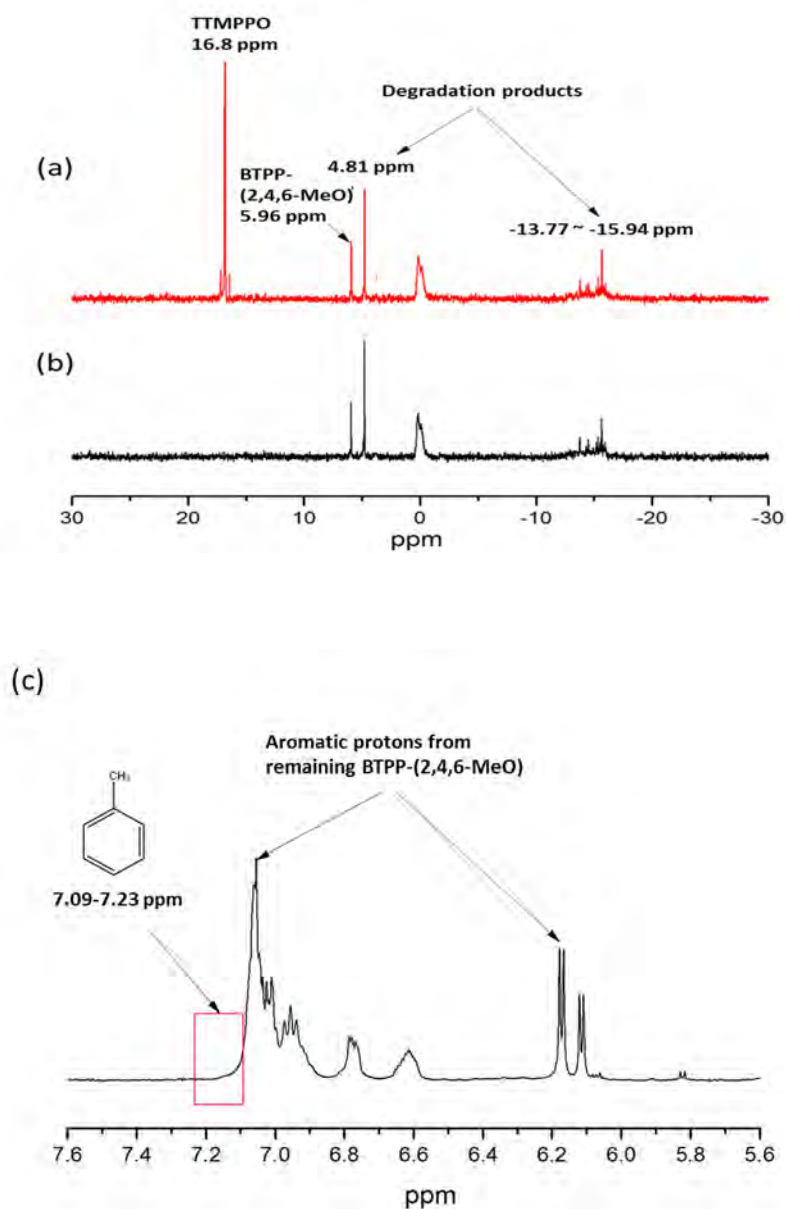


Figure 3.15: Evidence that the BTTP-(2,4,6-MeO) degrades by a different mechanism than QP analogs. (a)  $^{31}\text{P}$  NMR Spectra of BTTP-(2,4,6-MeO) after 32 days' test, with phosphine oxide (TTMPPO) added; (b)  $^{31}\text{P}$  NMR of BTTP-(2,4,6-MeO) after 32 days' test, showing no trace of TTMPPO at 16.8 ppm; (c)  $^1\text{H}$  NMR spectrum showing no trace of toluene from 7.09 to 7.23 ppm. The box indicate where the toluene would be found, if present.

To account for BTPP-(2,4,6-MeO)'s degradation behavior, a multi-step mechanism (Fig. 3.16) was proposed based on a detailed analysis of the degradation products, including ether hydrolysis, inner salt formation, ketone rearrangement and further hydrolysis. First, one methoxy group on the benzene ring is hydrolyzed in base to form a hydroxyl group, generating methanol. Second, a hydroxide in the solution strips the proton from the hydroxyl group, leading to the formation of phosphonium inner salt. Third, the inner salt rearranges to form its resonance structure which has a ketone structure and a C=P double bond. Finally, the remaining methoxy groups undergo ether hydrolysis to form hydroxyl groups. To verify the proposed mechanism, we investigated each step individually.

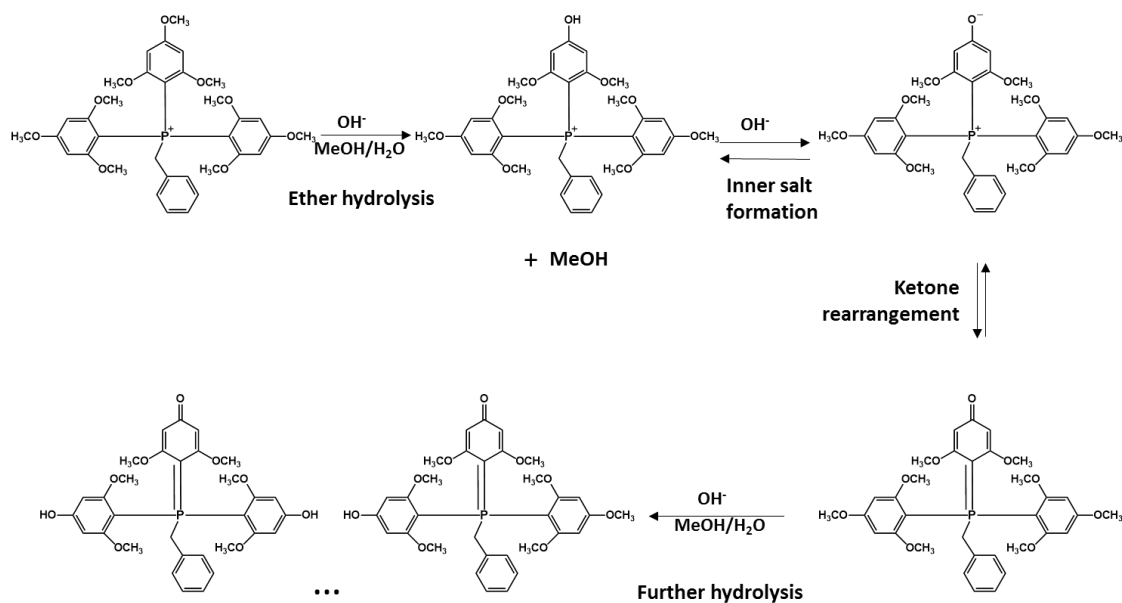


Figure 3.16: Proposed degradation mechanism of BTPP-(2,4,6-MeO) in alkaline media.

### 3.3.3 Verification of the proposed degradation mechanism of BTPP-(2,4,6-MeO)

Degradation step 1 is the hydrolysis of methoxy group on the benzene ring to form a phenol. Researches have shown that anisole can degrade into phenol in KOH/ethanol solution at high temperature (180-200 °C), producing methanol.<sup>[253]</sup> Thus, analogous step can be verified by detecting the formation of methanol as a degradation product. However, deuterated methanol was already present in our test solution as the solvent, rendering detection of a small quantity of methanol by <sup>1</sup>H NMR difficult. We solved this problem by changing the solvent from deuterated methanol to deuterated ethanol for one test (Fig. 3.17). A new peak (<sup>1</sup>H NMR:  $\delta$  = 3.33 ppm) was produced over time. With additional methanol added to the degradation product (at  $t$  = 7 days), the new NMR peak overlapped perfectly with methanol peak, confirming that ether hydrolysis takes place.

Step 2 is the formation of phosphonium inner salt from the phenol structure. Researchers have reported the formation of phosphonium inner salt from their corresponding hydroxyphenyl phosphonium salts in the presence of a base.<sup>[254]</sup> In verifying this step, hydrochloric acid was added to the degradation products to force the back reaction from inner salt to *p*-hydroxyphenyl phosphonium salt. Before adding the acid (Fig. 3.18(a)), A is the initial BTPP-(2,4,6-MeO) peak (<sup>31</sup>P NMR:  $\delta$  = 5.96 ppm), and B is the inner salt peak (<sup>31</sup>P NMR:  $\delta$  = 4.81 ppm). After adding the acid, B in Fig. 3.18(a) shifted downfield to become C in Fig. 3.18(b), which is the peak for *p*-hydroxyphenyl phosphonium (<sup>31</sup>P NMR:  $\delta$  = 5.83 ppm). The proximity of the resultant C to A in the <sup>31</sup>P spectrum is due to the strong structural similarity of these species near the P center.



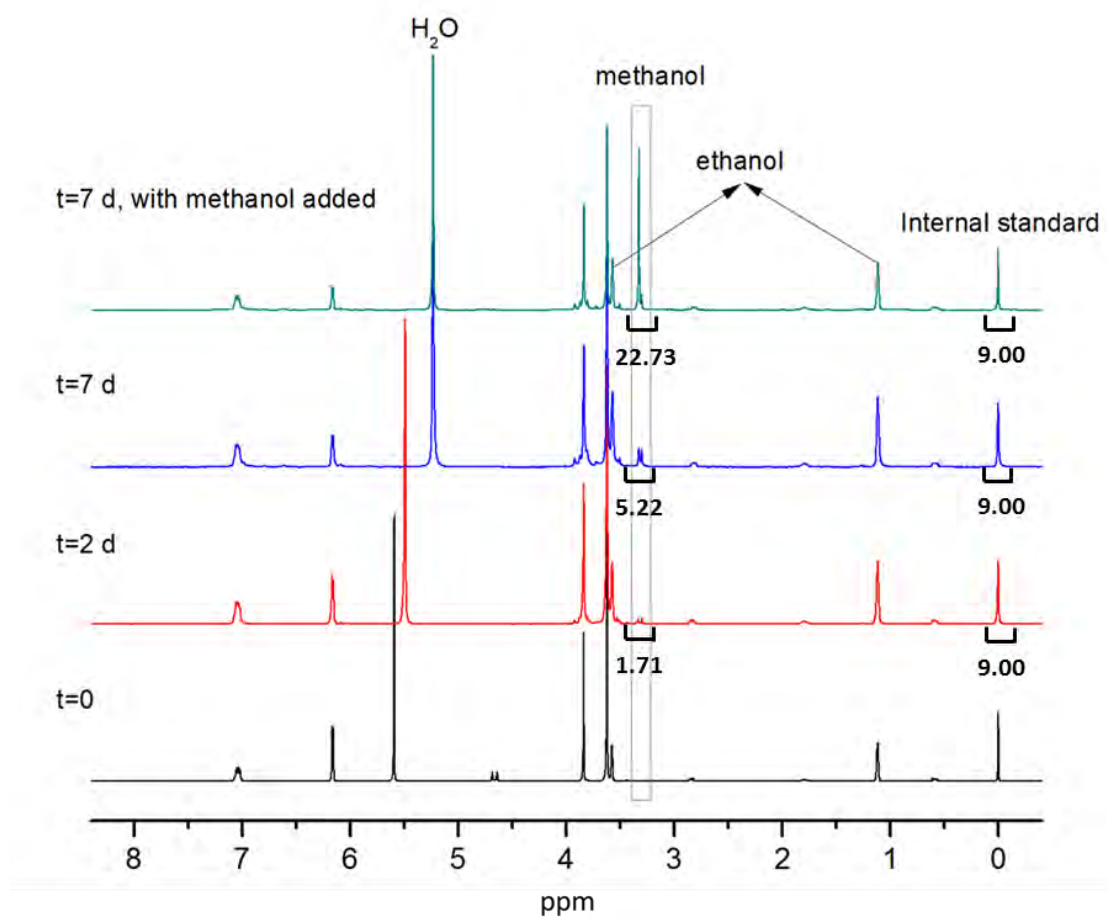


Figure 3.17: Evidence of ether hydrolysis during degradation. Another degradation test was performed in ethanol instead of methanol, resulting in the  $^1\text{H}$  NMR spectra shown above. The methanol production peak is boxed. Solvent: 1 M KOD in  $\text{CD}_3\text{CD}_2\text{OD}/\text{D}_2\text{O}$  (5/1 vol).

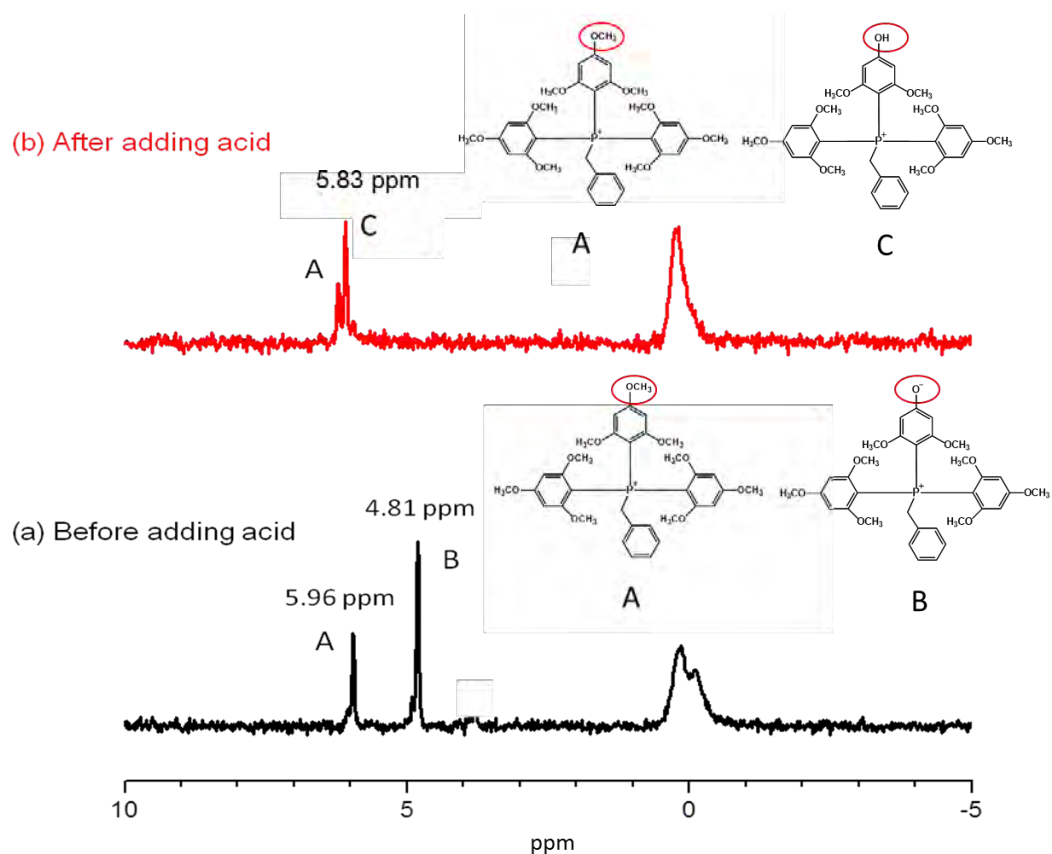


Figure 3.18: Evidence of inner salt formation during degradation. (a)  $^{31}\text{P}$  NMR spectrum of degradation products, showing BTTPP-(2,4,6-MeO) (peak A) and the inner salt degradation product (peak B); (b) Same spectrum after addition of HCl. The acid protonates the inner salt, eliminating peak B and generating peak C.

Step 3 is the ketone rearrangement of the inner salt. Horner et al. proposed that phosphonium inner salt generated from *p*-hydroxyphenyl phosphonium salt could rearrange into a resonance-stabilized structure.<sup>[254-255]</sup> ATR-FTIR spectra identified that a characteristic ketone absorption peak ( $1738\text{ cm}^{-1}$ ) showed up after degradation (Fig. 3.19), indicating the formation of the resonance structure. In  $^{31}\text{P}$  NMR spectra (Fig. 3.20), the product of ketone arrangement appears at  $-13.5\text{ ppm}$ .

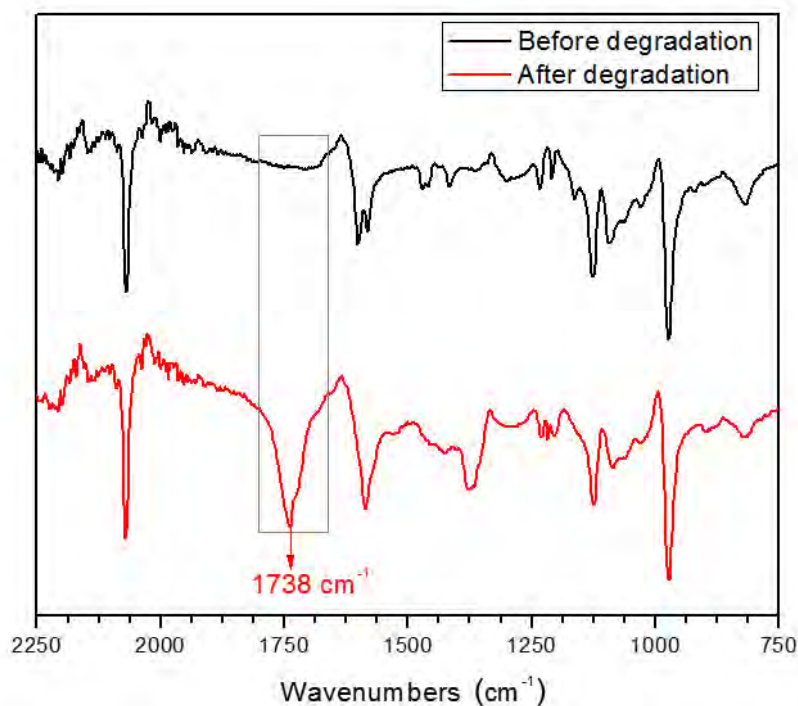


Figure 3.19: Evidence of ketone formation during degradation. This ATR-FTIR spectrum shows a characteristic ketone peak only after degradation.

The first three steps demonstrate the degradation process of one methoxy group in BTPP-(2,4,6-MeO). However, BTPP-(2,4,6-MeO) possesses nine methoxy groups, and all of them could be hydrolyzed. As for Step 4 (further hydrolysis), the  $^{31}\text{P}$  NMR spectra (Fig. 3.20) suggested that multiple similar products form after ketone rearrangement ( $^{31}\text{P}$  NMR:  $-13.8\sim-15.6$  ppm), consistent with statistical hydrolysis of the remaining methoxy substituents into hydroxyl groups.

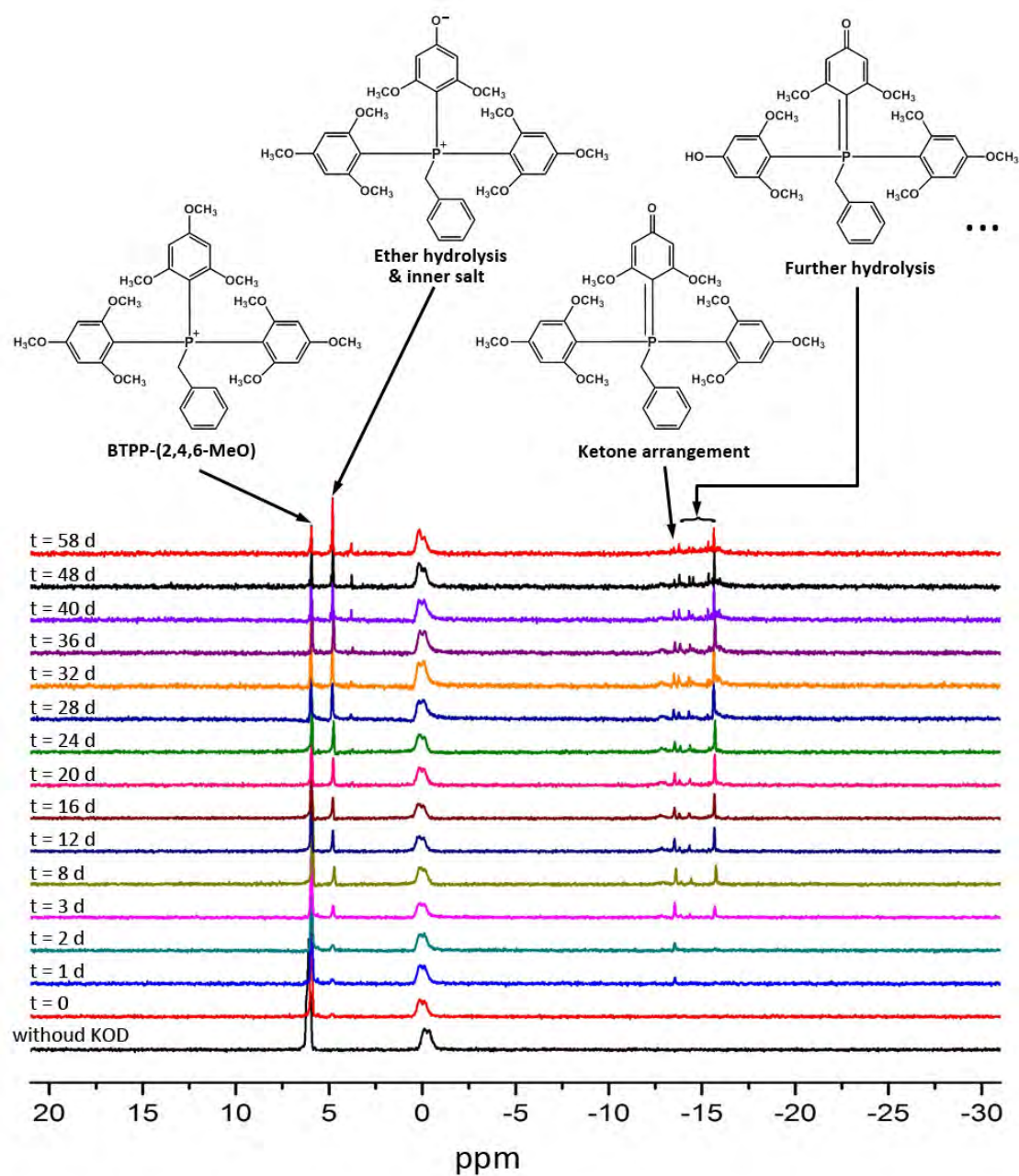


Figure 3.20:  $^{31}\text{P}$  NMR assignment of BTPP-(2,4,6-MeO) after degradation at 80 °C. Phosphoric acid as the external standard. 1 M KOD in  $\text{CD}_3\text{OD}/\text{D}_2\text{O}$  (5/1 vol) as the solvent.

This new mechanism demonstrates that due to the strong electron donation of the nine methoxy groups on benzene rings, the P center becomes less susceptible to  $\text{OH}^-$  nucleophilic attack so that the essential structure of BTPP-(2,4,6-MeO) remains intact during the durability test. It explains why the overall alkaline stability of BTPP-(2,4,6-MeO) is significantly higher compared with the three QP analogs and even BTMA. However, because the methoxy group itself is not resistant to alkaline aqueous environment, it becomes the weakest point within the QP cation and causes the degradation before the entire cation structure falling apart. This finding indicates that if we could find some phenyl-substituent that not only provides sufficient electron donation but also has high stability in alkaline aqueous environment, the cation stability would be further improved.

### 3.4 Conclusion

In summary, the alkaline stabilities of BTPP-(2,4,6-MeO) and three QP analogs were quantitatively studied.  $k_{80}$  of each cation was calculated and compared with the benchmark BTMA (Table 3.1). BTPP-(2,4,6-MeO) shows better alkaline stability than the three QP analogs and even the ammonium benchmark BTMA. For the three QP analogs, as the electron-donating ability of the phenyl-substituent increasing, the cation stability improves.

Different from QA cations (hydroxide usually attacks the substituents on N atom, not the center N atom itself), all of the three QP analogs degrade through Cahours-Hofmann pathway. No  $\alpha\text{-C S}_{\text{N}}2$  degradation takes place, confirming the benzylic position is well protected in QP cations.

With respects to BTPP-(2,4,6-MeO), it undergoes a completely different degradation mechanism, which is substituent-related. Neither  $\alpha\text{-C S}_{\text{N}}2$  attack nor

center atom degradation takes place. A new degradation mechanism has been proposed and verified, which demonstrates that not only the P center atom, but also the phenyl-substituents can undergo degradation in alkaline environment. With nine strong electron-donating phenyl-substituents, the P center becomes less susceptible to  $\text{OH}^-$  nucleophilic attack so that the essential structure of BTPP-(2,4,6-MeO) remains intact during the durability test. It explains why the overall alkaline stability of BTPP-(2,4,6-MeO) is significantly higher than that of the three QP analogs and even BTMA. However, the methoxy group itself is susceptible to nucleophilic attack in alkaline environment, and thus becomes point of decomposition within the cation. The methoxy group undergoes ether hydrolysis, and triggers an alternative degradation before the entire cation structure decomposes.

Through the novel design of BTPP-(2,4,6-MeO), we have successfully eliminated the two primary degradation pathways for QP cations ( $\alpha$ -C degradation and central atom degradation). The remaining degradation pathway *via*  $\text{OH}^-$  attack is the substituents degradation. Further efforts will focus on phenyl-substituents that provide sufficient electron donation and high stability in alkaline environment, to further the cation stability. Chapter 4 will show our efforts in further stabilizing QP cations.

## Chapter 4

### DESIGN OF AN ALKALINE STABLE PHOSPHONIUM CATION

Inspired by the unusual degradation mechanism of (BTPP-(2,4,6-MeO)), a superior QP cation, methyl tris(2,4,6-trimethoxyphenyl)phosphonium (MTPP-(2,4,6-Me)) was developed with ultra-high alkaline stability (80 °C, 1 M KOD, CD<sub>3</sub>OD/D<sub>2</sub>O (v/v = 5/1) solution, less than 20% degradation over 200 days test), which is 31 times as stable as BTPP-(2,4,6-MeO) (the most stable QP cation before) and 64 times as stable as BMTA (the benchmark cation). MTPP-(2,4,6-Me) demonstrates a level of stability that has not been achieved by any other known HEM cation.

Through a systematic study of a series of QP cations, the structure-property relationships were evaluated, to aid in the design of superior QP cations for HEM applications.

#### 4.1 Introduction

In Chapter 3, we studied the degradation kinetics and degradation mechanism of BTPP-(2,4,6-MeO). BTPP-(2,4,6-MeO) was shown to eliminated two primary degradation pathways for QP cations ( $\alpha$ -C degradation and central atom degradation). The remaining degradation pathway triggered by OH<sup>-</sup> attack is the substituent's degradation, i.e. the methoxy substituent undergoes ether hydrolysis in alkaline environment, and triggers a new type of degradation. Accordingly, we propose that if we could find some phenyl-substituent that not only provides sufficient electron

donation but also has high stability in alkaline environment, the cation stability would be further improved.

The methyl group is stable in alkaline media, and it also possesses an electron-donation ability which can increase the electron density on P to prevent the OH<sup>-</sup> attack. Additionally, according to Taft's theory<sup>[256-258]</sup>, the methyl group has a more negative steric substituent constant ( $E_s$ ) (the definition of  $E_s$  and can be found in Appendix B) than the methoxy group ( $E_s(\text{Me}) = -1.24$ ,  $E_s(\text{MeO}) = -0.55$ ; reference:  $E_s(\text{H}) = 0$ ), meaning that the methyl substituent has a larger steric hindrance than the methoxy substituent.<sup>[259]</sup> Despite methoxy's larger size, C-O bond rotation allows the trailing methyl substituent to minimize steric repulsion. Therefore, in order to design a superior QP cation, we target to replace all nine methoxy groups with methyl groups to eliminate the ether hydrolysis degradation and take the advantage of methyl's larger steric hindrance.

Understanding the structure-property relationships would provide important guidance for further improving the cation stability. Therefore, we decide to extend our study to a wider range of QP cations and try to find out some useful principles.

## 4.2 Materials and methods

### 4.2.1 Materials and characterization

All the chemicals mentioned in the synthesis were purchased from Sigma-Aldrich and used as received. The <sup>1</sup>H NMR spectra were measured in deuterated solvents on a Bruker AV400 spectrometer (<sup>1</sup>H, 400 MHz). The <sup>1</sup>H NMR chemical shifts are expressed as  $\delta$  downfield from tetramethylsilane (TMS) and calibrated to the residual proton of the deuterated solvent ( $\delta = 7.26$  ppm for chloroform-d). The <sup>31</sup>P



NMR spectra were measured in deuterated solvents on a Bruker AV400 spectrometer ( $^{31}\text{P}$ , 161 MHz). The  $^{31}\text{P}$  NMR chemical shifts are expressed as downfield from external 85%  $\text{H}_3\text{PO}_4$ .

#### 4.2.2 Experimental methods

**General procedure for synthesizing methyl based quaternary phosphonium salts:** A mixture of the corresponding phosphine (10 mmol) and 2 mL iodomethane (32 mmol) was stirred at room temperature for 24 h. The precipitated product was collected by filtration, rinsed three times with THF, and dried under vacuum.<sup>[260]</sup>

Methyl tris(2,4,6-trimethylphenyl)phosphonium iodide (MTPP-(2,4,6-Me)-I) (Table. 4.2(a)):  $^1\text{H}$  NMR (400 MHz,  $\text{CDCl}_3$ )  $\delta$  7.06 (6H, dd,  $J = 84.0, 3.2$  Hz), 2.94 (3H, d,  $J = 11.2$  Hz), 2.35 (18H, d,  $J = 5.2$  Hz), 1.91 (9H, s).  $^{31}\text{P}$  NMR (161 MHz,  $\text{CDCl}_3$ )  $\delta$  6.53 (s). Yield: 95 wt%.

Methyl tris(2,4,6-trimethoxyphenyl)phosphonium iodide (MTPP-(2,4,6-MeO)-I) (Table. 4.2(b)):  $^1\text{H}$  NMR (400 MHz,  $\text{CDCl}_3$ )  $\delta$  6.14 (6H, d,  $J = 4.8$  Hz), 3.90 (9H, s), 3.61 (18H, s), 2.47 (3H, d,  $J = 15.2$  Hz).  $^{31}\text{P}$  NMR (161 MHz,  $\text{CDCl}_3$ )  $\delta$  -3.79 (s). Yield: 96 wt%.

Methyl tris(2,6-trimethoxyphenyl)phosphonium iodide (MTPP-(2,6-MeO)-I) (Table. 4.2(d)):  $^1\text{H}$  NMR (400 MHz,  $\text{CDCl}_3$ )  $\delta$  7.54 (3H, t,  $J = 8.4$  Hz), 6.63 (6H, dd,  $J = 8.8, 5.6$  Hz), 3.59 (18H, s), 2.60 (3H, d,  $J = 15.2$  Hz).  $^{31}\text{P}$  NMR (161 MHz,  $\text{CDCl}_3$ )  $\delta$  -1.84 (s). Yield: 92 wt%.

Methyl tris(*o*-methoxyphenyl)phosphonium iodide (MTPP-(*o*-MeO)-I) (Table. 4.2(f)):  $^1\text{H}$  NMR (400 MHz,  $\text{CDCl}_3$ )  $\delta$  7.80 (3H, t,  $J = 7.6$  Hz), 7.25 (3H, t,  $J = 6.4$

Hz), 7.13 (3H, td,  $J = 7.6, 2.8$  Hz), 6.97 (3H, ddd,  $J = 23.6, 8.0, 1.6$  Hz), 3.87 (9H, s), 2.74 (3H, d,  $J = 15.2$  Hz).  $^{31}\text{P}$  NMR (161 MHz,  $\text{CDCl}_3$ )  $\delta$  20.1 (s). Yield: 89 wt%.

Methyl tris(*o*-methylphenyl)phosphonium iodide (MTPP-(*o*-Me)-I) (Table. 4.2(h)):  $^1\text{H}$  NMR (400 MHz,  $\text{CDCl}_3$ )  $\delta$  7.73 (3H, t,  $J = 7.6$  Hz), 7.55 (3H, t,  $J = 6.0$  Hz), 7.43 (3H, t,  $J = 8.0$  Hz), 7.23 (3H, dd,  $J = 15.2, 7.6$  Hz), 3.20 (3H, d,  $J = 13.2$  Hz), 2.40 (9H, s).  $^{31}\text{P}$  NMR (161 MHz,  $\text{CDCl}_3$ )  $\delta$  21.7 (s). Yield: 86 wt%.

Methyl tris(*p*-methoxyphenyl)phosphonium iodide (MTPP-(*p*-MeO)-I) (Table. 4.2(i)):  $^1\text{H}$  NMR (400 MHz,  $\text{CDCl}_3$ )  $\delta$  7.59 (6H, dd,  $J = 12.8, 8.8$  Hz), 7.14 (6H, dd,  $J = 2.8$  Hz), 3.89 (9H, s), 2.93 (3H, d,  $J = 13.2$  Hz).  $^{31}\text{P}$  NMR (161 MHz,  $\text{CDCl}_3$ )  $\delta$  18.8 (s). Yield: 91 wt%.

**General procedure for synthesizing benzyl based quaternary phosphonium salts:** A mixture of the corresponding phosphine (10 mmol) and 2.54 g benzyl chloride (20 mmol) in 10 mL THF was stirred at 60 °C for 24 h. The precipitated product was collected by filtration, rinsed three times with THF, and dried under vacuum.

Benzyl (tris(2,6-trimethoxyphenyl)phosphonium chloride (BTPP-(2,6-MeO)-Cl) (Table. 4.2(e)):  $^1\text{H}$  NMR (400 MHz,  $\text{CDCl}_3$ )  $\delta$  7.45 (3H, t,  $J = 8.8$  Hz), 7.03-6.97 (5H, m), 6.53 (6H, dd,  $J = 8.4, 5.2$  Hz), 4.72 (2H, d,  $J = 17.6$  Hz), 3.61 (18H, s).  $^{31}\text{P}$  NMR (161 MHz,  $\text{CDCl}_3$ )  $\delta$  7.85 (s). Yield: 89 wt%.

Benzyl tris(*o*-methoxyphenyl)phosphonium chloride (BTPP-(*o*-MeO)-Cl) (Table. 4.2(g)):  $^1\text{H}$  NMR (400 MHz,  $\text{CDCl}_3$ )  $\delta$  7.77 (3H, t,  $J = 7.6$  Hz), 7.26 (3H, td,  $J = 12.8, 1.6$  Hz), 7.18-7.13 (9H, m), 6.97 (2H, dd,  $J = 17.6, 1.6$  Hz), 4.59 (2H, d,  $J = 16.0$  Hz), 3.66 (9H, s).  $^{31}\text{P}$  NMR (161 MHz,  $\text{CDCl}_3$ )  $\delta$  24.7 (s). Yield: 87 wt%.

**Durability test QP model compounds:** 1 M deuterated potassium hydroxide (KOD) in CD<sub>3</sub>OD/D<sub>2</sub>O (5/1 vol) solution was prepared by dissolving KOD (40 wt% in D<sub>2</sub>O, 4.28 g, 30.0 mmol) in a mixture of deuterated methanol and heavy water (CD<sub>3</sub>OD/D<sub>2</sub>O) (25 mL/2.67 mL). QP cations (1.00 mmol) was added to the alkaline solution to obtain a molar ratio of 30 KOD : 1 model compound (i.e. 0.033 M). TMS(CH<sub>2</sub>)<sub>3</sub>SO<sub>3</sub>Na) (0.107 g, 0.490 mmol) was added to serve as an internal standard for <sup>1</sup>H NMR measurements. The mixture was placed in a fluoropolymer lined autoclave held at 80 °C. Before the test (t = 0), an aliquot of the testing solution was removed and analyzed by both <sup>1</sup>H NMR and <sup>31</sup>P NMR spectroscopy to determine the initial quantity of the QP cation. Then, the testing solution was held at 80 °C. Aliquots of the reaction mixture were removed periodically and analyzed by both <sup>1</sup>H NMR and <sup>31</sup>P NMR spectroscopy to determine the quantity of the QP cation remaining. A control sample with the same recipe but without adding KOD was prepared, and its <sup>1</sup>H NMR and <sup>31</sup>P NMR were also measured.

**Calculation of the degradation rate constants (*k*) of QP model compounds:** *k*<sub>80</sub> (the degradation rate constant at 80 °C) of QP cations studied in this chapter were calculated by correlating ln(C<sub>0</sub>/C) at 80 °C and time (chemical structures in Table 4.2, kinetic data in Table 4.3). Here, C<sub>0</sub> is the initial QP cation concentration, and C is the QP cation concentration at the sampling time.

### 4.3 Results and discussion

#### 4.3.1 Synthesis of the MTPP-(2,4,6-Me)

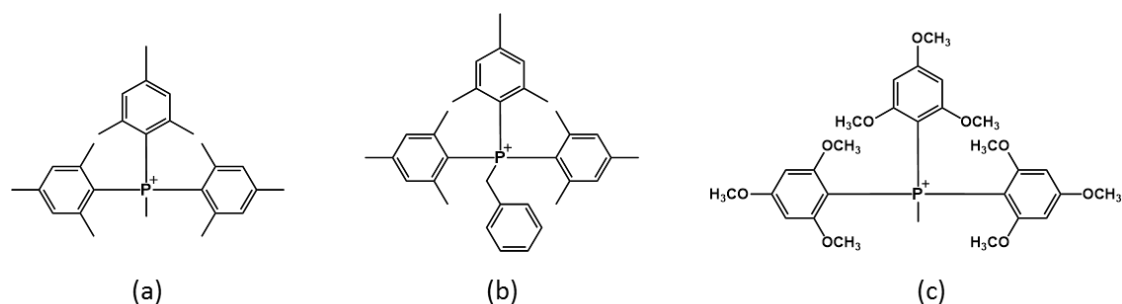


Figure 4.1: Chemical structures of (a) MTPP-(2,4,6-Me), (b) BTPP-(2,4,6-Me) and (c) MTPP-(2,4,6-MeO).

Initially, an attempt was made to synthesize benzyl tris(2,4,6-trimethylphenyl)-phosphonium (BTPP-(2,4,6-Me), Fig. 4.1(b)) by quaternization with benzyl chloride, as seen with BTPP-(2,4,6-MeO). No reaction occurred. Two more reactive benzyl halides (benzyl bromide and benzyl iodide) under a variety of conditions, were tested with no success (Table 4.1). **Note:** dimethylformamide (DMF) could react with benzyl halides at high temperature (>150 °C) to form ammonium salts (chemical equation in Fig 4.2; <sup>1</sup>H NMR spectrum in Fig. 4.3). The much lower reactivity of tris(2,4,6-trimethylphenyl)phosphine compared with tris(2,4,6-trimethoxyphenyl)phosphine was expected to be attributed to its increased steric hindrance. Despite methoxy's larger size, C-O bond rotation allows the trailing methyl substituent to minimize the interactions with the reacting species. Thus, a quaternizing agent with smaller size, iodomethane was used to further reduce the large steric hindrance and finally methyl tris(2,4,6-trimethylphenyl)phosphonium (MTPP-(2,4,6-Me), Fig. 4.1(a)) was success-

fully synthesized. The methyl group instead of benzyl group was introduced as the fourth substituent on the P center. The precursor's reduced reactivity also indicated that its quaternization form might have further enhanced steric hindrance, hence better protecting the central P atom from OH<sup>-</sup> attack and thus improve the alkaline stability. The <sup>31</sup>P NMR chemical shift of MTPP-(2,4,6-Me) was very close to that of BTPP-(2,4,6-MeO) (<sup>31</sup>P NMR in CDCl<sub>3</sub>:  $\delta$  = 5.71 ppm vs  $\delta$  = 6.53 ppm), which suggested they have similar conformation and bonding to the P center and should have similar electronic properties.

Table 4.1: Unsuccessful reaction conditions for quaternization with benzyl halides (BnX) to produce BTPP-(2,4,6-Me).

X	T (°C)	Time (day)	Solvent	Result (if other than 'no reaction')
Cl	40	1	THF	The solvent quaternized.
Cl	60	1	THF or hexane	
Cl	100	1	Toluene	
Cl	100	1	DMF	
Cl	150	1	DMF	
Cl	180	7	None (neat)	
Br	40	1	THF	
Br	60	1	THF	
Br	100	1	Toluene	
Br	100	1	DMF	
Br	180	7	None (neat)	
I	40	1	THF	
I	60	1	THF or hexane	
I	100	1	Toluene	
I	100	1	DMF	
I	180	7	None (neat)	

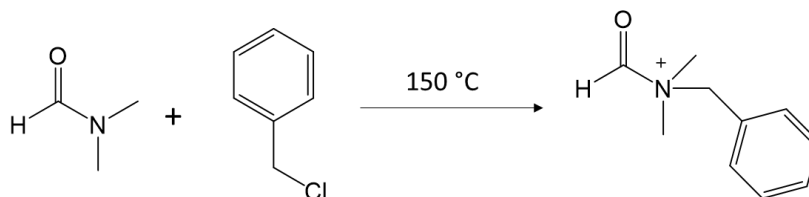


Figure 4.2: Chemical equation for quaternization of DMF with benzyl chloride.

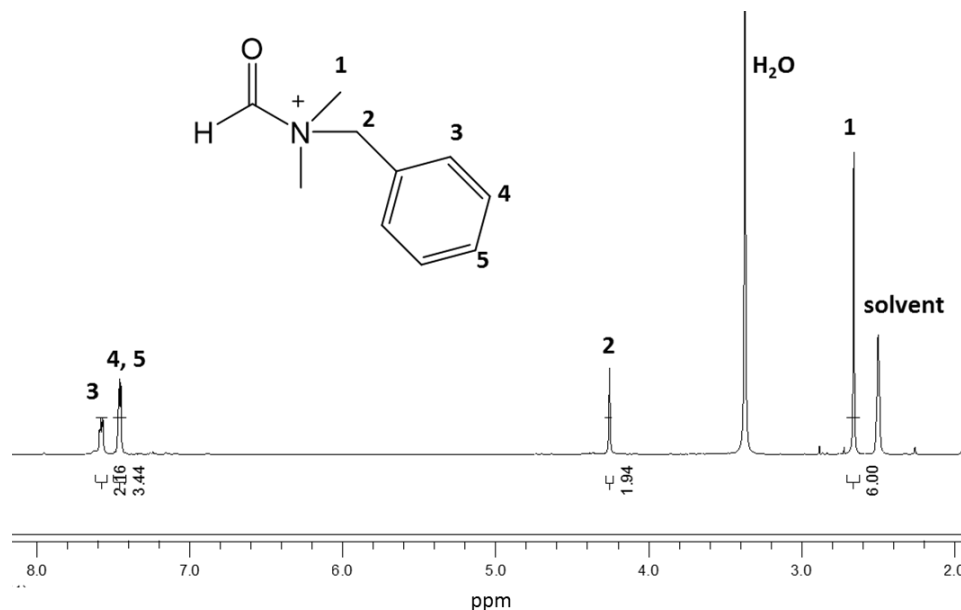


Figure 4.3:  $^1\text{H}$  NMR spectrum ( $\text{DMSO-d}_6$ ) of DMF after quaternization with benzyl chloride.

We anticipated the concern that any superior durability of MTPP-(2,4,6-Me) could also be attributed to the switch from a benzyl to a methyl, and accordingly prepared methyl tris(2,4,6-trimethoxyphenyl)phosphonium (MTPP-(2,4,6-MeO), Fig. 4.1(c)), a control version of BTPP-(2,4,6-MeO) for the following durability test to eliminate the influence of the fourth substituent.

### 4.3.2 Alkaline durability test of MTPP-(2,4,6-Me)

The alkaline stabilities of MTPP-(2,4,6-Me) and MTPP-(2,4,6-MeO) were quantified by our standard procedure (1 M KOD, 80 °C, CD<sub>3</sub>OD/D<sub>2</sub>O = 5/1 (vol)). <sup>1</sup>H NMR and <sup>31</sup>P NMR spectra for MTPP-(2,4,6-Me) (<sup>1</sup>H NMR in Fig. 4.4, <sup>31</sup>P NMR in Fig. 4.5) and MTPP-(2,4,6-MeO) (<sup>1</sup>H NMR in Fig. 4.6, <sup>31</sup>P NMR in Fig. 4.7) were taken periodically. For MTPP-(2,4,6-Me), as expected, no degradation of the methyl groups was detected. Only phosphine oxide was produced with a very slow rate over the test, indicating the general Cahours–Hofmann mechanism.

The degradation percentage of MTPP-(2,4,6-Me) was judged by the gradual decrease in area of the aromatic region ( $\delta = 7.32\sim 7.08$  ppm) as compared to the constant area of the largest internal standard peak (methyl proton,  $\delta = 0$  ppm) in <sup>1</sup>H NMR spectra (Fig. 4.4). And the degradation percentage was verified by  $A_2/(A_1+A_2)$  in <sup>31</sup>P NMR spectra (Fig. 4.5).  $A_1$  is the peak area of generated phosphine oxide peak (<sup>31</sup>P NMR:  $\delta = 40.9$  ppm) and  $A_2$  is the peak area of the remaining MTPP-(2,4,6-Me) (<sup>31</sup>P NMR,  $\delta = 7.44$  ppm). The disappearing of methyl peaks was due to the hydrogen-deuterium exchange not the degradation of MTPP-(2,4,6-Me). The degradation percentage of MTPP-(2,4,6-MeO) was judged by the gradual decrease in area of the largest peak (ortho-methoxy proton,  $\delta = 3.60$  ppm) as compared to the constant area of the largest internal standard peak (methyl proton,  $\delta = 0$  ppm) in <sup>1</sup>H NMR spectra (Fig. 4.6). And the degradation percentage can be verified by  $A_4/(A_1+A_2+A_3+A_4)$  in <sup>31</sup>P NMR spectra (Fig. 4.7).  $A_1$  is the peak area of generated phosphine oxide peak;  $A_2$  is the peak area of degradation product generated by ether hydrolysis;  $A_3$  is the peak area of the other degradation products and  $A_4$  is the peak area of the remaining MTPP-(2,4,6-MeO).

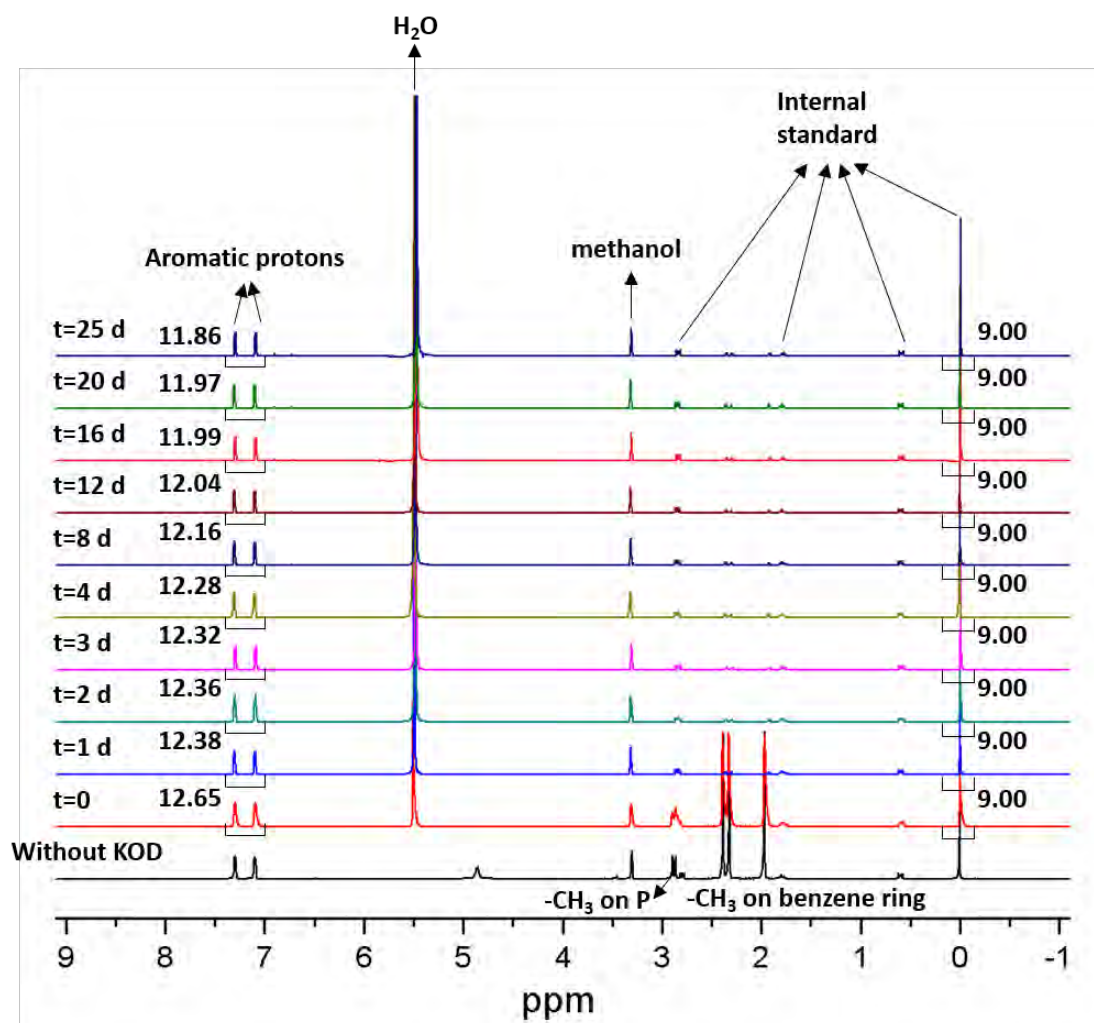


Figure 4.4: Time series of  $^1\text{H}$  NMR spectra during durability test of the MTPP-(2,4,6-Me) at 80 °C. TMS(CH<sub>2</sub>)<sub>3</sub>SO<sub>3</sub>Na as the internal standard; 1 M KOD in CD<sub>3</sub>OD/D<sub>2</sub>O (5/1 vol) as the solvent.



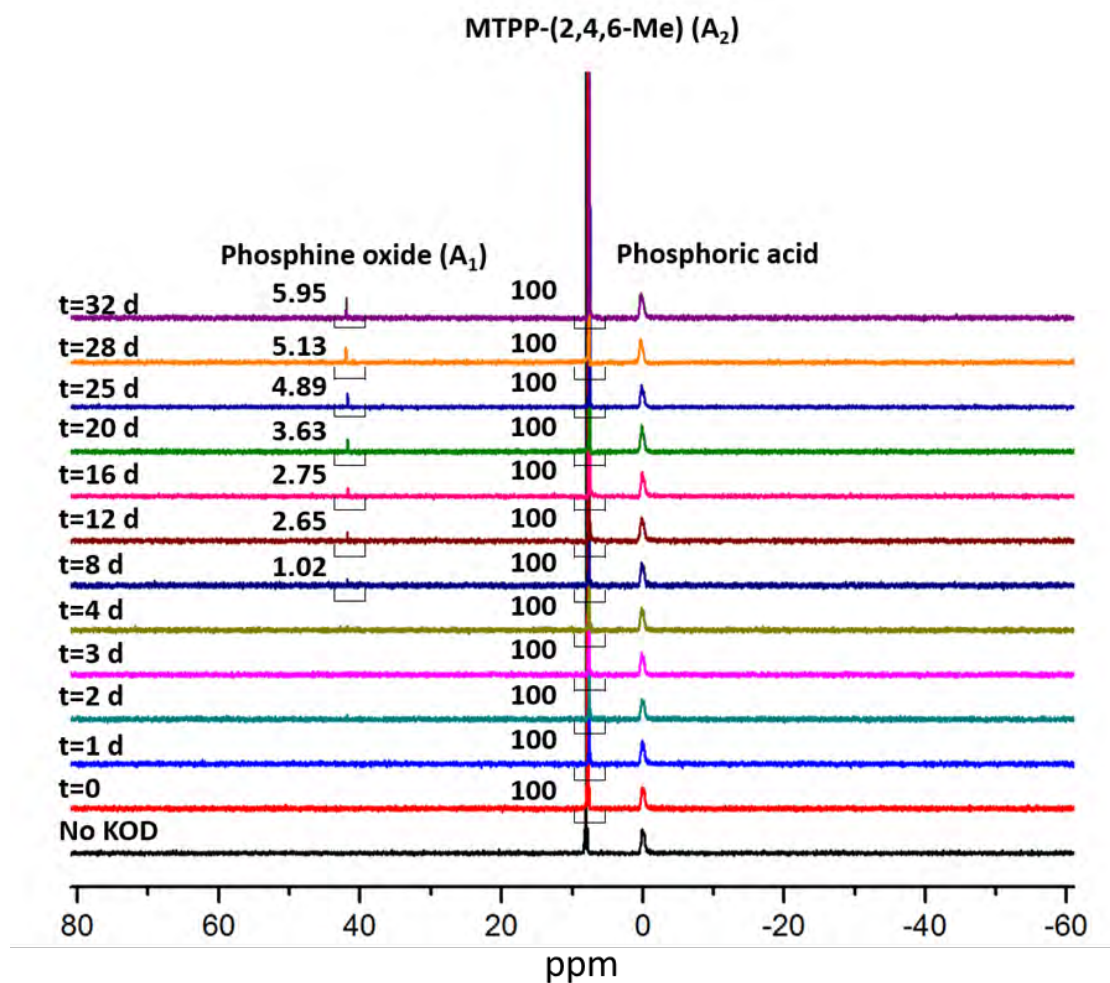


Figure 4.5: Time series of  $^{31}\text{P}$  NMR spectra during durability test of the MTPP-(2,4,6-Me) at 80 °C. Phosphoric acid as the external standard; 1 M KOD in  $\text{CD}_3\text{OD}/\text{D}_2\text{O}$  (5/1 vol) as the solvent.

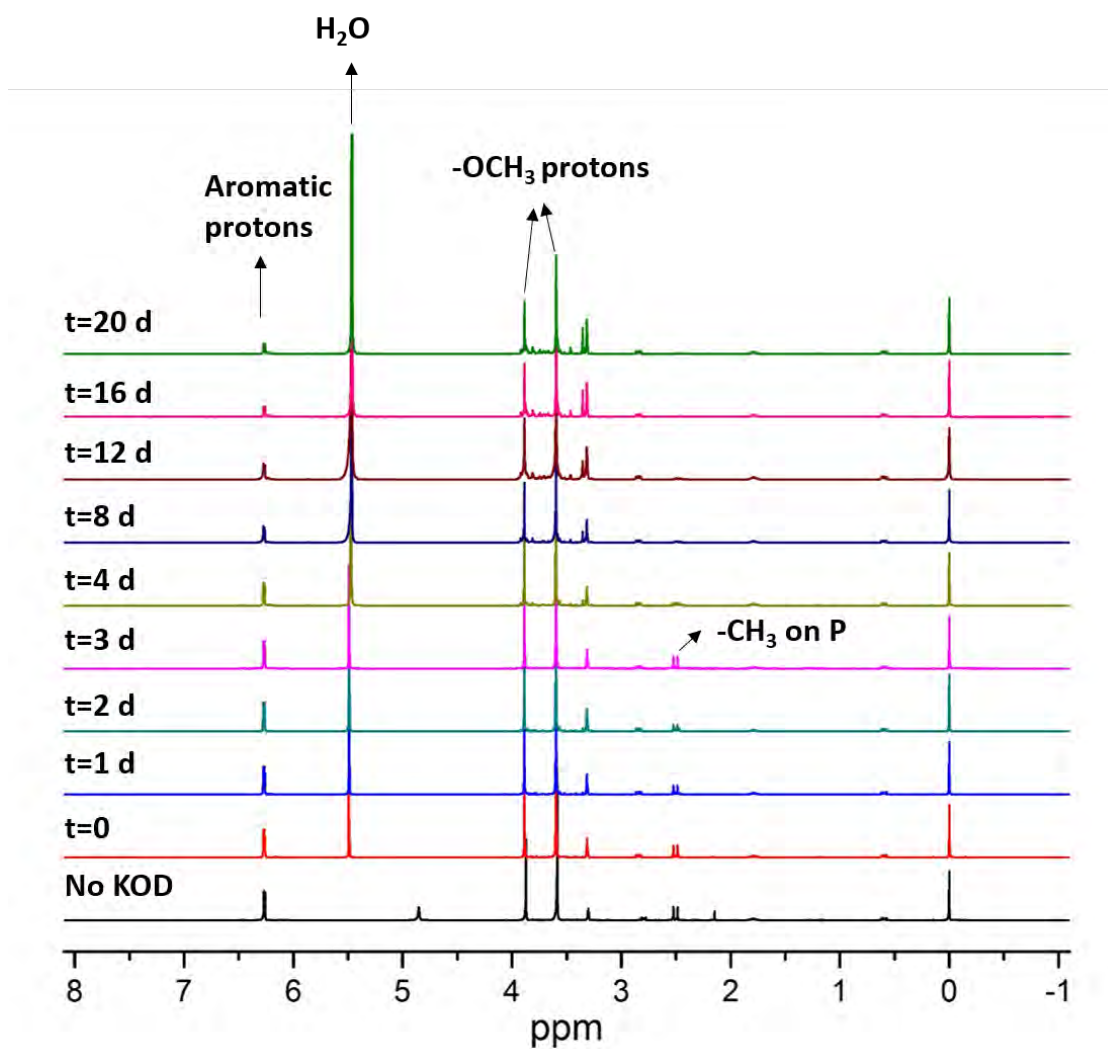


Figure 4.6: Time series of  $^1\text{H}$  NMR spectra during durability test of the MTPP-(2,4,6-MeO) at  $80^\circ\text{C}$ . TMS( $\text{CH}_2$ )<sub>3</sub>SO<sub>3</sub>Na as the internal standard; 1 M KOD in  $\text{CD}_3\text{OD}/\text{D}_2\text{O}$  (5/1 vol) as the solvent.

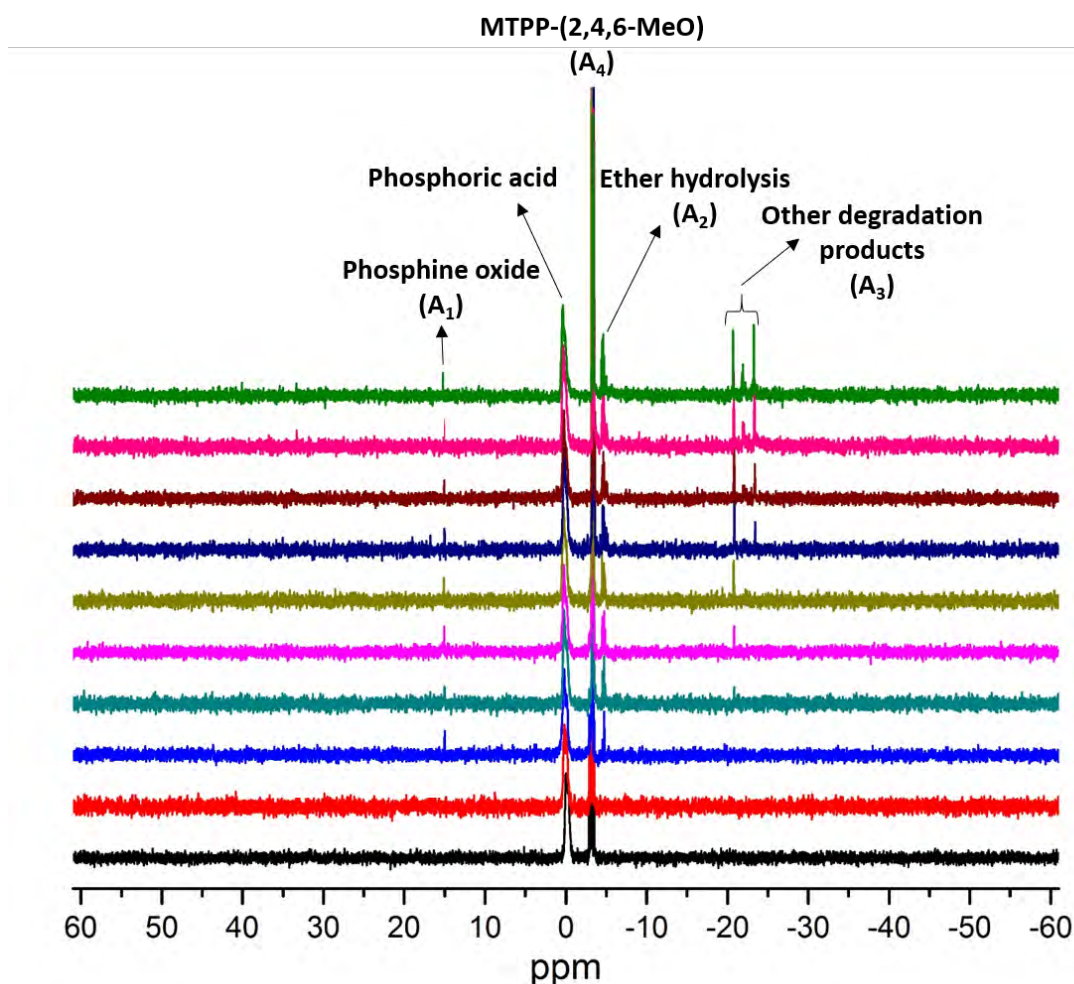
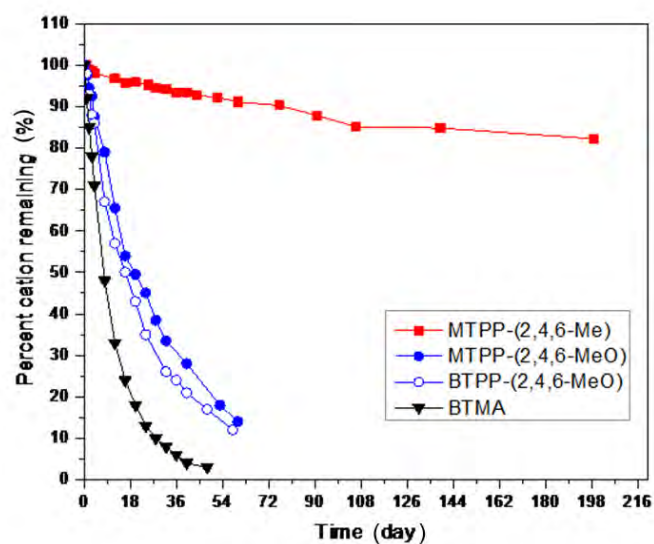


Figure 4.7: Time series of  $^{31}\text{P}$  NMR spectra during durability test of the MTPP-(2,4,6-MeO) at 80 °C. Phosphoric acid as the external standard; 1 M KOD in  $\text{CD}_3\text{OD}/\text{D}_2\text{O}$  (5/1 vol) as the solvent.

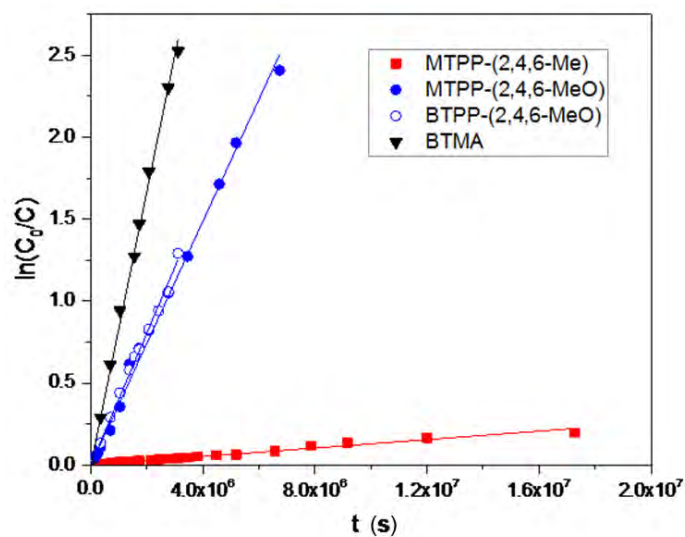
Fig. 4.8(a) shows the degradation profiles of MTPP-(2,4,6-Me), MTPP-(2,4,6-MeO), BTPP-(2,4,6-MeO) and the benchmark BTMA. MTPP-(2,4,6-Me) is much more stable than the other three cations. After 60 days, 93% of MTPP-(2,4,6-Me) remained, whereas only 14% of MTPP-(2,4,6-MeO) remained. After 200 days, still 82% of MTPP-(2,4,6-Me) remained. While MTPP-(2,4,6-MeO) degradation was

slightly less than BTPP-(2,4,6-MeO) over the testing timeframe (e.g. after 40 days, 72% vs 79% degradation), the difference is insignificant when compared to the improvement of MTPP-(2,4,6-Me) (e.g. after 40 days, 7% vs 72% degradation). Thus, the switch of the quaternizing agent is not the primary reason for the superiority of MTPP-(2,4,6-Me).  $k_{80}$  for MTPP-(2,4,6-Me) and MTPP-(2,4,6-MeO) were calculated to be  $1.3\text{E}-8 \text{ s}^{-1}$  and  $3.7\text{E}-7 \text{ s}^{-1}$ , respectively (Fig. 4.6(a)). The stability of MTPP-(2,4,6-Me) is 64 times that of the benchmark BTMA and 31 times that of BTPP-(2,4,6-MeO) ( $k = 4.0 \text{ E}-7 \text{ s}^{-1}$ ), the previously most stable QP cation, demonstrating significant cation enhancement is possible using this methodology.

Fig. 4.9 shows the comparison of alkaline stability of MTPP-(2,4,6-Me) with other reported cations in 1 M KOD or NaOD solution. Here, cation lifetime is defined as the average time for 20% cation degradation. Among these cations, MTPP-(2,4,6-Me) demonstrates the highest alkaline stability. **Note:** all of the other cations were tested in the alkaline aqueous solution (unless otherwise noted) whereas MTPP-(2,4,6-Me) was tested in the mixed solvent of methanol and water. The addition of methanol would likely accelerate the degradation rate by about two orders of magnitude as seen previously.<sup>[212, 223]</sup> Thus, the actual stability of MTPP-(2,4,6-Me) could be even higher. MTPP-(2,4,6-Me) demonstrates a level of stability that has not been achieved by any other known HEM cations.



(a)



(b)

Figure 4.8: (a) Degradation profiles and (b) plots of  $\ln(C_0/C)$  versus time of MTPP-(2,4,6-Me), MTPP-(2,4,6-MeO), BTPP-(2,4,6-MeO) and BTMA at 80 °C. 1 M KOD in CD<sub>3</sub>OD/D<sub>2</sub>O (5/1 vol) as the solvent.

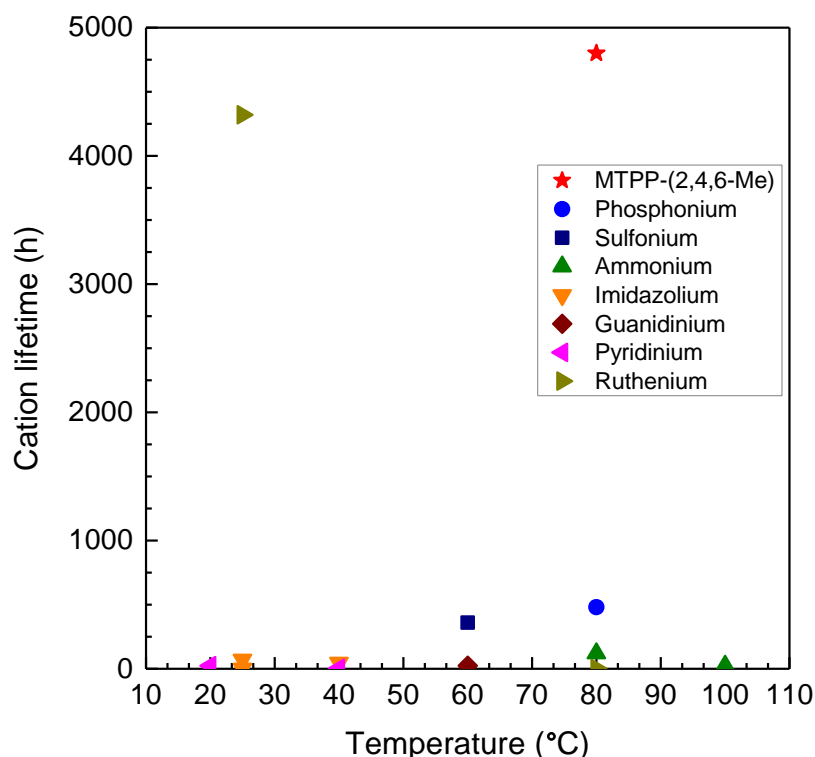


Figure 4.9: Comparison of alkaline stability of MTPP-(2,4,6-Me) and other reported cations. Test conditions: 1 M KOD or NaOD in D<sub>2</sub>O, 20% degradation threshold on <sup>1</sup>H NMR basis (unless otherwise noted). Ammonium: trimethyl-benzylammonium [80 °C in 1 M NaOD/(D<sub>2</sub>O+CD<sub>3</sub>OD)]<sup>[212]</sup> and 100 °C in 1 M NaOD/D<sub>2</sub>O]. Imidazolium: 1-methyl-benzylimidazolium<sup>[177]</sup>, 2-phenyl benzimidazolium (0.3 M KOH)<sup>[72]</sup>, 1,3-dimethyl-2-(2,4,6-trimethylphenyl)-benzimidazolium (1.3 M KOH)<sup>[72]</sup>. Guanidinium: pentamethyl-benzylguanidium. Pyridinium: benzylpyridinium. Phosphonium: tetrakis(dialkylamino)phosphonium [1 M NaOD/(D<sub>2</sub>O+CD<sub>3</sub>OD)]<sup>[212]</sup>. Sulfonium: methoxy-triphenylsulfonium<sup>[261]</sup>. Ruthenium: bis(terpyridine)ruthenium (UV-vis spectroscopy)<sup>[216]</sup>.

#### 4.3.3 Reasons for the ultra-high alkaline stability of MTPP-(2,4,6-Me)

Different from BTPP-(2,4,6-MeO), minor phosphine oxide (TTMPPO) (<sup>31</sup>P NMR in CDCl<sub>3</sub>: δ = 16.8 ppm) was detected in <sup>31</sup>P NMR spectra after the degradation of MTPP-(2,4,6-MeO) (Fig. 4.5). This suggests that MTPP-(2,4,6-MeO) undergoes

competing degradation pathways (ether hydrolysis and Cahours–Hofmann reactions), although ether hydrolysis is the predominant one. At 80 °C, with a  $k_{80}$  (the overall rate constant) of  $3.7\text{E-}7\text{ s}^{-1}$ , MTPP-(2,4,6-MeO) has a  $k_{OF}$  (the rate constant of oxide formation) of  $1.5\text{E-}8\text{ s}^{-1}$  and a  $k_{EH}$  (the rate constant of ether hydrolysis) of  $3.6\text{E-}7\text{ s}^{-1}$ . For comparison, MTPP-(2,4,6-Me) has  $k = k_{OF} = 1.3\text{E-}8\text{ s}^{-1}$ .

The ether hydrolysis results from the instability of the methoxy group which is the major cause for MTPP-(2,4,6-MeO)'s degradation. By replacing all of the methoxy groups with methyl groups, the degradation caused by ether hydrolysis which was predominant for MTPP-(2,4,6-MeO) is eliminated, and accordingly a significant enhancement of QP's alkaline stability is observed.

The rate of oxide formation is controlled by both electronic (electron density on the P center) and steric effects. Although MTPP-(2,4,6-MeO) has higher electron density on the P center than MTPP-(2,4,6-Me) ( $^{31}\text{P}$  NMR in  $\text{CDCl}_3$ :  $-3.79\text{ ppm}$  vs  $6.53\text{ ppm}$ ), indicating higher resistance to oxide formation, MTPP-(2,4,6-Me) has a comparable  $k_{OF}$  with MTPP-(2,4,6-MeO) ( $1.3\text{E-}8\text{ s}^{-1}$  vs  $1.5\text{E-}8\text{ s}^{-1}$ ). It suggests that the steric effect is dominant in stabilizing MTPP-(2,4,6-Me). The methyl substituent has a larger steric envelope than the methoxy substituent, and thus blocks  $\text{OH}^-$  from approaching the P center more effectively, which offsets the stability loss caused by lower electron density on the P center. Consequently, the alkaline stability of QP cation was further improved.

In summary, the elimination of the ether hydrolysis is the major contribution to MTPP-(2,4,6-Me)'s ultra-high alkaline stability. Additionally, the large steric hindrance of methyl substituents further stabilizes MTPP-(2,4,6-Me).

#### 4.3.4 Exploration of the structure-property relationship

In further exploring the structure-property relationship, a systematical study on the degradation kinetics and mechanisms of a wider range of QP cations (Table 4.2) were carried out at 80 °C by going through the same procedures. The degradation rate constants and  $^{31}\text{P}$  NMR chemical shifts ( $\delta$ ) for all of these cations are shown in Table 4.3. According to their degradation mechanisms, these cations can be divided into three categories (Table 4.4): (1) cations only degrade through oxide formation pathway,  $k = k_{OF}$ , where  $k_{OF}$  is the rate constant of oxide formation; this category includes the methyl substituted cations and some of the methoxy-substituted cations; the latter ones' oxide formation rates are much larger than their ether hydrolysis rates and thus  $k = k_{OF}$ ; (2) cations only undergo the ether hydrolysis pathway,  $k = k_{EH}$ , where  $k_{EH}$  is the rate constant of ether hydrolysis; (3) cations undergo both oxide formation and ether hydrolysis pathways,  $k = k_{OF} + k_{EH}$ . Because  $k_{EH}$  only comes from the individual behavior of methoxy group in the alkaline environment, not under the control of either electronic effects or steric effects, only  $k_{OF}$  will be considered in the following discussions.



Table 4.2: Structure of QP cations studied in this chapter.

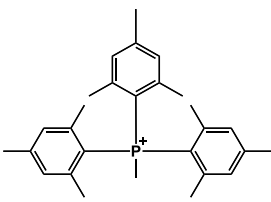
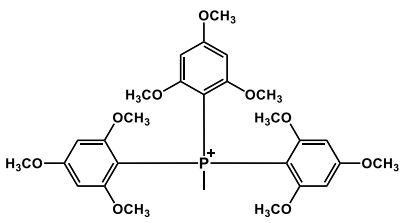
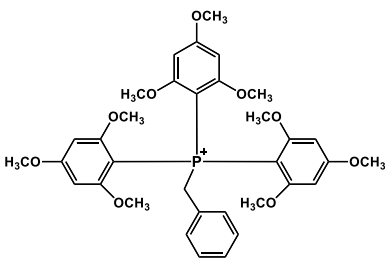
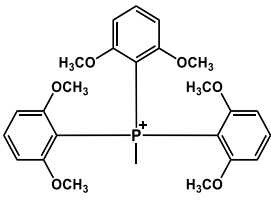
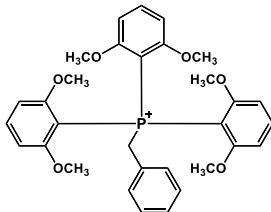
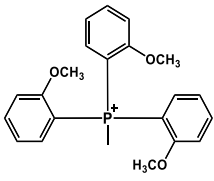
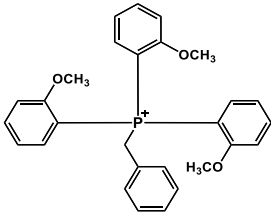
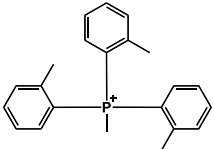
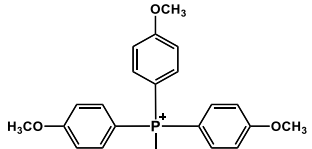
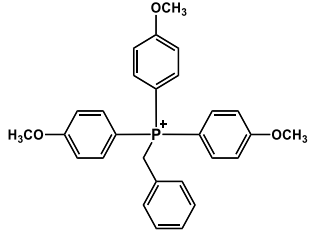
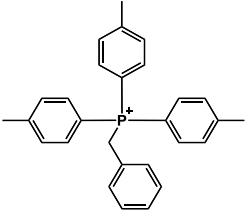
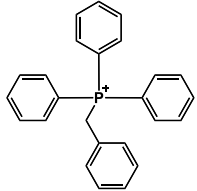
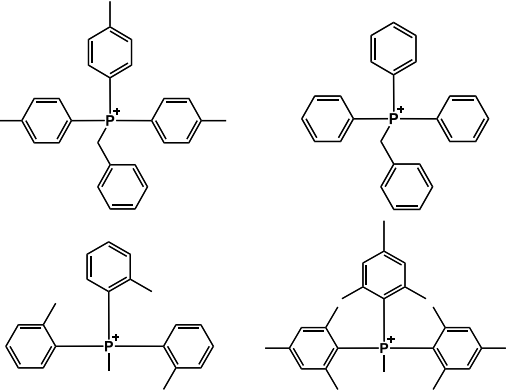
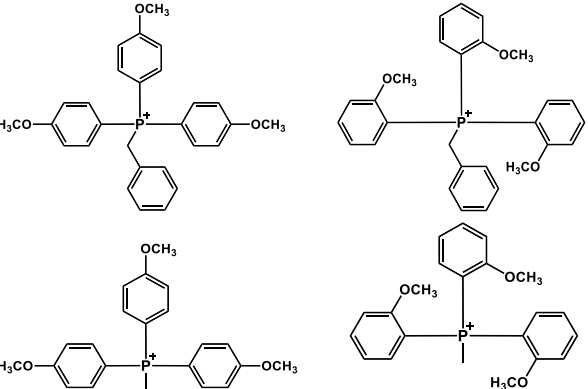
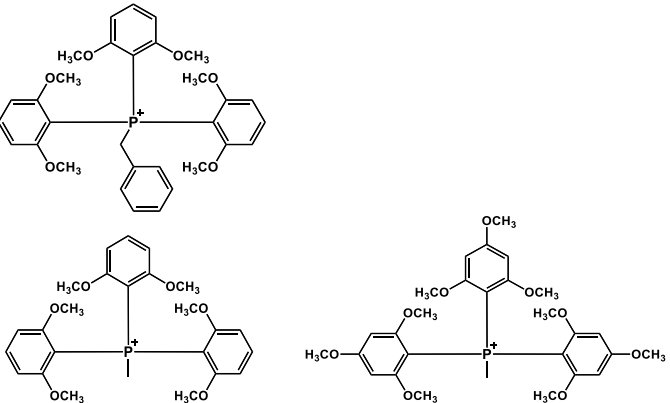
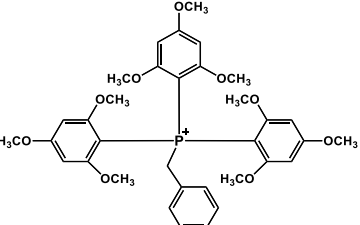
		
(a) MTPP-(2,4,6-Me)	(b) MTPP-(2,4,6-MeO)	(c) BTPP-(2,4,6-MeO)
		
(d) MTPP-(2,6-MeO)	(e) BTPP-(2,6-MeO)	(f) MTPP-( <i>o</i> -MeO)
		
(g) BTPP-( <i>o</i> -MeO)	(h) MTPP-( <i>o</i> -Me)	(i) MTPP-( <i>p</i> -MeO)
		
(j) BTPP-( <i>p</i> -MeO)	(k) BTPP-( <i>p</i> -Me)	(l) BTPP

Table 4.3:  $^{31}\text{P}$  NMR chemical shift ( $\delta$ ) and degradation rate ( $k$ ,  $k_{OF}$  and  $k_{EH}$ ) of QP cations at 80 °C.

Cation	$\delta$ (ppm)	$k_{OF}$ ( $\text{s}^{-1}$ )	$k_{EH}$ ( $\text{s}^{-1}$ )	$k$ ( $\text{s}^{-1}$ )
(a) MTPP-(2,4,6-Me)	6.53	1.3E-8	0	1.3E-8
(b) MTPP-(2,4,6-MeO)	-3.79	1.5E-8	3.6E-7	3.7E-7
(c) BTPP-(2,4,6-MeO)	5.71	~0	4.0E-7	4.0E-7
(d) MTPP-(2,6-MeO)	-1.84	5.0E-7	1.0E-7	6.0E-7
(e) BTPP-(2,6-MeO)	7.85	1.9E-7	1.8E-7	3.7E-7
(f) MTPP-( <i>o</i> -MeO)	20.1	2.0E-5	0	2.0E-5
(g) BTPP-( <i>o</i> -MeO)	24.7	2.8E-5	0	2.8E-5
(h) MTPP-( <i>o</i> -Me)	21.7	3.9E-4	0	3.9E-4
(i) MTPP-( <i>p</i> -MeO)	18.8	2.2E-4	0	2.2E-4
(j) BTPP-( <i>p</i> -MeO)	20.8	1.3E-3	0	1.3E-3
(k) BTPP-( <i>p</i> -Me)	22.0	9.7E-2	0	9.7E-2
(l) BTPP	23.1	N/A	0	N/A

Table 4.4: Degradation mechanisms of QP cations studied in this chapter.

<p>Oxidation formation</p> $k_{EH} \ll k_{OF}$ $k = k_{OF}$	
	
<p>Oxidation formation &amp; Ether hydrolysis</p> $k = k_{EH} + k_{OF}$	
<p>Ether hydrolysis</p> $k_{EH} \gg k_{OF}$ $k = k_{EH}$	

The Hammett equation predicts a linear relationship between the reaction rate and the substituent constant ( $\sigma$ ) (Eq. 4.1).<sup>[262-264]</sup>

$$\log \frac{k}{k_0} = \sigma \rho \quad \text{Eq. 4.1}$$

In this equation,  $k_0$  is the reference reaction rate of the unsubstituted reactant, and  $k$  is the reaction rate of a substituted reactant.  $\rho$  is the reaction constant which depends only on the type of reaction but not on the substituent used.  $\sigma$  depends on the resonance, inductive and direct electrostatic effect from the substituents (i.e. the electronic effect). It was found that  $\sigma$  can be replaced by the  $^{31}\text{P}$  NMR chemical shifts ( $\delta$ ) in the Hammett equation for the phosphorus compound.<sup>[265]</sup> The smaller value of  $\delta$  (shift upfield) indicates the stronger electron-donating ability of the substituents. For the three QP analogs studied in Chapter 3 (BTPP, BTPP-(*p*-Me) and BTPP-(*p*-MeO)), the alkaline stability increases as  $\delta$  shifting more upfield ( $^{31}\text{P}$  NMR in  $\text{CDCl}_3$ : 23.3 ppm, 22.0 ppm and 20.8 ppm, respectively), revealed significance of the electron effect to the cation stability.

According to Hammett equation<sup>[266]</sup>,  $-\ln(k_{OF})$  of each QP cation was plotted as a function of its  $^{31}\text{P}$  NMR chemical shift ( $\delta$ ) (Fig. 4.10). In terms of the overall trend, a linear relationship between  $-\ln(k_{OF})$  and  $\sigma$  seems to exist, as QP cations with smaller chemical shifts have higher stabilities. Especially for the para-substituted QP cations (i, j and k in Fig. 4.10), the linear relationship is apparent, which means electronic effect is dominant for these cations. However, for ortho-substituted QP cations, the linear relationship breaks down. For example, cation (f) and cation (j) have identical chemical shifts (20.1 ppm vs 20.8 ppm), but the ortho-substituted one (f) is 650 times as stable as the para-substituted one (j). The similar phenomenon has been observed for cation (h) and cation (k). The deviation from Hammett relationship suggests that

electronic effect is not the only factor that controls the degradation rate. Hammett equation is generally applicable for reactions of para- and meta-substituted derivatives, because para- or meta- substitution on the benzene ring has little influence on the steric hindrance adjacent to the P center. In this case, the steric effect is negligible. However, when ortho-substituents are involved, due to their proximity to the reaction center, the overall steric influence can be significantly increased,<sup>[267]</sup> and thus may become the dominant factor to develop the highest stabilizing strategy. Consequently, it is critical to occupy the ortho-positions of P-bond ligand.

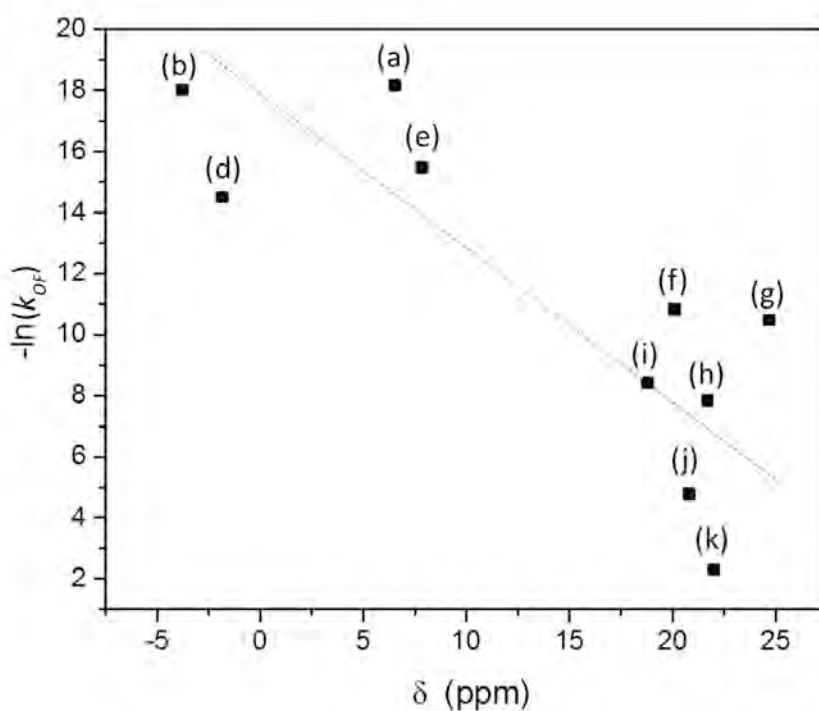


Figure 4.10: Plot of  $-\ln(k_{OF})$  versus  $\delta$  for QP cations shown in Table 4.3. (a) MTPP-(2,4,6-Me), (b) MTPP-(2,4,6-MeO), (d) MTPP-(2,6-MeO), (e) BTPP-(2,6-MeO), (f) MTPP-(*o*-MeO), (g) BTPP-(*o*-MeO), (h) MTPP-(*o*-Me), (i) MTPP-(*p*-MeO), (j) BTPP-(*p*-MeO) and (k) BTPP-(*p*-Me).

For the cation pair derived from the same phosphine precursor but only different in the fourth substituent (benzyl or methyl) (e.g. cation (i)/cation (j)), the slope of the straight line connecting the cation pair decreases as the steric hindrance of phosphine precursor increases (cation (i)/cation (j) > cation (f)/cation (g) > cation (d)/cation (e)) (Fig. 4.11). The fourth substituent affects the degradation rate both electronically and sterically, and these two effects influence the degradation rate in opposite directions. Compared with the benzyl substituent, the methyl substituent has stronger electron donation but smaller steric hindrance. For cation (i)/cation (j) and cation (f)/cation (g) (both with a positive slope), the electronic effect dominates but to a smaller extent in the latter case. For cation (d)/cation (e) (with a negative slope), the steric effect is dominant. It indicates that as the overall steric hindrance of the QP cations increases, the ability for  $\text{OH}^-$  to attack the P center decreases, and this has been shown to significantly enhance the stability of the cation.

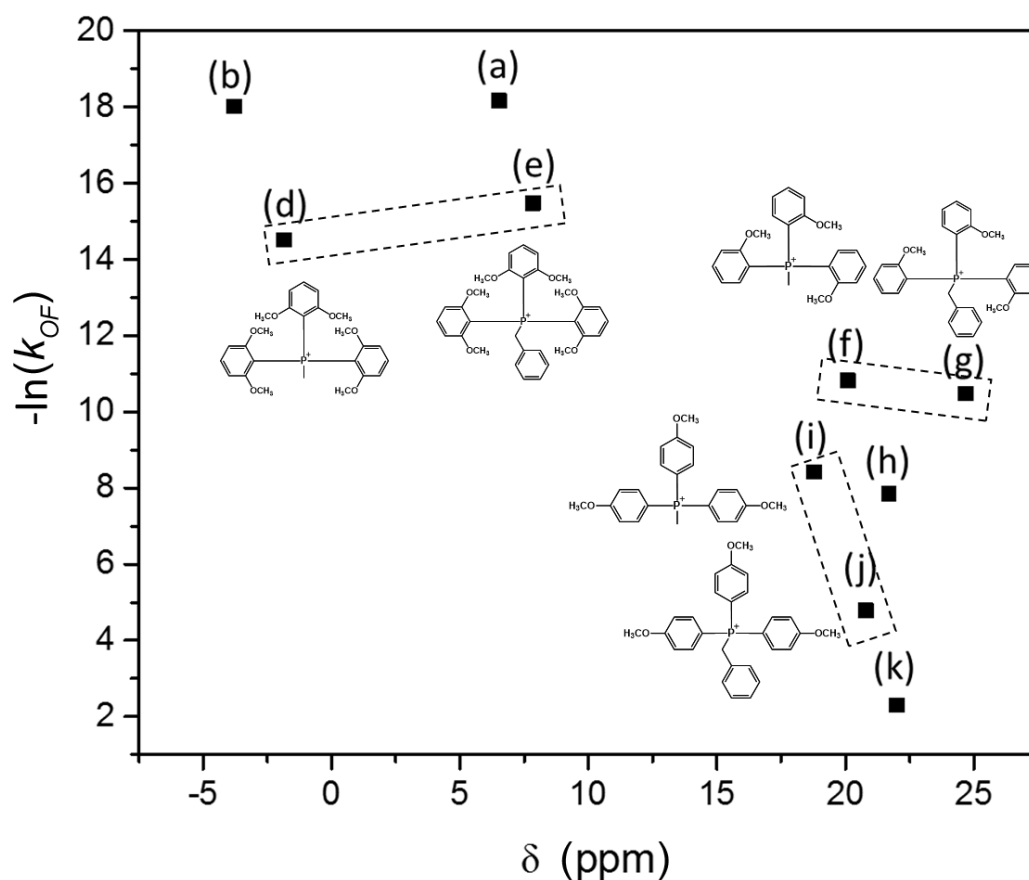


Figure 4.11: Comparison of cation pairs with different phosphine precursors (cation (i)/cation (j), cation (f)/cation (g) and cation (d)/cation (e)). (a) MTPP-(2,4,6-Me), (b) MTPP-(2,4,6-MeO), (d) MTPP-(2,6-MeO), (e) BTPP-(2,6-MeO), (f) MTPP-(*o*-MeO), (g) BTPP-(*o*-MeO), (h) MTPP-(*o*-Me), (i) MTPP-(*p*-MeO), (j) BTPP-(*p*-MeO) and (k) BTPP-(*p*-Me).

#### 4.4 Conclusion

In summary, a new phosphonium cation, MTPP-(2,4,6-Me) has been developed, with ultra-high alkaline stability. It is 31 times as stable as BTPP-(2,4,6-MeO), the previous most stable QP cation to date, and 64 times as stable as BMTA, the benchmark cation. MTPP-(2,4,6-Me) demonstrates a level of stability that has not been achieved by any other known HEM cations.

The ultra-high alkaline stability of MTPP-(2,4,6-Me) is attributed to two factors: (a) by replacing the methoxy groups with methyl groups, the substituent degradation (i.e. ether hydrolysis) has been successfully eliminated; and (b) the steric hindrance of the methyl group in the ortho-position, significantly reduces the rate of OH<sup>-</sup> attack at the P center. Due to its excellent alkaline stability, MTPP-(2,4,6-Me) is a very promising candidate for the cationic group served in HEMs, which is important for the energy conversion devices, such as fuel cells.

From the systematic study of a series of QP cations, it can be concluded that electronic effect and steric effect combined determine the rate of P center atom degradation. For para-substituted QP cations, electronic effect controls the degradation rate whereas for ortho-substituted QP cations, steric effect becomes the major controlling factor. For cations with the same phosphine precursor, the cation stability is dependent on the choice of the fourth substituent (comes from the quaternizing agent). The selection criteria of the phosphine precursor should combine both steric and electronic attributes. Choosing candidates with large steric effect (ortho-substitution) and strong electron-donating (*p*- and *m*-substitutions) would provide the best QP stabilizing strategy.

To take the advantage of MTPP-(2,4,6-Me)'s outstanding alkaline stability, we are very interested in linking this cation to the polymer backbone and making the polymer into a HEM. This work will be discussed in Chapter 5.



## Chapter 5

### SYNTHESIS OF MTPP-(2,4,6-ME)-FUNCTIONALIZED POLYMER FOR HEMS

Three synthesis routes have been designed to synthesize MTPP-(2,4,6-Me) functionalized polymers for HEMs. Although Route 1 and 2 have been shown to be infeasible, Route 3 demonstrated a facile route to link MTPP-(2,4,6-Me) to the polymer backbone.

#### 5.1 Introduction

In Chapter 4, it was shown that MTPP-(2,4,6-Me) demonstrated ultra-high alkaline stability. In order to take the advantage of MTPP-(2,4,6-Me)'s outstanding alkaline stability, we explored linking this cation to a polymer backbone in order to make a high performance HEM.

Due to the strong steric effect, the general 'chloromethylation-quaternization-alkalization' protocol cannot be applied to synthesize MTPP-(2,4,6-Me) functionalized polymers. Accordingly, three new synthesis routes were constructed to link MTPP-(2,4,6-Me) cation to the polymer backbone.

Three synthesis routes were developed to link MTPP-(2,4,6-Me) cation to the polymer backbone. The first route directly attaches the MTPP-(2,4,6-Me) cation through its side group to the polymer backbone, including three major steps (Fig. 5.1): (a) bromination of one of the methyl groups on the phenyl rings of MTPP-(2,4,6-Me)-I; (b) synthesis of butylaminated polysulfone (PSf-BA) through a chloromethylation and amination reaction to introduce a nitrogen atom bridge; and (c) incorporation of

the MTPP-(2,4,6-Me) cation to the polysulfone backbone *via* the reaction between the bromomethyl group of MTPP-(2,4,6-Me)-I and the butylamine group of PSf-BA.

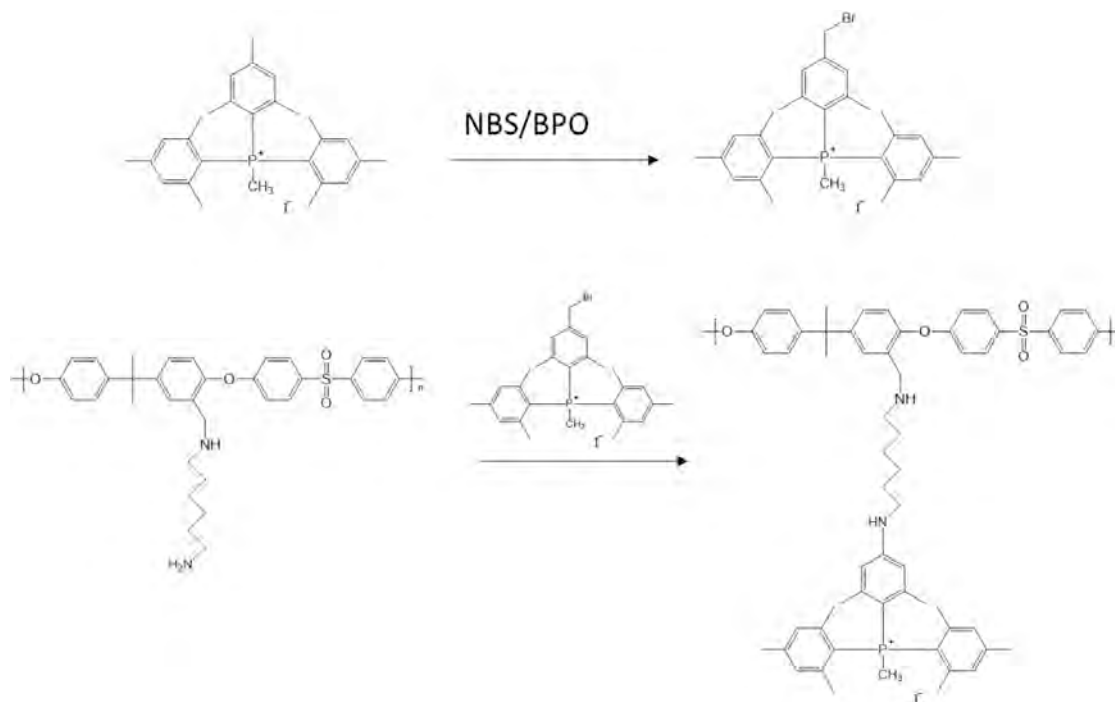


Figure 5.1: Synthesis of MTPP-(2,4,6-Me) functionalized polymer (Route 1).

The second route focuses on synthesizing polymer acylating agent to quaternize the phosphine precursor, including three major steps (Fig. 5.2): (a) acylation of the PPO backbone to give the polymer acylating agent; (b) reduction of the carbonyl group; and (c) quaternization of the phosphine precursor with the polymer acylating agent to give MTPP-(2,4,6-Me) functionalized PPO.

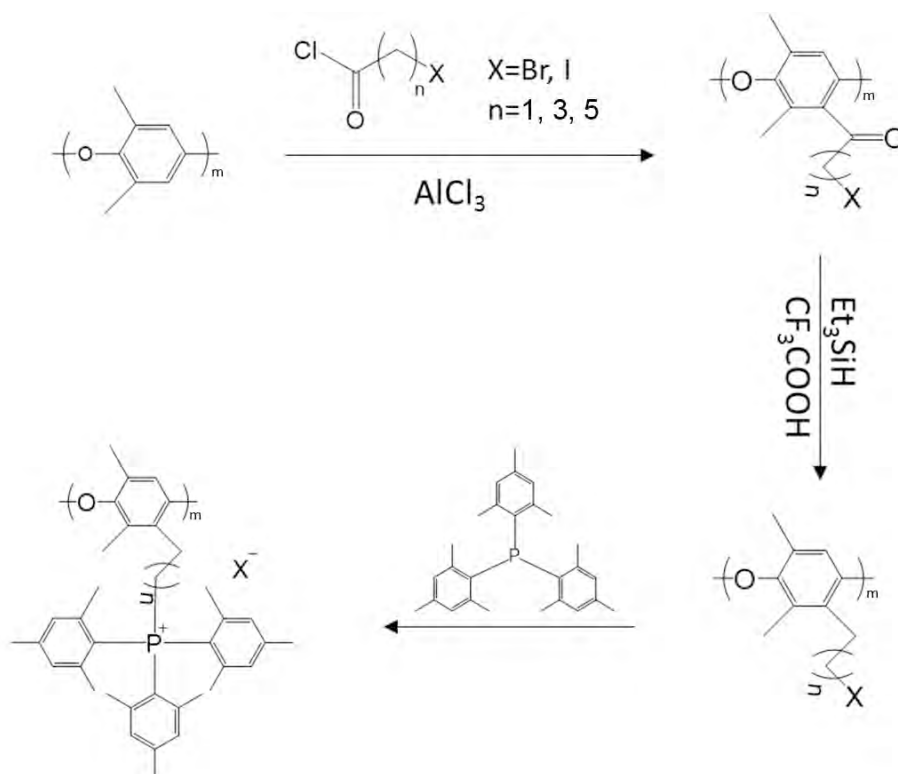


Figure 5.2: Synthesis of MTPP-(2,4,6-Me) functionalized polymer (Route 2).

The final route attempts to attach the phosphine precursor to the polymer backbone followed by the quaternization of the phosphine, including three major steps (Fig. 5.3): (a) synthesis of the phosphine precursor with eight methyl groups and one vinyl group on the phenyl rings; (b) link the phosphine precursor the polystyrene (PSt) backbone *via* Heck coupling; and (c) quaternization of the phosphine precursor with alkyl halide to give MTPP-(2,4,6-Me) functionalized PSt. This route was identified as being the easiest and most efficient.

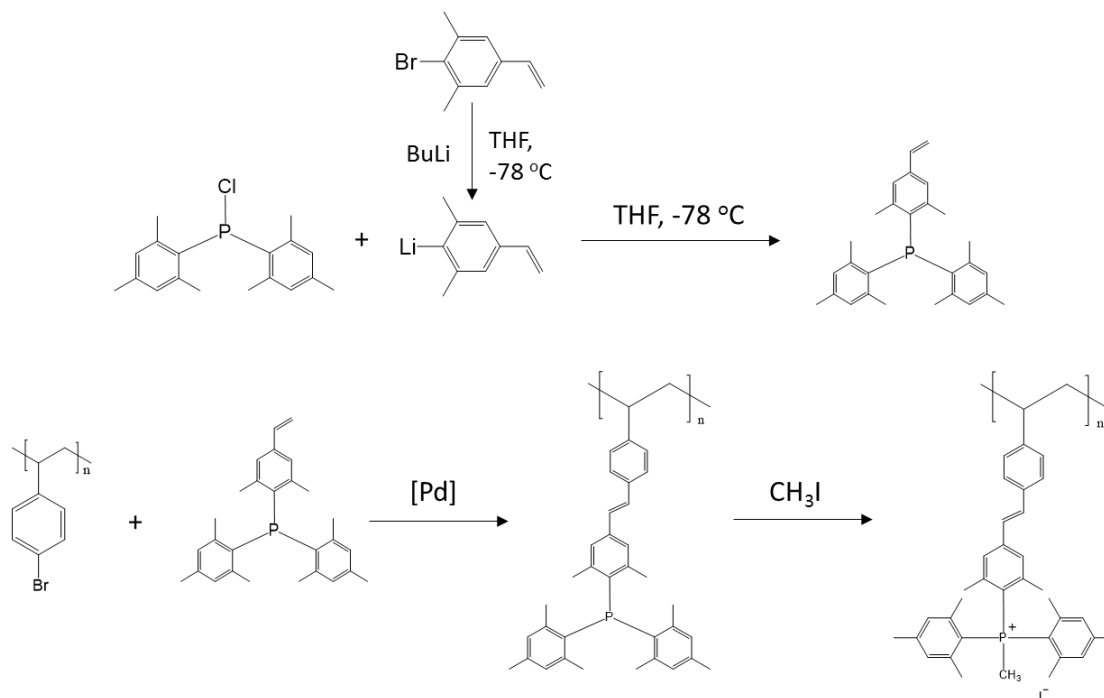


Figure 5.3: Synthesis of MTPP-(2,4,6-Me) functionalized polymer (Route 3).

## 5.2 Materials and methods

### 5.2.1 Materials and characterization

All the chemicals mentioned in the synthesis were purchased from Sigma-Aldrich and used as received. The  $^1\text{H}$  spectra were measured in deuterated solvents on a Bruker AV400 spectrometer ( $^1\text{H}$ , 400 MHz). The  $^1\text{H}$  NMR chemical shifts are expressed as  $\delta$  downfield from tetramethylsilane (TMS) and calibrated to the residual proton of the deuterated solvent ( $\delta = 7.26$  ppm for chloroform-d). The  $^{31}\text{P}$  NMR spectra were measured in deuterated solvents on a Bruker AV400 spectrometer ( $^{31}\text{P}$ , 161 MHz). The  $^{31}\text{P}$  NMR chemical shifts are expressed as downfield from external 85%  $\text{H}_3\text{PO}_4$ .

## 5.2.2 Experimental methods

### 5.2.2.1 Route 1

**Bromination of Methyl tris(2,4,6-trimethylphenyl)phosphonium iodide (MTPP-(2,4,6-Me)-I):** 3.99 g (7.5 mmol) MTPP-(2,4,6-Me)-I and 1.33 g (7.5 mmol) *N*-bromosuccinimide (NBS) was dissolved in 100 mL dichloroethane. The solution was heated to 85 °C, followed by addition of 0.09 g (0.375 mmol) benzoyl peroxide (BPO). The mixture was stirred at room temperature for 24 h. After the reaction, the mixture was added dropwise into 500 mL diethyl ether to precipitate the product. The precipitate was washed three times with diethyl ether and dried under vacuum at room temperature for 24 h to give the product. The  $^1\text{H}$  NMR and  $^{31}\text{P}$  NMR spectra are shown in Fig. 5.4 and 5.5. The degree of bromination can be calculated by comparing the peak area of bromomethyl proton (Peak 5) to that of methyl on P center (Peak 4).

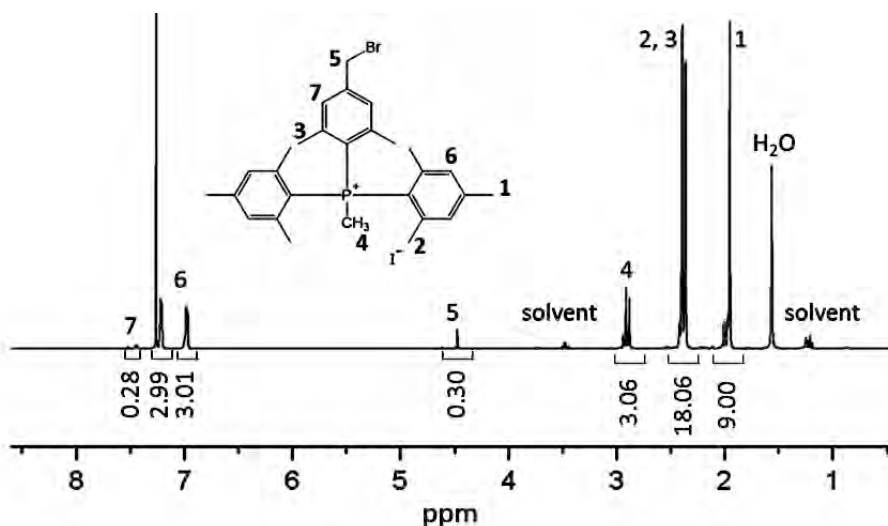


Figure 5.4:  $^1\text{H}$  NMR spectrum ( $\text{CDCl}_3$ ) of MTPP-(2,4,6-Me) after the bromination.

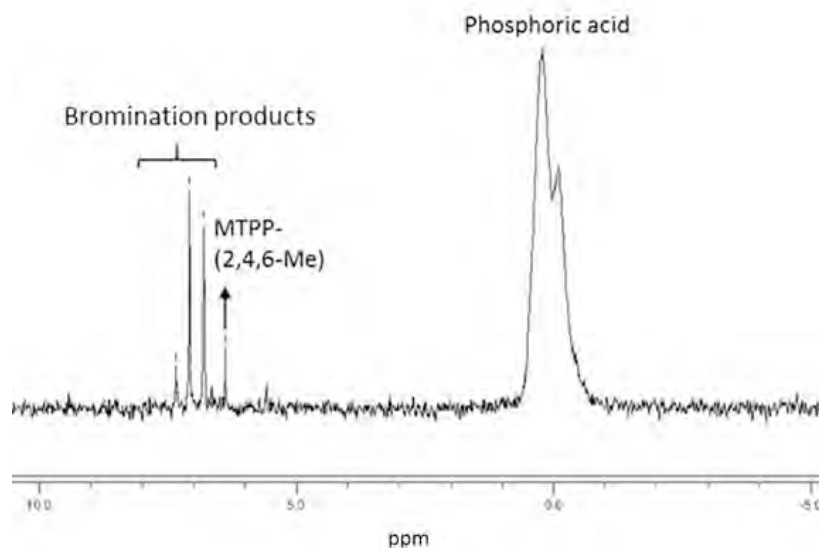


Figure 5.5:  $^{31}\text{P}$  NMR spectrum ( $\text{CDCl}_3$ ) of MTPP-(2,4,6-Me) after the bromination.

#### 5.2.2.2 Route 2

**General procedure to acylate poly(phenylene oxide) (PPO):** 1.2 g (10 mmol) PPO was dissolved in 100 mL dichloromethane in a flask under argon. The flask was cooled down to 0 °C and the acylating agent (10 mmol) was added. 1.33 g (10 mmol) aluminum chloride ( $\text{AlCl}_3$ ) was added to the flask. The bath was removed and the reaction was allowed to warm to room temperature over 6 h while stirring. The solution was concentrated to 50 mL and poured into 200 mL ethanol to precipitate the product. The precipitate was separated by filtration, washed three times with ethanol and dried under vacuum at room temperature for 24 h.<sup>[268]</sup> The  $^1\text{H}$  NMR spectra are shown in Fig. 5.6 and Fig. 5.7. For  $L = 2$ , the degree of acylation can be calculated by  $A_4/(A_{4'}/2 + A_4)$ . Here  $A_4$  is the peak area of aromatic protons of the acylated units;  $A_{4'}$  is the peak area of aromatic protons of the unreacted units. For  $L = 4$ , the degree of acylation can be calculated by  $A_6/(A_{6'}/2 + A_6)$ . Here  $A_6$  is the peak area of aromatic

protons of the acylated units;  $A_{6'}$  is the peak area of aromatic protons of the unreacted units. The degree of acylation can be controlled by varying reaction temperature and the amount of acylating agent (Table 5.1).

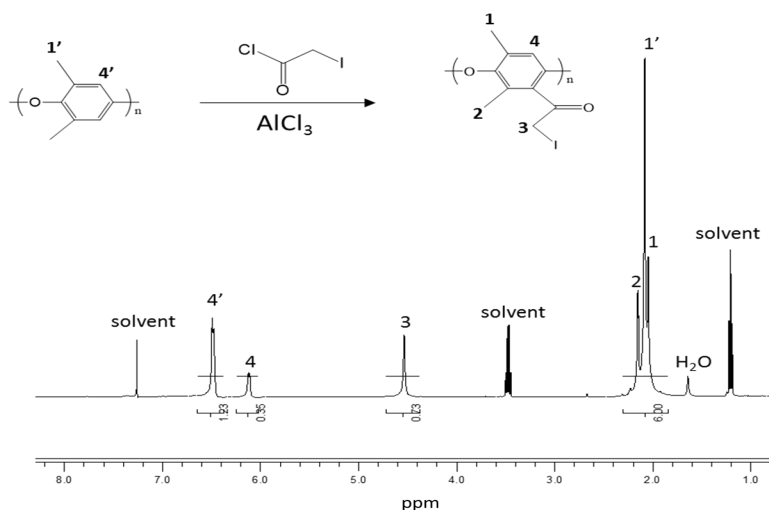


Figure 5.6:  $^1\text{H}$  NMR spectrum ( $\text{CDCl}_3$ ) of acylated PPO,  $L = 2$ .  $L$  is the number of carbons of the acylating agent.

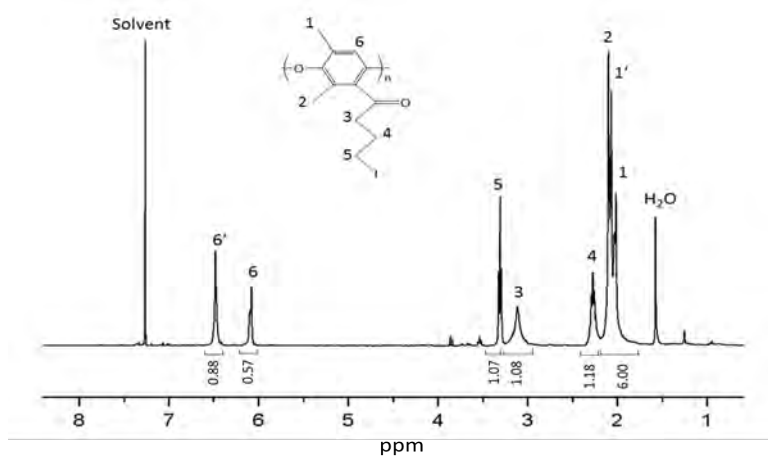


Figure 5.7:  $^1\text{H}$  NMR spectrum ( $\text{CDCl}_3$ ) of acylated PPO,  $L = 4$ .  $L$  is the number of carbons of the acylating agent.

Table 5.1: Reaction conditions and degree of acylation of acylated PPO.

Temperature (°C)	L	Time (h)	Amount of acylating agent (eq)	Degree of acylation (%)
20	2	1	0.5	0.2
20	2	1	1	0.37
0	4	1	1	0.44
20	4	1	1	0.57

**Synthesis of 4-iodobutyric chloride:** To a solution of 1 g (4.67 mmol) 4-iodobutyric acid in 10 mL chloroform was dropwise added 3.65 mL (50 mmol) thionyl chloride. The solution was stirred at room temperature for 24 h. The solvent was evaporated to afford a brown oil.<sup>[269]</sup>

4-iodobutyric chloride: <sup>1</sup>H NMR (400 MHz, CDCl<sub>3</sub>)  $\delta$  3.22 (2H, t), 3.07 (2H, t), 2.09 (2H, m). Yield: 83 wt%.

### 5.2.2.3 Route 3

**Synthesis of 4-vinylphenyl-bis(2,4,6-trimethylphenyl) phosphine:** Under an anhydrous and oxygen-free atmosphere, 5 mL butyllithium/cyclohexane solution (2.0 M) was added dropwise to a solution of 1.35 g (10 mmol) 4-bromostyrene in 15 mL anhydrous THF at  $-78$  °C. The solution was stirred for 24 h at  $-78$  °C to afford 4-lithostyrene.<sup>[270]</sup> To the freshly prepared 4-lithostyrene THF solution at  $-78$  °C, was added bis(2,4,6-trimethylphenyl)phosphorus chloride (10 mmol, 3.05 g) in 40 mL of anhydrous THF dropwise with stirring over 20 min. After stirring at  $-78$  °C for 30 min, the reaction mixture was allowed to warm to room temperature. After stirring at room temperature for 1 h, the reaction mixture was hydrolyzed with HCl (1 M, 20 mL), followed by addition of chloroform and then the organic solution was separated and dried over anhydrous MgSO<sub>4</sub>. The solvent was evaporated at reduced pressure.



The residue was washed with methanol three times, separated by filtration and dried under vacuum at room temperature for 24 h.<sup>[271]</sup>

4-vinylphenyl-bis(2,4,6-trimethylphenyl) phosphine: <sup>1</sup>H NMR (400 MHz, CDCl<sub>3</sub>) δ 7.30 (4H, d, *J* = 4.4 Hz), 6.83 (4H, d, *J* = 2.8 Hz), 6.69 (1H, dd, *J* = 17.6 Hz, *J* = 10.8 Hz), 5.76 (1H, d, *J* = 17.6 Hz), 5.24 (1H, d, *J* = 17.6 Hz), 2.27 (6H, s), 2.11 (12H, s) <sup>31</sup>P NMR (161 MHz, CDCl<sub>3</sub>) δ -22.6 (s). Yield: 83 wt%.

**Synthesis of phosphine functionalized polymer:** To 4-vinylphenyl bis(2,4,6-trimethylphenyl) phosphine (0.093 g, 0.25 mmol) and bis(triphenylphosphine)-palladium(II) dichloride (PdCl<sub>2</sub>(PPh<sub>3</sub>)<sub>2</sub>) (7.0 mg, 0.01 mmol) in 5 mL *N,N*-dimethylformamide (DMF), was added triethylamine (0.11 mL, 0.75 mmol), and formic acid (88 wt%, 0.02 mL, 0.5 mmol). The solution was then heated to 80 °C for 24 h. The solution was dropwise added to 50 mL methanol to precipitate the product. The precipitate was collected by filtration, rinsed three times with methanol, and dried under vacuum.<sup>[272-273]</sup> The <sup>1</sup>H NMR spectra before and after the reaction are shown in Fig. 5.8. The degree of functionalization (DF) can be calculated by  $DF = \frac{A_7/4}{(A_3 + A_{3'})/2}$ .

Here *A*<sub>7</sub> is the peak area of the methoxy groups on the cation; *A*<sub>3</sub> is the peak area of aromatic protons adjacent to the reacted repeat units; *A*<sub>3'</sub> is the peak area of aromatic protons adjacent to the unreacted repeat units. The calculated DF = 27 at%.

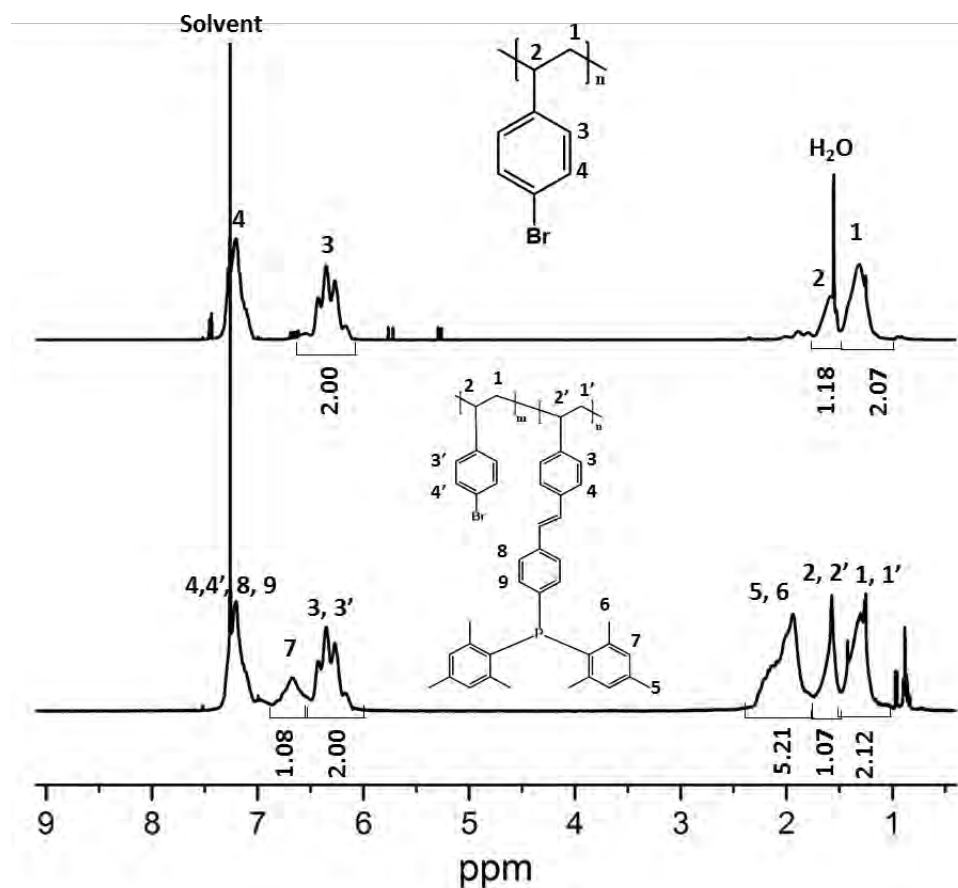


Figure 5.8:  $^1\text{H}$  NMR spectra ( $\text{CDCl}_3$ ) of poly(4-bromostyrene) and 4-vinylphenyl-bis(2,4,6-trimethylphenyl) phosphine functionalized polystyrene.

**Quaternization of phosphine functionalized polymer:** A mixture of the 1 g phosphine functionalized polymer and 4 mL iodomethane (64 mmol) was stirred at room temperature for 24 h. The solution was added dropwise to 40 mL ethyl ether to precipitate the product. The precipitate was collected by filtration, rinsed three times with ethyl ether, and dried under vacuum. The  $^{31}\text{P}$  NMR spectra before and after the reaction are shown in Fig. 5.9.

The complete disappearance of the phosphine peak ( $^{31}\text{P}$  NMR in  $\text{CDCl}_3$ :  $\delta = -23.2$  ppm) and appearance of the phosphonium peak ( $^{31}\text{P}$  NMR in  $\text{CDCl}_3$ :  $\delta = 12.6$  ppm) indicates that the degree of quaternization is 100%.

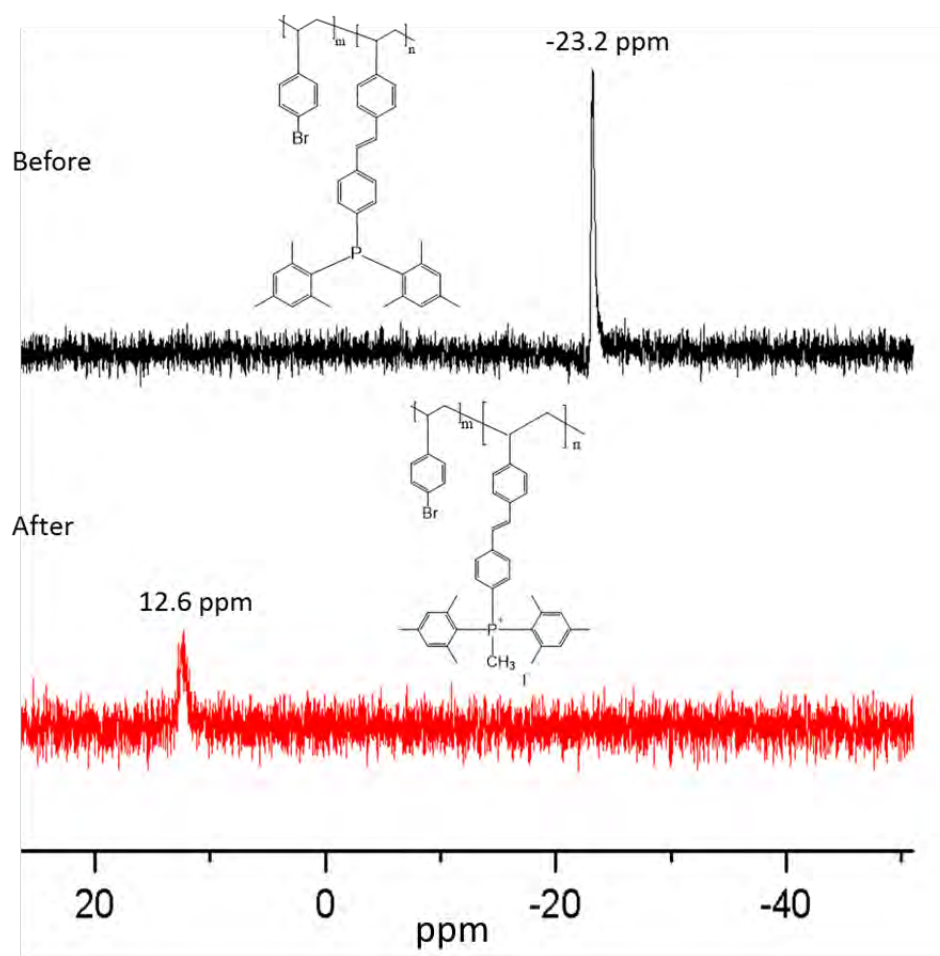


Figure 5.9:  $^{31}\text{P}$  NMR spectra ( $\text{CDCl}_3$ ) of 4-vinylphenyl-bis(2,4,6-trimethylphenyl) phosphine functionalized polystyrene and methyl 4-vinylphenyl-bis(2,4,6-trimethylphenyl)phosphonium functionalized polystyrene.

#### 5.2.2.4 Synthesis of 2-bromo-5-vinyl-*m*-xylene

**Synthesis of 4-bromo-3,5-dimethylaniline:** 12.7 mL (0.1 mol) 3,5-dimethylaniline in 100 mL anhydrous acetonitrile (ACN) was added to 17.8 g (0.1 mol) *N*-bromosuccinimide (NBS) in 100 mL ACN acetonitrile at 0 °C. The solution was allowed to warm to room temperature and stirred for 18 h. The solvent was evaporated after the reaction. The resulting mixture was diluted with 1 L hexane and the precipitate was removed by filtration. The filtrate was concentrated at reduced pressure to afford the crude product. The crude product was recrystallized from hexane to yield desired pure product.<sup>[274]</sup>

4-bromo-3,5-dimethylaniline: <sup>1</sup>H NMR (400 MHz, CDCl<sub>3</sub>) δ 6.44 (2H, s), 3.54 (2H, s), 2.32 (6H, s). Yield: 90 wt%.

**Synthesis of 2-bromo-5-iodo-*m*-xylene:** To a solution of 4-bromo-3,5-dimethylaniline (5.0 g, 25 mmol) in aqueous HCl (200 mL, 6.0 M) at 0 °C, a solution of sodium nitrite (NaNO<sub>2</sub>) (1.95 g, 28.3 mmol) in DI water (9 mL) was added dropwise over a period of 15 min. The mixture was stirred at 0 °C for 20 min. Then, a solution of potassium iodide (KI) (41.5 g, 0.25 mol) in DI water (69 mL) was slowly added to the mixture over a period of 15 min. The reaction mixture was stirred at 0 °C for 2 h and allowed to warm to room temperature. After 18 h, the resulting mixture was neutralized by adding sodium carbonate (Na<sub>2</sub>CO<sub>3</sub>) and was subsequently extracted with ethyl ether (100 mL × 4). The combined organic layers were washed with DI water (200 mL), aqueous sodium sulfite (Na<sub>2</sub>SO<sub>3</sub>) (1 M, 75 mL × 3) and were dried over anhydrous MgSO<sub>4</sub>. After filtration, the filtrate was evaporated to afford the crude product. The crude product was purified by silica gel column chromatography using hexane as an eluent. Remove of the solvent gave colorless oil.<sup>[275]</sup>

2-bromo-5-iodo-*m*-xylene:  $^1\text{H}$  NMR (400 MHz,  $\text{CDCl}_3$ )  $\delta$  7.40 (2H, s), 2.36 (6H, s). Yield: 72 wt%.

**Synthesis of 2-bromo-5-vinyl-*m*-xylene:** A mixture of 2-bromo-5-iodo-*m*-xylene (3.3 g, 10.7 mmol), triethoxyvinylsilane (2.77 mL, 12.8 mmol), palladium(II) chloride ( $\text{PdCl}_2$ ) (0.1 g, 5 mol%) and tetrabutylammonium fluoride (TBAF) (1 M solution in THF; 12.8 mL, 12.8 mmol) in THF (32 mL) was heated under reflux (65  $^\circ\text{C}$ ) for 9 h. The reaction mixture was extracted with ethyl ether three times, the combined ether extract washed with brine and then DI water, and dried over anhydrous  $\text{MgSO}_4$ . Evaporation of the solvent left the crude product, which was purified by column chromatography over silica gel (hexane : ether = 98 : 2 vol) to give 2-bromo-5-vinyl-*m*-xylene as a colorless oil.<sup>[276]</sup>

2-bromo-5-vinyl-*m*-xylene:  $^1\text{H}$  NMR (400 MHz,  $\text{CDCl}_3$ )  $\delta$  7.09 (2H, s), 6.56 (1H, q), 5.75 (1H, d,  $J = 4.8$  Hz), 5.25 (1H, d,  $J = 4.8$  Hz), 2.45 (6H, s). Yield: 50 wt%.

#### 5.2.2.5 Alkaline stability study of MTPP-(2,4,6-Me) analog

**Synthesis of MTPP-(2,4,6-Me) analog:** A mixture of the 4-vinylphenyl-bis(2,4,6-trimethylphenyl) phosphine (10 mmol) and 2 mL iodomethane (32 mmol) was stirred at room temperature for 24 h. The precipitated product was collected by filtration, rinsed three times with THF, and dried under vacuum.

MTPP-(2,4,6-Me) analog:  $^1\text{H}$  NMR (400 MHz,  $\text{CDCl}_3$ )  $\delta$  7.70 (2H, dd,  $J = 6$  Hz,  $J = 3.6$  Hz), 7.53 (2H, dd,  $J = 6.0$  Hz,  $J = 3.6$  Hz), 7.03 (4H, d,  $J = 4.4$  Hz), 6.76 (1H, dd,  $J = 17.6$  Hz,  $J = 10.8$  Hz), 5.99 (1H, d,  $J = 17.6$  Hz), 5.53 (1H, d,  $J = 17.6$  Hz), 3.18 (3H, d,  $J = 12.0$  Hz), 2.35 (6H, s), 2.09 (12H, s).  $^{31}\text{P}$  NMR (161 MHz,  $\text{CDCl}_3$ )  $\delta$  14.0 (s). Yield: 73 wt%.

**Durability test of MTPP-(2,4,6-Me) analog:** 1 M deuterated potassium hydroxide (KOD) in CD<sub>3</sub>OD/D<sub>2</sub>O (5/1 vol) solution was prepared by dissolving KOD (40 wt% in D<sub>2</sub>O, 4.28 g, 30.0 mmol) in a mixture of deuterated methanol and heavy water (CD<sub>3</sub>OD/D<sub>2</sub>O) (25 mL/2.67 mL). MTPP-(2,4,6-Me) analog (0.514 g, 1.00 mmol) was added to the alkaline solution to obtain a molar ratio of 30 KOD : 1 model compound (i.e. 0.033 M). TMS(CH<sub>2</sub>)<sub>3</sub>SO<sub>3</sub>Na (0.107 g, 0.490 mmol) was added to serve as an internal standard for <sup>1</sup>H NMR measurements. The mixture was placed in a fluoropolymer lined autoclave. Before the test (t = 0), an aliquot of the testing solution was removed and analyzed by both <sup>1</sup>H NMR and <sup>31</sup>P NMR spectroscopy to determine the initial quantity of MTPP-(2,4,6-Me) analog. Then, the testing solution was held at 60 °C. Aliquots of the reaction were removed hourly and analyzed by both <sup>1</sup>H NMR and <sup>31</sup>P NMR spectroscopy to determine the quantity of MTPP-(2,4,6-Me) analog remaining.

### 5.3 Results and discussion.

#### 5.3.1 Route 1- link the side group of MTPP-(2,4,6-Me)-I to the polymer backbone

We targeted to brominate one of the nine methyl groups on the phenyl rings of MTPP-(2,4,6-Me)-I using NBS as the brominating agent and BPO as the initiator. The key point for this step is that we need to ensure only one methyl get brominated per cation, otherwise, crosslinking may occur in the following steps. <sup>1</sup>H NMR spectra (Fig. 5.4) show that after the bromination reaction, a new peak appears at 4.5 ppm which is attributed to the bromomethyl group. The generation of new aromatic peak (Peak 7) also suggests the bromination takes place. The degree of bromination can be calculated by comparing the peak area of bromomethyl proton (Peak 5) to that of

methyl on P center (Peak 4). Besides the degree of bromination, we also need to know whether multi-bromination takes place in one cation. The  $^{31}\text{P}$  NMR spectrum (Fig. 5.5) shows that besides the initial MTPP-(2,4,6-Me) cation peak, there are three new P peaks generate after the bromination, which indicates multi-bromination takes place in one cation. With multi-bromination, more than one bromomethyl group could react with butylamine groups of PSf-BA in the subsequent step, affording a crosslinking opportunity for the polymer chains, which would make the characterization and processing of the HEMs problematic. Therefore, this synthesis route was abandoned.

### 5.3.2 Route 2- link the P center to the polymer backbone

In Chapter 4, it was demonstrated that it is necessary to quaternize the phosphine precursor with a methyl halide instead of the sterically hindered benzyl halide to synthesize MTPP-(2,4,6-Me). Analogously, our standard synthetic route for linking the cation to a polymer must be modified to reduce the bulkiness of the polymer's functional sites. Our approach is to introduce a long haloalkyl chain from the polymer to move the reaction away from the large rings on the PPO backbone.

Haloalkylated PPO (Fig. 5.2,  $L = 2, 4, 6$ ,  $L$  is the number of carbons of the acylating agent) was synthesized by acylation. We chose  $L = 2$  at the beginning because the acylating agent is commercially available.  $^1\text{H}$  NMR confirms that this step was successful (Fig. 5.6). However, the subsequent quaternization reaction with the phosphine precursor failed under various conditions (0% conversion, Table 5.1). The primary reason for the failure of the quaternization reaction is likely that the  $L = 2$  spacer is not long enough to completely prevent backbone interference. Therefore, the simplest solution is to increase  $L$ . An  $L = 4$  acylating agent is also commercially available, but in the form of a carboxylic acid instead of an acyl chloride, so that an

additional conversion step is required.  $^1\text{H}$  NMR spectrum suggests that we have succeeded in iodoalkylated PPO with  $L = 4$  (Fig. 5.7). The subsequent quaternization reaction was carried out to link iodoalkylated PPO to the phosphine precursor under various conditions (Table 5.2). Only 5% conversion was achieved when the reaction temperature was raised to 120 °C. Higher temperatures did not improve conversion but caused additional side reactions. We also tried  $L = 6$  acylating agent, however, the iodide form was not commercially available. Thus bromide form was used instead. The subsequent quaternization reaction failed again under various conditions (0% conversion, Table 5.2).

The reason for the low conversion of the quaternization reaction may be the improper balance between steric and electronic effects. Although the longer spacer reduces steric hindrance, its extra carbon atoms donate more electron density to the  $\alpha$ -carbon, decreasing its reactivity for an electrophilic attack. Also, the polymer version of the reaction may be inherently less favorable due to higher viscosity, inadequate solvation, and/or spatial mobility constraints.



Table 5.2: Conditions for and results of polymer quaternization reaction (Route 2).

Side chain	Temperature (°C)	Molar ratio (phosphine/polymer)	Conversion
C <sub>2</sub> I	20	1	0
C <sub>2</sub> I	40	1	0
C <sub>2</sub> I	60	1	0
C <sub>2</sub> I	80	1	0
C <sub>2</sub> I	120	1	0
C <sub>2</sub> I	20	5	0
C <sub>2</sub> I	40	5	0
C <sub>2</sub> I	60	5	0
C <sub>2</sub> I	80	5	0
C <sub>2</sub> I	120	5	0
C <sub>4</sub> I	80	5	0
C <sub>4</sub> I	120	5	~5%
C <sub>6</sub> Br	80	5	0
C <sub>6</sub> Br	120	5	0

### 5.3.3 Route 3- link the side group of the phosphine precursor to the polymer backbone

In order to overcome the large steric hindrance to the quaternization, phosphine instead of phosphonium cation was designed to link to the polymer backbone through the side group on the benzene ring. Thus, an additional step is required to synthesize this particular phosphine which has eight methyl groups and one vinyl group on the phenyl rings. Then, Heck coupling is carried out to link the vinyl-substituted phosphine to the polymer backbone followed by the quaternization with iodomethane. However, 4-bromo-3,5-dimethylstyrene, the reactant to begin with, is not commercial, and it needs additional three steps to synthesize (Fig. 5.10).

Before the synthesis, 4-bromostyrene was used as the reactant to verify the feasibility of Route 3 (Fig. 5.11), because it is commercial and has very similar

structure to 4-bromo-3,5-dimethylstyrene. After going through the all the steps, methyl 4-vinylphenyl bis(2,4,6-trimethylphenyl)phosphonium (MTPP-(2,4,6-Me) analog)) functionalized PSt was obtained. (NMR evidences for final product are shown in Fig. 5.8 and 5.9). Accordingly, Route 3 has proved to be feasible.

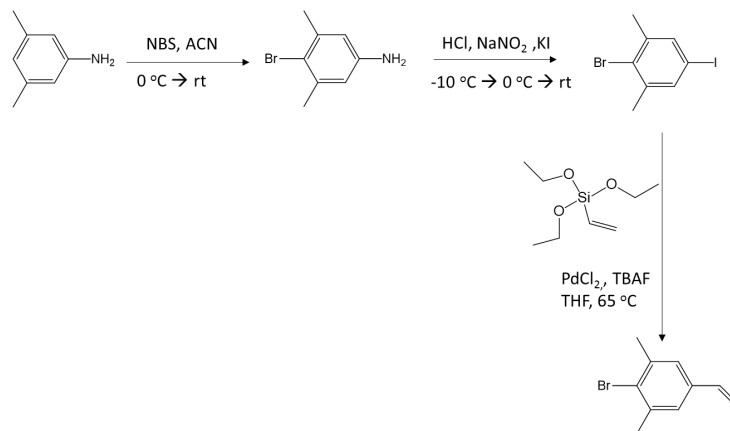


Figure 5.10: Synthesis route of 4-bromo-3,5-dimethylstyrene.

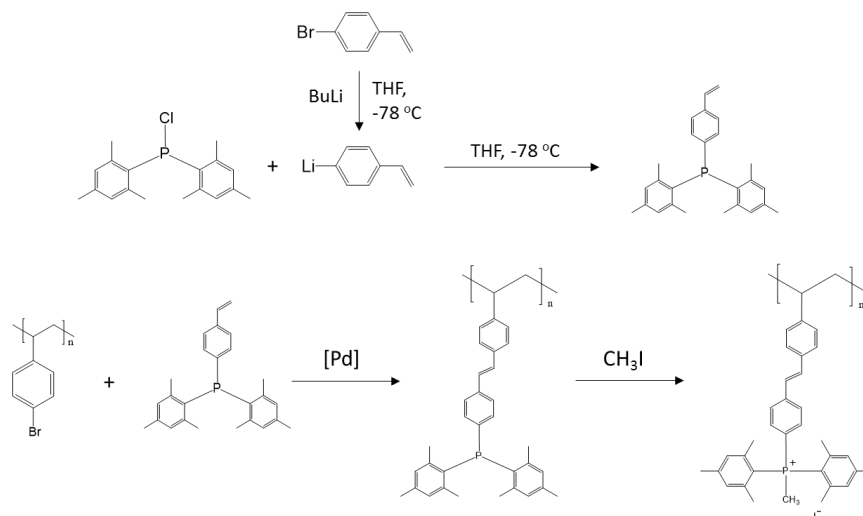


Figure 5.11: Synthesis route of MTPP-(2,4,6-Me) analog functionalized polymer (verification of Route 3).

By exploring the multi-step synthesis route including bromination, iodination and Hiyama coupling (Fig. 5.10). 4-bromo-3,5-dimethylstyrene has been successfully synthesized (see 5.2.2.4). This successful result indicates that Route 3, with this new reactant, affords MTPP-(2,4,6-Me) functionalized PSt.

#### 5.3.4 Alkaline durability test of MTPP-(2,4,6-Me) analog

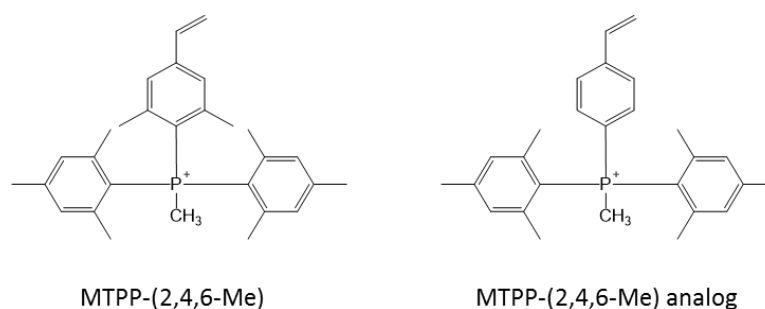


Figure 5.12: Chemical structures of MTPP-(2,4,6-Me) and MTPP-(2,4,6-Me) analog.

MTPP-(2,4,6-Me) analog has very similar chemical structure to MTPP-(2,4,6-Me) (Fig. 5.19), only lacks two methyl groups on one benzene rings. Its alkaline stability has also been studied. **Note:** the temperature here is 60 °C other than 80 °C which was applied to MTPP-(2,4,6-Me) due to its expected lower stability. The other conditions are the same as noted previously.  $^{31}\text{P}$  NMR spectra over 24 h (Fig. 5.13) indicate a gradual degradation resulting in the phosphine oxide peak gradually increasing (Peak 1). The degradation percentage of MTPP-(2,4,6-Me) analog was judged by  $A_2/(A_1+A_2)$ .  $A_1$  is the peak area of generated phosphine oxide peak and  $A_2$  is the peak area of the remaining MTPP-(2,4,6-Me) analog. Even with a lower temperature, after 24 h, only 14% of MTPP-(2,4,6-Me) analog remained.

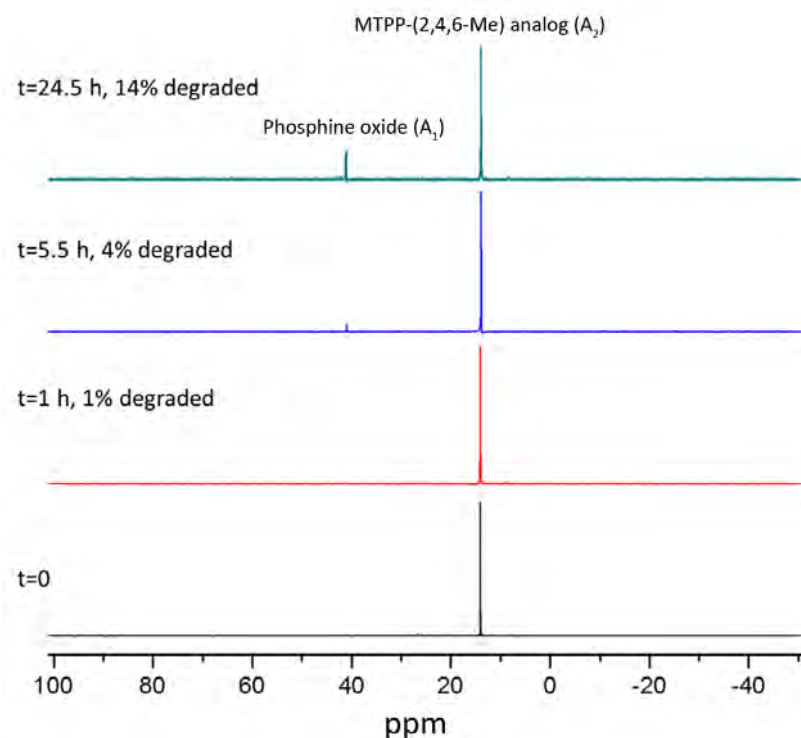


Figure 5.13: Time series of  $^{31}\text{P}$  NMR spectra during durability test of MTPP-(2,4,6-Me) analog at 60 °C. Phosphoric acid as the external standard; 1M KOD in  $\text{CD}_3\text{OD}/\text{D}_2\text{O}$  (5/1 vol) as the solvent.

When compared with MTPP-(2,4,6-Me), with the only difference being two methyl groups, the alkaline stability of MTPP-(2,4,6-Me) analog drops significantly. It provides further evidence to the role that steric hindrance plays in stabilizing MTPP-(2,4,6-Me). When it loses two ortho-substituents on one benzene ring, an opening to  $\text{OH}^-$  attack is significantly enhanced. Accordingly, the alkaline stability of MTPP-(2,4,6-Me) analog is much worse than that of MTPP-(2,4,6-Me). This observation again verified the superiority of the design of MTPP-(2,4,6-Me).

## 5.4 Conclusion

Three synthesis routes have been developed to link MTPP-(2,4,6-Me) to the polymer backbone. Route 1 has issues arising from the multi-bromination which would cause crosslinking of the polymer chains. In terms of Route 2, the large steric hindrance of the phosphine precursor and high viscosity of the polymer reactant prevented quaternization step to take place.

In Route 3, phosphine precursor instead of MTPP-(2,4,6-Me) cation is designed to link to the polymer backbone to overcome the large steric hindrance to quaternization. By using 4-bromostyrene instead of 4-bromo-3,5-dimethylstyrene (the reactant for synthesizing MTPP-(2,4,6-Me) functionalized polymer, but not commercially available), MTPP-(2,4,6-Me) analog functionalized polymer was successfully synthesized, which verified the feasibility of Route 3. MTPP-(2,4,6-Me) analog, the one only lacks two methyl groups compared with MTPP-(2,4,6-Me), showed much worse alkaline stability than MTPP-(2,4,6-Me), due to the reduction of steric hindrance. Thus MTPP-(2,4,6-Me) based HEM is still desired. The desired reactant for MTPP-(2,4,6-Me) based HEM, 4-bromo-3,5-dimethylstyrene, has been successfully synthesized. Accordingly, by going through Route 3 with the desired reactant, MTPP-(2,4,6-Me) functionalized Polymer can be obtained.

## Chapter 6

### CONCLUSIONS AND FUTURE WORK

#### 6.1 Conclusions

The nature of the cationic group to a large extent determines the alkaline stability of the HEM. Thus, efforts were made to develop alkaline stable cations and understand the degradation pathways.

TAS cations were firstly explored due to their capabilities to avoid the degradations from  $\alpha$ -C  $S_N2$  attack and Hofmann elimination. By adopting a novel nitrogen-bridge strategy, TAS functionalized polysulfones were successfully synthesized and made into HEMs. The methoxy-substituted TAS based HEM (i.e. PSf-MeOTASOH) exhibits good alkaline stability (maintained 80% of hydroxide conductivity after 12 days in 1 M KOH aqueous solution at 60 °C), excellent thermal stability ( $T_{OD} = 242$  °C), acceptable hydroxide conductivity ( $15.4 \text{ mS cm}^{-1}$  at 20 °C) and high IEC-normalized hydroxide conductivity ( $22.3 \text{ mS g cm}^{-1} \text{ mmol}^{-1}$ ).

The alkaline stability study of a series of TAS species uncovered the influence of the aryl-substituents on cation stability. By introducing more and stronger electron donating aryl-substituents, the alkaline stability of TAS cation was improved (9MeOTAS > MeOTAS > MeTAS). However, the alkaline stability of the most stable TAS cation (9MeOTAS) is still inferior to the benchmark cation BTMA, because the central S atom is susceptible to  $\text{OH}^-$  attack. This is deemed to be an intrinsic limitation for TAS cations. Consequently, this effort shifted to develop a more protected central atom to increase the alkaline stability of these cations.

Triaryl-substituted QP cations are expected to have higher alkaline stability than TAS cations, due to their increased steric hindrance around to the central P atom. The alkaline stabilities of previous developed BTPP-(2,4,6-MeO) and its three QP analogs with different phenyl-substituents were quantitatively studied. BTPP-(2,4,6-MeO) showed much enhanced alkaline stability as compared to the three QP analogs and the benchmark cation, BTMA. Different from QA cations, all of the three QP analogs degraded through Cahours-Hofmann pathway to form phosphine oxide. No  $\alpha$ -C S<sub>N</sub>2 degradation took place, confirming the benzylic position is well protected in QP cations.

BTPP-(2,4,6-MeO) undergoes a completely different degradation mechanism, which is substituent-related. It was determined that neither an  $\alpha$ -C S<sub>N</sub>2 attack or nor a central atom degradation took place. A new degradation mechanism is proposed that includes ether hydrolysis, inner salt formation, ketone rearrangement and further hydrolysis. This mechanism was verified and reveals that not only the central P atom, but also the phenyl-substituents could undergo degradation in alkaline environment. With nine strong electron-donating phenyl-substituents, the P center became less susceptible to OH<sup>-</sup> nucleophilic attack so that the essential structure of BTPP-(2,4,6-MeO) remained intact during the durability test. This explained why the overall alkaline stability of BTPP-(2,4,6-MeO) is significantly higher than that of the three QP analogs and even BTMA. However, the methoxy group itself is susceptible to alkaline attack, and thus illustrates another potential degradation pathway for these cations. The methoxy group undergoes ether hydrolysis and triggers another type of degradation before the entire cation structure falls apart. Accordingly, by replacing the

methoxy substituent with an alkaline stable electron-donating substituent, the alkaline stability of QP cation could be further improved.

Inspired by the new degradation mechanism, a superior QP system, MTPP-(2,4,6-Me), was designed. MTPP-(2,4,6-Me) exhibited excellent alkaline stability, which is 31 times as stable as BTTP-(2,4,6-MeO), the most stable QP cation to date and 64 times as stable as BMTA. MTPP-(2,4,6-Me) demonstrated a level of stability that has not been achieved by any other known HEM cations. The ultra-high alkaline stability of MTPP-(2,4,6-Me) is resultant from methyl's high alkaline stability, decent electron-donating ability and large steric hindrance. Due to its excellent alkaline stability, MTPP-(2,4,6-Me) is considered to be a very promising candidate for the cationic group served in HEMs.

Through the systematic study of a series of QP cations, structure-property relationship was evaluated. The electronic effect and the steric effect together combined determine the rate of P center degradation. For para-substituted QP cations, electronic effect controls the degradation rate whereas for ortho-substituted QP cations, steric effect becomes the major controlling factor. For cations with the same phosphine precursor, the cation stability is dependent upon the fourth substituent (from the quaternizing agent). The selection criteria of the phosphine precursor should combine both steric and electronic attributes. Choosing candidates with large steric effect (ortho-substitutions) and strong electron-donating (para- and meta-substitutions) would provide the best QP stabilizing strategy.

To take the advantage of MTPP-(2,4,6-Me)'s outstanding alkaline stability, three synthesis routes were designed to synthesize MTPP-(2,4,6-Me) functionalized polymers for constructing HEMs. Linking through the side group of MTPP-(2,4,6-Me)



(Route 1) or through the P center of the phosphine precursor (Route 2) to the polymer backbone was proved to be infeasible. In order to overcome the large steric hindrance from both the P center and the polymer chains, Route 3 (linking through the side group of the phosphine precursor to the polymer backbone) was designed. By using 4-bromostyrene instead of 4-bromo-3,5-dimethylstyrene, the feasibility of Route 3 was verified. The desired reactant, 4-bromo-3,5-dimethylstyrene, was successfully synthesized. Accordingly, by going through Route 3 with the desired reactant, MTPP-(2,4,6-Me) functionalized polymer should be obtained.

## **6.2 Future work**

### **6.2.1 Preparation and characterization of MTPP-(2,4,6-Me) based HEMs**

Route 3 will be adopted to synthesize MTPP-(2,4,6-Me) functionalized polymers. By adjusting the reaction conditions (e.g. reaction temperature, reaction time and stoichiometric ratio of the reactants), polymers with different degree of functionalization could be achieved.  $^1\text{H}$  and  $^{31}\text{P}$  NMR spectroscopies will be used to confirm the chemical structures of the products.

With the cation functionalized polymers, MTPP-(2,4,6-Me)-based HEMs can be fabricated by drop-casting method. The IECs of the HEMs can be determined by titration. The conductivities of HEMs with different IECs will be measured under various temperatures to determine whether they meet the requirement for HEMFC applications ( $>10^{-2} \text{ S cm}^{-1}$ ), and how the IEC and temperature influence the conductivity. The water uptake and swelling ratio of the HEMs will be measured to determine whether the HEMs have sufficient dimensional stabilities. And the

mechanical properties will be measured to determine whether they have enough strength and flexibility for practical applications.

The alkaline durability test of the HEMs will be carried out to determine whether the excellent alkaline stability of MTPP-(2,4,6-Me) cation efficiently transfers to its membrane form. With 20% conductivity loss as the criteria, the durability of the HEMs will be determined.

### **6.2.2 Further improvement of alkaline stabilities of MTPP-(2,4,6-Me) based HEMs**

The comparison of the alkaline stability between the cation and its membrane form could tell us how the interactions between the cation and the polymer backbone affect the overall alkaline stability of the HEM. Recent investigations found that the cationic groups bound to the polymer chains might facilitate the alkaline degradation of the polymer backbone.<sup>[230, 277]</sup> With cationic groups attached to polymer backbone, the polymer backbone becomes partially hydrophilic, allowing close approach of OH<sup>-</sup>. Therefore, some alkaline stable polymers (e.g. polysulfone), when functionalized with the cationic groups, might lose their stability in the alkaline environment. This cation-triggered alkaline degradation of the polymer backbones would cause a degradation of the HEM before the cationic groups decompose. If such degradation takes place in MTPP-(2,4,6-Me) based HEMs, strategies need to be developed to address this issue.

One effective approach to mitigate the cation-triggered backbone degradation is to elongate the length of the linkage between the cationic group and the polymer backbone (Fig. 6.1). The longer linkage could reduce the electron effect of the cationic groups on the polymer backbone.<sup>[278-279]</sup> In order to introduce the longer linkage, some modifications will be made to Route 3 (Fig. 6.2). Additionally, with the extended

linkage, the flexibility of the polymer chains would be increased, which could mitigate the brittleness and thus increase the durability of the HEM.

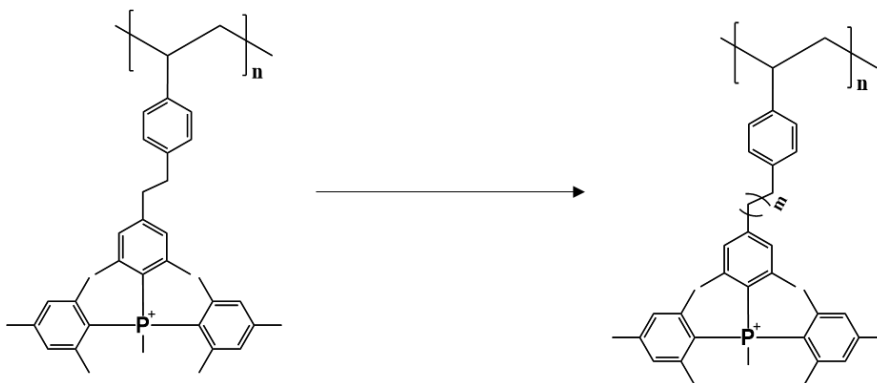


Figure 6.1: A strategy to mitigate the cation-triggered polymer backbone degradation.

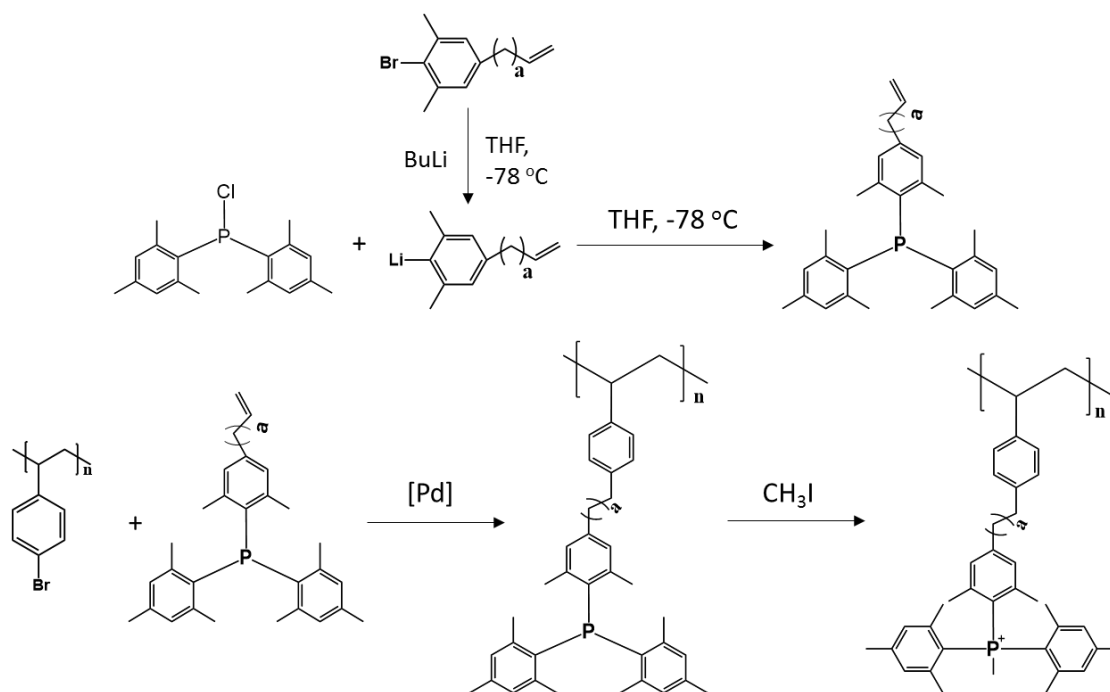


Figure 6.2: Synthesis route of MTPP-(2,4,6-Me) functionalized polymer with elongated linkage.

### 6.2.3 Further improvement of hydroxide conductivities of MTPP-(2,4,6-Me) based HEMs

To improve the hydroxide conductivities of the HEMs without making changes to the cations, an efficient way is to construct phase-segregated microstructure in HEMs. The cationic groups functionalized polymer segments would form hydrophilic ionic clusters and channels, which could enhance the effective mobility of  $\text{OH}^-$ , and thus increase the  $\text{OH}^-$  conductivity. To achieve better phase-segregated HEMs, one strategy is to introduce a longer linkage between the cationic groups and the polymer backbone. This approach is very important because it could also increase HEM's alkaline stability and flexibility at the same time.

Another interesting approach is to fabricate the HEMs based on block copolymers (Fig. 6.3). Due to the demixing of incompatible segments, strong phase-segregated morphologies generally exist in block copolymers. By adjusting the volume ratio of different blocks, well-connected ionic channels could be achieved in HEM, and the  $\text{OH}^-$  conductivity would be significant enhanced.

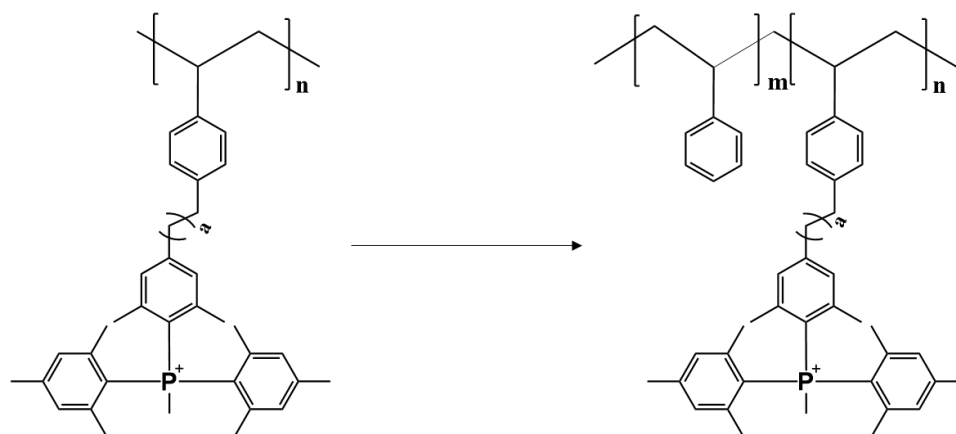


Figure 6:3 A strategy to improve the hydroxide conductivities of MTPP-(2,4,6-Me)-based HEMs.

#### 6.2.4 Further exploration of alkaline stable QP cations

As discussed in Chapter 4, in order to increase the alkaline stabilities of QP cations, the selection criteria of the phosphine precursor should combine both steric and electronic attributes. Choosing candidates with large steric effect (ortho-substitution) and strong electron-donating (para- and meta-substitutions) would provide the best QP stabilizing strategy.

By replacing the methyl substituents with some alkaline stable chemical groups that are bulkier and more electro-donating, the alkaline stability of QP could be further enhanced. For example, the *t*-butyl group has an  $E_s$  more negative than the methyl group ( $-2.78$  vs  $-1.24$ ) (see Appendix B for the definition of  $E_s$ ), indicating an increased steric effect. Additionally, the *t*-butyl group also has a stronger electron-donating ability than the methyl group ( $\sigma$ :  $-0.197$  vs  $-0.170$ ).<sup>[263, 280]</sup> Therefore, the QP with nine *t*-butyl groups as the phenyl-substituents, methyl (tris(2,4,6-*t*-butylphenyl)phosphonium (MTPP-(2,4,6-*t*-Bu)) (Fig. 6.4 (b)) is expected to have even higher alkaline stability. The major challenge in developing this QP cation would be the difficulties of synthesizing and quaternizing its phosphine precursor due to the increased steric effect.

To simplify the synthesis, some compromises might be made. The QP with six *t*-butyl groups and three methyl groups, methyl (2,4,6-trimethylphenyl)-bis(2,4,6-tri-*t*-butylphenyl)phosphonium (Fig. 6.5) would be easier to synthesize. The proposed synthesis route of the new phosphine precursor is shown in Fig. 6.6. With the phosphine precursor, Heck reaction demonstrated in Route 3 would be able to link it to the polymer backbone, and the quaternization step will be followed to obtain the new QP cation functionalized polymer.

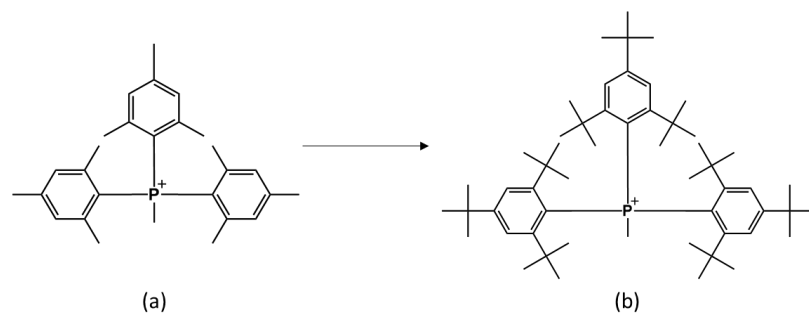


Figure 6.4: A strategy to further improve the alkaline stability of the QP cation. (a) MTPP-(2,4,6-Me) and (b) MTPP-(2,4,6-*t*-Bu).

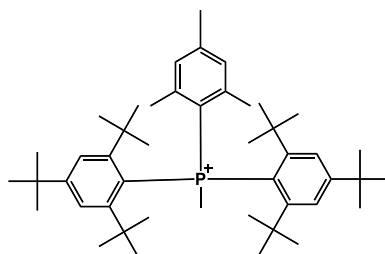


Figure 6.5: Chemical structure of a possibly superior QP cation, methyl (2,4,6-trimethylphenyl)-bis(2,4,6-tri-*t*-butylphenyl)phosphonium.

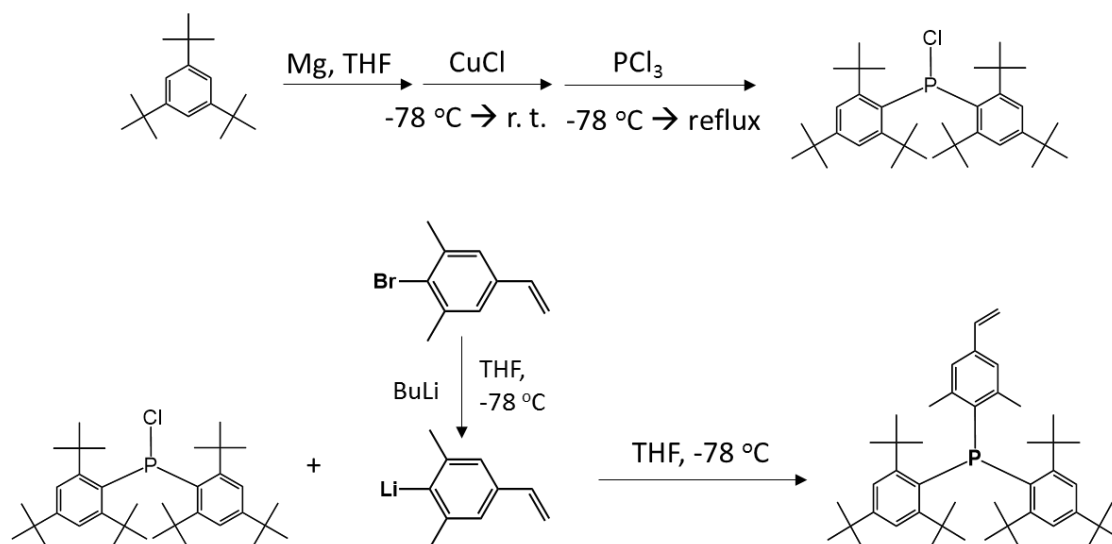


Figure 6.6: Proposed synthesis route of the new phosphine precursor.

## REFERENCES

- [1] R. Devanathan, *Energy & Environmental Science* **2008**, *1*, 101-119.
- [2] J. R. Varcoe, P. Atanassov, D. R. Dekel, A. M. Herring, M. A. Hickner, P. A. Kohl, A. R. Kucernak, W. E. Mustain, K. Nijmeijer, K. Scott, T. Xu, L. Zhuang, *Energy & Environmental Science* **2014**, *7*, 3135-3191.
- [3] G. Merle, M. Wessling, K. Nijmeijer, *Journal of Membrane Science* **2011**, *377*, 1-35.
- [4] J. Marcinkoski, J. P. Kopasz, T. G. Benjamin, *International Journal of Hydrogen Energy* **2008**, *33*, 3894-3902.
- [5] W. G. Grot, in *US Pat., Vol. 3718627* (Ed.: U. Pat.), **1968**.
- [6] J. Roziere, D. J. Jones, *Annual Review of Materials Research* **2003**, *33*, 503-555.
- [7] R. Borup, J. Meyers, B. Pivovar, Y. S. Kim, R. Mukundan, N. Garland, D. Myers, M. Wilson, F. Garzon, D. Wood, P. Zelenay, K. More, K. Stroh, T. Zawodzinski, J. Boncella, J. E. McGrath, M. Inaba, K. Miyatake, M. Hori, K. Ota, Z. Ogumi, S. Miyata, A. Nishikata, Z. Siroma, Y. Uchimoto, K. Yasuda, K.-i. Kimijima, N. Iwashita, *Chemical Reviews* **2007**, *107*, 3904-3951.
- [8] J. S. Spendelow, A. Wieckowski, *Physical Chemistry Chemical Physics* **2007**, *9*, 2654-2675.
- [9] Y. Kiros, S. Schwartz, *Journal of Power Sources* **2000**, *87*, 101-105.
- [10] J. Hernandez, J. Solla-Gullon, E. Herrero, A. Aldaz, J. M. Feliu, *Electrochimica Acta* **2006**, *52*, 1662-1669.
- [11] L. Demarconnay, C. Coutanceau, J. M. Leger, *Electrochimica Acta* **2004**, *49*, 4513-4521.
- [12] J. A. Vega, C. Chartier, W. E. Mustain, *Journal of Power Sources* **2010**, *195*, 7176-7180.
- [13] E. Gulzow, M. Schulze, *Journal of Power Sources* **2004**, *127*, 243-251.
- [14] G. F. McLean, T. Niet, S. Prince-Richard, N. Djilali, *International Journal of Hydrogen Energy* **2002**, *27*, 507-526.

- [15] P. Gouerec, L. Poletto, J. Denizot, E. Sanchez-Cortezon, J. H. Miners, *Journal of Power Sources* **2004**, 129, 193-204.
- [16] A. Schulze, E. Gulzow, *Journal of Power Sources* **2004**, 127, 252-263.
- [17] J. Larminie, Docks, A., *Fuel cell systems explained*, J. Wiley, **2002**.
- [18] E. Agel, J. Bouet, J. F. Fauvarque, *Journal of Power Sources* **2001**, 101, 267-274.
- [19] T. W. Xu, Z. M. Liu, W. H. Yang, *Journal of Membrane Science* **2005**, 249, 183-191.
- [20] J. R. Varcoe, R. C. T. Slade, G. L. Wright, Y. Chen, *Journal of Physical Chemistry B* **2006**, 110, 21041-21049.
- [21] S. Gu, W. Sheng, R. Cai, S. M. Alia, S. Song, K. O. Jensen, Y. Yan, *Chemical Communications* **2013**, 49, 131-133.
- [22] S. Lu, J. Pan, A. Huang, L. Zhuang, J. Lu, *Proceedings of the National Academy of Sciences of the United States of America* **2008**, 105, 20611-20614.
- [23] J. Pan, S. Lu, Y. Li, A. Huang, L. Zhuang, J. Lu, *Advanced Functional Materials* **2010**, 20, 312-319.
- [24] J. R. Varcoe, R. C. T. Slade, *Fuel Cells* **2005**, 5, 187-200.
- [25] L. Li, Y. X. Wang, *Journal of Membrane Science* **2005**, 262, 1-4.
- [26] G. Hebrard, J. Zeng, K. Loubiere, *Chemical Engineering Journal* **2009**, 148, 132-138.
- [27] E. H. Yu, K. Scott, *Journal of Power Sources* **2004**, 137, 248-256.
- [28] J.-S. Park, S.-H. Park, S.-D. Yim, Y.-G. Yoon, W.-Y. Lee, C.-S. Kim, *Journal of Power Sources* **2008**, 178, 620-626.
- [29] H. Hou, G. Sun, R. He, Z. Wu, B. Sun, *Journal of Power Sources* **2008**, 182, 95-99.
- [30] J. R. Varcoe, R. C. T. Slade, E. Lam How Yee, *Chemical Communications* **2006**, 1428-1429.
- [31] Y. Wu, C. Wu, F. Yu, T. Xu, Y. Fu, *Journal of Membrane Science* **2008**, 307, 28-36.



- [32] Y. Xiong, J. Fang, Q. H. Zeng, Q. L. Liu, *Journal of Membrane Science* **2008**, *311*, 319-325.
- [33] E. H. Yu, K. Scott, *Electrochemistry Communications* **2004**, *6*, 361-365.
- [34] H. Long, K. Kim, B. S. Pivovar, *Journal of Physical Chemistry C* **2012**, *116*, 9419-9426.
- [35] J. B. Edson, C. S. Macomber, B. S. Pivovar, J. M. Boncella, *Journal of Membrane Science* **2012**, *399*, 49-59.
- [36] S. Chempath, J. M. Boncella, L. R. Pratt, N. Henson, B. S. Pivovar, *Journal of Physical Chemistry C* **2010**, *114*, 11977-11983.
- [37] S. Chempath, B. R. Einsla, L. R. Pratt, C. S. Macomber, J. M. Boncella, J. A. Rau, B. S. Pivovar, *Journal of Physical Chemistry C* **2008**, *112*, 3179-3182.
- [38] C. S. Macomber, J. M. Boncella, B. S. Pivovar, J. A. Rau, *Journal of Thermal Analysis and Calorimetry* **2008**, *93*, 225-229.
- [39] D. Stoica, F. Alloin, S. Marais, D. Langevin, C. Chappey, P. Judeinstein, *Journal of Physical Chemistry B* **2008**, *112*, 12338-12346.
- [40] J. R. Varcoe, *Physical Chemistry Chemical Physics* **2007**, *9*, 1479-1486.
- [41] J. Yan, M. A. Hickner, *Macromolecules* **2010**, *43*, 2349-2356.
- [42] D. Marx, A. Chandra, M. E. Tuckerman, *Chemical Reviews* **2010**, *110*, 2174-2216.
- [43] X. Lin, Y. Liu, S. D. Poynton, A. L. Ong, J. R. Varcoe, L. Wu, Y. Li, X. Liang, Q. Li, T. Xu, *Journal of Power Sources* **2013**, *233*, 259-268.
- [44] W. Wang, S. Wang, W. Li, X. Xie, Y. Lv, *International Journal of Hydrogen Energy* **2013**, *38*, 11045-11052.
- [45] A. Katzfuss, V. Gogel, L. Joerissen, J. Kerres, *Journal of Membrane Science* **2013**, *425*, 131-140.
- [46] S. Gu, J. Skovgard, Y. S. Yan, *Chemsuschem* **2012**, *5*, 843-848.
- [47] L. Gubler, *Advanced Energy Materials* **2014**, *4*, 1300827.
- [48] S. Zhang, C. Li, X. Xie, F. Zhang, *International Journal of Hydrogen Energy* **2014**, *39*, 13718-13724.

- [49] J. Wang, G. He, X. Wu, X. Yan, Y. Zhang, Y. Wang, L. Du, *Journal of Membrane Science* **2014**, 459, 86-95.
- [50] L. Wang, M. A. Hickner, *Polymer Chemistry* **2014**, 5, 2928-2935.
- [51] M. R. Hibbs, M. A. Hickner, T. M. Alam, S. K. McIntyre, C. H. Fujimoto, C. J. Cornelius, *Chemistry of Materials* **2008**, 20, 2566-2573.
- [52] G. L. Han, P. Y. Xu, K. Zhou, Q. G. Zhang, A. M. Zhu, Q. L. Liu, *Journal of Membrane Science* **2014**, 464, 72-79.
- [53] H.-C. Lee, K.-L. Liu, L.-D. Tsai, J.-Y. Lai, C.-Y. Chao, *Rsc Advances* **2014**, 4, 10944-10954.
- [54] J. Ran, L. Wu, X. Lin, L. Jiang, T. Xu, *Rsc Advances* **2012**, 2, 4250-4257.
- [55] P. Zschocke, D. Quellmalz, *Journal of Membrane Science* **1985**, 22, 325-332.
- [56] M. Zhang, H. K. Kim, E. Chalkova, F. Mark, S. N. Lvov, T. C. M. Chung, *Macromolecules* **2011**, 44, 5937-5946.
- [57] H. A. Kostalik, T. J. Clark, N. J. Robertson, P. F. Mutolo, J. M. Longo, H. D. Abruna, G. W. Coates, *Macromolecules* **2010**, 43, 7147-7150.
- [58] N. J. Robertson, H. A. Kostalik, T. J. Clark, P. F. Mutolo, H. D. Abruna, G. W. Coates, *Journal of the American Chemical Society* **2010**, 132, 3400-3404.
- [59] R. Janarthanan, J. L. Horan, B. R. Caire, Z. C. Ziegler, Y. Yang, X. Zuo, M. W. Liberatore, M. R. Hibbs, A. M. Herring, *Journal of Polymer Science Part B-Polymer Physics* **2013**, 51, 1743-1750.
- [60] C. Fujimoto, D.-S. Kim, M. Hibbs, D. Wroblewski, Y. S. Kim, *Journal of Membrane Science* **2012**, 423, 438-449.
- [61] E. E. Switzer, T. S. Olson, A. K. Datye, P. Atanassov, M. R. Hibbs, C. Fujimoto, C. J. Cornelius, *Electrochimica Acta* **2010**, 55, 3404-3408.
- [62] M. A. Vandiver, J. L. Horan, Y. Yang, E. T. Tansey, S. Seifert, M. W. Liberatore, A. M. Herring, *Journal of Polymer Science Part B-Polymer Physics* **2013**, 51, 1761-1769.
- [63] D. S. Kim, C. H. Fujimoto, M. R. Hibbs, A. Labouriau, Y.-K. Choe, Y. S. Kim, *Macromolecules* **2013**, 46, 7826-7833.

- [64] X. Kong, K. Wadhwa, J. G. Verkade, K. Schmidt-Rohr, *Macromolecules* **2009**, 42, 1659-1664.
- [65] A. Bosnjakovic, M. Danilczuk, S. Schlick, P. N. Xiong, G. M. Haugen, S. J. Hamrock, *Journal of Membrane Science* **2014**, 467, 136-141.
- [66] C.-C. Yang, *Journal of Applied Electrochemistry* **2012**, 42, 305-317.
- [67] T. Y. Guo, Q. H. Zeng, C. H. Zhao, Q. L. Liu, A. M. Zhu, I. Broadwell, *Journal of Membrane Science* **2011**, 371, 268-275.
- [68] C. Sollogoub, A. Guinault, C. Bonnebat, M. Bennjima, L. Akrou, J. F. Fauvarque, L. Ogier, *Journal of Membrane Science* **2009**, 335, 37-42.
- [69] D. Stoica, L. Ogier, L. Akrou, F. Alloin, J. F. Fauvarque, *Electrochimica Acta* **2007**, 53, 1596-1603.
- [70] D. Henkensmeier, H. Cho, M. Brela, A. Michalak, A. Dyck, W. Germer, D. Ngoc My Hanh, J. H. Jang, H.-J. Kim, N.-S. Woo, T.-H. Lim, *International Journal of Hydrogen Energy* **2014**, 39, 2842-2853.
- [71] L. An, L. Zeng, T. S. Zhao, *International Journal of Hydrogen Energy* **2013**, 38, 10602-10606.
- [72] O. D. Thomas, K. J. W. Y. Soo, T. J. Peckham, M. P. Kulkarni, S. Holdcroft, *Journal of the American Chemical Society* **2012**, 134, 10753-10756.
- [73] Z. Xia, S. Yuan, G. Jiang, X. Guo, J. Fang, L. Liu, J. Qiao, J. Yin, *Journal of Membrane Science* **2012**, 390, 152-159.
- [74] H. Luo, G. Vaivars, B. Agboola, S. Mu, M. Mathe, *Solid State Ionics* **2012**, 208, 52-55.
- [75] O. D. Thomas, K. J. W. Y. Soo, T. J. Peckham, M. P. Kulkarni, S. Holdcroft, *Polymer Chemistry* **2011**, 2, 1641-1643.
- [76] H. Hou, G. Sun, R. He, B. Sun, W. Jin, H. Liu, Q. Xin, *International Journal of Hydrogen Energy* **2008**, 33, 7172-7176.
- [77] B. Xing, O. Savadogo, *Electrochemistry Communications* **2000**, 2, 697-702.
- [78] A. M. Maes, T. P. Pandey, M. A. Vandiver, L. K. Lundquist, Y. Yang, J. L. Horan, A. Krosovsky, M. W. Liberatore, S. Seifert, A. M. Herring, *Electrochimica Acta* **2013**, 110, 260-266.

- [79] W. Lu, Z.-G. Shao, G. Zhang, Y. Zhao, B. Yi, *Journal of Power Sources* **2014**, 248, 905-914.
- [80] T.-H. Tsai, A. M. Maes, M. A. Vandiver, C. Versek, S. Seifert, M. Tuominen, M. W. Liberatore, A. M. Herring, E. B. Coughlin, *Journal of Polymer Science Part B-Polymer Physics* **2013**, 51, 1751-1760.
- [81] J. Zhou, J. Guo, D. Chu, R. Chen, *Journal of Power Sources* **2012**, 219, 272-279.
- [82] C. Chen, A. R. Hess, A. R. Jones, X. Liu, G. D. Barber, T. E. Mallouk, H. R. Allcock, *Macromolecules* **2012**, 45, 1182-1189.
- [83] T. Zhou, J. Zhang, J. Jingfu, G. Jiang, J. Zhang, J. Qiao, *Synthetic Metals* **2013**, 167, 43-50.
- [84] L. Zeng, T. S. Zhao, Y. S. Li, *International Journal of Hydrogen Energy* **2012**, 37, 18425-18432.
- [85] G. Merle, S. S. Hosseiny, M. Wessling, K. Nijmeijer, *Journal of Membrane Science* **2012**, 409, 191-199.
- [86] Y. Wu, J. Luo, L. Yao, C. Wu, F. Mao, T. Xu, *Journal of Membrane Science* **2012**, 399, 16-27.
- [87] C.-C. Yang, S.-S. Chiu, S.-C. Kuo, T.-H. Liou, *Journal of Power Sources* **2012**, 199, 37-45.
- [88] J. Fu, J. Qiao, X. Wang, J. Ma, T. Okada, *Synthetic Metals* **2010**, 160, 193-199.
- [89] C.-C. Yang, S.-J. Chiu, W.-C. Chien, *Journal of Power Sources* **2006**, 162, 21-29.
- [90] T. Sata, K. Kawamura, K. Matsusaki, *Journal of Membrane Science* **2001**, 181, 167-178.
- [91] X. Li, Q. Liu, Y. Yu, Y. Meng, *Journal of Materials Chemistry A* **2013**, 1, 4324-4335.
- [92] A. Jasti, V. K. Shahi, *Journal of Materials Chemistry A* **2013**, 1, 6134-6137.
- [93] D. Chen, M. A. Hickner, S. Wang, J. Pan, M. Xiao, Y. Meng, *International Journal of Hydrogen Energy* **2012**, 37, 16168-16176.

- [94] M. Tanaka, M. Koike, K. Miyatake, M. Watanabe, *Polymer Chemistry* **2011**, 2, 99-106.
- [95] J. Fang, P. K. Shen, *J Membrane Sci* **2006**, 285, 317-322.
- [96] X. Li, Y. Yu, Y. Meng, *Acs Applied Materials & Interfaces* **2013**, 5, 1414-1422.
- [97] D. W. Seo, Y. D. Lim, M. A. Hossain, S. H. Lee, H. C. Lee, H. H. Jang, S. Y. Choi, W. G. Kim, *International Journal of Hydrogen Energy* **2013**, 38, 579-587.
- [98] D. W. Seo, M. A. Hossain, D. H. Lee, Y. D. Lim, S. H. Lee, H. C. Lee, T. W. Hong, W. G. Kim, *Electrochimica Acta* **2012**, 86, 360-365.
- [99] Q. Zhang, Q. Zhang, J. Wang, S. Zhang, S. Li, *Polymer* **2010**, 51, 5407-5416.
- [100] J. Zhou, M. Unlu, J. A. Vega, P. A. Kohl, *Journal of Power Sources* **2009**, 190, 285-292.
- [101] D. Xing, S. Zhang, C. Yin, C. Yan, X. Jian, *Materials Science and Engineering B-Advanced Functional Solid-State Materials* **2009**, 157, 1-5.
- [102] J. Kerres, A. Ullrich, M. Hein, *Journal of Polymer Science Part a-Polymer Chemistry* **2001**, 39, 2874-2888.
- [103] N. T. Rebeck, Y. Li, D. M. Knauss, *Journal of Polymer Science Part B-Polymer Physics* **2013**, 51, 1770-1778.
- [104] X. Lin, C. Wu, Y. Wu, T. Xu, *Journal of Applied Polymer Science* **2012**, 123, 3644-3651.
- [105] A. L. Ong, S. Saad, R. Lan, R. J. Goodfellow, S. Tao, *Journal of Power Sources* **2011**, 196, 8272-8279.
- [106] Y. Wu, C. Wu, J. R. Varcoe, S. D. Poynton, T. Xu, Y. Fu, *Journal of Power Sources* **2010**, 195, 3069-3076.
- [107] L. Wu, T. Xu, D. Wu, X. Zheng, *Journal of Membrane Science* **2008**, 310, 577-585.
- [108] L. Wu, T. Xu, W. Yang, *Journal of Membrane Science* **2006**, 286, 185-192.
- [109] T. W. Xu, F. F. Zha, *Journal of Membrane Science* **2002**, 199, 203-210.

- [110] X. Yan, S. Gu, G. He, X. Wu, J. Benziger, *Journal of Power Sources* **2014**, 250, 90-97.
- [111] J. Han, H. Peng, J. Pan, L. Wei, G. Li, C. Chen, L. Xiao, J. Lu, L. Zhuang, *Acs Applied Materials & Interfaces* **2013**, 5, 13405-13411.
- [112] Z. Liu, X. Li, K. Shen, P. Feng, Y. Zhang, X. Xu, W. Hu, Z. Jiang, B. Liu, M. D. Guiver, *Journal of Materials Chemistry A* **2013**, 1, 6481-6488.
- [113] Z. Liu, X. Zhu, G. Wang, X. Hou, D. Liu, *Journal of Polymer Science Part B- Polymer Physics* **2013**, 51, 1632-1638.
- [114] K. Shen, J. Pang, S. Feng, Y. Wang, Z. Jiang, *Journal of Membrane Science* **2013**, 440, 20-28.
- [115] X. Yan, G. He, X. Wu, J. Benziger, *Journal of Membrane Science* **2013**, 429, 13-22.
- [116] A. Jasti, S. Prakash, V. K. Shahi, *Journal of Membrane Science* **2013**, 428, 470-479.
- [117] J. Wang, J. Wang, S. Zhang, *Journal of Membrane Science* **2012**, 415, 205-212.
- [118] H. Zhang, Z. Zhou, *Solid State Ionics* **2008**, 179, 1296-1299.
- [119] X. Yan, S. Gu, G. He, X. Wu, W. Zheng, X. Ruan, *Journal of Membrane Science* **2014**, 466, 220-228.
- [120] C. Li, S. Wang, W. Wang, X. Xie, Y. Lv, C. Deng, *International Journal of Hydrogen Energy* **2013**, 38, 11038-11044.
- [121] Q. Hu, Y. Shang, Y. Wang, M. Xu, S. Wang, X. Xie, Y. Liu, H. Zhang, J. Wang, Z. Mao, *International Journal of Hydrogen Energy* **2012**, 37, 12659-12665.
- [122] G. Wang, Y. Weng, D. Chu, D. Xie, R. Chen, *Journal of Membrane Science* **2009**, 326, 4-8.
- [123] G. Wang, Y. Weng, J. Zhao, D. Chu, D. Xie, R. Chen, *Polymers for Advanced Technologies* **2010**, 21, 554-560.
- [124] D.-H. Kim, J.-H. Park, S.-J. Seo, J.-S. Park, S. Jung, Y. S. Kang, J.-H. Choi, M.-S. Kang, *Journal of Membrane Science* **2013**, 447, 80-86.

- [125] S.-H. Park, Y.-W. Choi, C.-S. Kim, S. B. Park, *Journal of Solid State Electrochemistry* **2013**, *17*, 1247-1254.
- [126] H. Jung, H. Ohashi, T. Tamaki, T. Yamaguchi, *Chemistry Letters* **2013**, *42*, 14-16.
- [127] H. Zhang, H. Ohashi, T. Tamaki, T. Yamaguchi, *Journal of Physical Chemistry C* **2012**, *116*, 7650-7657.
- [128] H. Jung, K. Fujii, T. Tamaki, H. Ohashi, T. Ito, T. Yamaguchi, *Journal of Membrane Science* **2011**, *373*, 107-111.
- [129] X. Zhang, S. W. Tay, Z. Liu, L. Hong, *Journal of Power Sources* **2011**, *196*, 5494-5498.
- [130] A. K. Pandey, R. F. Childs, M. West, J. N. A. Lott, B. E. McCarry, J. M. Dickson, *Journal of Polymer Science Part a-Polymer Chemistry* **2001**, *39*, 807-820.
- [131] H. Koshikawa, K. Yoshimura, W. Sinnananchi, T. Yamaki, M. Asano, K. Yamamoto, S. Yamaguchi, H. Tanaka, Y. Maekawa, *Macromolecular Chemistry and Physics* **2013**, *214*, 1756-1762.
- [132] J. P. Kizewski, N. H. Mudri, J. R. Varcoe, *Radiation Physics and Chemistry* **2013**, *89*, 64-69.
- [133] M. Mamlouk, J. A. Horsfall, C. Williams, K. Scott, *International Journal of Hydrogen Energy* **2012**, *37*, 11912-11920.
- [134] B.-S. Ko, J.-Y. Sohn, J. Shin, *Polymer* **2012**, *53*, 4652-4661.
- [135] L. Ajis, A. A. Nazli, M. A. Abd Malik, M. D. Khairul Zaman, Y. Muhd Zu Azhan, in *New Materials and Processes, Pts 1-3, Vol. 476-478* (Eds.: W. Z. Chen, Q. Li, Y. L. Chen, P. Q. Dai, Z. Y. Jiang), **2012**, pp. 636-641.
- [136] J. Fang, Y. Yang, X. Lu, M. Ye, W. Li, Y. Zhang, *International Journal of Hydrogen Energy* **2012**, *37*, 594-602.
- [137] J. R. Varcoe, R. C. T. Slade, E. L. H. Yee, S. D. Poynton, D. J. Driscoll, D. C. Apperley, *Chemistry of Materials* **2007**, *19*, 2686-2693.
- [138] T. N. Danks, R. C. T. Slade, J. R. Varcoe, *Journal of Materials Chemistry* **2003**, *13*, 712-721.

- [139] B. L. Svarfvar, K. B. Ekman, M. J. Sundell, J. H. Nasman, *Polymers for Advanced Technologies* **1996**, 7, 839-846.
- [140] J. Hu, Y. Meng, C. Zhang, S. Fang, *Thin Solid Films* **2011**, 519, 2155-2162.
- [141] G. Li, J. Pan, J. Han, C. Chen, J. Lu, L. Zhuang, *Journal of Materials Chemistry A* **2013**, 1, 12497-12502.
- [142] Y. Zhao, J. Pan, H. Yu, D. Yang, J. Li, L. Zhuang, Z. Shao, B. Yi, *International Journal of Hydrogen Energy* **2013**, 38, 1983-1987.
- [143] Y. Zhao, H. Yu, D. Yang, J. Li, Z. Shao, B. Yi, *Journal of Power Sources* **2013**, 221, 247-251.
- [144] Y.-C. Cao, K. Scott, X. Wang, *International Journal of Hydrogen Energy* **2012**, 37, 12688-12693.
- [145] F. Zhang, H. Zhang, J. Ren, C. Qu, *Journal of Materials Chemistry* **2010**, 20, 8139-8146.
- [146] A. M. Park, F. E. Turley, R. J. Wycisk, P. N. Pintauro, *Macromolecules* **2014**, 47, 227-235.
- [147] S. Roddecha, Z. Dong, Y. Wu, M. Anthamatten, *Journal of Membrane Science* **2012**, 389, 478-485.
- [148] Z. Jiang, Z.-J. Jiang, *Journal of Membrane Science* **2014**, 456, 85-106.
- [149] J. Hu, C. Zhang, L. Jiang, S. Fang, X. Zhang, X. Wang, Y. Meng, *Journal of Power Sources* **2014**, 248, 831-838.
- [150] N. Follain, S. Roualdes, S. Marais, J. Frugier, M. Reinholdt, J. Durand, *Journal of Physical Chemistry C* **2012**, 116, 8510-8522.
- [151] C. Zhang, J. Hu, J. Cong, Y. Zhao, W. Shen, H. Toyoda, M. Nagatsu, Y. Meng, *Journal of Power Sources* **2011**, 196, 5386-5393.
- [152] C. Zhang, J. Hu, Y. Meng, M. Nagatsu, H. Toyoda, *Chemical Communications* **2011**, 47, 10230-10232.
- [153] M. Sudoh, S. Niimi, N. Takaoka, M. Watanabe, *Alkaline Electrochemical Power Sources* **2010**, 25, 61-70.
- [154] K. Matsuoka, S. Chiba, Y. Iriyama, T. Abe, M. Matsuoka, K. Kikuchi, Z. Ogumi, *Thin Solid Films* **2008**, 516, 3309-3313.



- [155] M. Schieda, S. Roualdes, J. Durand, A. Martinet, D. Marsacq, *Desalination* **2006**, *199*, 286-288.
- [156] K.-D. Kreuer, *Chemistry of Materials* **2014**, *26*, 361-380.
- [157] M. A. Hickner, A. M. Herring, E. B. Coughlin, *Journal of Polymer Science Part B-Polymer Physics* **2013**, *51*, 1727-1735.
- [158] Y.-J. Wang, J. Qiao, R. Baker, J. Zhang, *Chemical Society Reviews* **2013**, *42*, 5768-5787.
- [159] A. Brouzgou, A. Podias, P. Tsiakaras, *Journal of Applied Electrochemistry* **2013**, *43*, 119-136.
- [160] J. Pan, C. Chen, L. Zhuang, J. Lu, *Accounts of Chemical Research* **2012**, *45*, 473-481.
- [161] H. Zhang, P. K. Shen, *Chemical Reviews* **2012**, *112*, 2780-2832.
- [162] H. Zhang, P. K. Shen, *Chemical Society Reviews* **2012**, *41*, 2382-2394.
- [163] G. Couture, A. Alaaeddine, F. Boschet, B. Ameduri, *Progress in Polymer Science* **2011**, *36*, 1521-1557.
- [164] Y. A. Elabd, M. A. Hickner, *Macromolecules* **2011**, *44*, 1-11.
- [165] D. Tang, J. Pan, S. Lu, L. Zhuang, J. Lu, *Science China-Chemistry* **2010**, *53*, 357-364.
- [166] E. Antolini, E. R. Gonzalez, *Journal of Power Sources* **2010**, *195*, 3431-3450.
- [167] A. Serov, C. Kwak, *Applied Catalysis B-Environmental* **2010**, *98*, 1-9.
- [168] F. Bidault, D. J. L. Brett, P. H. Middleton, N. P. Brandon, *Journal of Power Sources* **2009**, *187*, 39-48.
- [169] T. W. Xu, *Journal of Membrane Science* **2005**, *263*, 1-29.
- [170] S. Maurya, S.-H. Shin, M.-K. Kim, S.-H. Yun, S.-H. Moon, *Journal of Membrane Science* **2013**, *443*, 28-35.
- [171] X. Wang, M. Li, B. T. Golding, M. Sadeghi, Y. Cao, E. H. Yu, K. Scott, *International Journal of Hydrogen Energy* **2011**, *36*, 10022-10026.

- [172] M. Faraj, E. Elia, M. Boccia, A. Filpi, A. Pucci, F. Ciardelli, *Journal of Polymer Science Part a-Polymer Chemistry* **2011**, 49, 3437-3447.
- [173] A. K. Pandey, A. Goswami, D. Sen, S. Mazumder, R. F. Childs, *Journal of Membrane Science* **2003**, 217, 117-130.
- [174] B. Bauer, H. Strathmann, F. Effenberger, *Desalination* **1990**, 79, 125-144.
- [175] O. I. Deavin, S. Murphy, A. L. Ong, S. D. Poynton, R. Zeng, H. Herman, J. R. Varcoe, *Energy & Environmental Science* **2012**, 5, 8584-8597.
- [176] M. A. Hossain, Y. Lim, S. Lee, H. Jang, S. Choi, Y. Jeon, S. Lee, H. Ju, W. G. Kim, *Solid State Ionics* **2014**, 262, 754-760.
- [177] J. Wang, S. Gu, R. B. Kaspar, B. Zhang, Y. Yan, *Chemsuschem* **2013**, 6, 2079-2082.
- [178] O. M. M. Page, S. D. Poynton, S. Murphy, A. L. Ong, D. M. Hillman, C. A. Hancock, M. G. Hale, D. C. Apperley, J. R. Varcoe, *Rsc Advances* **2013**, 3, 579-587.
- [179] B. Lin, H. Dong, Y. Li, Z. Si, F. Gu, F. Yan, *Chemistry of Materials* **2013**, 25, 1858-1867.
- [180] D. Chen, M. A. Hickner, *Acs Applied Materials & Interfaces* **2012**, 4, 5775-5781.
- [181] J. Ran, L. Wu, J. R. Varcoe, A. L. Ong, S. D. Poynton, T. Xu, *Journal of Membrane Science* **2012**, 415, 242-249.
- [182] B. Qiu, B. Lin, Z. Si, L. Qiu, F. Chu, J. Zhao, F. Yan, *Journal of Power Sources* **2012**, 217, 329-335.
- [183] B. S. Aitken, C. F. Buitrago, J. D. Heffley, M. Lee, H. W. Gibson, K. I. Winey, K. B. Wagener, *Macromolecules* **2012**, 45, 681-687.
- [184] B. Qiu, B. Lin, L. Qiu, F. Yan, *Journal of Materials Chemistry* **2012**, 22, 1040-1045.
- [185] B. Lin, L. Qiu, B. Qiu, Y. Peng, F. Yan, *Macromolecules* **2011**, 44, 9642-9649.
- [186] Y. Ye, Y. A. Elabd, *Macromolecules* **2011**, 44, 8494-8503.
- [187] F. Zhang, H. Zhang, C. Qu, *Journal of Materials Chemistry* **2011**, 21, 12744-12752.

- [188] B. Lin, L. Qiu, J. Lu, F. Yan, *Chemistry of Materials* **2010**, 22, 6718-6725.
- [189] M. Guo, J. Fang, H. Xu, W. Li, X. Lu, C. Lan, K. Li, *Journal of Membrane Science* **2010**, 362, 97-104.
- [190] X. Lin, X. Liang, S. D. Poynton, J. R. Varcoe, A. L. Ong, J. Ran, Y. Li, Q. Li, T. Xu, *Journal of Membrane Science* **2013**, 443, 193-200.
- [191] J. Miyake, K. Fukasawa, M. Watanabe, K. Miyatake, *Journal of Polymer Science Part a-Polymer Chemistry* **2014**, 52, 383-389.
- [192] X. Li, Y. Yu, Q. Liu, Y. Meng, *International Journal of Hydrogen Energy* **2013**, 38, 11067-11073.
- [193] L. I. Sanli, S. A. Gursel, *Journal of Applied Polymer Science* **2011**, 120, 2313-2323.
- [194] Y. Li, T. Xu, *Separation and Purification Technology* **2008**, 61, 430-435.
- [195] A. B. Huang, C. Y. Xia, C. B. Xiao, L. Zhuang, *Journal of Applied Polymer Science* **2006**, 100, 2248-2251.
- [196] A. B. Huang, C. B. Xiao, L. Zhuang, *Journal of Applied Polymer Science* **2005**, 96, 2146-2153.
- [197] L.-c. Jheng, S. L.-c. Hsu, B.-y. Lin, Y.-l. Hsu, *Journal of Membrane Science* **2014**, 460, 160-170.
- [198] S. D. Sajjad, Y. Hong, F. Liu, *Polymers for Advanced Technologies* **2014**, 25, 108-116.
- [199] C. H. Zhao, Y. Gong, Q. L. Liu, Q. G. Zhang, A. M. Zhu, *International Journal of Hydrogen Energy* **2012**, 37, 11383-11393.
- [200] X. Lin, L. Wu, Y. Liu, A. L. Ong, S. D. Poynton, J. R. Varcoe, T. Xu, *Journal of Power Sources* **2012**, 217, 373-380.
- [201] D. S. Kim, A. Labouriau, M. D. Guiver, Y. S. Kim, *Chemistry of Materials* **2011**, 23, 3795-3797.
- [202] M. Li, L. Yang, S. Fang, S. Dong, *Journal of Membrane Science* **2011**, 366, 245-250.
- [203] J. Wang, S. Li, S. Zhang, *Macromolecules* **2010**, 43, 3890-3896.

- [204] Q. Zhang, S. Li, S. Zhang, *Chemical Communications* **2010**, 46, 7495-7497.
- [205] L. Jiang, X. Lin, J. Ran, C. Li, L. Wu, T. Xu, *Chinese Journal of Chemistry* **2012**, 30, 2241-2246.
- [206] S. Gu, R. Cai, Y. Yan, *Chemical Communications* **2011**, 47, 2856-2858.
- [207] K. K. Stokes, J. A. Orlicki, F. L. Beyer, *Polymer Chemistry* **2011**, 2, 80-82.
- [208] C. G. Arges, S. Kulkarni, A. Baranek, K.-J. Pan, M.-s. Jung, D. Patton, K. A. Mauritz, V. Ramani, *Polymer Electrolyte Fuel Cells 10, Pts 1 and 2* **2010**, 33, 1903-1913.
- [209] S. Gu, R. Cai, T. Luo, K. Jensen, C. Contreras, Y. Yan, *Chemsuschem* **2010**, 3, 555-558.
- [210] S. Gu, R. Cai, T. Luo, Z. Chen, M. Sun, Y. Liu, G. He, Y. Yan, *Angewandte Chemie-International Edition* **2009**, 48, 6499-6502.
- [211] M. Wada, S. Higashizaki, *Journal of the Chemical Society-Chemical Communications* **1984**, 482-483.
- [212] K. J. T. Noonan, K. M. Hugar, H. A. Kostalik, E. B. Lobkovsky, H. D. Abruna, G. W. Coates, *Journal of the American Chemical Society* **2012**, 134, 18161-18164.
- [213] Y. Wang, A. Rapakousiou, D. Astruc, *Macromolecules* **2014**, 47, 3767-3774.
- [214] M. L. Disabb-Miller, Y. Zha, A. J. DeCarlo, M. Pawar, G. N. Tew, M. A. Hickner, *Macromolecules* **2013**, 46, 9279-9287.
- [215] P. Y. Xu, C. H. Zhao, Q. L. Liu, *Journal of Applied Polymer Science* **2013**, 130, 1172-1178.
- [216] Y. Zha, M. L. Disabb-Miller, Z. D. Johnson, M. A. Hickner, G. N. Tew, *Journal of the American Chemical Society* **2012**, 134, 4493-4496.
- [217] S. Gu, J. H. Wang, Q. R. Fang, R. B. Kaspar, B. Z. Zhang, Y. S. Yan, *ECS Meeting Abstracts* **2013**, MA2013-02.
- [218] B. R. Einsla, Chempath, S., Pratt, L. R., Boncella, J. M., Rau, J., Macomber, C. S., Pivovar, B. S., *Electrochem. Soc. Trans* **2007**, 11, 1173-1180.
- [219] C. G. Arges, L. Wang, J. Parrondo, V. Ramani, *Journal of the Electrochemical Society* **2013**, 160, F1258-F1274.

- [220] C. Iojoiu, F. Chabert, M. Marechal, N. E. Kissi, J. Guindet, J. Y. Sanchez, *Journal of Power Sources* **2006**, *153*, 198-209.
- [221] U. S. Hwang, J. H. Choi, *Separation and Purification Technology* **2006**, *48*, 16-23.
- [222] T. Sata, M. Tsujimoto, T. Yamaguchi, K. Matsusaki, *Journal of Membrane Science* **1996**, *112*, 161-170.
- [223] M. R. Sturgeon, C. S. Macomber, C. Engtrakul, H. Long, B. S. Pivovar, *Journal of the Electrochemical Society* **2015**, *162*, F366-F372.
- [224] S. Smiles, R. Le Rossignol, *Journal of the Chemical Society* **1906**, *89*, 696-708.
- [225] K. Gyoryova, B. Mohai, *Thermochimica Acta* **1985**, *92*, 771-774.
- [226] A. T. G. Cameron J. F., Orellana A. J., Sinta R. F., *J. Proc. SPIE* **1997**, *3049*, 473-484.
- [227] J. V. Crivello, *Advances in Polymer Science* **1984**, *62*, 1-48.
- [228] K. C. Lethesh, W. Dehaen, K. Binnemans, *Rsc Advances* **2014**, *4*, 4472-4477.
- [229] Y. Ye, K. K. Stokes, F. L. Beyer, Y. A. Elabd, *Journal of Membrane Science* **2013**, *443*, 93-99.
- [230] C. G. Arges, V. Ramani, *Journal of the Electrochemical Society* **2013**, *160*, F1006-F1021.
- [231] H. Matsumoto, T. Matsuda, Y. Miyazaki, *Chemistry Letters* **2000**, 1430-1431.
- [232] O. O. Okoturo, T. J. VanderNoot, *Journal of Electroanalytical Chemistry* **2004**, *568*, 167-181.
- [233] L. Xiao, K. E. Johnson, *Canadian Journal of Chemistry-Revue Canadienne De Chimie* **2004**, *82*, 491-498.
- [234] H. Matsumoto, H. Sakaebe, K. Tatsumi, *Journal of Power Sources* **2005**, *146*, 45-50.
- [235] L. Yang, Z. Zhang, X. Gao, H. Zhang, K. Mashita, *Journal of Power Sources* **2006**, *162*, 614-619.

- [236] J. von Braun, W. Teuffert, K. Weissback, *Justus Liebigs Annalen Der Chemie* **1929**, 472, 121-142.
- [237] C. K. Ingold, J. A. Jessop, K. I. Kuriyan, A. M. M. Mandour, *Journal of the Chemical Society* **1933**, 533-537.
- [238] C. K. Ingold, K. I. Kuriyan, *Journal of the Chemical Society* **1933**, 991-993.
- [239] S. Lindenbaum, G. E. Boyd, G. E. Myers, *Journal of Physical Chemistry* **1958**, 62, 995-999.
- [240] S. V. Bhilare, A. R. Deorukhkar, N. B. Darvatkar, M. S. Rasalkar, M. M. Salunkhe, *Journal of Molecular Catalysis a-Chemical* **2007**, 270, 123-126.
- [241] H. Herman, R. C. T. Slade, J. R. Varcoe, *Journal of Membrane Science* **2003**, 218, 147-163.
- [242] G. G. Wang, Y. M. Weng, D. Chu, D. Xie, R. R. Chen, *J Membrane Sci* **2009**, 326, 4-8.
- [243] Y. Xiong, Q. L. Liu, Q. H. Zeng, *J. Power Sources* **2009**, 193, 541-546.
- [244] J. H. Wang, Z. Zhao, F. X. Gong, S. H. Li, S. B. Zhang, *Macromolecules* **2009**, 42, 8711-8717.
- [245] S. Gu, R. Cai, Y. S. Yan, *Chem. Commun.* **2011**, 47, 2856-2858.
- [246] J. H. Wang, S. H. Li, S. B. Zhang, *Macromolecules* **2010**, 43, 3890-3896.
- [247] B. C. Lin, L. H. Qiu, B. Qiu, Y. Peng, F. Yan, *Macromolecules* **2011**, 44, 9642-9649.
- [248] G. W. Fenton, C. K. Ingold, *Journal of the Chemical Society* **1929**, 2342-2357.
- [249] Pagilaga.Ru, W. E. McEwen, *Chemical Communications* **1966**, 652-653.
- [250] M. Zanger, C. A. Vanderwerf, W. E. McEwen, *Journal of the American Chemical Society* **1959**, 81, 3806-3807.
- [251] A. Taladriz, A. Healy, E. J. Flores Perez, V. Herrero Garcia, C. Rios Martinez, A. A. M. Alkhaldi, A. A. Eze, M. Kaiser, H. P. de Koning, A. Chana, C. Dardonville, *Journal of Medicinal Chemistry* **2012**, 55, 2606-2622.
- [252] K. R. Dunbar, S. C. Haefner, *Polyhedron* **1994**, 13, 727-736.

- [253] R. L. Burwell, *Chemical Reviews* **1954**, 54, 615-685.
- [254] L. Horner, H. Hoffmann, H. G. Wippel, G. Hassel, *Chemische Berichte-Recueil* **1958**, 91, 52-57.
- [255] G. Singh, *Journal of Organic Chemistry* **1987**, 52, 1647-1648.
- [256] R. W. Taft, *Journal of the American Chemical Society* **1952**, 74, 2729-2732.
- [257] R. W. Taft, *Journal of the American Chemical Society* **1952**, 74, 3120-3128.
- [258] R. W. Taft, *Journal of the American Chemical Society* **1953**, 75, 4538-4539.
- [259] D. D. A. Anslyn E.V., University Science Books, **2005**, p. 455.
- [260] E. C. Alyea, J. Malito, *Phosphorus Sulfur and Silicon and the Related Elements* **1989**, 46, 175-181.
- [261] B. Zhang, S. Gu, J. Wang, Y. Liu, A. M. Herring, Y. Yan, *Rsc Advances* **2012**, 2, 12683-12685.
- [262] S. L. Keenan, K. P. Peterson, K. Peterson, K. Jacobson, *Journal of Chemical Education* **2008**, 85, 558-560.
- [263] L. P. Hammett, *Journal of the American Chemical Society* **1937**, 59, 96-103.
- [264] C. Hansch, A. Leo, R. W. Taft, *Chemical Reviews* **1991**, 91, 165-195.
- [265] C. C. Mitsch, L. D. Freedman, C. G. Moreland, *Journal of Magnetic Resonance* **1971**, 5, 140-144.
- [266] W. E. McEwen, G. Axelrad, M. Zanger, Vanderwe.Ca, *Journal of the American Chemical Society* **1965**, 87, 3948-3952.
- [267] R. W. Taft, *Progress in Physical Organic Chemistry, Vol. 12*, **1976**.
- [268] M. R. Hibbs, *Journal of Polymer Science Part B-Polymer Physics* **2013**, 51, 1736-1742.
- [269] D. Macmillan, A. M. Daines, M. Bayrhuber, S. L. Flitsch, *Organic Letters* **2002**, 4, 1467-1470.
- [270] T. Oshikawa, M. Yamashita, *Chemistry & Industry* **1985**, 126-127.

- [271] M. Joshaghani, E. Faramarzi, E. Rafiee, M. Daryanavard, J. Xiao, C. Baillie, *Journal of Molecular Catalysis a-Chemical* **2007**, 273, 310-315.
- [272] A. M. Harned, H. S. He, P. H. Toy, D. L. Flynn, P. R. Hanson, *Journal of the American Chemical Society* **2005**, 127, 52-53.
- [273] R. El Abed, F. Aloui, J.-P. Genet, B. Ben Hassine, A. Marinetti, *Journal of Organometallic Chemistry* **2007**, 692, 1156-1160.
- [274] E. Zysman-Colman, K. Arias, J. S. Siegel, *Canadian Journal of Chemistry- Revue Canadienne De Chimie* **2009**, 87, 440-447.
- [275] T. Fujihara, Y. Tomike, T. Ohtake, J. Terao, Y. Tsuji, *Chemical Communications* **2011**, 47, 9699-9701.
- [276] T. Chatterjee, R. Dey, B. C. Ranu, *New Journal of Chemistry* **2011**, 35, 1103-1110.
- [277] S. A. Nunez, M. A. Hickner, *Acs Macro Letters* **2013**, 2, 49-52.
- [278] A. D. Mohanty, Y.-B. Lee, L. Zhu, M. A. Hickner, C. Bae, *Macromolecules* **2014**, 47, 1973-1980.
- [279] X. Li, G. Nie, J. Tao, W. Wu, L. Wang, S. Liao, *Acs Applied Materials & Interfaces* **2014**, 6, 7585-7595.
- [280] L. P. Hammett, *Chemical Reviews* **1935**, 17, 125-136.



## Appendix A

### ABBREVIATIONS AND IMPORTANT VARIABLES

$^1\text{H}$ NMR	Proton NMR
$^{31}\text{P}$ NMR	Phosphorus NMR
9MeOTAS	Tris(1,3,5-trimethoxyphenyl)sulfonium
9MeOTASCl	9MeOTAS chloride
9MeOTASTf	9MeOTAS triflate
ACN	Acetonitrile
AFC	Alkaline fuel cell
ATR-FTIR	Attenuated total reflectance Fourier transform infrared
BPO	Benzyl peroxide
BTMA	Benzyltrimethylammonium
BTPP	Benzyl triphenylphosphonium
BTPP-(2,4,6-MeO)	Benzyl tris(2,4,6-trimethoxyphenyl)phosphonium
BTPP-(2,6-MeO)	Benzyl tris(2,6-trimethoxyphenyl)phosphonium
BTPP-( <i>o</i> -MeO)	Benzyl tris( <i>o</i> -methoxyphenyl)phosphonium
BTPP-( <i>p</i> -Me)	Benzyl tris( <i>p</i> -methylphenyl)phosphonium
BTPP-( <i>p</i> -MeO)	Benzyl tris( <i>p</i> -methoxyphenyl)phosphonium
C	The cation concentration at the sampling time
C <sub>0</sub>	The initial cation concentration
CD <sub>3</sub> OD	Deuterated methanol
CD <sub>3</sub> CD <sub>2</sub> OD	Deuterated ethanol

CDCl <sub>3</sub>	Deuterated chloroform
CMPSf	Chloromethylated polysulfone
D <sub>2</sub> O	Heavy water
DB	Degree of bromination
DC	Degree of chloromethylation
DF	Degree of functionalization
DMF	<i>N,N</i> -Dimethylformamide
DMSO-d <sub>6</sub>	Deuterated dimethylsulfoxide
DS	Degree of functionalization of MeOTAS
$E_a$	Activation energy
$E_s$	Steric substituent constant
HC	Hydroxide conductivity
HC <sub>IEC</sub>	IEC normalized HC
HEM	Hydroxide exchange membrane
HEMFC	Hydroxide exchange membrane fuel cell
HOR	Hydrogen oxidation reaction
IEC	Ion exchange capacity
$k$	Rate constant of degradation
$k_{80}$	Adjusted rate constant of degradation at 80 °C
$k_{EH}$	Adjusted rate constant of ether hydrolysis
$k_{OF}$	Adjusted rate constant of oxide formation
KOD	Deuterated potassium hydroxide
MEA	Membrane-electrode-assembly
MeOTAS	Diphenyl (3-methyl-4-methoxyphenyl)sulfonium

MeOTASCl	MeOTAS chloride
MeOTASOH	MeOTAS hydroxide
MeOTASTf	MeOTAS triflate
MeTAS	Diphenyl(4-methylphenyl)sulfonium
MeTASCl	MeTAS chloride
MeTASOH	MeTAS hydroxide
MeTASTf	MeTAS triflate
MTPP-(2,4,6-Me)	Methyl tris(2,4,6-trimethylphenyl)phosphonium
MTPP-(2,4,6-MeO)	Methyl tris(2,4,6-trimethoxyphenyl)phosphonium
MTPP-(2,6-MeO)	Methyl tris(2,6-trimethoxyphenyl)phosphonium
MTPP-( <i>o</i> -Me)	Methyl tris( <i>o</i> -methylphenyl)phosphonium
MTPP-( <i>o</i> -MeO)	Methyl tris( <i>o</i> -methoxyphenyl)phosphonium
MTPP-( <i>p</i> -MeO)	Methyl tris( <i>p</i> -methoxyphenyl)phosphonium
NBS	<i>N</i> -Bromosuccinimide
NaOD	Deuterated sodium hydroxide
NMP	<i>N</i> -Methyl-2-pyrrolidone
NMR	Nuclear magnetic resonance
ORR	Oxygen reduction reaction
QA	Quaternary ammonium
QP	Quaternary phosphonium
PEM	Proton exchange membrane
PEMFC	Proton exchange membrane fuel cell
PPO	Poly(phenylene oxide)
PSf	Polysulfone

PSf-BA	Butylaminated polysulfone
PSf-MeOTAS	MeOTAS functionalized polysulfone
PSf-MeOTASOH	MeOTAS functionalized polysulfone based HEM
PSf-MeTAS	MeTAS functionalized polysulfone
PSf-MeTASOH	MeTAS functionalized polysulfone based HEM
PSf-TPQP	TPQP functionalized PSf
PS <sub>t</sub>	Polystyrene
SAXS	Small-angle X-ray scattering
T <sub>g</sub>	Glass transition temperature
T <sub>FD</sub> ,	Fastest-weight-loss decomposition temperature
T <sub>OD</sub>	Onset decomposition temperature
TAS	Triarylsulfonium
TBAF	Tetrabutylammonium fluoride
TGA	Thermogravimetric analysis
THF	Tetrahydrofuran
TMS	Tetramethylsilane
TMS(CH <sub>2</sub> ) <sub>3</sub> SO <sub>3</sub> Na	3-(trimethylsilyl)-1-propanesulfonic acid sodium salt
TPQP	Tris(2,4,6-trimethoxyphenyl) quaternary phosphonium
TS	Tertiary sulfonium
TTMPP	Tris(2,4,6-trimethoxyphenyl)phosphine
TTMPPO	Tris(2,4,6-trimethoxyphenyl)phosphine oxide
$\delta$	<sup>1</sup> H NMR or <sup>31</sup> P NMR chemical shift
$\sigma$	The substituent constant
$\rho$	The reaction constant

## Appendix B

### TAFT EQUATION AND STERIC SUBSTITUENT CONSTANT ( $E_s$ )

The Taft equation was developed by Robert W. Taft in 1952 as a modification to the Hammett equation.<sup>[256-258]</sup> While the Hammett equation accounts for how electronic effects influence reaction rates, the Taft equation also describes the steric effects of a substituent. The Taft equation is written as Eq. B.1.  $k_s$  is the rate of the studied reaction, and  $k_H$  is the rate of the reference reaction ( $R = H$ ).  $\log(k_s/k_H)$  is the ratio of the rate of the substituted reaction compared to the reference reaction.  $\sigma^*$  is the polar substituent constant that describes the field and inductive effects of the substituent.  $E_s$  is the steric substituent constant.  $\rho^*$  is the sensitivity factor for the reaction to polar effects, and  $\delta_T$  is a reaction constant that describes the susceptibility of a reaction series to steric effects. For the definition reaction series,  $\delta_T$  was set to 1, and  $E_s$  for the reference reaction was set to zero.

$$\log\left(\frac{k_s}{k_H}\right) = \rho^* \sigma^* + \delta_T E_s \quad \text{Eq. B.1}$$

Although the acid catalyzed and base catalyzed hydrolysis of esters gives transition states for the rate determining steps that have differing charge densities, their structures differ only by two hydrogen atoms. Taft thus assumed that steric effects would influence both reaction mechanisms equally. Due to this, the steric substituent constant  $E_s$  was determined from solely the acid catalyzed reaction, as this would not include polar effects.  $E_s$  was defined as Eq. B.2. Some commonly used  $E_s$  are lists in Table B.1.

$$E_s = \frac{1}{\delta_T} \log \left( \frac{k_s}{k_H} \right) \quad \text{Eq. B.2}$$

Table B.1: Some  $E_s$  used in the Taft equation.<sup>[256-258]</sup>

Substituent	$E_s$
-H	0
-OCH <sub>3</sub>	-0.55
-CH <sub>3</sub>	-1.24
-CH <sub>2</sub> CH <sub>3</sub>	-1.31
-CH(CH <sub>3</sub> ) <sub>2</sub>	-1.71
-C(CH <sub>3</sub> ) <sub>3</sub>	-2.78
-CH <sub>2</sub> Ph	-1.62
-Ph	-3.79

## Appendix C

### DEGRADATION MECHANISM STUDY OF QP ANALOGS IN CHAPTER 3 AND DEGRADATION KINETICS STUDY OF QP CATIONS IN CHAPTER 4

Here show the evidence to determine the degradation mechanism of QP analogs in Chapter 3 and the original data used to calculate  $k_{80}$  of QP cations which are not shown in the main text of Chapter 4. The  $^1\text{H}$  NMR spectra of the degradation products of the three QP analogs are shown in Fig. C.1-C.3. The time series of  $^{13}\text{P}$  NMR spectra and plots of  $\ln(C_0/C)$  versus time for of MTPP-(2,6-MeO), BTPP-(2,6-MeO), MTPP-(*o*-MeO), BTPP-(*o*-MeO), MTPP-(*o*-Me) and MTPP-(*p*-MeO) tested at 80 °C are shown in Fig. C.4-C.15.

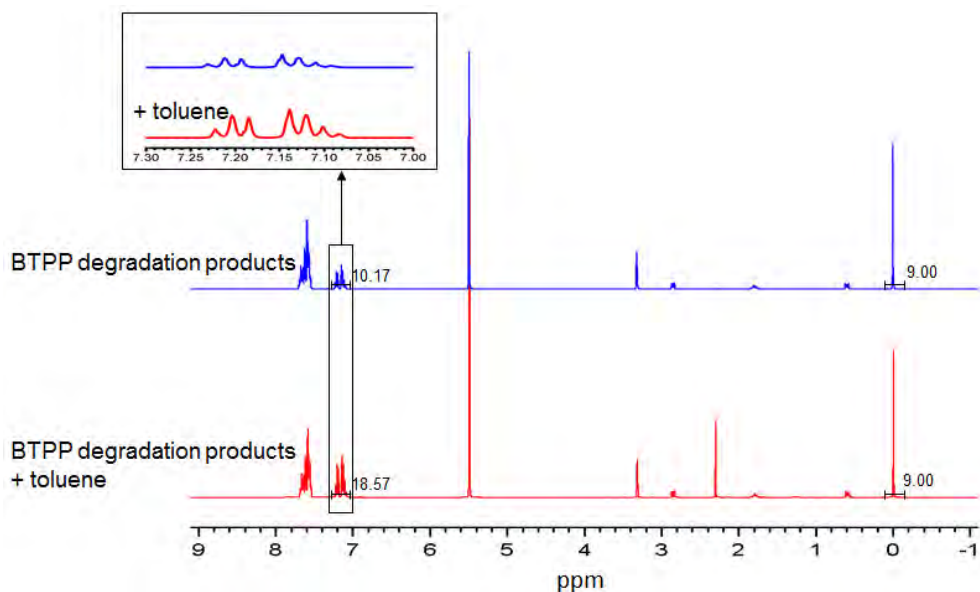


Figure C.1:  $^1\text{H}$  NMR evidence for the toluene production in the alkaline degradation of BTPP.

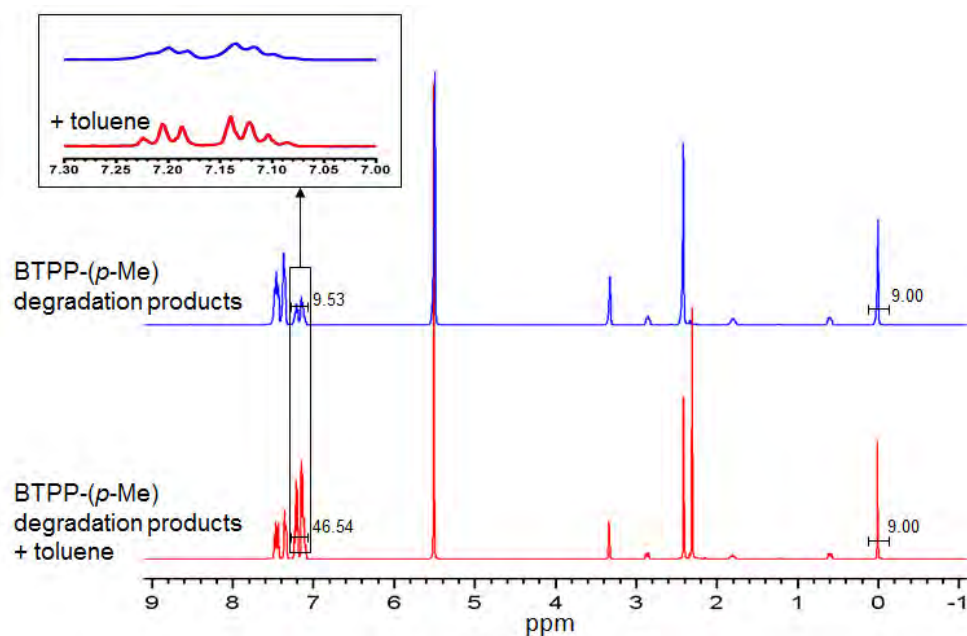


Figure C.2:  $^1\text{H}$  NMR evidence for the toluene production in the alkaline degradation of BTPP-(*p*-Me).

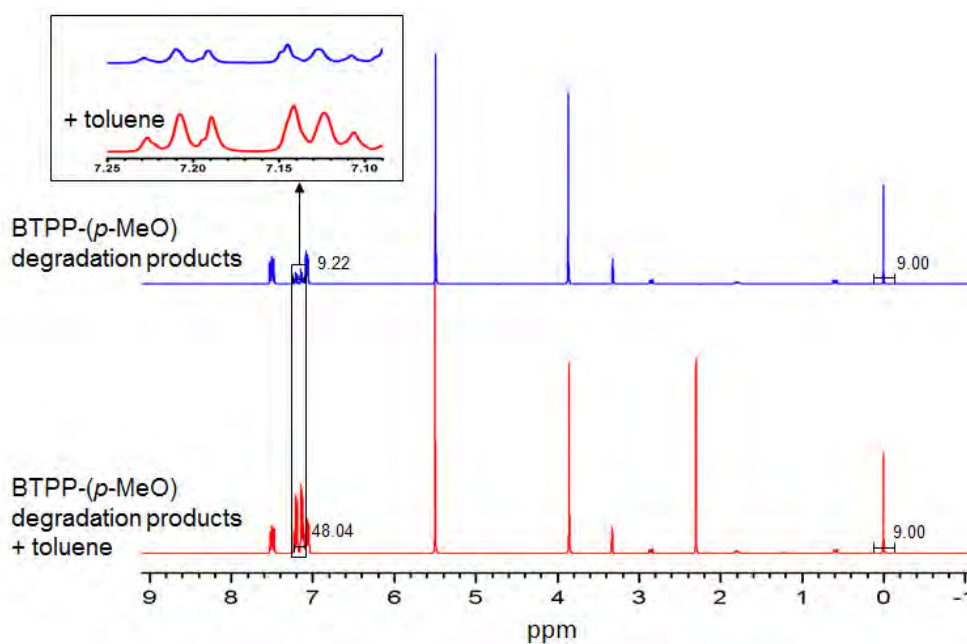


Figure C.3:  $^1\text{H}$  NMR evidence for the toluene production in the alkaline degradation of BTPP-(*p*-MeO).



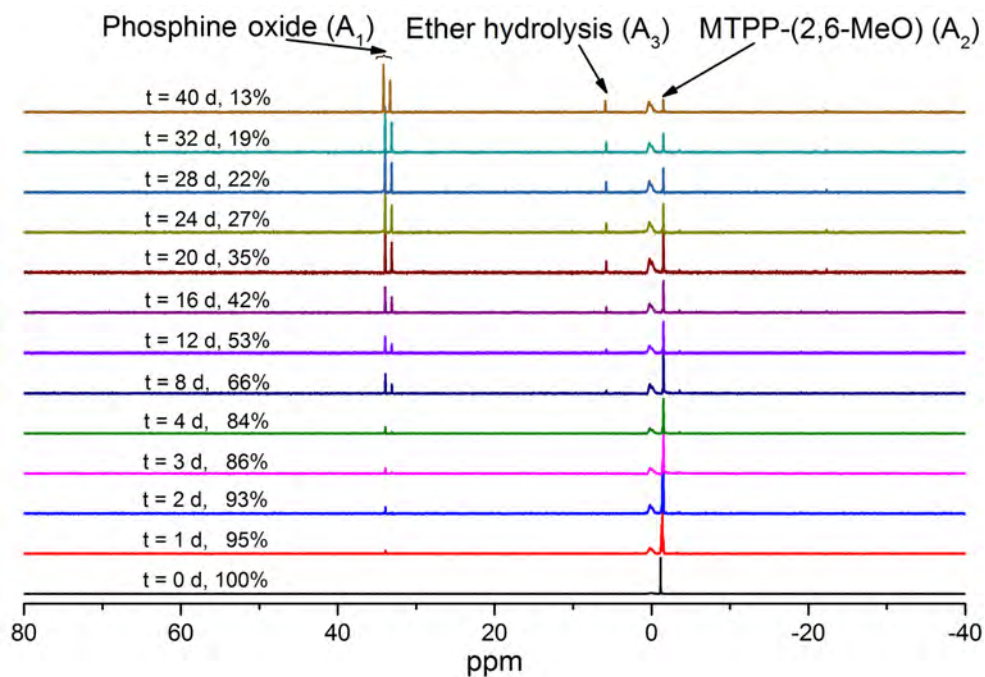


Figure C.4: Time series of  $^{31}\text{P}$  NMR spectra during durability test of MTPP-(2,6-MeO) at 80 °C. Phosphoric acid as the external standard; 1 M KOD in  $\text{CD}_3\text{OD}/\text{D}_2\text{O}$  (5/1 vol) as the solvent. The degradation percentage is calculated by  $A_2/(A_1+A_2+A_3)$ .  $A_1$  is the peak area of the phosphine oxide;  $A_2$  is the peak area of MTPP-(2,6-MeO);  $A_3$  is the peak area of ether hydrolysis products.

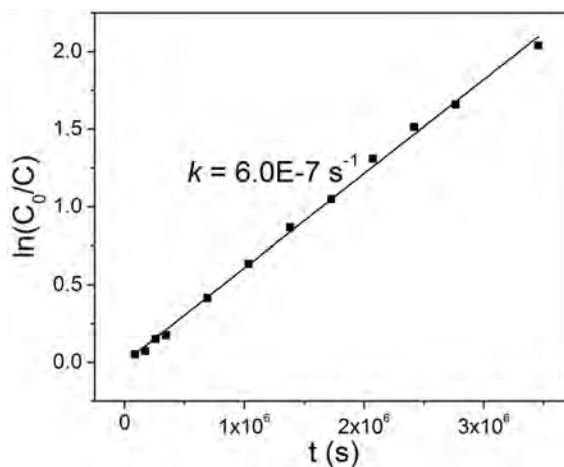


Figure C.5: The plot of  $\ln(C_0/C)$  versus time of MTPP-(2,6-MeO) at 80 °C. 1 M KOD in  $\text{CD}_3\text{OD}/\text{D}_2\text{O}$  (5/1 vol) as the solvent.

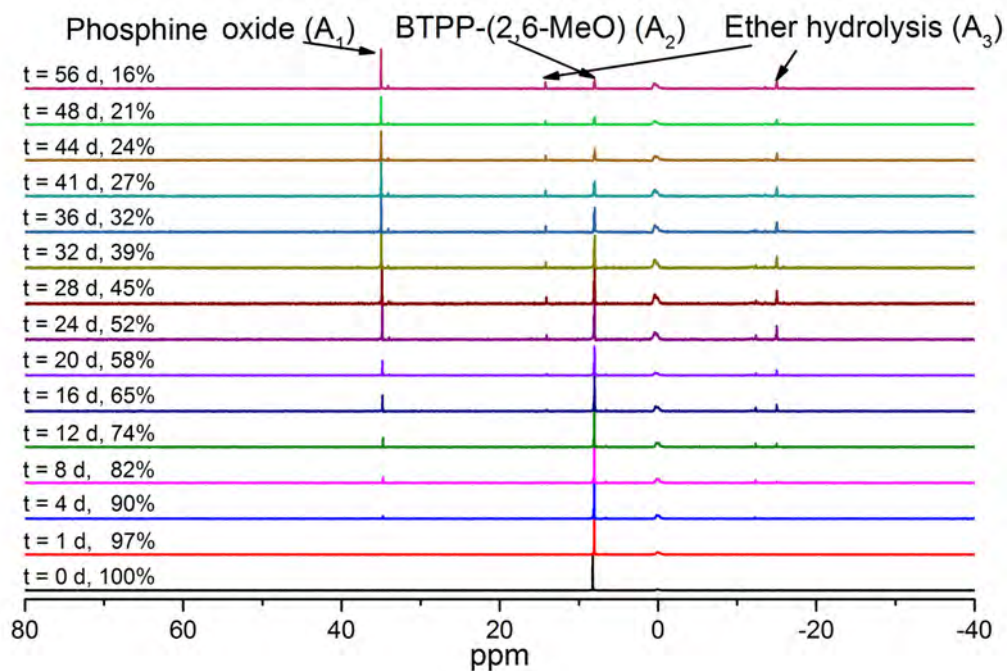


Figure C.6: Time series of  $^{31}\text{P}$  NMR spectra during durability test of BTPP-(2,6-MeO) at 80 °C. Phosphoric acid as the external standard; 1 M KOD in  $\text{CD}_3\text{OD}/\text{D}_2\text{O}$  (5/1 vol) as the solvent. The degradation percentage is calculated by  $A_2/(A_1+A_2+A_3)$ .  $A_1$  is the peak area of the phosphine oxide;  $A_2$  is the peak area of BTPP-(2,6-MeO);  $A_3$  is the peak area of ether hydrolysis products.

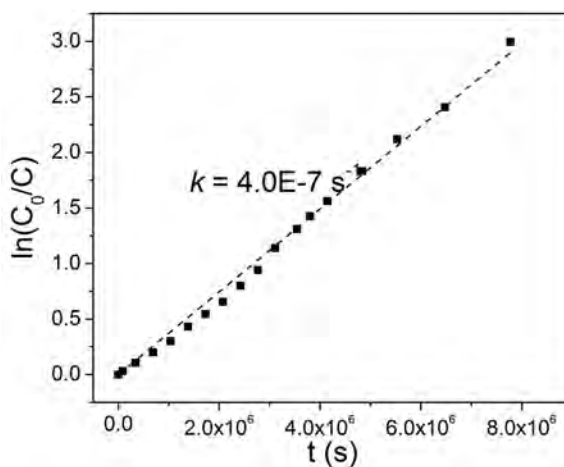


Figure C.7: The plot of  $\ln(C_0/C)$  versus time of BTPP-(2,6-MeO) at 80 °C. 1 M KOD in  $\text{CD}_3\text{OD}/\text{D}_2\text{O}$  (5/1 vol) as the solvent.

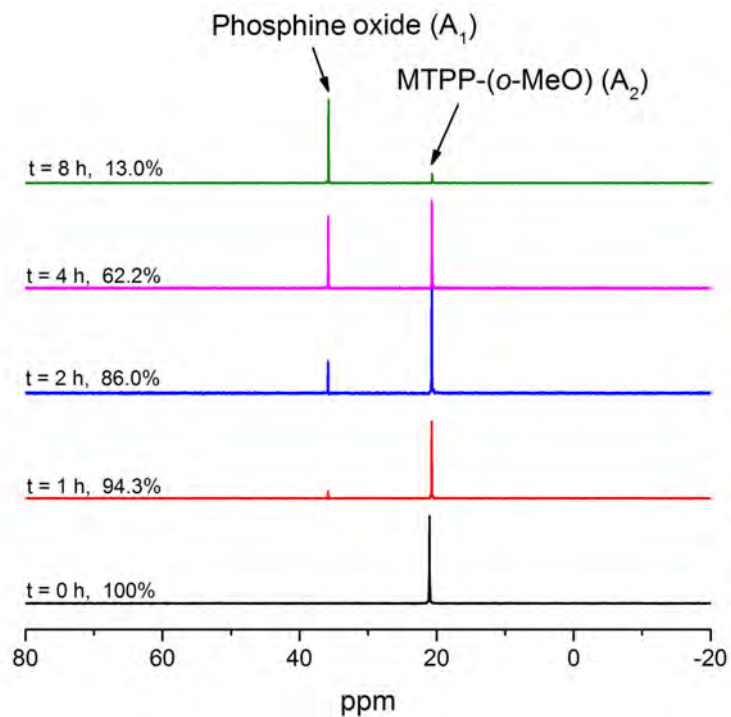


Figure C.8: Time series of  $^{31}\text{P}$  NMR spectra during durability test of MTPP-(*o*-MeO) at 80 °C. Phosphoric acid as the external standard; 1 M KOD in  $\text{CD}_3\text{OD}/\text{D}_2\text{O}$  (5/1 vol) as the solvent. The degradation percentage is calculated by  $A_2/(A_1+A_2)$ .  $A_1$  is the peak area of the phosphine oxide;  $A_2$  is the peak area of MTPP-(*o*-MeO).

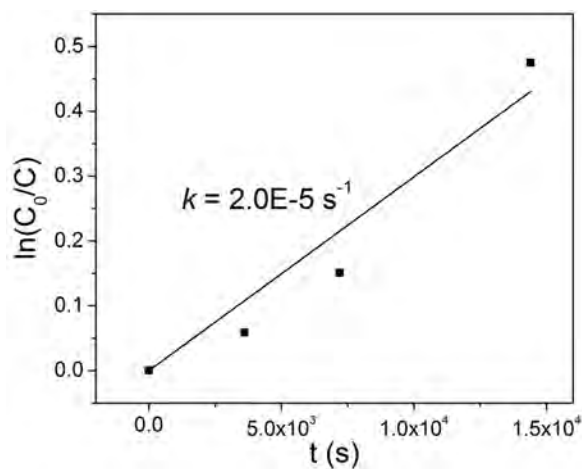


Figure C.9: The plot of  $\ln(C_0/C)$  versus time of MTPP-(*o*-MeO) at 80 °C. 1 M KOD in  $\text{CD}_3\text{OD}/\text{D}_2\text{O}$  (5/1 vol) as the solvent.

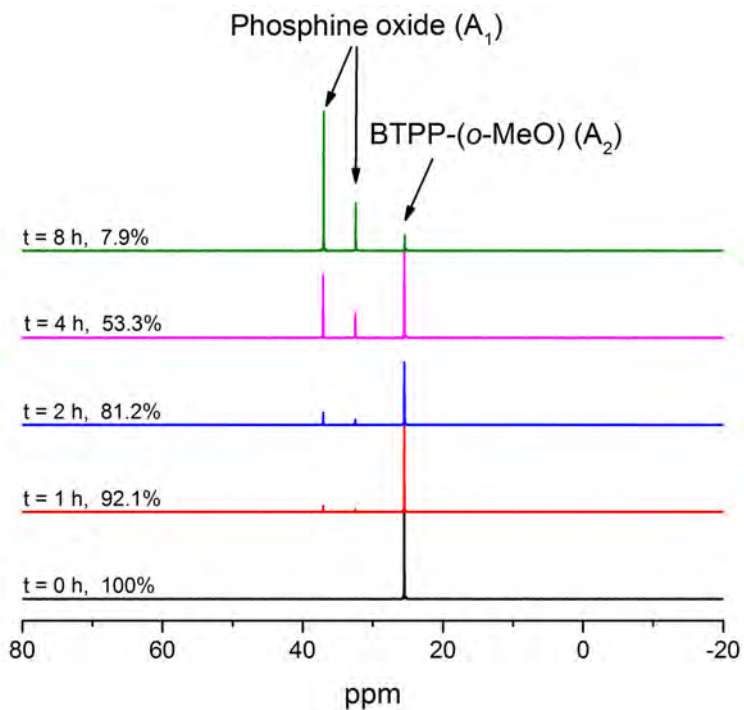


Figure C.10: Time series of  $^{31}\text{P}$  NMR spectra during durability test of BTPP-(*o*-MeO) at 80 °C. Phosphoric acid as the external standard; 1 M KOD in  $\text{CD}_3\text{OD}/\text{D}_2\text{O}$  (5/1 vol) as the solvent. The degradation percentage is calculated by  $A_2/(A_1 + A_2)$ .  $A_1$  is the peak area of the phosphine oxide;  $A_2$  is the peak area of BTPP-(*o*-MeO).

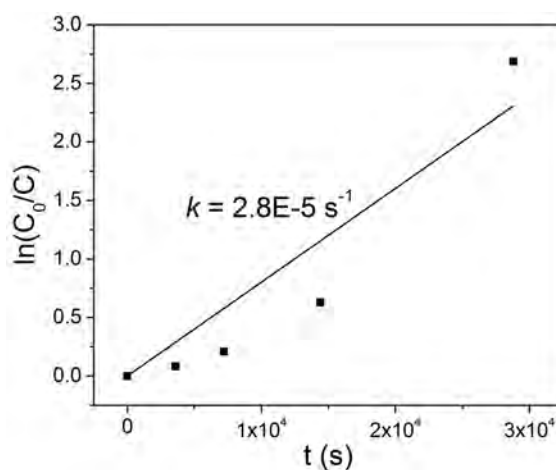


Figure C.11: The plots of  $\ln(C_0/C)$  versus time of BTPP-(*o*-MeO) at 80 °C. 1 M KOD in  $\text{CD}_3\text{OD}/\text{D}_2\text{O}$  (5/1 vol) as the solvent.

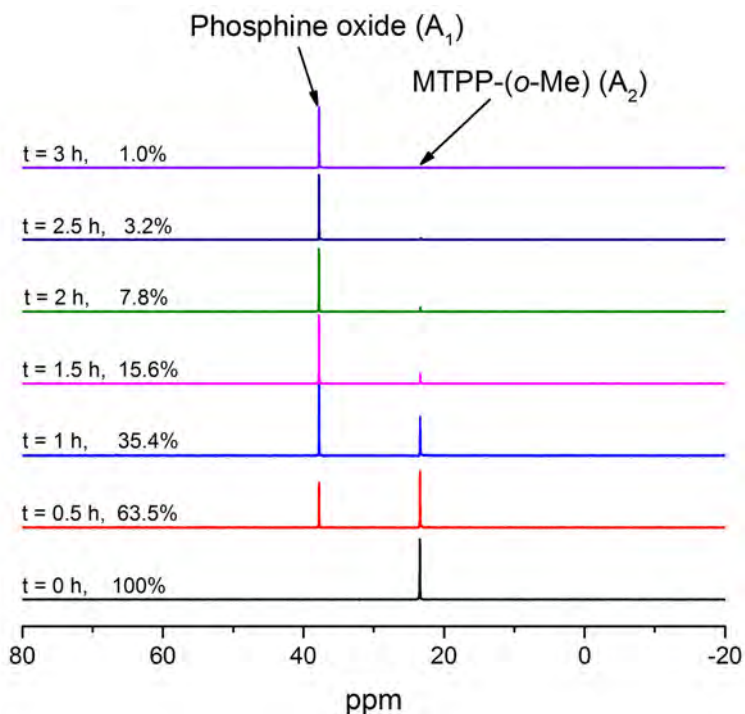


Figure C.12: Time series of  $^{31}\text{P}$  NMR spectra during durability test of MTPP-(*o*-Me) at 80 °C. Phosphoric acid as the external standard; 1 M KOD in  $\text{CD}_3\text{OD}/\text{D}_2\text{O}$  (5/1 vol) as the solvent. The degradation percentage is calculated by  $A_2/(A_1+A_2)$ .  $A_1$  is the peak area of the phosphine oxide;  $A_2$  is the peak area of MTPP-(*o*-Me).

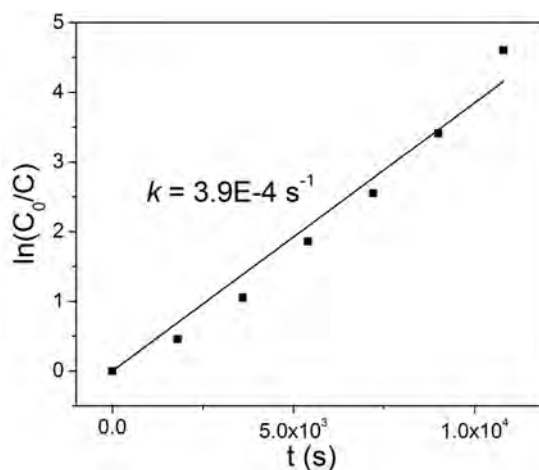


Figure C.13: The plot of  $\ln(C_0/C)$  versus time of MTPP-(*o*-Me) at 80 °C. 1 M KOD in  $\text{CD}_3\text{OD}/\text{D}_2\text{O}$  (5/1 vol) as the solvent.

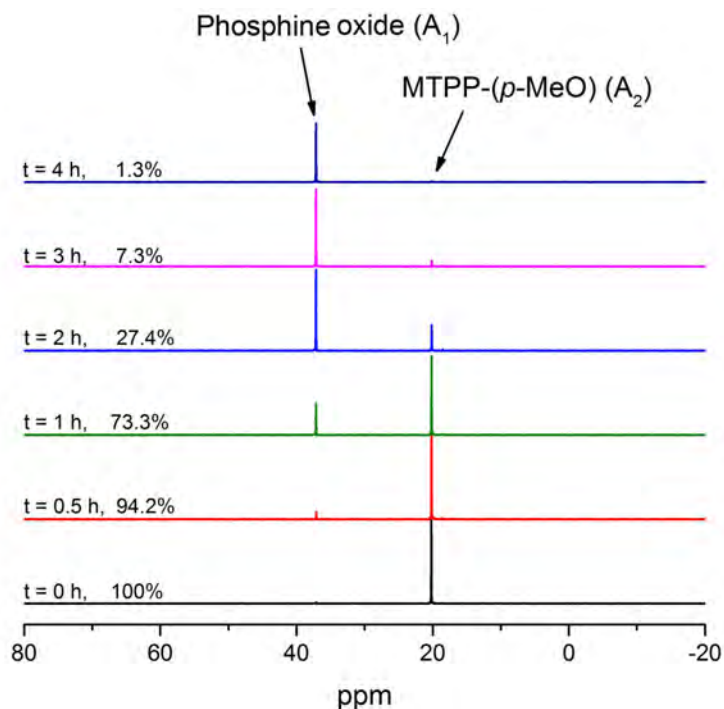


Figure C.14: Time series of  $^{31}\text{P}$  NMR spectra during durability test of MTPP-(*p*-MeO) at 80 °C. Phosphoric acid as the external standard; 1 M KOD in  $\text{CD}_3\text{OD}/\text{D}_2\text{O}$  (5/1 vol) as the solvent. The degradation percentage is calculated by  $A_2/(A_1 + A_2)$ .  $A_1$  is the peak area of MTPP-(*p*-MeO) oxide;  $A_2$  is the peak area of MTPP-(*p*-MeO).

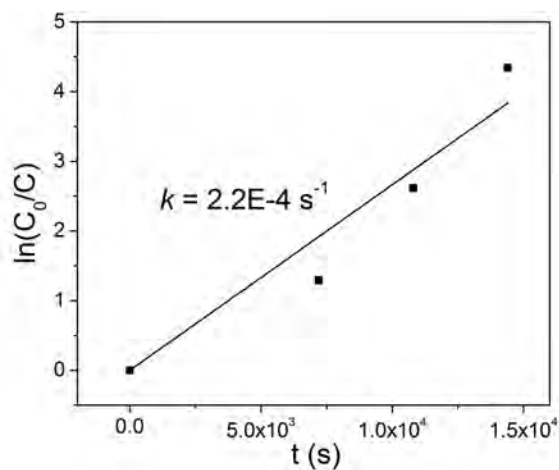


Figure C.15: Plots of  $\ln(C_0/C)$  versus time of MTPP-(*p*-MeO) at 80 °C. 1 M KOD in  $\text{CD}_3\text{OD}/\text{D}_2\text{O}$  (5/1 vol) as the solvent.